กระบวนการที่ปรับปรุงขึ้นสำหรับการดีราซิไมเซชัน ของระบบผลึกคอนโกลเมอเรต

นายกิตติศักดิ์ สุวรรณแสง

วิทยานิพนธ์นี้เป็นส่วนหนึ่งของการศึกษาตามหลักสูตรปริญญาวิศวกรรมศาสตรดุษฎีบัณฑิต
สาขาวิชาวิศวกรรมเคมี
มหาวิทยาลัยเทคโนโลยีสุรนารี
ปีการศึกษา 2557

AN IMPROVED PROCESS FOR DERACEMIZATION OF A CONGLOMERATE FORMING SYSTEM

Kittisak Suwannasang

A Thesis Submitted in Partial Fulfillment of the Requirements for the

Degree of Doctor of Philosophy in Chemical Engineering

Suranaree University of Technology

Academic Year 2014

กิตติศักดิ์ สุวรรณแสง : กระบวนการที่ปรับปรุงขึ้นสำหรับการดีราซิไมเซชันของระบบผลึกคอนโกลเมอเรต (AN IMPROVED PROCESS FOR DERACEMIZATION OF A CONGLOMERATE FORMING SYSTEM) อาจารย์ที่ปรึกษา : ศาสตราจารย์ ดร.เอเดรียน อีแวน ฟลัด, 208 หน้า.

กระบวนการเพิ่มความบริสุทธิ์ของสารอิแนนทิโอเมอร์มีความสำคัญเป็นอย่างยิ่งในการผลิตส่วนผสมของยา วิทยานิพนธ์นี้จึงได้พัฒนาแนวทางใหม่เพื่อนำไปประยุกต์ใช้ในการเพิ่มความบริสุทธิ์ของสารประกอบอินทรีย์ที่เป็นไครัลและมีการตกผลึกแบบคอนโกลเมอเรต โดยสองกระบวนการที่ถูกพัฒนาขึ้นมานั้น มีประสิทธิภาพที่ดีและง่ายต่อการนำไปใช้ในกระบวนการผลิต กระบวนการแรกคือการดีราซิไมเซชัน โดยใช้การโปรแกรมวัฏจักรความร้อน-ความเย็นร่วมกับปฏิกิริยาราซิไมเซชันซึ่งเกิดขึ้นอย่างรวดเร็วในวัฏภาคของสารละลาย กระบวนการที่สองได้รวมกระบวนการแรกเข้ากับกระบวนการตกผลึกแบบพรีเฟอเรนเชียล เพื่อให้ได้สารอิแนนทิโอเมอร์ตามที่ต้องการ จากการศึกษาวิจัยพบว่าทั้งสองกระบวนการที่กล่าวมาข้างต้นนั้นสามารถนำไปใช้เพื่อทำให้สารอิแนนทิโอเมอร์ซึ่งเป็นสารผลิตภัณฑ์ มีความบริสุทธิ์ได้สูงถึง 100% และมีผลได้เป็น 100% โดยคิดจากการเปลี่ยนสารอิแนนทิโอเมอร์ในวัฏภาคแขวนลอยทั้งหมดไปเป็นสารอิแนนทิโอเมอร์ที่เป็นสารผลิตภัณฑ์

สาขาวิชา วิศวกรรมเคมี ลายมือชื่อนักศึกษา _____

ปีการศึกษา 2557 ลายมือชื่ออาจารย์ที่ปรึกษา _____

KITTISAK SUWANNASANG : AN IMPROVED PROCESS FOR DERACEMIZATION OF A CONGLOMERATE FORMING SYSTEM. THESIS ADVISOR : PROF. ADRIAN EVAN FLOOD, Ph.D., 208 PP.

ENANTIOPURIFICATION / CHIRAL SYMMETRY BREAKING / PREFERENTIAL CRYSTALLIZATION / POPULATION BALANCE MODELING

Enantiopurification is very important in the production of pharmaceutical ingredients. This dissertation has developed novel routes of purification of those chiral organic compounds that can crystallize into a conglomerate system. Enantiopurification has been achieved in two effective and uncomplicated processes. The first process is deracemization via the use of programmed heating-cooling cycles combined with a fast solution phase racemization. The second process combines the first process with preferential crystallization to ensure the desired enantiomer is produced. It was found that these two processes can be used for chiral discrimination and can achieve 100% chiral purification at a yield of 100% recovery of the desired enantiomer, based on the recovery of all the crystalline material in the suspension into the preferred enantiomer.

School of Chemical Engineering Student's Signature_____

Academic Year 2014 Advisor's Signature_____

AN IMPROVED PROCESS FOR DERACEMIZATION OF A CONGLOMERATE FORMING SYSTEM

Suranaree University of Technology has approved this thesis submitted in partial fulfillment of the requirements for the Degree of Doctor of Philosophy.

Thesis Examining Committee

_____
(Dr. Terasut Sookkumnerd)
Chairperson

_____
(Prof. Dr. Adrian Evan Flood)
Member (Thesis Advisor)

_____
(Prof. Dr. Gérard Coquerel)
Member

_____
(Asst. Prof. Dr. Atichat Wongkoblap)
Member

_____
(Asst. Prof. Dr. Panarat Rattanaphanee)
Member

_____
(Asst. Prof. Dr. Sopark Sonwai)
Member

_____
(Prof. Dr. Sukit Limpijumnong)
Vice Rector for Academic Affairs and Innovation

_____
(Assoc. Prof. Flt. Lt. Dr. Kontorn Chamniprasart)
Dean of Institute of Engineering

ACKNOWLEDGEMENT

First of all, I would like to express the deepest gratitude to my beloved family for their unconditional support and encouragement which helped me to realize my own potential. Without them, I would not be where I am today.

With the achievement of this dissertation research, I would especially like to thank my thesis advisor, Professor Dr. Adrian Evan Flood, for giving me the opportunity to pursue my Ph.D. study. His motivation, suggestions and valuable ideas helped me to complete my dissertation research. His logical way of scientific thinking and his attitude have been of great value for me.

I would like to express my sincere appreciation to my foreign supervisor, Professor Dr. Gérard Coquerel, for giving me the valuable opportunity to twice visit the Sciences et Méthodes Séparatives (SMS) laboratory at the University of Rouen in France for research work. During the periods of my study abroad, Prof. Coquerel introduced me to the world of chiral resolution and his extensive research in this area. His valuable guidance was very fruitful for me.

In addition, I would like to especially express my gratitude to Dr. Céline Rougeot for kindly answering all of my scientific questions and creating a good atmosphere in the SMS laboratory. She synthesized the materials used in my study and also briefly trained me to synthesize these two substances.

Next, I am sincerely thankful to my thesis examining committee; Dr. Terasut Sookkumnerd, Asst. Prof. Dr. Atichat Wongkoblap, Asst. Prof. Dr. Panarat Rattanaphanee and Asst. Prof. Dr. Sopark Sonwai, for taking time to read my thesis and also for their effort in checking, valuable comments and suggestions during

the thesis defense.

I am very grateful to all the academic members in the School of Chemical Engineering; Prof. Dr. Chaiyot Tangsathikulchai, Asst. Prof. Dr. Chalongsri Flood, Dr. Guntima Sirijeerachai, Asst. Prof. Dr. Boris Golman, Dr. Supunnee Junpirom and Dr. Atthaphon Maneedaeng, for teaching me the skills and abilities in their own fields. These people have given me the spirit, important skills and deep knowledge of the chemical engineering profession.

During my study abroad, I had helpful technical support from Dr. Morgane Sanselme, Dr. Nicolas Couvrat, and all the Ph.D. students in the SMS laboratory. I would like to sincerely thank all of you for giving me friendship and valuable scientific insights. My thanks also extend to all of the graduate students in the Chemical Engineering School at SUT for their encouragement and academic support.

Also, I would like to thank the assistances from the technical staffs in the Center for Scientific and Technological Equipment at SUT, especially Mr. Saran Dokmaikul. My thanks also go to Mrs. Amporn Ladnongkun (at SUT) and Mrs. Ghislaine Chevalier (at SMS laboratory) for their skillful secretarial work.

Finally, I would like to acknowledge with gratitude the Royal Golden Jubilee Ph.D. Program by the Thailand Research Fund (TRF) in co-operation with Suranaree University of Technology (SUT) for their full financial support and also for giving me the great opportunity to spend eleven months at Rouen in France, in the SMS laboratory. I am also thankful to the French Embassy in Thailand for the partial financial support of six-month extension of my study at the University of Rouen in France.

Kittisak Suwannasang

TABLE OF CONTENTS

Page

TABLE OF CONTENTS (Continued)

Page

TABLE OF CONTENTS (Continued)

Page

TABLE OF CONTENTS (Continued)

Page

TABLE OF CONTENTS (Continued)

Page

TABLE OF CONTENTS (Continued)

Page

TABLE OF CONTENTS (Continued)

Page

LIST OF TABLES

Table **Page**

LIST OF TABLES (Continued)

Table **Page**

LIST OF FIGURES

Figure **Page**

LIST OF FIGURES (Continued)

Figure **Page**

LIST OF FIGURES (Continued)

Figure **Page**

LIST OF FIGURES (Continued)

Figure **Page**

LIST OF FIGURES (Continued)

Figure **Page**

LIST OF FIGURES (Continued)

Figure **Page**

LIST OF FIGURES (Continued)

Figure **Page**

LIST OF FIGURES (Continued)

Figure **Page**

LIST OF FIGURES (Continued)

Figure **Page**

LIST OF FIGURES (Continued)

Figure **Page**

LIST OF FIGURES (Continued)

Figure **Page**

SYMBOLS AND ABBREVIATIONS

AS3PC	=	Auto-seeded polythermic programmed preferential crystallization
APIs	=	Active pharmaceutical ingredients
b	=	Exponential decay constant, s^{-1}
C	=	Concentration, g solute/g solution
Cl-Tak	=	1-(4-chlorophenyl)-4,4-dimethyl-2-(1H-1,2,4-triazol-1-yl)pentan-3-one
C_s	=	Saturated concentration, g solute/g solution
CSD	=	Crystal size distributions
D-	=	*D*-crystals
DBU	=	1,8-diazabicyclo[5.4.0]undec-ene
D_R	=	Dissolution rate of *R*-crystals, μm s^{-1}
D_S	=	Dissolution rate of *S*-crystals, μm s^{-1}
DSC	=	Differential scanning calorimetry
ds/dT	=	Variation of solubility versus temperature, g solute/(g solution °C)
e.e.	=	Enantiomeric excess
E1	=	Enantiomer 1
E2	=	Enantiomer 2
FD	=	Fraction of mass dissolved

SYMBOLS AND ABBREVIATIONS (Continued)

f_G	=	The distribution of growth rate activity
$G_{j\to\infty}^{(i)}$	=	Final Growth rate of *i* crystals, μm s^{-1}
G_R	=	Growth rate of *R*-crystals, μm s^{-1}
G_S	=	Growth rate of *S*-crystals, μm s^{-1}
$\overline{G}_R$	=	Mean of the growth rate distribution of *R*-crystal, μm s^{-1}
$\overline{G}_S$	=	Mean of the growth rate distribution of *S*-crystal, μm s^{-1}
GRD	=	Crystal growth rate dispersion
h	=	Hour
HPLC	=	High-performance liquid chromatography
KCl	=	Potassium chloride
L-	=	*L*-crystals
L	=	Size of crystals, μm
$\overline{L}^{(i)}$	=	Mode of the distribution of the enantiomorph *i*, μm
$L_{minD(j)}^{(i)}$	=	Minimum size of *i* crystals after the heating period of cycle *j*, μm
$L_{minG(j)}^{(i)}$	=	Minimum size of *i* crystals after the cooling period of cycle *j*, μm
$\Delta L_{D(j)}^{(i)}$	=	Change in the size of any *i* crystal due to dissolution during the heating period *j*, μm

SYMBOLS AND ABBREVIATIONS (Continued)

$\bar{L}_{D(j)}^{(i)}$	=	Mean of the population density of the *i* crystals after the heating period of cycle *j*, μm
$\Delta L_{D(j)}^{(i)}$	=	Decrease in the size due to dissolution during the heating period, μm
$\Delta L_{G(j)}^{(i)}$	=	Increase in the size of crystals due to crystal growth during the cooling period, μm
$L_{initial}$	=	Initial size of crystals, μm
L_{min}	=	Minimum size of crystals, μm
L_{∞}	=	Maximum size of crystals, μm
MeCN	=	Acetonitrile
Me-Tak	=	4,4-dimethyl-1-(p-toluyl)-2-(1H-1,2,4-triazol-1-yl)pentan-3-one
Min	=	Minute
m_R	=	Mass of the *R*-enantiomer, g
m_S	=	Mass of the *S*-enantiomer, g
MSZW	=	Metastable zone width
$n^{(i)}$	=	Number density distribution of the *i* crystals
$NaClO_3$	=	Sodium chlorate
NaOH	=	Sodium hydroxide
PC	=	Preferential crystallization

SYMBOLS AND ABBREVIATIONS (Continued)

PCR	=	Preferential crystallization in cooperation with a solution phase racemization
PCRT	=	A combination of temperature cycles and preferential crystallization in-situ solution phase racemization
R-	=	*R*-enantiomer
RM1	=	Raw material prepared by solvent evaporation
RM2	=	Raw material prepared by fast cooling
S-	=	*S*-enantiomer
SEM	=	Scanning electron microscope
SOAT	=	Second-order asymmetric transformation
T	=	Temperature, $^{\circ}$C
T_{cryst}	=	Crystallization temperature, $^{\circ}$C
TP	=	Temperature program
XRPD	=	X ray powder diffraction

Greek Symbols

$\mu_3^{(i)}$	=	Third moment of the *i* crystals, μm^3
$\mu_{3,(j)}^{T}$	=	Total third moment of the crystals, μm^3
$\sigma^{(i)}$	=	Standard deviation of the crystal size distribution of the *i* crystals, μm

SYMBOLS AND ABBREVIATIONS (Continued)

$\left(\sigma^{(i)}\right)^2$	=	Variance of the crystal size distribution of the the *i* crystals, μm^2
$\tau_G^{(i)}$	=	Mean life time of the growth rate of *i* crystals, s
Δ	=	Differential

Subscripts

0	=	Initial condition
cryst	=	Crystallization
D	=	Dissolution period
G	=	Growth period
initial	=	Initial condition
j	=	Number of temperature cycle
R	=	*R*-enantiomer
S	=	*S*-enantiomer

Superscripts

i	=	Component *i*
T	=	Total

CHAPTER I

GENERAL INTRODUCTION

1.1 Background and Significance of the Study

Enantiomers are pairs of stereoisomers which are non-superimposable mirror images of each other. Only one of the two enantiomers will typically be present in the biospheres (Nagata et al., 1998); for instance amino acids appear in the *L*-form (for instance *L*-serine) and sugars typically appear in the *D*-form (for instance *D*-glucose). Such molecules are very significant in biological system because many active biological molecules are one of a pair of enantiomers (Ávalos et al., 2010). Enantiopurification has been of interest since Everhardus Jacobus Ariëns' paper in 1984 (Ariëns, 1984); before this work most chiral drugs were a racemic mixture. Ariëns declared that even though only one of the enantiomers is therapeutically active, it does not mean that the other enantiomer is really inactive. Ariëns compared the effect of the non-active enantiomer and other impurities on the therapeutic action and concluded that the non-active enantiomer should be consider as an impurity (at a level of 50% or more). This is unfortunate, since in biological systems the two enantiomers will have very different properties due to the presence of other chiral materials in the body. In many cases one of the two enantiomers may have very good therapeutic or pharmaceutical effect, whereas the second enantiomer may be inert, or even toxic in many cases (McConathy and Owens, 2003). This makes it necessary to produce active phamaceutical ingredients (APIs) in enantiomerically pure form – the

active enantiomer must be separated essentially completely from the other form, although this had been neglected for a long time.

After the discovery of the need to produce enantiomerically pure APIs, reseach and development of enantioseparation and marketing of pure enantiomers has grown. The use of racemic mixtures of APIs has been substantially decreased. Finally, in 2001, racemic mixtures were not sold in the API market, as depicted in Figure 1.1 (Caner et al., 2004).

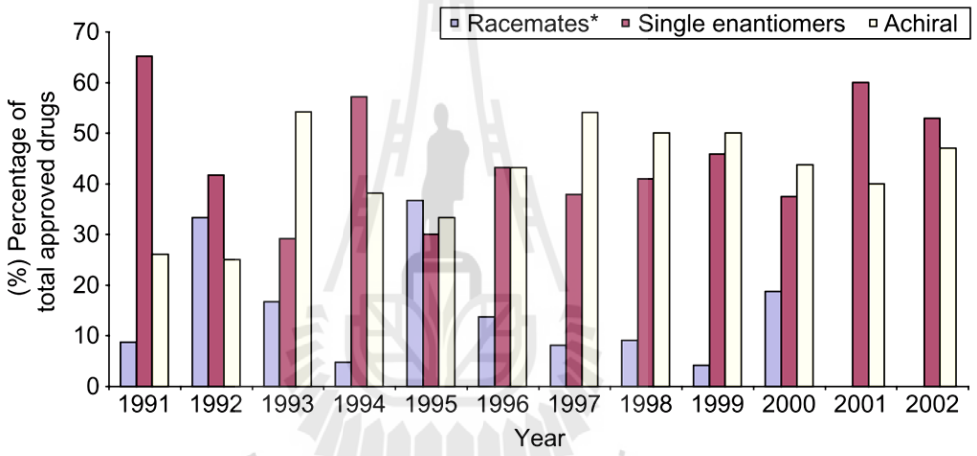

Figure 1.1 Annual distribution of FDA-approved drugs (NMEs) according to chirality in the period 1991-2002. *Including diastermeric mixtures (Caner et al., 2004).

After the need for using pure enantiomers in medication forced authorities to tighten regulations on drugs, there has been much research into producing single enantiomers. Despite an increasing number of asymmetric synthesis or stereoselective synthesis for APIs with a single chirality (Collins et al., 1992), there are still a lot of reactions that produce a racemic mixture of the two enantiomers. In between 1985 and 2004, about 46% of APIs were obtained from a resolution of a racemic mixture

produced from a synthesis in comparison to a synthesis using molecules from the chiral pool (45%) and a synthesis based upon an asymmetric procedure (9%) (Murakami, 2007).

1.2 Enantiomers

Unfortunately, the two enantiomers have the same physical and chemical properties (apart from having opposite values of optical rotation) in non-chiral solvents, and they are particularly difficult to separate via traditional separations used in the chemical process industries.

A convenient value used to determine the purity of a chiral substance is the enantiomeric excess (*e.e.*) (Morrison and Mosher, 1971), expressed as following;

$$e.e. = \left[\frac{m_R - m_S}{m_R + m_S}\right] \times 100\% \quad (1.1)$$

where m_i represents the mass of component *i*. The *e.e.* is zero if there is an equal amount of the two enantiomers, but if there is a pure enantiomer the *e.e.* is 100%. The *e.e.* can be a positive or negative value depending on which is normally assigned to being the preferred enantiomer. In the above definition the pure *R*-form is considered as +100% *e.e.*

There are many possible outcomes in condensed phases if a racemic mixture of two enantiomers is crystallized (Coquerel, 2000). Even if partial solid solutions and solid-solid transitions are neglected there remain three possible outcomes which are most frequently observed. The binary phase diagram for those outcomes,

conglomerate forming compound, racemic compound, and total solid solution forming systems are presented schematically in Figure 1.2.

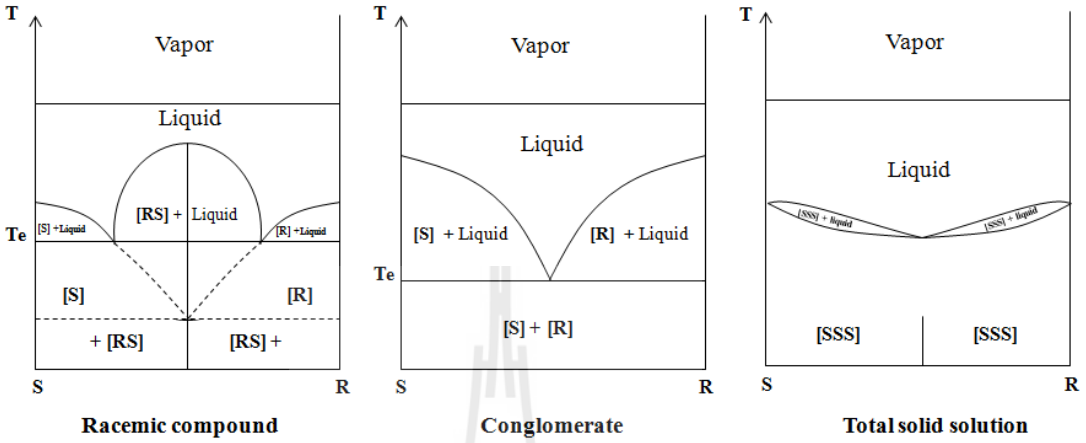

Figure 1.2 Illustration of typical binary phase diagrams of enantiomer pair in absence of partial solid solution and solid-solid transition.

1.2.1 A Racemic Compound Forming System

The first possibility is that a racemic mixture crystallizes into a racemic compound forming system, where there is one crystal phase consisting of an equimolar mixture of the two enantiomers. More than 90% of known racemic mixtures (composed of 1:1 mixture of the two enantiomers in any physical state) of chiral organic molecules crystallize as racemic compounds (Eliel et al., 1994). Typically a molecule has a greater affinity for the opposite type than its own kind, leading to a crystal with equal amounts of the two enantiomers in one structured crystalline phase (i.e. a *DL*-crystal form). This type of compound exhibits two symmetrical eutectic points and its melting temperature can be either lower or higher than the melting temperature of the pure enantiomer crystal.

1.2.2 A Racemic Conglomerate Forming System

The second possibility is that the racemic mixture is a conglomerate forming system. This is where the two pure enantiomers crystallize independently because the molecules have a greater affinity for the same enantiomer than for the opposite enantiomer. The conglomerate forming system exists in only 5-10% of known racemic mixtures. A conglomerate forming system involves chiral discrimination in the crystalline phase: an equimolar amount of the two enantiomeric molecules are arranged in pure separated crystalline phases (i.e. a conglomerate containing both pure *D*- and pure *L*-crystals). The phase diagram for this system consists of a simple eutectic in which the minimum melting point always occurs at the 50:50 enantiomeric composition even if there is partial solid solution (Coquerel, 2000).

1.2.3 A Total Solid Solution Forming System

The third possibility is that a total solid solution forms from the racemic mixture. Less than 1% of known racemic mixtures crystallize as a total solid solution. Each crystal is composed of a random mixture of the two enantiomers because there is no significant difference in the affinity between the same and opposite enantiomers. Chiral discrimination in the solid state of this type of material is almost impossible. However, there are few cases of purifications of this kind of enantiomers proposed in the literature (Tamura et al., 2002).

1.3 How to Have Access to Pure Enantiomer of a Racemic Conglomerate Forming System

There are several routes to obtain a desired pure enantiomer depending on the physical and chemical properties of the species involved:

1.3.1 Pure Enantiomer Derived From a Stereoselective Synthesis

If a starting chiral material (an enantiopure molecule) can be derived from the chiral pool, the desired enantiopure product can be produced based upon classical organic synthesis (Collins et al., 1992). This method is not expensive and also readily available (for instance the amino acids). When a starting chiral material cannot be prepared from the chiral pool, the chiral center has to be generated during a special organic synthesis: a synthesis using a chiral reagent (Corey et al., 1988), a synthesis using a chiral auxiliary (Ensley et al., 1978), or a synthesis using a chiral catalyst (Takaya et al., 1986).

1.3.2 Pure Enantiomer Derived From a Racemic Mixture

When a desired product cannot be produced based upon synthesis using a pure chiral molecule because of an economic aspect or a process difficulty the synthesis will produce a racemic mixture (an equal amount of the two enantiomers). Consequently, an additional process will be performed to separate the target enantiomer from the unwanted enantiomer. The resolution of racemic mixtures can be classified into several different categories such as biocatalytic processes (Leijondahl et al., 2009), chiral chromatography (Ikai and Okamoto, 2009), chiral membrane separation (Maximini et al., 2006) and chiral resolution via crystallization which is presented in the next section.

1.4 Resolution by Crystallization

Having access to a target enantiopure molecule is important, however the economic aspects have to be considered for the industrial scale operation, including the operating cost of the method and the operating time. Although there are a variety of routes for enantioseparation, crystallization is the favored method for separating and purifying enantiomers in the pharmaceutical and chemical industries since its operating cost is relatively low compared with the other separation methods (e.g. chromatography and membrane processes).

Resolution by crystallization may be classified into two categories according to the formation of condensed phase of the racemic mixture. Pasteurian resolution is typically used for enantiopurification of a racemic compound forming system. However if the enantiomers crystallize as a racemic conglomerate, separation by preferential crystallization is typically preferred.

1.4.1 Pasteurian Resolution

In 1853, Louis Pasteur discovered a method of breaking the symmetry of two enantiomorphs by transforming the pair of enantiomers into a diastereomeric pair by reacting them with another pure chiral agent in an achiral solvent (Pasteur, 1853). These two diastereomers have differences in chemical and physical properties (e.g. in solubility) and the two molecules are no longer mirror images (Jacques et al., 1981). This creates a potential route to obtain a pure diastereomer by a classical crystallization. However an additional step is required for the recovery of the pure target enantiomer from the chiral agent.

1.4.2 Preferential Crystallization

A basic principle of preferential crystallization was shown in 1866 by Desire Gernez, Pasteur's student. During a resolution of sodium ammonium tartrate tetrahydrate, he observed that there was no occurrence of a new crystal if a saturated solution of a pure enantiomer was seeded by the opposite enantiomorphs. Another experiment showed that crystal growth of the same enantiomer occurred at the expense of the alternate enantiomer in the solution if a saturated solution of a racemic mixture was seeded by a few crystals of a pure enantiomer (Gernez, 1866). Years later in 1882, the predominant influence of supersaturation was described by Jungfleish (Jungfleish, 1882).

Preferential crystallization (PC) is a favored method of enantioseparation if racemic mixtures crystallize as a conglomerates. Typically, PC is operated as a cyclic process, alternating the crystallization of the two enantiomers. According to the schematic diagram of the PC process presented in Figure 1.3, starting at point A (monophasic domain) a solution contains a small amount of a selected enantiomer (i.e. an E1 enantiomer) in excess at high temperature ($T_{cryst}+\Delta T$). The solution is cooled down to a crystallization temperature (T_{cryst}). Then E1 crystals (typically 10 %wt of the mass of crystallized solute) are seeded into the solution. Only the E1 enantiomer ideally crystallizes and grows. When the solution reaches point B, the mother liquor is enriched with the E2 enantiomer. The solid is therefore quickly separated from the mother liquor by filtration or centrifugation to avoid primary nucleation of the E2. The mother liquor is then reheated up to the high temperature and after that a racemic mixture, with same amount of the harvested solid, is added into the mother liquor. Hence, the solution is slightly enriched with the E2 enantiomer

at point C. For this reason, the E2 enantiomer is selectively crystallized. The solution is cooled down to the T_{cryst} again and then seeded with the E2 crystals, leading to a stereoselective crystallization of the E2 enantiomer. When the solution reaches point D, the solid in the suspension is separated swiftly from the mother liquor to avoid the nucleation of the E1. After that the mother liquor is heated up and then added by a racemic mixture. Those bring the mother liquor back to the initial composition at point A again (with the slight enrichment of the E1 enantiomer). The following batches will be composed of the repeating steps as described above.

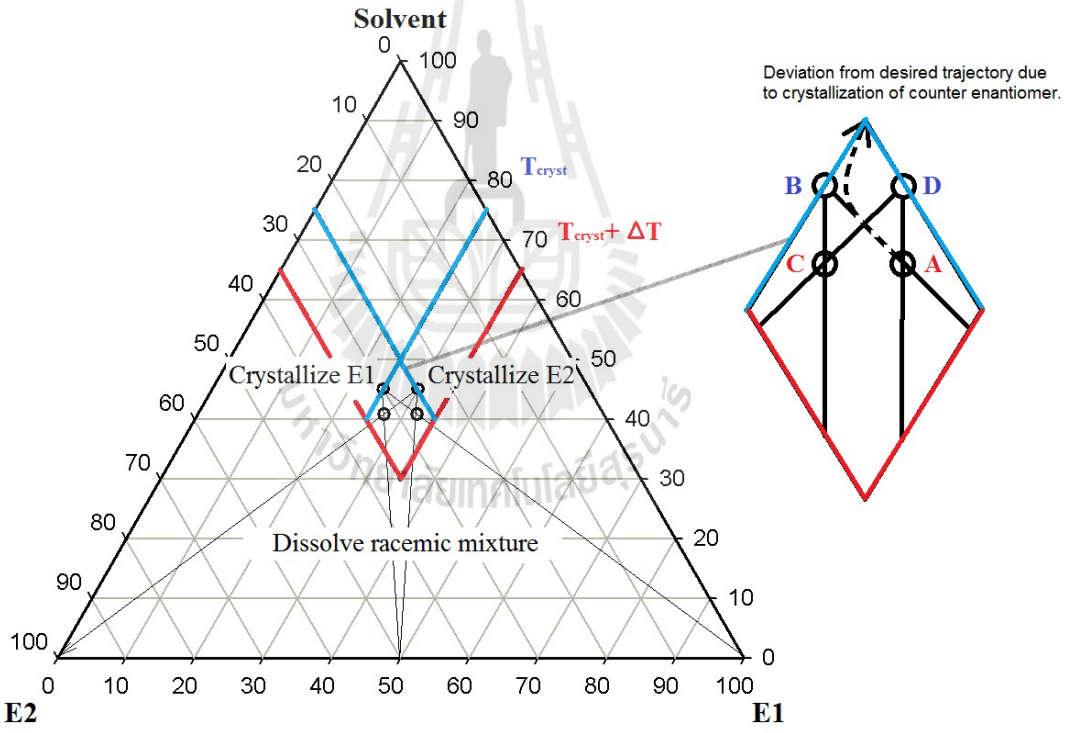

Figure 1.3 Basic description of preferential crystallization operated as a cyclic process.

Several methods of enantioseparation were developed based on PC, such as the auto-seeded polythermic programmed preferential crystallization (AS3PC)

and the second-order asymmetric transformation (SOAT). AS3PC, developed by the group of Coquerel, can be used effectively to separate a target enantiomer from a racemic mixture (Coquerel et al., 1995). Unfortunately, there is no configuration change between the two enantiomers, leading to the production yield being limited to 50%.

The SOAT is a combined technique of PC with simultaneous in-situ racemization in solution (Arai et al., 1983). Under operating by the combined method, a counter enantiomer can be converted to a desired enantiomer by the racemization reaction. Thanks to a slow cooling rate and the racemization, the entrainment effect has not been limited by the primary nucleation of the counter enantiomer during the crystallization. As a result, the SOAT process can achieve 100% yield of the desired enantiomer, which is derived from the racemic mixture in the initial solution (Nasipuri, 1994).

1.5 Spontaneous Symmetry Breaking

In 1898, Kipping and Pope investigated the crystallization of sodium chlorate by evaporating a saturated aqueous solution without stirring. The result was shown that there were 50.08 %wt of *D*-crystals, which were obtained from the 46 different experiments (3,137 crystals). They emphasized that the average amount of *D*-crystals obtained from a large number of crystallizations of sodium chlorate should consist of 50% of crystals of each handedness since there is an equal tendency to deposit *D*- and *L*- crystals (Kipping and Pope, 1898).

Almost a century later, in 1990, Kondepudi and his co-workers investigated the chiral symmetry breaking (Kondepudi et al., 1990) or “total spontaneous

resolution" of sodium chlorate ($NaClO_3$) — an achiral compound, but which forms optically active crystals (a racemic conglomerate forming system). The outcomes from their experiments showed that the sodium chlorate crystallized from an aqueous solution while the solution is not stirred were a statistically equal number of *D*- and *L*-$NaClO_3$ crystals, which agreed with the discovery of Kipping and Pope. When the solution was stirred, however, 99.7% of $NaClO_3$ crystals had the same chirality (either *D*-crystal or *L*-crystal) as shown in Figure 1.4b.

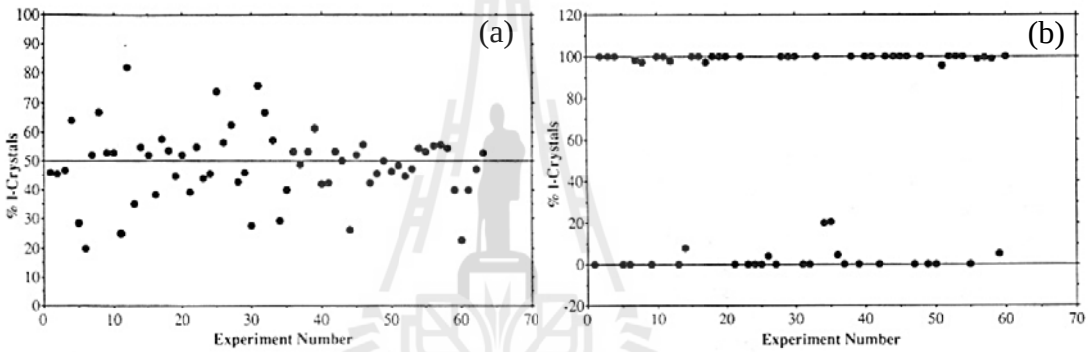

Figure 1.4 (a) Scatter gram showing percent *L*-crystals in a sample of 63 unstirred crystallizations of sodium chlorate. (b) Scatter gram showing percent *L*-crystals in a sample of 60 stirred crystallizations of sodium chlorate (Kondepudi et al., 1993).

Their explanation for the mechanisms involved in the total symmetry breaking, which was similar to the suggestion by Frank in 1953, is that there is a competition between the *D*- and the *L*- crystals due to an autocatalytic process (a nonlinear amplification process) in which an enantiomorph is able to catalyze its own creation and at the same time suppress the other enantiomorph (Frank, 1953; Kondepudi et al., 1990). A few years later, new experimental results from

Kondepudi's and Martine's groups have highlighted the importance of the stirring effect on a chiral symmetry breaking (Kondepudi et al., 1993; Kondepudi et al., 1995; Martin et al., 1996).

1.5.1 Theory of the Mother Crystal

In 1993, the theory of the mother crystal was proposed by the group of Kondepudi. Attempting to explain the phenomenon driving the racemic suspension to a single handedness in the case of stirred crystallization, they proposed a hypothesis of chiral symmetry breaking based upon the theory of nucleation. They explained that a first single parent crystal (called the "mother crystal") was swiftly produced from a supersaturated solution via a primary nucleation. Then the chiral symmetry breaking was initiated from the breakage of the mother crystal by stirring, producing a lot of secondary nuclei having the same handedness as the mother crystal. This secondary nucleation causes the chiral autocatalysis resulting in total symmetry breaking (Kondepudi et al., 1993).

A decade later, the idea of mother crystal became a question again when Viedma demonstrated new experimental results. These results clearly contradicted the emergence of homochirality as described based upon on the theory of the mother crystal. Viedma himself preformed crystallization experiments with sodium chlorate that were initiated at a very high supersaturation level (i.e. C/C_s is more than 1.5, and 60°C of supercooling). From a theoretical point of view a lot of primary nuclei must have been generated instantaneously. He observed that the crystals obtained from this procedure have the same handedness in every solution. Viedma concluded that the single mother crystal theory is not adequate to explain the chiral symmetry breaking in this example. His experimental results indicate that the total symmetry breaking

phenomenon can occur even if there is a significant amount of primary nuclei appearing simultaneously. Viedma also stated that "*the idea of the mother crystal is not appropriate to account for the symmetry breaking process, the mechanism to explain the chiral symmetry breaking in crystallization remains as an open question*" However, the first single mother crystal idea could be used to explain the mechanism of symmetry breaking in the case of a low supersaturation level; a relative supersaturation ranging from 1.001 (0.2 nuclei/min) to 1.04 (2 nuclei/min) (Viedma, 2004).

1.5.2 Viedma Ripening

In 2005, a new process of symmetry breaking named "Viedma ripening" (i.e. an attrition enhanced-deracemization) was proposed by Cristobal Viedma (Viedma, 2005). Typically, the term ripening (for instance Ostwald ripening, where bigger crystals grow by consuming the supersaturated solution produced from the dissolution of smaller crystals in an isothermal stagnant solution) refers to a process which is caused by the solubility dependence on the crystal size in a situation where primary nucleation does not occur due to the system is at low supersaturation.

Viedma preformed an experimental demonstration at a constant temperature to clarify the effect of stirring on total symmetry breaking of sodium chlorate crystals, an achiral molecule. Small glass beads were introduced into a suspension of a racemic mixture of sodium chlorate crystals in order to enhance the abrasive effect. He discovered a complete deracemization by this new process. Complete homochirality can be obtained even if there is an equal mass of the two enantiomeric crystals present initially. The time required to reach a pure enantiomeric crystal suspension depends strongly on the stirring rate and the number of glass balls.

He also noticed that the chiral outcome is random. However, if there is a small imbalance at the initial time, the crystal product is predominantly the enantiomorphs which was in excess at the initial time (Viedma, 2005).

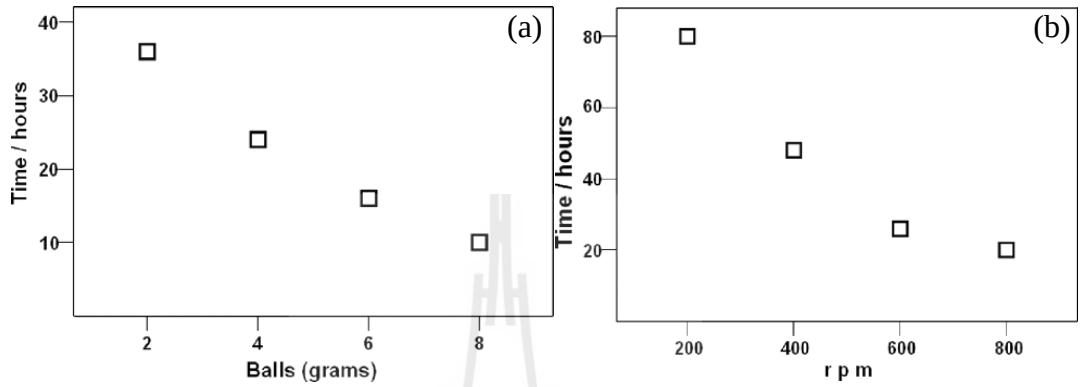

Figure 1.5 Solutions with initial symmetric mixture of *L*- and *D*- crystals of $NaClO_3$ and glass beads show total symmetry breaking and chiral purity. The data shows the time required to achieve chiral purity depending on: (a) the number of balls in the system (600 rpm) and (b) the speed of agitation of the system (4 g of balls) (Viedma, 2005).

In Viedma ripening the two populations of the enantiomorph crystals are continuously ground leading to production of a large amount of fragments. Some small crystals are likely to dissolve according to the Gibbs-Thomson effect; a small crystal has a higher solubility than a larger one. To minimize its surface energy, the small crystals is more likely to dissolve than the larger ones, leading the crystal growth of the big crystals at the expense of small crystals. Dissolution and crystallization in the isothermal system result from the mechanical effect of the abrasive grinding. Viedma suggested that the mechanisms of the attrition-enhanced

deracemization are a combination of the non-linear autocatalytic dynamics of secondary nucleation and the recycling of material from crystals dissolving due to Ostwald ripening to larger crystals that are growing (Viedma, 2005).

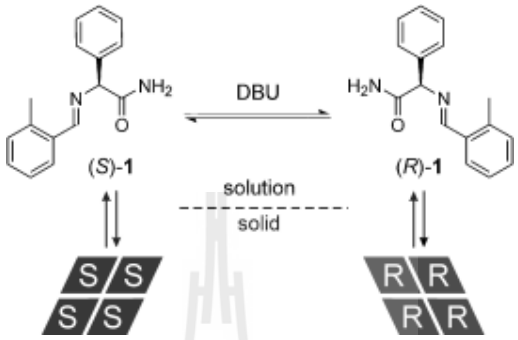

Figure 1.6 Equilibria involved in the attrition-enhanced crystallization/dissolution in the presence of DBU (1,8-diazabicyclo[5.4.0]undec-ene) as a racemizing agent for **1** (Noorduin et al., 2008b).

Inspired by Viedma, the group of Vlieg and Blackmond deracemized an intrinsically chiral organic molecule in 2008. They proved the principle of Viedma ripening could be extended to chiral molecules by deracemizing a chiral amino acid derivative, *N*-(2-methylbenzylidene)-phenylglycine amide (**1**), under racemization in solution (i.e. an equilibrium reaction by which the enantiomers interconvert, with the reaction having an equilibrium constant equal to 1). The chemical and physical equilibria involved deracemization is depicted in Figure 1.6 (Noorduin et al., 2008a).

The abrasive grinding ensured by small glass balls was used to deracemize a racemic mixture of the two enantiomeric crystals undergo racemization in solution which was faster than the crystallization step. This protocol has also been successfully used to achieve a single homochiral product as shown in Figure 1.7.

Meanwhile, the mechanisms behind attrition enhanced-deracemization are still uncertain. There is still debate regarding to the mechanisms involved in the deracemization, however, scientists generally agree that deracemization is a nonlinear autocatalytic process resulting in an exponential behavior in the kinetics.

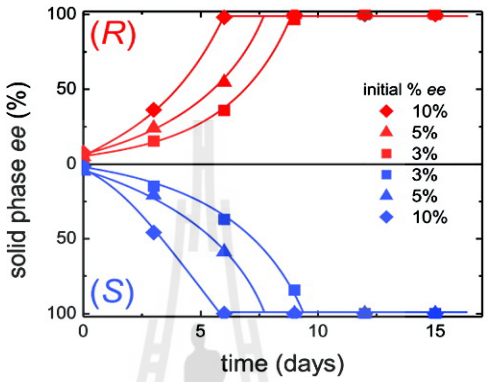

Figure 1.7 Attrition-enhanced evolution of solid-phase *e.e.* for **1** in MeCN in the presence of solution-phase racemization initiated by adding DBU, starting from initial *e.e.* values of **1**. Lines are a guide to the eye (Noorduin et al., 2008a).

1.5.3 Temperature Gradient Enhanced-Deracemization

In 2008, after the group of Vlieg had demonstrated the deracemization of an intrinsically chiral organic compound, the effect of temperature gradients on the deracemization of a proteinogenic amino acid was investigated (Viedma et al., 2008). As shown in Figure 1.8, the evolution of the enantiomeric excess in the solid phase was accelerated when the suspension was heated on a stirred hotplate. The temperature gradient has a strong effect on the length of the induction period in the abrasive grinding system as shown in Figure 1.8a. Since the kinetics depend on temperature, the fast amplification of the *e.e.* in the solid phase to single chirality

appearing in the temperature gradient system (with a maximum temperature near 160°C) is not appropriate to compare with the evolution of the enantiomeric excess in the solid phase occurring in the controlled isothermal system (at 90°C). On the other hand, their emphasis on the amplification of the enantiomeric excess is that "*Once the system has "taken off" under enhanced attrition conditions, the rate of evolution of the solid phase e.e. is not strongly sensitive to temperature*" (Viedma et al., 2008).

Deracemization of aspartic acid was also carried out in the absence of glass beads. The result indicated that under non-abrasive grinding the conversion to complete single handedness is possible in both the temperature gradient system and in the isothermal system as shown in Figure 1.8b.

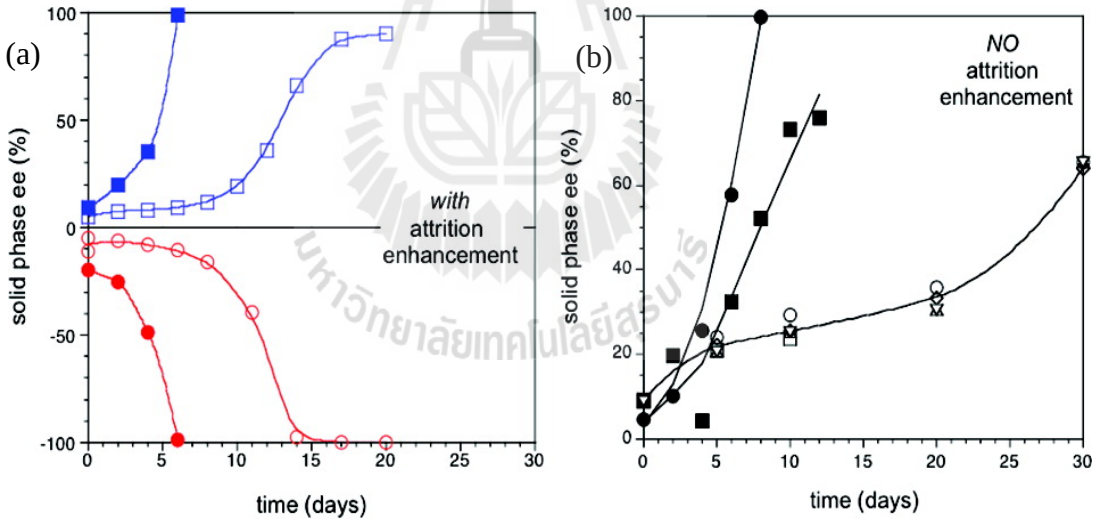

Figure 1.8 Evolution of solid-phase *e.e.* for *D*- and *L*- aspartic acid under racemizing conditions. (a) Attrition-enhanced conditions. Filled symbols: gradient heating to 160°C. Open symbols: isothermal at 90°C. Positive *e.e.* values are assigned to the naturally occurring *L*-aspartic acid. (b) Stirring in the absence of glass beads. Filled circles: gradient heating to 160°C. Filled

squares: under reflux at 125°C. Open symbols: isothermal heating to 105°C (Viedma et al., 2008).

Three years later, Viedma and Cintas proposed a novel technique of deracemization (Viedma and Cintas, 2011). They boiled a suspension of sodium chlorate crystals. The pure enantiomer crystals were obtained only from the non-stirred system. The outcome for the crystals in the stirring system was a mixture of the two enantiomorphous crystals since there is not a significant temperature gradient occurring in the stirred system. The appearance of complete deracemization in the boiling system is unlike grinding. The major mechanism involved deracemization is dissolution-growth cycling supplied by the gradient of temperature between the hot zone (at the bottom of the flask in contact with the hotplate) and the cool zone (at the surface of the heterogeneous system) as shown in Figure 1.9.

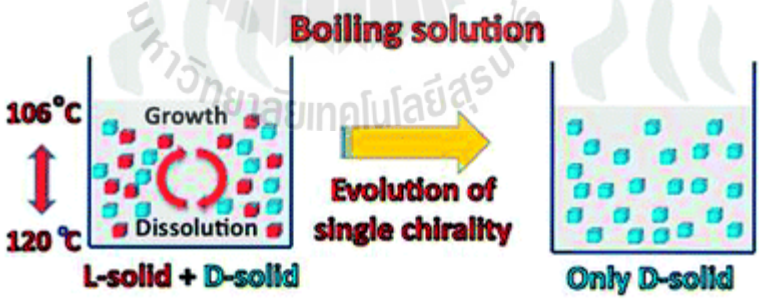

Figure 1.9 Deracemization of $NaClO_3$ under boiling. Cycles of dissolution and crystal growth result in a solid phase of one enantiomorph (Viedma and Cintas, 2011).

1.6 Objectives of the Research

1. To demonstrate a new protocol which is easy to implement for obtaining a pure enantiomer from a racemic suspension through a deracemization process using programmed-temperature cycles in a system where there is racemization of the solute in solution.

2. To present possible mechanisms of complete chiral symmetry breaking occurring in a temperature variation induced-deracemization system, independent of grinding.

3. To improve the temperature variation induced-deracemization process using a series of damped-temperature profiles in the presence of swift racemization in solution.

4. To develop a process to obtain a pure enantiomer using a combination of preferential crystallization with in-situ racemization, combined with periodic temperature fluctuations.

1.7 Scope and Limitation of the Research

This research attempts to propose a new easy to implement process by which it is possible to obtain a pure enantiomer. This novel process also aims to avoid the limitation in the production yield of ordinary enantioseparation processes (i.e. the maximum yield of preferential crystallization is limited at only 50%). The possible mechanisms responsible for the total symmetry breaking occurring in the new deracemization process will be explained. The research is composed of 6 parts as following:

Chapter 1: General introduction of the research.

Chapter 2: Using programmed heating-cooling cycles with racemization in solution for complete symmetry breaking of a conglomerate forming system.

Chapter 3: Mathematical modeling of chiral symmetry breaking towards complete deracemization due to differences in crystal growth kinetics.

Chapter 4: Benefit of temperature fluctuations in a damped pattern on deracemization of a conglomerate suspension.

Chapter 5: Combination of preferential crystallization, solution phase racemization and temperature cycles for rapid symmetry breaking of a conglomerate forming system.

Chapter 6: General conclusion of the research, and recommendations.

1.8 Output of the Research

1. A new process for deracemization, temperature fluctuation induced-deracemization, has been proposed. This process can be used to obtain a pure enantiomer in a suspension starting from a racemic mixture of a conglomerate forming system. Since the implementation of this novel process is simple, the scale up is easily possible.

2. Mathematical modeling of possible mechanisms occurring in the temperature fluctuation induced-deracemization has been proposed.

3. The route of improvement of the new deracemization has been proposed by monitoring and adjusting the temperature program while operating the process.

4. A combined technique of preferential crystallization with in-situ racemization combined with periodic temperature fluctuations has been proposed as

an effective enantiopurification process. 100% yield based on the material in the initial crystalline phase of the suspension can be obtained.

1.9 References

Arai, K., Ohara, Y., Takakuwa, Y., and Iizumi, T. (1983). Process for preparing an optical active ester of naphthylpropionic acid. **Patent US4417070 A.**

Ariëns, E. J. (1984). Stereochemistry, a basis for sophisticated nonsense in pharmacokinetics and clinical pharmacology. **European Journal of Clinical Pharmacology.** 26: 663-668.

Ávalos, M., Babiano, R., Cintas, P., Jiménez, J. L., and Palacios, J. C. (2010). Homochirality and chemical evolution: new vistas and reflections on recent models. **Tetrahedron: Asymmetry.** 21: 1030-1040.

Caner, H., Groner, E., Levy, L., and Agranat, I. (2004). Trends in the development of chiral drugs. **Drug Discovery Today.** 9: 105-110.

Collins, A. N., Sheldrake, G. N., and Crosby, J. (1992). **Chirality in industry: the commercial manufacture and applications of optically active compounds.** Wiley: Chichester.

Coquerel, G. (2000). Review on the heterogeneous equilibria between condensed phases in binary systems of enantiomers. **Enantiomer.** 5: 481-498.

Coquerel, G., Petit, M.-N., and Bouaziz, R. (1995). Procédé de dédoublement (AS3PC) de deux antipodes optiques par entraînement polythermique programmé et auto-ensemencé. **Patent WO1995/008522.**

Corey, E. J., Shibata, S., and Bakshi, R. K. (1988). An efficient and catalytically enantioselective route to (S)-(-)-phenyloxirane. **The Journal of Organic Chemistry.** 53: 2861-2863.

Eliel, E., Wilen, S. H., and Mander, L. N. (1994). **Stereochemistry of Organic Compounds.** Wiley: New York.

Ensley, H. E., Parnell, C. A., and Corey, E. J. (1978). Convenient synthesis of a highly efficient and recyclable chiral director for asymmetric induction. **The Journal of Organic Chemistry.** 43: 1610-1612.

Frank, F. C. (1953). On spontaneous asymmetric synthesis. **Biochimica et Biophysica Acta.** 11: 459-463.

Gernez, D. (1866). Séparation des tartrates droits et des tartrates gauches à l'aide de solutions saturées. **Compte-rendus de l'Académie des Sciences 63.** 843-888.

Ikai, T., and Okamoto, Y. (2009). Structure Control of Polysaccharide Derivatives for Efficient Separation of Enantiomers by Chromatography. **Chemical Reviews.** 109: 6077-6101.

Jacques, J., Collet, A., and Wilen, S. H. (1981). **Enantiomers, Racemates, and Resolutions.** John Wiley & Sons, New York.

Jungfleish, M. E. (1882). **Journal of Pharmaceutical Chemistry.** 5: 346-357.

Kipping, F. S., and Pope, W. J. (1898). **LXIII.-Enantiomorphism. Journal of the Chemical Society.** Transactions 73: 606-617.

Kondepudi, D. K., Bullock, K. L., Digits, J. A., Hall, J. K., and Miller, J. M. (1993). Kinetics of chiral symmetry breaking in crystallization. **Journal of the American Chemical Society.** 115: 10211-10216.

Kondepudi, D. K., Bullock, K. L., Digits, J. A., and Yarborough, P. D. (1995). Stirring Rate as a Critical Parameter in Chiral Symmetry Breaking Crystallization. **Journal of the American Chemical Society.** 117: 401-404.

Kondepudi, D. K., Kaufman, R. J., and Singh, N. (1990). Chiral Symmetry Breaking in Sodium Chlorate Crystallizaton. **Science.** 250: 975-976.

Leijondahl, K., Borén, L., Braun, R., and Bäckvall, J.-E. (2009). Enzyme- and Ruthenium-Catalyzed Dynamic Kinetic Asymmetric Transformation of 1,5-Diols. Application to the Synthesis of (+)-Solenopsin A. **The Journal of Organic Chemistry.** 74: 1988-1993.

Martin, B., Tharrington, A., and Wu, X. l. (1996). Chiral Symmetry Breaking in Crystal Growth: Is Hydrodynamic Convection Relevant? **Physical Review Letters.** 77: 2826-2829.

Maximini, A., Chmiel, H., Holdik, H., and Maier, N. W. (2006). Development of a supported liquid membrane process for separating enantiomers of N-protected amino acid derivatives. **Journal of Membrane Science.** 276: 221-231.

McConathy, J., and Owens, M. J. (2003). Stereochemistry in Drug Action. **Primary Care Companion to The Journal of Clinical Psychiatry.** 5: 70-73.

Morrison, J. D., and Mosher, H. S. (1971). **Asymmetric organic reactions.** Prentice-Hall: Englewood Cliffs, N.J.

Murakami, H. (2007). From Racemates to Single Enantiomers - Chiral Synthetic Drugs over the last 20 Years. **Topics in current chemistry.** 269: 273-299.

Nagata, Y., Fujiwara, T., Kawaguchi-Nagata, K., Yoshihiro, F., and Yamanaka, T. (1998). Occurrence of peptidyl d-amino acids in soluble fractions of several

eubacteria, archaea and eukaryotes. **Biochimica et Biophysica Acta (BBA) - General Subjects.** 1379: 76-82.

Nasipuri, D. (1994). **Stereochemistry of Organic Compounds: Principles and Applications.** Second edition/Ed. New Age International (P) Ltd., New Delhi.

Noorduin, W. L., Izumi, T., Millemaggi, A., Leeman, M., Meekes, H., Van Enckevort, W. J. P., Kellogg, R. M., Kaptein, B., Vlieg, E., and Blackmond, D. G. (2008a). Emergence of a Single Solid Chiral State from a Nearly Racemic Amino Acid Derivative. **Journal of the American Chemical Society.** 130: 1158-1159.

Noorduin, W. L., Meekes, H., van Enckevort, W. J. P., Millemaggi, A., Leeman, M., Kaptein, B., Kellogg, R. M., and Vlieg, E. (2008b). Complete Deracemization by Attrition-Enhanced Ostwald Ripening Elucidated. **Angewandte Chemie International Edition.** 47: 6445-6447.

Pasteur, L. (1853). Transformation des acides tartriques en acide racémique - Découverte de l'acide tartrique inactif. Nouvelle méthode de séparation de l'acide racémique en acides tartriques droit et gauche. **Compte-rendus de l'Académie des Sciences.** 37: 162-166.

Takaya, H., Mashima, K., Koyano, K., Yagi, M., Kumobayashi, H., Taketomi, T., Akutagawa, S., and Noyori, R. (1986). Practical synthesis of (R)- or (S)-2,2'-bis(diarylphosphino)-1,1'-binaphthyls (BINAPs). **The Journal of Organic Chemistry.** 51: 629-635.

Tamura, R., Fujimoto, D., Lepp, Z., Misaki, K., Miura, H., Takahashi, H., Ushio, T., Nakai, T., and Hirotsu, K. (2002). Mechanism of Preferential Enrichment, an Unusual Enantiomeric Resolution Phenomenon Caused by Polymorphic

Transition during Crystallization of Mixed Crystals Composed of Two Enantiomers. **Journal of the American Chemical Society.** 124: 13139-13153.

Viedma, C. (2004). Experimental evidence of chiral symmetry breaking in crystallization from primary nucleation. **Journal of Crystal Growth.** 261: 118-121.

Viedma, C. (2005). Chiral Symmetry Breaking During Crystallization: Complete Chiral Purity Induced by Nonlinear Autocatalysis and Recycling. **Physical Review Letters.** 94: 065504.

Viedma, C., and Cintas, P. (2011). Homochirality beyond grinding: deracemizing chiral crystals by temperature gradient under boiling. **Chemical Communications.** 47: 12786-12788.

Viedma, C., Ortiz, J. E., Torres, T. d., Izumi, T., and Blackmond, D. G. (2008). Evolution of Solid Phase Homochirality for a Proteinogenic Amino Acid. **Journal of the American Chemical Society.** 130: 15274-15275.

CHAPTER II

USING PROGRAMMED HEATING-COOLING CYCLES WITH RACEMIZATION IN SOLUTION FOR COMPLETE SYMMETRY BREAKING OF A COMGLOMERATE FORMING SYSTEM

2.1 Abstract

A deracemization technique using periodic temperature fluctuations on a conglomerate forming system undergoing a swift racemization in solution is demonstrated. The method uses heating and cooling periods of the suspension in order to create cycles of partial dissolution of the crystal phase followed by crystal regrowth: this enables symmetry breaking in the solid phase. The technique is an effective, simple, and cheap operation, and can promote understanding of the effects of dissolution and recrystallization on chiral symmetry breaking in the solid phase. The heating period leads to the decrease of the size of crystals and the destruction of small crystals; the surviving crystals can then grow during the cooling period. A succession of such cycles allows the autocatalytic transformation from a racemic suspension into pure enantiomer, with an enantiomeric excess (*e.e.*) > 99% within a few days. The results demonstrate a possible mechanism for the emergence of homochirality of molecules of biological significance on earth.

2.2 Introduction

Access to pure enantiomers remains an important scientific and industrial issue. Recently, a new crystallization process called Viedma ripening was designed (Viedma, 2005). Viedma showed that it was possible to completely break the symmetry of a racemic mixture of *D*- and *L*-crystals of $NaClO_3$ by using a continuous grinding technique in suspension. Though achiral in solution, $NaClO_3$ has the special feature to crystallize in the chiral space group $P2_13$ (Abrahams and Bernstein, 1977), giving two kinds of enantiomorphous crystals. An older technique named total symmetry breaking, which was described by Kipping and Pope in 1898, was used to obtain an enantiomeric excess over 90% by seeding a saturated solution of $NaClO_3$ with solid composed of pure enantiomorphous crystals (Kipping and Pope, 1898). In 2008, the first example of the total symmetry breaking of an intrinsically chiral component, an amino acid derivative, was jointly given by a Dutch consortium and the group of Blackmond by combining Viedma ripening and in situ racemization in solution (Noorduin et al., 2008a). After this initial research, further chiral organic compounds have been deracemized (Levilain et al., 2009; Noorduin et al., 2009a; Noorduin et al., 2010a; Noorduin et al., 2010b; Noorduin et al., 2009b; van der Meijden et al., 2009). Unfortunately, the number of candidates is limited by the important restrictions of this process: compounds must crystallize as a conglomerate (i.e., a physical mixture of the two enantiomers) and must undergo a fast racemization in solution under the same operating conditions. The number of publications on the topic has also significantly increased as researchers attempt to explain how racemic suspensions in contact with a saturated solution and a racemizing agent are able to evolve toward an enantiopure final state. Additionally, the full resolution of the

mechanism of the deracemization could give the keys to understand why only one enantiomer of many natural chiral compounds is prevalent in nature. The understanding of how biological systems may have naturally become homochiral is one of the most important questions for the scientists (Frank, 1953; Saito and Hyuga, 2011; Sato et al., 2003; Soai et al., 1995).

Numerous studies have been carried out to explain the mechanism of chiral symmetry breaking of the crystal phase. After vigorous debates, the current standard model involves the combination of Ostwald ripening and the reincorporation of chiral clusters by crystals of the same chirality (Cartwright et al., 2007; Crusats et al., 2006; Hein et al., 2012; Noorduin et al., 2010b; Noorduin et al., 2009b). Indeed, attrition produced by grinding enables the production of a high number of chiral clusters that increase the exchange of matter between particles and thus the rate of the evolution of the *e.e.* of the solid phase. Moreover, due to the minimization of the energy surfaces, the smaller particles produced by grinding are quickly dissolved to the benefit of the growth of the larger ones (Ostwald ripening) which also speeds up the evolution of the *e.e.* Numerous computer models have been produced to simulate the evolution of such a process by taking in account the reincorporation of clusters, the effect of Ostwald ripening, the size dependent solubility, the agglomeration of particles, and of course, the crystallization as a conglomerate together with fast racemization in solution (Iggland and Mazzotti, 2011; McBride and Tully, 2008; Noorduin et al., 2008b; Saito and Hyuga, 2004; Skrdla, 2011; Uwaha, 2004). These studies also demonstrated that the grinding and the resulting processes were not necessary to complete deracemization, but they serve to significantly accelerate the evolution of the *e.e.* (Noorduin et al., 2009b). Ripening occurs somewhere between the solubility

of an infinite size crystal and the solubility of a nucleus, which will result in slow kinetics since these two limits are very close and both dissolution and growth processes will occur at very low levels of supersaturation.

In 2011, Viedma and Cintas showed that boiling suspensions of sodium chlorate can also lead to chiral symmetry breaking of the crystals (Viedma and Cintas, 2011). They suggested that dissolution/crystallization cycles due to the temperature gradient existing between the bottom of the flask (in contact with a hot plate) and the top of the flask (in contact with atmosphere at ambient temperature) are responsible for the process of deracemization. Recent modeling performed by Iggland and Mazzotti (Iggland and Mazzotti, 2013) has shown that simultaneous growth of crystals larger than the critical size and dissolution of crystals smaller than the critical size may be able to produce relatively fast chiral symmetry breaking. It should be emphasized that this process (a form of ripening) is very distinct from growth and dissolution cycles due to temperature gradient where essentially all the crystals in the suspension grow in the lower temperature part of the gradient and dissolve (either partially or totally) in the upper temperature part. It is possible that similar effects occur in suspensions undergoing grinding. Indeed, attrition induces localized volumes of high energy/temperature in the system, which leads to the dissolution/ recrystallization phenomenon.

This paper aims at contributing to a better understanding of deracemization in heterogeneous systems. This study is focused on the effect of temperature fluctuations at near ambient conditions in a gently stirred system on the deracemization of a model compound, 1-(4-chlorophenyl)-4,4-dimethyl-2-(1H-1,2,4-triazol-1-yl)pentan-3-one (Cl-Tak) (Figure 2.1). This compound, a precursor of Paclobutrazol, a plant growth

inhibitor (Black et al., 1989), is known to crystallize as a stable conglomerate without detectable solid solution and can be easily racemized using an alkaline aqueous solution (Black et al., 1990).

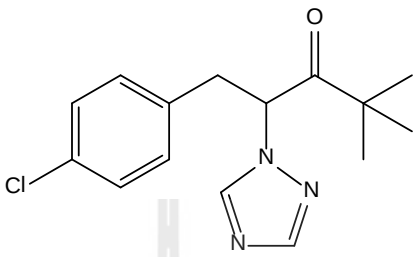

Figure 2.1 Chemical structure of Cl-Tak.

The deracemization of this compound was previously described in the literature at 25°C (Levilain et al., 2009). This compound was thus an appropriate candidate to study the possibility to perform deracemization by means of temperature cycles at near ambient conditions to simulate the natural temperature cycling and in order to address the question of how chiral symmetry breaking occurs.

2.3 Experimental Section

2.3.1 Materials

Racemic 1-(4-chlorophenyl)-4,4-dimethyl-2-(1H-1,2,4-triazol-1-yl) pentan-3-one (Cl-Tak) was synthesized according to the literature (Balasubramanyan and Shephard, 1977).

Distilled water was used for deracemization experiments. HPLC-grade n-heptane and ethanol, and reagent-grade methanol were purchased from Fisher Scientific.

2.3.2 Deracemization Experiments

The deracemizations were carried out as follows: in a 50 mL round-bottom thermostatted flask, Cl-Tak was suspended in a methanol/water mixture (80/20 %wt, 25 g) and then the racemizing agent, sodium hydroxide (0.2 g, i.e., 8 g per kg of solvent), was added. An oval magnetic stirrer operated at 500 rpm was used to ensure a uniform distribution of particles and temperature in the heterogeneous system, and then a temperature program (TP) was applied. Different masses of Cl-Tak and different TPs (Figure 2.2) were used to achieve the symmetry breaking in the study, as summarized in Table 2.1.

Table 2.1 Required number of cycles and required time to achieve complete symmetry breaking (defined as reaching an *e.e.* > 98%) for the experiments described.

	TP	Total mass of Cl-Tak (g)	Required time to complete deracemization (h)	Number of cycles required to complete deracemization
Experiment I	1	3.3	91	91
Experiment II	2	2.5	51	86
Experiment III	3	2.5	51	121
Experiment IV	4	2.5	51	67
Experiment V	2	1.8	32	55

The first temperature program TP1 consisted of 4 steps; holding at 20°C for 5 min, ramping up to 30°C over a period of 5 min, holding at 30°C for

5 min, and then ramping down to 20°C over a period of 45 min. The second temperature program TP2 starting by holding the temperature of the suspension at 20°C for 5 min, then ramping it up to 25°C over a period of 2 min, then holding it at 25°C for 5 min, and finally ramping it down to 20°C over 23 min. The third temperature program TP3 and fourth temperature program TP4 were identical to TP2 with the exception that the final ramp from 25°C to 20°C occurred over periods of 13 min (TP3) and 33 min (TP4).

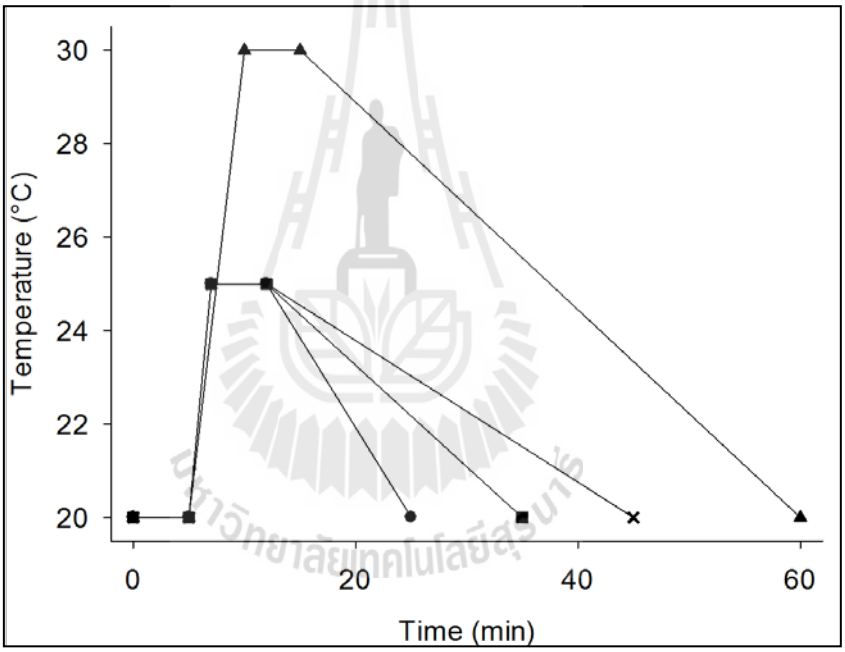

Figure 2.2 The different temperature programs. ▲ TP1, ■ TP2, ● TP3 and x TP4.

These temperature cycles were continued over a large number of cycles until deracemization was substantial. The suspension was partially dissolved during the heating period. The remaining crystals then recrystallize and grow during the cooling period by consumption of the supersaturation in the solution phase. The recrystallized amount is the same as the mass lost during the heating step.

2.3.3 HPLC Analysis

The *e.e.* was monitored by chiral HPLC (Levilain et al., 2009). Samples were taken off at the end of cycles (at 20°C) using a plastic pipette. The solid was then filtered under a vacuum and washed with a sufficient amount of water to remove the rest of the sodium hydroxide (the solubility of Cl-Tak in water at 20°C is lower than 0.1%) (Levilain et al., 2009). A small amount of solid (*ca* 5 mg) was then dissolved into 1 mL of ethanol. A 20 μL sample of this solution was injected into a Chiracel OD column (250 × 4.6 mm) using a solution of 5 %vol ethanol in *n*-heptane as eluent at a flow rate of 1.5 $mL.min^{-1}$. The two enantiomers were detected at retention times of *ca* 8 and *ca* 10 min using UV detection at a wavelength of 227 nm.

2.3.4 Solubility Measurement

Solubilities of the racemic mixture and of the pure enantiomer of Cl-Tak were determined at different temperatures using the gravimetric method. Without racemization (i.e., in a 80/20 methanol/water mixture), the solubilities of the racemic mixture and of the pure enantiomer are 5.0% and 2.4%, respectively at 25°C and are in accordance with Meyerhoffer's rule. Under racemizing conditions, the solubilities of the racemic mixture and of the pure enantiomer are very close (Table 2.2), probably because both the solid phases are in equilibrium with a racemic liquid phase. The presence of sodium hydroxide seems to decrease the solubility of Cl-Tak. It should be noted that HPLC analyses confirmed that the chirality of the solid phases was the expected chirality (racemic for determination of the solubility of racemic Cl-Tak, enantiomerically pure for determination of the solubility of pure enantiomer of Cl-Tak) and that the liquid phases (that is to say the dry extracts) were racemic.

Table 2.2 Solubilities of Cl-Tak in an 80/20 %wt methanol/water mixture containing 8 g of NaOH per kg of solvent. Solubilities are given in mass of Cl-Tak per 100 g of saturated solution.

Temperature (°C)	Solubility of the racemic mixture Cl-Tak (%)	Solubility of pure enantiomer of Cl-Tak (%)
20	3.9	3.6
25	4.6	4.4
30	5.8	5.5

2.3.5 Enantiomeric Excess in the Solid Phase

Enantiomeric excess (*e.e.*) in the solid phase is defined in terms of the predominant enantiomer at complete deracemization (at the end of the experiment). The experimental results demonstrated that the deracemization was random; the final product of the deracemization could be either of the *R*-form or the *S*-form of the compound. The presentation here is focused on the absolute value of the *e.e.* in order to compare the results more conveniently.

2.4 Experimental Results

First, experiments were carried out to give the proof that temperature cycles at near ambient conditions were able to totally break the symmetry of the solid phase. TP1 and TP2, respectively experiment I (Figure 2.3a) and experiment II (Figure 2.4a), were applied to a suspension of Cl-Tak. After few dozens of hours (*ca* 90 h and *ca* 50 h, respectively) and cycles (*ca* 90 cycles and *ca* 85 cycles, respectively), the solid phase became enantiomerically pure. The time required to achieve complete

deracemization in the solid phase using the temperature cycling technique is shorter than when using grinding by small glass beads at constant temperature, which requires around a week for complete deracemization. These results indicate that it is possible to achieve total symmetry breaking of the solid phase by using cyclic temperature fluctuations in the system. The behavior of the conversion is a sigmoidal curve with an exponential part as illustrated by the curve ln(*e.e.*) = *f(t)* (see Figure 2.3b).

TP2 is shorter than TP1 and with smaller temperature fluctuations (between 20 and 25°C instead of 20 and 30°C for TP1). Therefore, for a usual *ds/dT* – variation of solubility versus temperature- there is no need for a high temperature gradient to break the symmetry.

It is known that grinding due to a magnetic stirrer is also able to perform deracemization (Viedma, 2004). Similar experiments were thus conducted in the same operating conditions than experiments I and II but with some periods of constant temperature to demonstrate that the symmetry breaking found in this study was due to temperature cycling rather than grinding. Experiment I´ was carried out at constant temperature (20°C) for the first 142 h, and then TP1 cycles were applied (Figure 2.3a). No evolution of the *e.e.* is visible in the absence of temperature cycles during the observation period. But, once TP1 is applied, symmetry breaking of the solid phase significantly increases, leading to complete deracemization at *ca* 90 temperature cycles (90 h) after the initiation of the temperature program. Figure 2.3b shows that the linear part of the curve ln(*e.e.*) = *f(t)* of experiment I and I´ is parallel, meaning that the evolution of the *e.e.* is not disturbed by the initial constant temperature period.

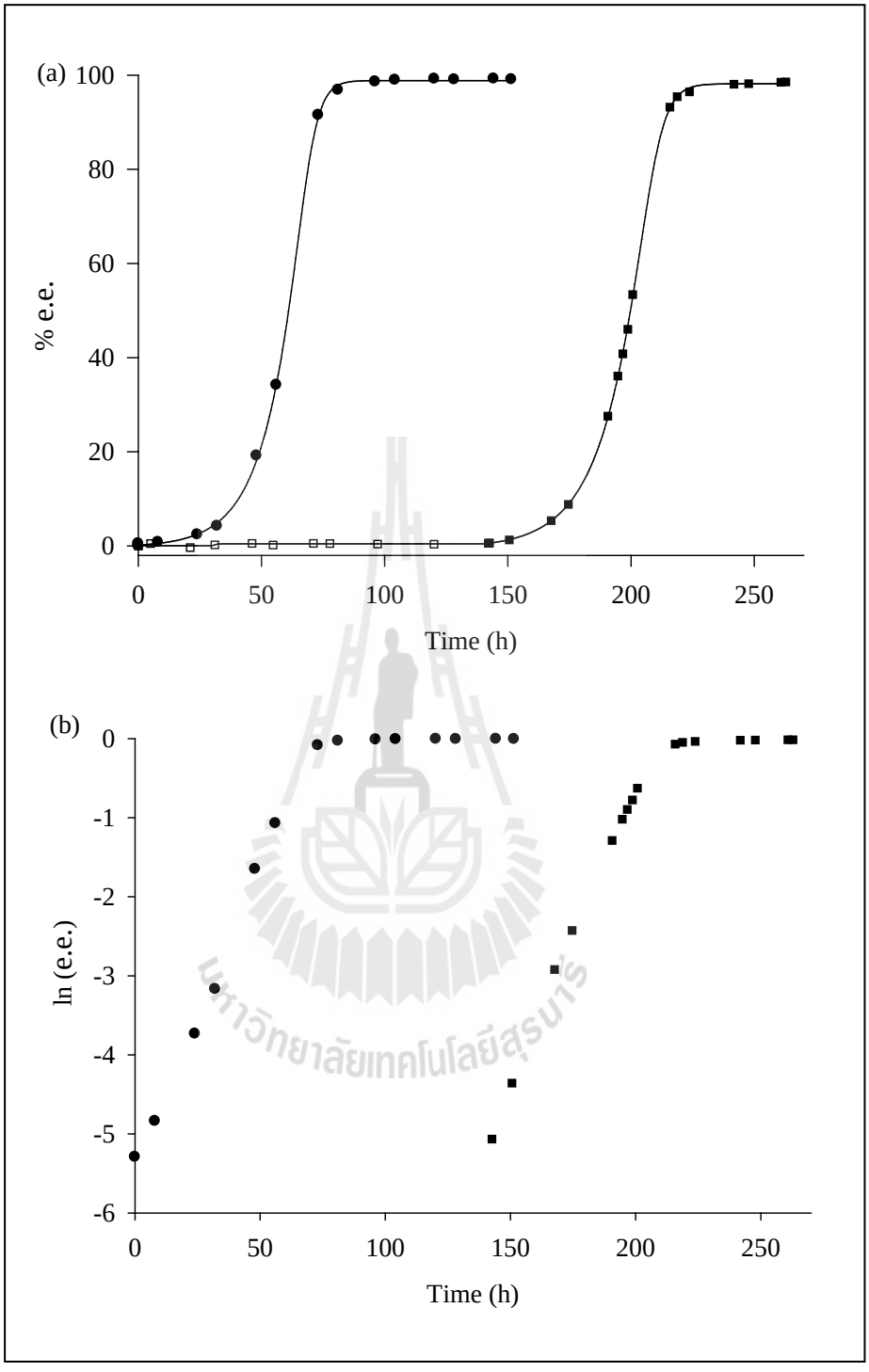

Figure 2.3 Deracemization by using TP1. (a) Evolution of *e.e.* versus time. (b) Evolution of ln(*e.e.*) versus time. ● Experiment I, □ experiment I´ - constant temperature period (20°C), ■ experiment I´ - TP1 period.

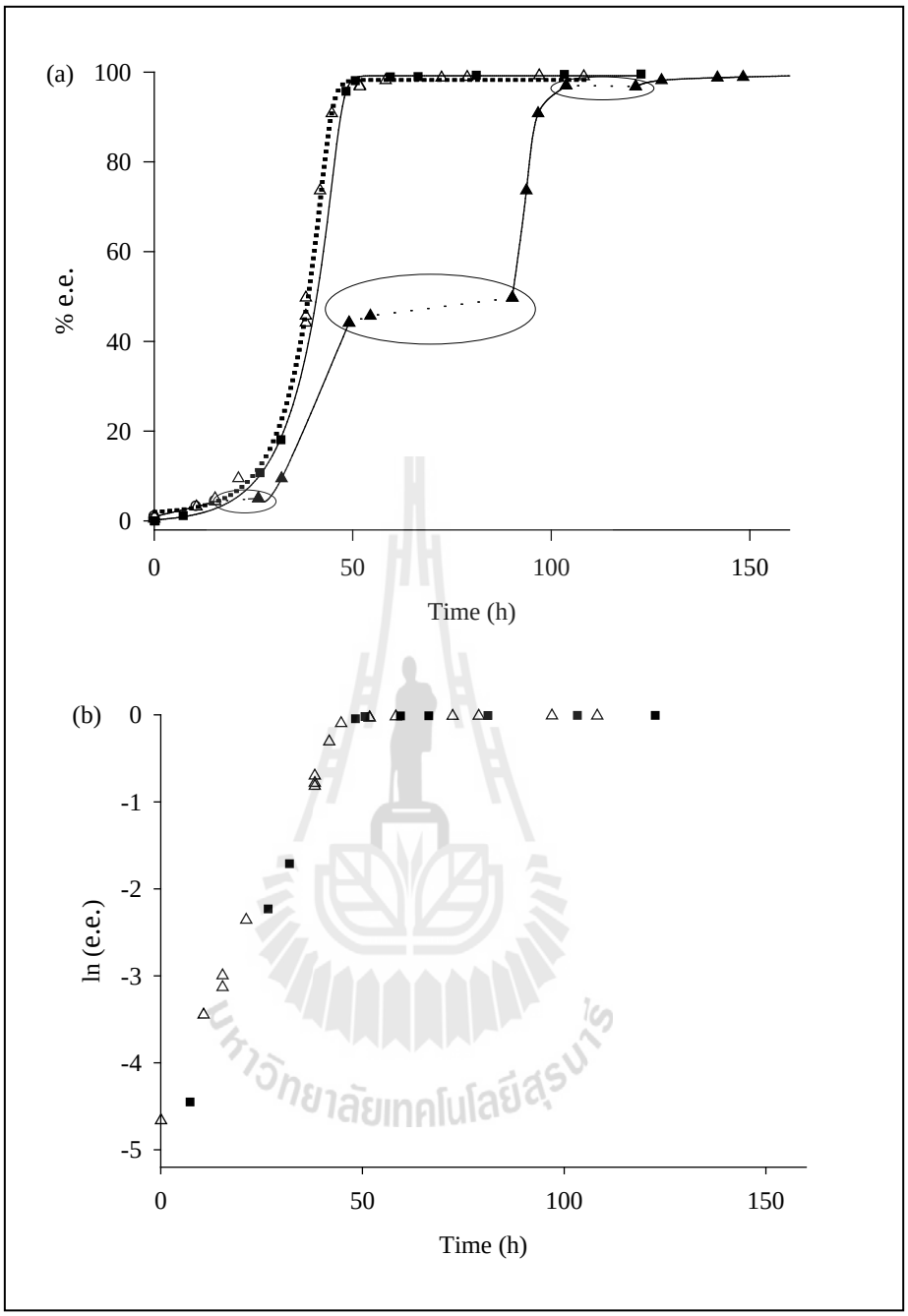

Figure 2.4 Deracemization by using TP2. (a) Evolution of *e.e.* versus time. (b) Evolution of ln(*e.e.*) versus time. ■ Experiment II, ▲ experiment II´, full line: TP2 periods, dashed line: constant temperature periods (20°C). The constant temperature periods are encircled. △ Experiment II´ ignoring the constant temperature periods.

In the case of experiment II′, three periods of constant temperature were applied between periods of temperature cycles (Figure 2.4a). The evolution of the *e.e.* of the solid phase when the temperature is constant is much slower (almost without evolution) than during the TP2 periods even at high values of *e.e.* (≈ 45%). When merging the TP2 periods together (removing data at constant temperature), the evolution of *e.e.* in the solid phase (dotted line) is similar to the continuous use of TP2 throughout the experiment. The curves $\ln(e.e.) = f(t)$ are also superimposable (Figure 2.4b).

The fast evolution of the *e.e.* observed in this study is therefore due to the temperature fluctuations applied to the suspension and not due to the grinding ensured by the magnetic stirrer.

The effect of the cooling rate on the evolution of *e.e.* of the solid was investigated; the temperature programs TP2, TP3 and TP4 were compared. They differ only by the duration of the ramp to return to 20°C (Figure 2.5). This is a critical parameter since it will determine the evolution of the supersaturation during the crystal growth period; faster cooling rates will lead to larger supersaturation values during the crystallization and therefore a greater likelihood of nucleation during the crystallization period rather than simply growth of existing crystals. The cooling rates of TP2, TP3 and TP4 are 13, 23 and 9 °C h^{-1}, respectively.

The results show that the evolution of *e.e.* over time is unchanged for the three temperature programs used (Figure 2.5a). The programs have no significant effect on the time required to achieve complete chiral purity. However, when the evolution of *e.e.* in the solid phase is plotted against the number of heating-cooling cycles (Figure

2.5b), the evolution of the *e.e.* is different. The faster cooling rate system requires more cycles than the lower cooling rate system.

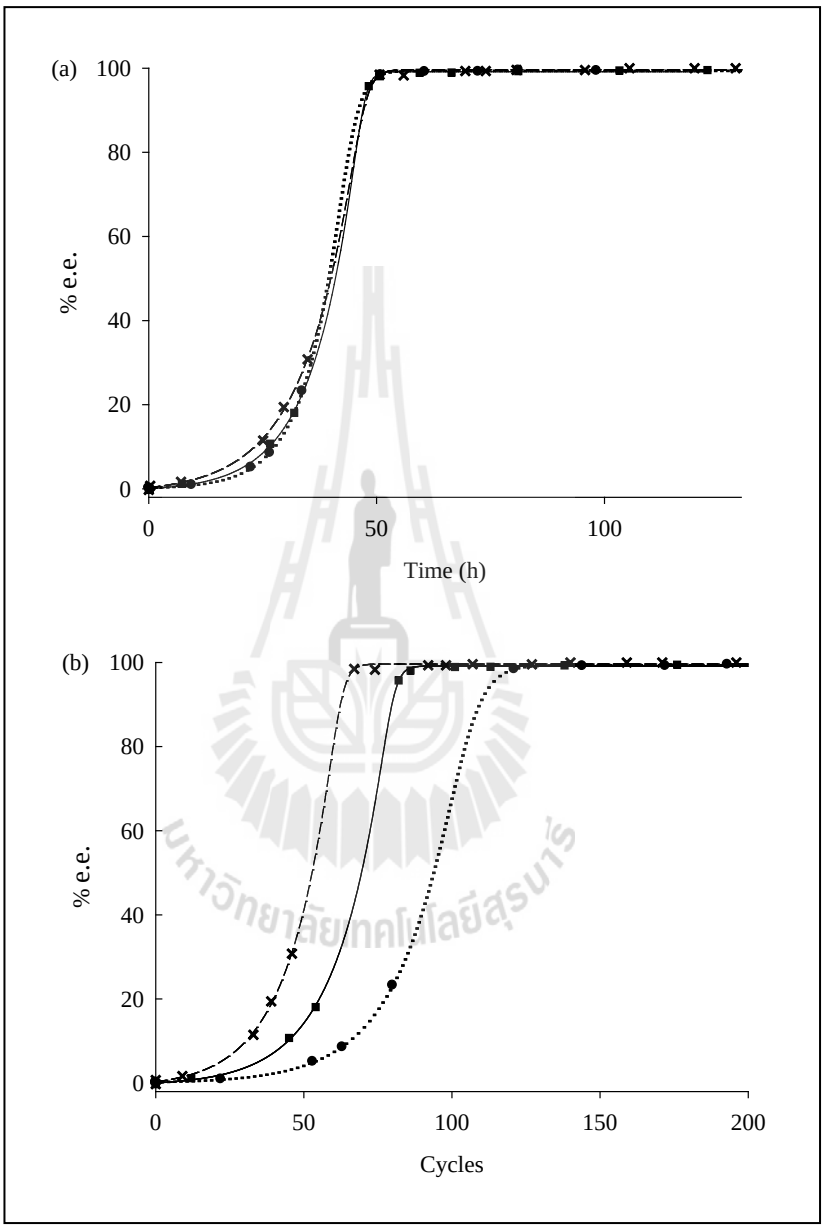

Figure 2.5 Effect of the cooling rate on deracemizations. (a) Evolution of the *e.e.* versus time. (b) Evolution of *e.e.* versus the number of heating-cooling cycles. ■ Experiment II (TP2), ● experiment III (TP3), × experiment IV (TP4).

In the case of a rapid cooling, the creation of a high supersaturation puts the solution point beyond the Ostwald limit (Ostwald, 1900), and the enantiomer in minor amount can produce small crystals by secondary nucleation, resulting in a time delay for complete conversion. However, in the case of a slow cooling, the crystallization of the major enantiomer is favored and not limited by the decrease of its concentration due to racemization in the liquid phase.

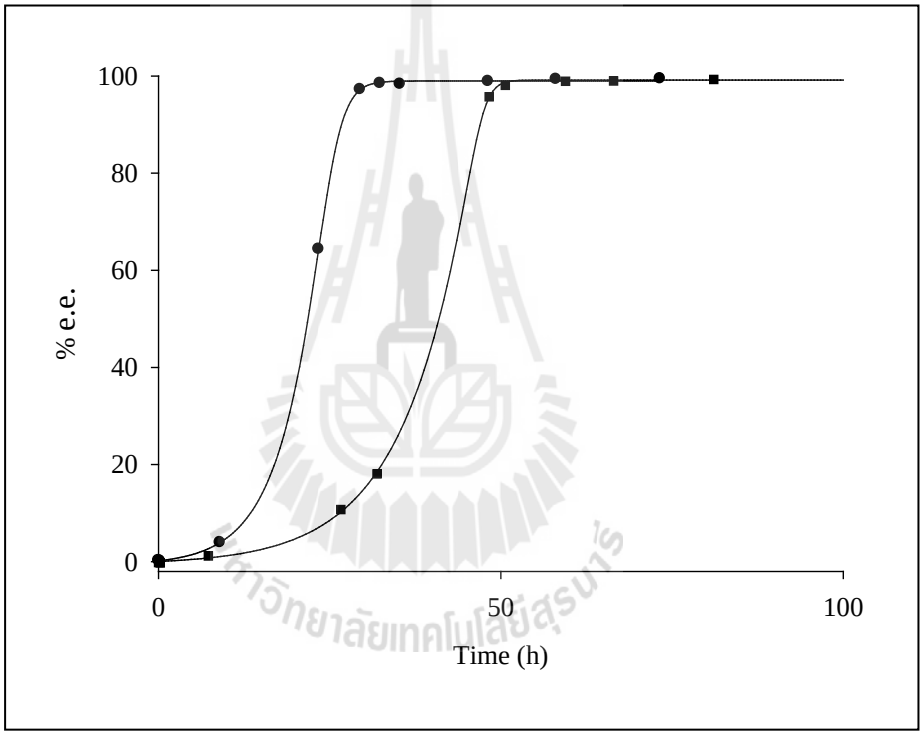

Figure 2.6 Comparison between two deracemizations carried out in the same experimental conditions, using TP2, except for the total mass of Cl-Tak: ■ experiment II: 2.5 g of Cl-Tak and ● experiment V: 1.8 g of Cl-Tak.

The effect of the amount of solid to deracemize on the duration of the experiment was studied. Two experiments were carried out in the same operating

conditions, except for the initial mass of Cl-Tak: 2.5 g (experiment II) and 1.8 g (experiment V) were used. In the two cases, the same mass of solid is dissolved during the heating period. The resulting masses and the resulting supersaturations are therefore the same, as illustrated on Figure 2.7. It is not surprising that the time required to achieve complete chiral purity is shorter when the mass of solid is smaller (Figure 2.6), the amount of Cl-Tak to deracemize being smaller. However the relative percentage of solid involved by each cycle is different: *ca* 10% of the solid phase is dissolved in the experiment II instead of *ca* 20% in the experiment V. It is therefore possible that all the processes that occur due to dissolution/recrystallization are magnified when a higher percentage of solid is involved by the temperature fluctuations, accelerating the evolution of the *e.e.*

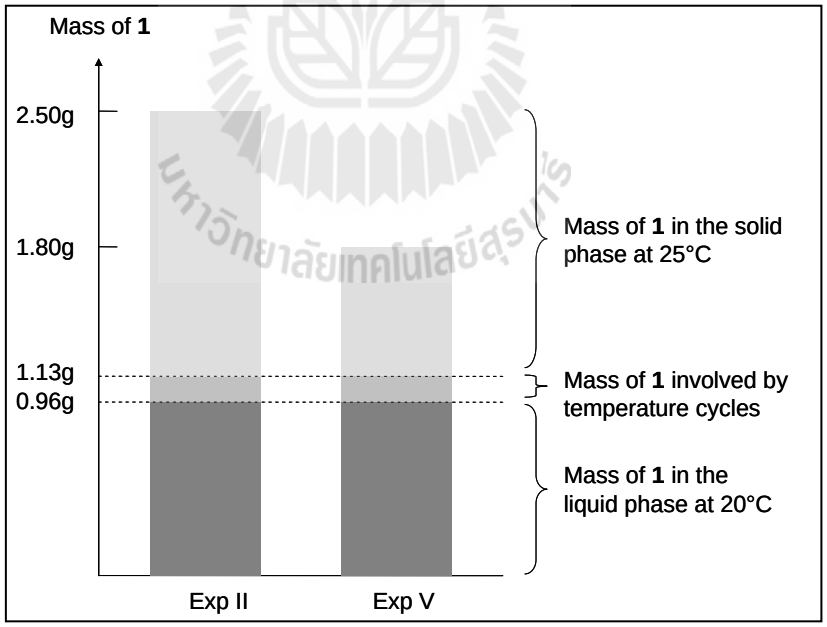

Figure 2.7 Schematic representation of the distribution of Cl-Tak (**1**) in the different phases of the suspension for the experiments II and V.

2.5 Discussion

The results presented in this study demonstrate conclusively that deracemization can also occur in the absence of abrasive grinding. The evolution of a racemic mixture of a chiral compound to single handedness is possible due to the combination of racemization in solution and dissolution/recrystallization cycles in the system. These temperature fluctuations are responsible for two phenomena that result in an increase of the *e.e.* of the solid phase: (i) dissolution of the racemic mixture during heating periods, (ii) growth of crystals and entrainment effect during cooling periods.

During the heating periods, according to thermodynamic principles and for low and medium *e.e.* in the solid phase, only the racemic mixture is dissolved (obviously, if the *e.e.* of the solid phase is too high, the enantiomer in excess will be also dissolved). Proportionally, crystals of the less abundant enantiomer are more dissolved than crystals of the enantiomer in excess; the *e.e.* of the solid phase is therefore magnified. Then, during the cooling periods, a supersaturation is created and the remaining crystals can grow (Levilain and Coquerel, 2010).

For a system in equilibrium without racemization, the initial and the final compositions of a heating/cooling event must be the same: a racemic liquid phase in equilibrium with two mirror related solid phases. The entrainment effect is therefore limited to a short period of time, when the system is out of equilibrium. In the most favorable case, the enantiomer in default is completely dissolved at the highest temperature. The system is autoseeded by the crystals of the single enantiomer remaining in the solid phase (Coquerel, 2007; Levilain and Coquerel, 2010; Viedma, 2007). The entrainment effect takes place as soon as the system is cooled, and it is

exhausted when the mother liquor reaches the metastable solubility of the crystallizing enantiomer. The return to equilibrium corresponds to the crystallization of the second enantiomer, then the *e.e.* of the mother liquor decreases down to zero.

With racemization in solution, the composition of the liquid phase is always racemic. Therefore, the entrainment effect has no thermodynamic limit.

A preferential crystallization method called second order asymmetric transition (SOAT) (Collins et al., 1992; Sheldon, 1993) is based on this concept. The combination of a controlled cooling with racemization in solution prevents, up to a certain point, the crystallization of the counter enantiomer and improves the efficiency of the preferential crystallization. If the enantiomeric excess in the solid is not high enough, they are actually two simultaneous SOATs, but the larger the imbalance in the two solid phases the higher the imbalance in the crystal growth so the faster the evolution of toward high *e.e.* The net result is therefore an autocatalytic effect.

Viedma previously described a similar model, the "*thermodynamic-kinetic feedback near equilibrium*", to explain the spontaneous chiral symmetry breaking observed for $NaBrO_3$ (Viedma, 2007). The appearance of a single handedness was due to a "*feedback between the thermodynamic control of dissolution and the kinetics of the growth process near equilibrium*". This model was described for the slight growth-dissolution cycles that occur at constant temperature (Ostwald ripening), but he suggested that this model could be applied to intrinsically chiral molecules.

Recently, Viedma's research group in collaboration with Blackmond's group gave the proof that deracemization can be achieved only through the use of a temperature gradient, at high temperatures (*ca* 105°C), due to the type of heating used, but without grinding (Viedma et al., 2008). This is likely to be due to a similar

mechanism as in the current work, since crystals may cycle through regions of different temperatures; however, the use of deliberate temperature cycling may result in a clearer picture of the mechanism of the deracemization which is still matter of debate.

The general consensus is that Viedma ripening occurs due to Ostwald ripening and the reincorporation of chiral clusters. At the initial stage of the deracemization, a difference between the two enantiomers can be created by any departure from a perfectly symmetric situation: stochastic slight variation of *e.e.* or of the crystal size distribution due to continuous exchanges of matter between the solid and the liquid phase, presence of an impurity (Noorduin et al., 2008a) which promotes or disrupts the crystallization of one of the two enantiomers, etc. This imbalance is then progressively increased due to Ostwald ripening and reincorporation of chiral clusters. However, it is evident that grinding also introduces fluctuations in energy and therefore fluctuations in temperature in a suspension. Friction induces by glass beads may cause high numbers of small localized cycles of heating/cooling in the system. These fluctuations (with respect to time and space) in temperature will lead to the creation of local dissolution and thus supersaturation after cooling and then entrainment.

In this report, we demonstrate deracemization using a technique that is not dependent on grinding. The phenomenon of dissolution/growth in our system has been induced by controlled temperature cycles similar to those occurring in nature. All crystals are simultaneously dissolved during the heating period; the same mass of the two enantiomers is affected. The crystals remaining after the heating cycle are then grown during the cooling period by consuming the excess of the solute

molecules in the supersaturated solution. Since the solution has rapid racemization, the supersaturation of the *R*- and *S*-components are equal throughout the crystallization period and the entrainment effect can efficiently occur. Possible mechanisms for the phenomena do not necessarily require an initial asymmetry in either the solution or the crystalline phase; a very slight imbalance stochastically created by statistical fluctuations is sufficient to trigger the evolution of the whole system. It is possible that there are different histories involved in the nucleation and growth of the two populations (due to the stochastic nature of some of the phenomena) which may have been carried over from events occurring before the temperature cycles where initiated that may result in an imbalance in the kinetics of the two enantiomorphs.

The results may also have implications for the origin of the homochirality of biologically significant molecules on Earth. Natural temperature cycles occur over short time intervals due to natural convection and buoyancy induced flow, and over longer time intervals due to diurnal and annual temperature cycles. Thus, if deracemization can occur due only to repeated temperature cycles at near ambient conditions, it seems a highly likely cause for homochirality in nature. There is no need for a racemization agent in the liquid phase for the deracemization in a crystalline phase to occur, since amino acids will naturally racemize in solution over very long periods of time, which is plausible since geological time frames were available for the event.

Another well-known theory is that undersea volcanic vents (hydrothermal vents) might have been the original source of life on earth, and this has been reviewed recently by Holm (Holm, 1992). These vents will result in strong temperature

gradients due to the temperature difference between the vent and the surrounding deep water, creating buoyancy flow. This creates a natural temperature cycle for pockets of fluid around the vent and potentially has led to a deracemization event due to these temperature cycles. It can be noted that such systems have the necessary precursor compounds required to form amino acids and also suitable reaction conditions.

2.6 Conclusions

This work presents a possible mechanism of complete chiral symmetry breaking occurring in the system via temperature fluctuations, and this is independent from grinding. The dissolution and recrystallization phenomena induced by temperature fluctuations in the system are enough to break the symmetry and finally to achieve complete deracemization. The interplay between (i) dissolution and regrowth with dispersion of rates (Flood, 2010), (ii) racemization in solution and (iii) the entrainment effect seem to be responsible of this process.

The heating/cooling cycle can be produced by several procedures, such as friction caused by glass beads in agitated systems or sonication, causing localized energy inputs into the system, temperature programming via the use of a thermostat, or temperature fluctuations in nature. Their effects are therefore to be added to the effect of the other phenomena, such as Ostwald ripening or reincorporation of clusters.

Our results help to fill crucial gaps in the understanding of the mechanism of the deracemization process.

To optimize this novel procedure, the temperature programming has to be adjusted. Optimal programming may use large temperature swings for the initial

cycles in order to initiate the breaking of symmetry, followed by smaller temperature variations in later cycles where the preferred enantiomer has a significant excess. In the latter situation, only a small amount of crystal needs to be dissolved to remain in the biphasic domain at high temperature: crystals of a single enantiomer in equilibrium with a racemic saturated solution. This procedure should produce an optimum set of conditions, and the evolution of enantiomeric excess may tend toward an exponential increase to 100%, for conglomerates without partial solid solution (Gonella et al., 2011), rather than the sigmoidal shape as found in this work.

A combination of techniques using preferential crystallization in addition to periodic temperature fluctuations in order to completely deracemize conglomerate systems may accelerate the complete deracemization and yield high product purity and yield for industrial applications.

This method could also lead to a variety of industrial applications for deracemization; the process involving cycles of growth and dissolution due to temperature fluctuations is easier to implement at a large scale than a continuous grinding.

2.7 References

Abrahams, S. C., and Bernstein, J. L. (1977). Remeasurement of optically active NaClO3 and NaBrO3. **Acta Crystallographica Section B.** 33: 3601-3604.

Balasubramanyan, S., and Shephard, M. C. (1977). Fungicidal compounds. **Patent US4243405 A.**

Black, S. N., Williams, L. J., Davey, R. J., Moffatt, F., Jones, R. V. H., McEwan, D. M., and Sadler, D. E. (1989). The preparation of enantiomers of paclobutrazol: A crystal chemistry approach. **Tetrahedron.** 45. 2677-2682.

Black, S. N., Williams, L. J., Davey, R. J., Moffatt, F., McEwan, D. M., Sadler, D. E., Docherty, R., and Williams, D. J. (1990). Crystal chemistry of 1-(4-chlorophenyl)-4,4-dimethyl-2-(1H-1,2,4-triazol-1-yl)pentan-3-one, a paclobutrazol intermediate. **The Journal of Physical Chemistry.** 94: 3223-3226.

Cartwright, J. H. E., Piro, O., and Tuval, I. (2007). Ostwald Ripening, Chiral Crystallization, and the Common-Ancestor Effect. **Physical Review Letters.** 98: 165501.

Collins, A. N., Sheldrake, G. N., and Crosby, J. (1992). The commercial manufacture and applications of optically active compounds. **Chirality in industry.** Wiley: Chichester.

Coquerel, G. (2007). Preferential crystallization. **In Springer-Verlag: Berlin Heildelberg; Topics in Current Chemistry.** 269: pp. 1-51.

Crusats, J., Veintemillas-Verdaguer, S., and Ribó, J. M. (2006). Homochirality as a Consequence of Thermodynamic Equilibrium? **Chemistry – A European Journal.** 12: 7776-7781.

Flood, A. E. (2010). Feedback between crystal growth rates and surface roughness. **CrystEngComm.** 12: 313-323.

Frank, F. C. (1953). On spontaneous asymmetric synthesis. **Biochimica et Biophysica Acta.** 11: 459-463.

Gonella, S., Levilain, G., and Coquerel, G. (2011). Racemizable systems crystallizing as conglomerate and spontaneous symmetry breaking. **Journal of Thermal Analysis and Calorimetry**. 103: 125-129.

Hein, J. E., Huynh Cao, B., Viedma, C., Kellogg, R. M., and Blackmond, D. G. (2012). Pasteur's Tweezers Revisited: On the Mechanism of Attrition-Enhanced Deracemization and Resolution of Chiral Conglomerate Solids. **Journal of the American Chemical Society.** 134: 12629-12636.

Holm, N. G. (1992). Origins of Life and Evolution of the Biosphere. 22, 5-14.

Iggland, M., and Mazzotti, M. (2011). A Population Balance Model for Chiral Resolution via Viedma Ripening. **Crystal Growth & Design.** 11: 4611-4622.

Iggland, M., and Mazzotti, M. (2013). Solid state deracemisation through growth, dissolution and solution-phase racemisation. CrystEngComm 15, 2319-2328.

Kipping, F. S., and Pope, W. J. (1898). LXIII.-Enantiomorphism. **Journal of the Chemical Society, Transactions.** 73: 606-617.

Levilain, G., and Coquerel, G. (2010). Pitfalls and rewards of preferential crystallization. **CrystEngComm.** 12: 1983-1992.

Levilain, G., Rougeot, C., Guillen, F., Plaquevent, J.-C., and Coquerel, G. (2009). Attrition-enhanced preferential crystallization combined with racemization leading to redissolution of the antipode nuclei. **Tetrahedron: Asymmetry.** 20: 2769-2771.

McBride, J. M., and Tully, J. C. (2008). Physical chemistry: Did life grind to a start? **Nature.** 452: 161-162.

Noorduin, W. L., Izumi, T., Millemaggi, A., Leeman, M., Meekes, H., Van Enckevort, W. J. P., Kellogg, R. M., Kaptein, B., Vlieg, E., and Blackmond, D. G. (2008a). Emergence of a Single Solid Chiral State from a Nearly Racemic Amino Acid Derivative. **Journal of the American Chemical Society.** 130: 1158-1159.

Noorduin, W. L., Kaptein, B., Meekes, H., van Enckevort, W. J. P., Kellogg, R. M., and Vlieg, E. (2009a). Fast Attrition-Enhanced Deracemization of Naproxen by a Gradual In Situ Feed. **Angewandte Chemie International Edition.** 48: 4581-4583.

Noorduin, W. L., Meekes, H., Bode, A. A. C., van Enckevort, W. J. P., Kaptein, B., Kellogg, R. M., and Vlieg, E. (2008b). Explanation for the Emergence of a Single Chiral Solid State during Attrition-Enhanced Ostwald Ripening: Survival of the Fittest. **Crystal Growth & Design.** 8: 1675-1681.

Noorduin, W. L., Meekes, H., van Enckevort, W. J. P., Kaptein, B., Kellogg, R. M., and Vlieg, E. (2010a). Enantioselective Symmetry Breaking Directed by the Order of Process Steps. **Angewandte Chemie International Edition.** 49: 2539-2541.

Noorduin, W. L., van Enckevort, W. J. P., Meekes, H., Kaptein, B., Kellogg, R. M., Tully, J. C., McBride, J. M., and Vlieg, E. (2010b). The Driving Mechanism Behind Attrition-Enhanced Deracemization. **Angewandte Chemie International Edition.** 49: 8435-8438.

Noorduin, W. L., Vlieg, E., Kellogg, R. M., and Kaptein, B. (2009b). From Ostwald Ripening to Single Chirality. **Angewandte Chemie International Edition.** 48: 9600-9606.

Ostwald, F. W. Z. (1900). **Phys. Chem.** 34:, 495-503.

Saito, Y., and Hyuga, H. (2004). Complete Homochirality Induced by Nonlinear Autocatalysis and Recycling. **Journal of the Physical Society of Japan.** 73: 33-35.

Saito, Y., and Hyuga, H. (2011). Grinding-induced homochirality in crystal growth. **Journal of Crystal Growth.** 318: 93-98.

Sato, I., Omiya, D., Igarashi, H., Kato, K., Ogi, Y., Tsukiyama, K., and Soai, K. (2003). Relationship between the time, yield, and enantiomeric excess of asymmetric autocatalysis of chiral 2-alkynyl-5-pyrimidyl alkanol with amplification of enantiomeric excess. **Tetrahedron: Asymmetry.** 14: 975-979.

Sheldon, R. A. (1993). Industrial Synthesis of Optically Active Compounds. **Chirotechnology.** Marcel Dekker: New York.

Skrdla, P. J. (2011). Kinetics and Thermodynamics of Efficient Chiral Symmetry Breaking in Nearly Racemic Mixtures of Conglomerate Crystals. **Crystal Growth & Design.** 11: 1957-1965.

Soai, K., Shibata, T., Morioka, H., and Choji, K. (1995). Asymmetric autocatalysis and amplification of enantiomeric excess of a chiral molecule. **Nature.** 378: 767-768.

Uwaha, M. (2004). A Model for Complete Chiral Crystallization. **Journal of the Physical Society of Japan.** 73: 2601-2603.

van der Meijden, M. W., Leeman, M., Gelens, E., Noorduin, W. L., Meekes, H., van Enckevort, W. J. P., Kaptein, B., Vlieg, E., and Kellogg, R. M. (2009). Attrition-Enhanced Deracemization in the Synthesis of Clopidogrel - A Practical Application of a New Discovery. **Organic Process Research & Development.** 13: 1195-1198.

Viedma, C. (2004). Experimental evidence of chiral symmetry breaking in crystallization from primary nucleation. **Journal of Crystal Growth.** 261: 118-121.

Viedma, C. (2005). Chiral Symmetry Breaking During Crystallization: Complete Chiral Purity Induced by Nonlinear Autocatalysis and Recycling. **Physical Review Letters.** 94: 065504.

Viedma, C. (2007). Chiral Symmetry Breaking and Complete Chiral Purity by Thermodynamic-Kinetic Feedback Near Equilibrium: Implications for the Origin of Biochirality. **Astrobiology.** 7: 312-319.

Viedma, C., and Cintas, P. (2011). Homochirality beyond grinding: deracemizing chiral crystals by temperature gradient under boiling. **Chemical Communications.** 47: 12786-12788.

Viedma, C., Ortiz, J. E., Torres, T. d., Izumi, T., and Blackmond, D. G. (2008). Evolution of Solid Phase Homochirality for a Proteinogenic Amino Acid. **Journal of the American Chemical Society.** 130: 15274-15275.

CHAPTER III

MATHEMATICAL MODELING OF CHIRAL SYMMETRY BREAKING TOWARDS COMPLETE DERACEMIZATION DUE TO DIFFERENCES IN CRYSTAL GROWTH KINETICS

3.1 Abstract

Two simple models are proposed and tested for the mechanism of ripening of a conglomerate suspension to a single enantiomorph by temperature cycles. In both models, the initial crystal size distributions and masses of the two enantiomorphs are equal, but either the crystal growth rate or the growth rate distribution is varied. The difference in the crystal growth kinetics of the two enantiomorphs may be caused by the intrinsic thermodynamic stability of the crystals occurring in the initial suspension. The initial nucleation of one of the two enantiomers will occur earlier than that of the counter-enantiomer. This results in the formation of two populations occurring under different conditions, leading to different internal crystalline perfection and therefore different thermodynamic stability.

3.2 Introduction

Recently, a new process was experimentally demonstrated to obtain an enantiopure suspension from a racemic suspension of a conglomerate forming system, using a series of temperature cycles combined with a swift racemization in the

solution phase (Suwannasang et al., 2013). The material chosen as a model compound was 1-(4-chlorophenyl)-4,4-dimethyl-2-(1H-1,2,4-triazol-1-yl)pentan-3-one (Cl-Tak), because it is a conglomerate forming system and because it is rapidly racemized in the presence of sodium hydroxide. The previous study (Suwannasang et al., 2013) showed that ripening by temperature cycles can achieve complete deracemization from an initial racemic suspension within 2 - 4 days (see Figure 3.1 for an example of experimental results). During the periods when temperature cycling is stopped there was negligible change in enantiomeric excess (*e.e.*) in the crystalline phase. This demonstrated clearly that deracemization is caused by temperature cycling, not by grinding. This new ripening process appears distinct from Viedma ripening, and Ostwald ripening could not be the primary mechanism involved since the deracemization is too fast (Cartwright et al., 2007; McBride, 2008; Noorduin et al., 2010; Viedma, 2005).

Deracemization by temperature cycling occurs due to repeated cycles of partially dissolving the suspension during the heating period and then regrowth of the remaining crystals during the cooling period, which consumes the supersaturation in the solution phase. The mass of crystalline material regrown is the same as the mass lost during the heating step since the system fluctuates between saturated states at high and low temperatures. However, this new phenomenon of ripening is not well understood.

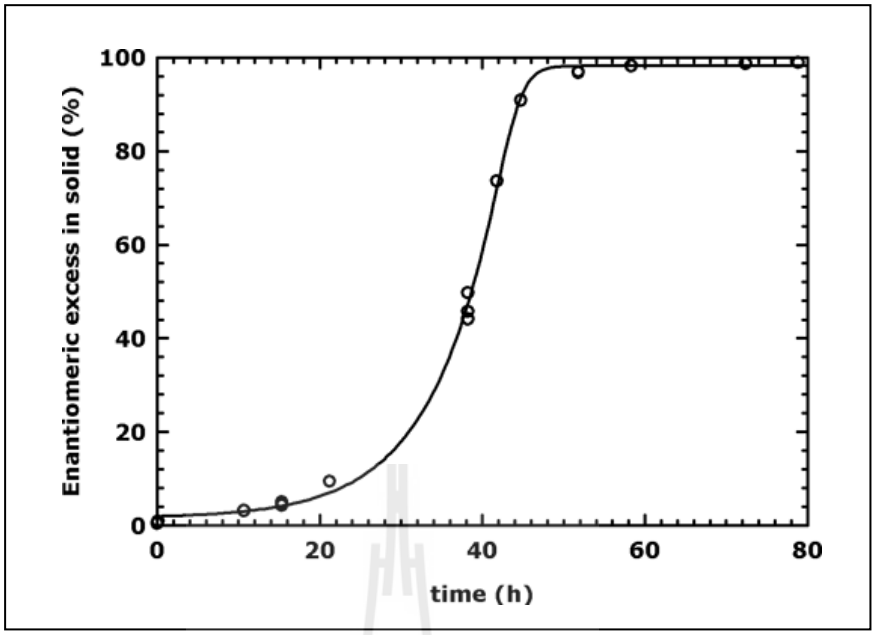

Figure 3.1 Deracemization of Cl-Tak using temperature cycling. Evolution of *e.e.* versus time during periods of temperature cycling; temperature cycles each with 1 h of duration.

Although the original racemic solution may be perfectly symmetric, this does not guarantee that the two enantiomorphs will nucleate or crystallize simultaneously. Garside et al. (John Garside, 2002) have noted that “as an example, the induction periods for aqueous solution of KCl show that the scatter of experimental data is rather large. This is often found and arises from the stochastic character of nucleation”. This suggests that the two enantiomorphs can nucleate at different times even though their properties are identical. Jones and Larson (Jones and Larson, 1999) have shown that crystals nucleating under different supersaturation levels have different levels of growth rate activity and different levels of crystal growth rate dispersion (GRD). If the two enantiomorphs nucleate under different supersaturations

or different temperatures, then the crystal growth rate kinetics of the two populations will be different, i.e., there is a memory effect.

One of the hypotheses is that deracemization may originate from the original nucleation events for the two enantiomorphs. Although the original racemic solution may be perfectly symmetric, this does not guarantee that the two enantiomorphs will nucleate or crystallize simultaneously since the nucleation is known as a stochastic phenomenon that does not occur at predictable times. Thus, deracemization might be caused –at least partially– by differences in crystal growth kinetics between the two enantiomorphs, which are caused by the initial formation of nuclei of the two enantiomers occurring at slightly different times, and therefore under different levels of supersaturation. Under rapid racemization in the solution phase, the enantiomorph nucleating first will nucleate at high supersaturation and will consume the solute of both enantiomers in the solution phase before the formation of the other enantiomer begins; the solution temperature may also change between the two nucleation events. This creates two populations of crystals that commenced nucleation at (slightly) different times and therefore under different conditions, leading to different internal crystalline perfection and thus slightly different thermodynamic stability.

The current study aims to use models of growth and dissolution kinetics under various assumptions for crystal growth and to determine whether such models are able to fit the functional forms of the experimental data in the deracemizations. It is important to note that the aim of this study is not try to achieve predictive models of the deracemization; the simple models are used to determine (i) whether the mechanism produces a time evolution of the *e.e.* and (ii) whether the functional form of the evolution in *e.e.* is similar to that seen in the experimental results in Figure 3.1.

Experimental studies of deracemization of chiral compounds tend to be very expensive, time consuming, and necessarily use small amounts of material. This is because the species involved must be conglomerate forming compounds and easily and quickly racemize in solution; this combination is very rare, and hence the compounds used are often not available commercially but need to be prepared and purified within the laboratory. This makes it beneficial to highlight some potential mechanisms and exclude other mechanisms based on the results of fundamental models using the mechanisms being investigated. In this way experimental studies can be optimized in order to search mainly the most probable mechanisms for the process.

Other studies have applied different mathematical modeling techniques to model Viedma ripening (deracemization in systems using grinding) and Ostwald ripening based on considerations including growth and dissolution. Iggland and Mazzotti (Iggland and Mazzotti, 2013) solved the full population balance including the use of size dependent solubility to model Ostwald ripening and concluded that the size-dependent solubility could induce deracemization. Ricci et al. (Ricci et al., 2013) investigated Viedma ripening using Monte-Carlo simulations. They conclude that "*size-dependent crystal solubility alone is insufficient to reproduce most of the experimental signatures of Viedma ripening, and that some form of a solid-phase chiral feedback mechanism must be invoked in order to reproduce experimentally observed behavior*". The apparent contradiction between these two results indicates that further work modeling such systems using a range of methods is warranted. Further work modeling Viedma ripening was made by Gherase et al. (Gherase et al., 2014), who modified the population balance formulation of Iggland and Mazzotti to include a surface area dependence for the mass transfer coefficient as well as the size-

dependent solubility model. This model suggests that the main factors driving deracemization may be the differences in the sizes and surface areas of the crystals of the two enantiomorphs, which is related to differences in sizes and numbers of crystals. In this model, agglomeration of “like-handed” particles is not needed to achieve amplification of the *e.e.*

Steendam et al. (Steendam et al., 2013) have recently experimentally investigated the effect of chiral impurities on Viedma ripening. It is known that even very small levels of impurities can have significant effects on crystal growth (and potentially dissolution) kinetics. Chiral impurities will have different effects for the two enantiomorphs and thus may influence the deracemization; in fact, it is shown that the deracemization does not progress to either one of the two enantiomorphs with equal probability, thus clearly illustrating the effect of the chiral impurity. However, this effect can be removed by enhancing the grinding, thus increasing the ratio of surface area to impurity concentration. The effect could also be removed with small amounts of chiral additive. This has a bearing on the present study since it shows that, under certain circumstances, the crystal growth kinetics of the two enantiomorphs may differ.

3.3 Conceptual Model Development

An initial thought was that deracemization could occur in systems where there is no difference between the crystal growth rate kinetics of the two enantiomorphs, and where there is no crystal GRD (growth rate occurs according to McCabe’s ΔL law) if there is an initial asymmetry in the crystal size distributions (CSD) of the two enantiomorphs. It could be imagined that dissolution cycles destroy more of the

population of the enantiomorph having a smaller mean crystal size, thus altering the *e.e.* Initial simulations modeling this effect show that this phenomenon does change the *e.e.* in the first dissolution-recrystallization cycle, but after this first cycle the two crystal populations oscillate between two fixed particle size distributions, and subsequent cycles make no change in the *e.e.* This mechanism is not a potential cause of the deracemization and will not be discussed further. It should be noted that, if the initial mean particle sizes of the two enantiomorphs are very large and a very large fraction of the suspension is dissolved, then a small population of the crystals of the larger enantiomorph survive to grow (in an autoseeded preferential crystallization (G. Coquerel; Levilain and Coquerel, 2010)) during the cooling part of the cycle, potentially leading to 100% *e.e.* in a single cycle. This is clearly not occurred in the experiments described in the prior experimental work (Suwannasang et al., 2013). An illustration of a simulation of this model is shown in Appendix C.1.

Based on the inability of McCabe's ΔL law with equal growth kinetics for the two enantiomorphs to explain the deracemization, two potential mechanisms are proposed that might explain the temperature-induced deracemization, and simple mathematical models, based on fundamental laws of crystal growth and dissolution kinetics, were made in order to check whether the proposed mechanisms are possible causes of the deracemization. The models should be able to reproduce the sigmoidal evolution of *e.e.* in the solid phase that is typically found in the deracemization experiments. The physical system to be modeled is illustrated in Figure 3.2. If simulation of a particular mechanism produces changes in *e.e.* that closely match the experimental trends, it provides a starting point for experimental validation of the mechanism for the process of deracemization.

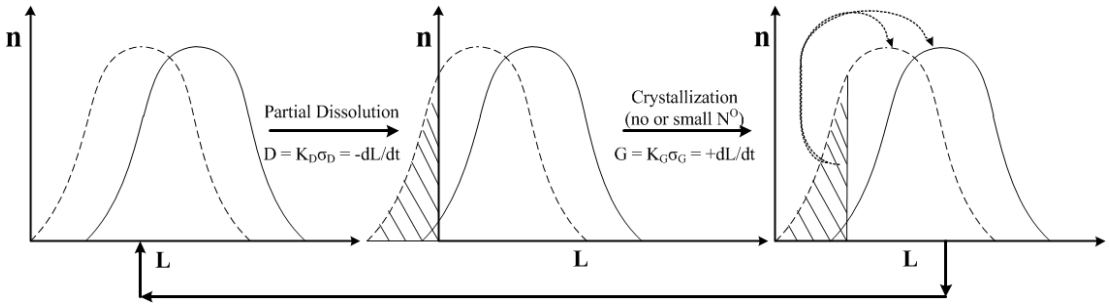

Figure 3.2 Schematic representation of the CSD during a partial dissolution/ recrystallization cycle. In the solution phase, fast racemization occurs to maintain equal amounts of the two enantiomers in solution.

In a typical deracemization experiment, a cycle in a temperature program consists of four steps: holding at 20°C for 5 min, ramping to 30°C over a period of 5 min, holding at 30°C for 5 min, then ramping down to 20°C over a period of 45 min. In this program, the time required for a cycle is 1 h. The cooling part of the cycle is deliberately performed slowly in order to promote crystal growth by maintaining a small supersaturation level and thus to inhibit crystal nucleation. The crystals in suspension were partially dissolved during the heating period. The remaining seeds then recrystallize and grow during the cooling period by consumption of the supersaturation in the solution phase. The amount recrystallized is the same amount as the mass lost during the heating step.

It is assumed in the simulations that the cycles are short enough and the supersaturation during growth is low enough so that nucleation does not occur for either enantiomorph. Crystal breakage and agglomeration are unlikely for the gentle agitation used in the experiments and are not considered in the models.

Two models are proposed to provide possible explanations of the experimental results. In the first model (Model 1), the two enantiomorphs have slightly different mean crystal growth rates, but the initial CSD and mass of the two populations are the same. In this model there is no crystal GRD for either enantiomorph. In the second model (Model 2), the two populations have the same initial CSD and mass: the two enantiomorphs have slightly different amounts of GRD but their mean crystal growth rate is equal.

3.4 Model 1: Simulation with Difference in Growth Rate Kinetics

The first model considers what can occur if there is a difference in the crystal growth rate kinetics of the two enantiomorphs related to the history of the crystals in the suspension. The two enantiomorphs possibly nucleate at different times where the primary nuclei of the two enantiomorphs occur at different levels of supersaturation and/or temperature. This causes the populations of the two enantiomorphs to have different crystal growth kinetics due to differences in internal crystal perfection or thermodynamic stability.

The assumptions in this model are: (i) there is no crystal GRD for either enantiomorph, (ii) size-independent crystal growth, (iii) no nucleation, breakage, nor agglomeration occur during the crystallization. The model uses only the average growth rate (or dissolution rate) during a cooling (or heating) part of a cycle. This is sufficient to find the CSD at the beginning and end of a cycle since each crystal in a particular population will grow or dissolve by the same ΔL, and therefore the CSD can be found by knowing the mass of crystal that is present at saturation. This is known since the solution of the population balance for a system in which there is no

nucleation, agglomeration nor breakage is a traveling wave, and hence the CSD at the end of a cycle will be the same function as at the beginning of the cycle, but shifted along the length axis. The ratio of the average growth rates of the two forms will be in the same as the ratio of the crystal growth activities (and therefore the ratio of the two growth rates at any point in time during a cooling cycle). The model uses the same dissolution rate kinetics for the two forms (since dissolution is often assumed to be mass transfer controlled).

Initial simulations were performed with the growth rates of the *R*- and *S*-forms being a constant ratio, for instance $\bar{G}_{S\text{-}} = 0.8\bar{G}_{R\text{-}}$. The *e.e.* evolved over time up to 100%; however, the evolution did not show the sigmoidal curve characteristic of the experimental results. Since the simulation results did not show the same functional form as the experimental results, the simulations were modified such that the two populations start with the same reduced growth rates (due to poor quality in the nuclei initially formed), but the crystals of both enantiomorphs undergo maturation due to the heating and cooling cycles such that their growth rates change. The model assumes that this maturation or healing process occurs at different rates for the two enantiomorphs, with the maturation of the *R*-crystals being significantly faster than that for the *S*-crystals, perhaps due to the poorer internal perfection of the *S*-crystals. The ratio of the growth rates (rate of slow maturing crystal/rate of fast maturing crystal) followed an exponential decay down to a constant value. This is due to the assumption that the slow maturing *S*-crystals nucleated under harsher conditions than the *R*-crystals (Jones and Larson, 1999, 2000).

Table 3.1 Key features of the two models.

	Model 1	Model 2
Initial CSD of *R*- and *S*-	equal; normal distributions	equal; monosize
Initial masses of *R*- and *S*-	equal	equal
Mean crystal growth rate	different, with the ratio $\frac{\overline{G}^{S-}}{\overline{G}^{R-}}$ being time dependent	equal (until slow growers in the distribution are fully dissolved)
Crystal GRD	none	modeled using discrete GRD

The first model is initiated with two equal population densities of *R*- and *S*-enantiomorphs. The CSD are assumed to be normal (Gaussian) distributions for the modeling here, with the exception that, due to the dissolution process, some of the smallest crystals completely disappear and are not replaced by nucleation (therefore, the number of particles decreases during the process), leaving the CSD without a lower tail; the distribution is cut at a size L_{min}. The CSD for the *S*-crystals after growth (Figure 3.2) illustrates this phenomenon. Table 3.1 summarizes the conditions used in this model (and the second model used).

The key to the present models is that, under the conditions assumed (no nucleation, agglomeration nor breakage in a batch system), solving the full population balance over time is not necessary, since the solution is known to be a travelling wave. The shape of the CSD at the end of a heating or cooling cycle (assuming that

equilibrium has been reached at that time) can be related to the initial CSD and a shift in size. The total masses of crystals at the beginning and end of the cycle are known (based on a mass balance for the solution and the saturation concentration at the high and low temperatures in the cycle). Thus, the correct solution can be found exactly via solving the third moment for the unknown parameter in the solution for the CSD, which is the amount by which the mode of the distribution has been shifted. The third moment and the number density distribution are defined by the equations:

$$\mu_3^{(i)} = \int_{L_{min}^{(i)}}^{\infty} \left\{ \left(L^{(i)}\right)^3 \cdot n^{(i)} \right\} dL^{(i)} \qquad \text{where } i = R\text{-}, S\text{-} \tag{3.1}$$

$$n^{(i)} = \begin{cases} 0 & \text{for } L < L_{min} \\ \frac{1}{(\sigma^{(i)})\sqrt{2\pi}} \exp\left(-\frac{(L^{(i)} - \bar{L}^{(i)})^2}{2(\sigma^{(i)})^2}\right) & \text{for } L_{min} \leq L < L_{\infty} \end{cases} \tag{3.2}$$

The third moment of the enantiomorph is proportional to the mass of this enantiomorph in the crystal phase. The initial total third moment is defined as:

$$\mu_{3,(j=0)}^{T} = \mu_{3,(j=0)}^{R-} + \mu_{3,(j=0)}^{S-} \tag{3.3}$$

This is also the total third moment for the suspension after the saturation point has been reached at the lower temperature for any cycle *j* because the same amount of crystal must occur whenever the system reaches saturation at this temperature.

The linear measure of particles size, rather than the volume of the particle, is chosen as the independent variable because the crystal growth rate is usually found to be approximately size independent if formulated in the term of an increase in a linear

dimension. The growth rate is a strong function of size if described in term of a volumetric increase, and so this form is unsuited to this modeling.

The average dissolution rates of all crystals of both enantiomorphs are the same during every heating cycle. At end of the dissolution period, the minimum size (L^{R-}_{minD}, L^{S-}_{minD}) of both populations are calculated using Maple 9.5. The equations to solve at the dissolution part at any cycle *j* are the following expressions:

$$\mu^{R-}_{3,D(j)} + \mu^{S-}_{3,D(j)} = (1 - FD) \cdot \mu^{T}_{3,G(j-1)} \tag{3.4}$$

where FD is the fraction of the suspension mass dissolved due to the change in the saturation temperature. The third moments of the *R*- and *S*- populations are

$$\mu^{R-}_{3,D(j)} = \int_{L^{R-}_{minD(j)}}^{\infty} \left\{ L^3 \cdot \frac{1}{(\sigma^{R-})\sqrt{2\pi}} \exp\left(-\frac{\left(L - \bar{L}^{R-}_{D(j)}\right)^2}{2(\sigma^{R-})^2} \right) \right\} dL \tag{3.5}$$

$$\mu^{S-}_{3,D(j)} = \int_{L^{S-}_{minD(j)}}^{\infty} \left\{ L^3 \cdot \frac{1}{(\sigma^{S-})\sqrt{2\pi}} \exp\left(-\frac{\left(L - \bar{L}^{S-}_{D(j)}\right)^2}{2(\sigma^{S-})^2} \right) \right\} dL \tag{3.6}$$

The lower limits of the populations ($L^{S-}_{minD(j)}$ and $L^{R-}_{minD(j)}$) may be zero if the smallest crystals in the population are entirely destroyed in the dissolution step or may be greater than zero if the amount of mass dissolved is not sufficient to destroy the smallest crystals.

The means of both populations will also change during a cycle (*j*) by the decrease in the size due to dissolution ($\Delta L^{(i)}_{D(j)}$) during the heating period, and the increase in the size of crystals due to crystal growth ($\Delta L^{(i)}_{G(j)}$) during the cooling

period. However, the shapes of the populations at the beginning and the end of the cycle are the same (since all crystals in the population may be assumed to be growing or dissolving with the same rate at any particular time), with the possible exception of the amount of the lower tail which no longer exists. Therefore

$$L^{i}_{\mathrm{minD(j)}} = L^{i}_{\mathrm{minG(j-1)}} - \Delta L^{i}_{\mathrm{D(j)}} \quad ; L^{i}_{\mathrm{minG(j=0)}} = 0 \quad i = R\text{-}, S\text{-} \tag{3.7}$$

where: $L^{i}_{\mathrm{minD(j)}}$ is the minimum size of *i* crystals after the heating period of cycle *j*.

$L^{i}_{\mathrm{minG(j)}}$ is the minimum size of *i* crystals after the cooling period of cycle *j*.

$\Delta L^{i}_{\mathrm{D(j)}}$ is the change in the size of any *i* crystals due to dissolution during the heating period *j*.

$$\bar{L}^{i}_{\mathrm{D(j)}} = \bar{L}^{i}_{\mathrm{G(j-1)}} - \Delta L^{i}_{\mathrm{D(j)}} \quad ; \bar{L}^{i}_{\mathrm{G(j=0)}} = \bar{L}^{i}_{\mathrm{initial}} \tag{3.8}$$

where $\bar{L}^{i}_{\mathrm{D(j)}}$ is the mean of the population density of the *i* enantiomorph after the heating period of cycle *j*.

$\bar{L}^{i}_{\mathrm{G(j-1)}}$ is the mean of the population density of the *i* enantiomorph after the previous cooling period.

The crystal size (L) cannot take on negative values; thus, the lower integration limit will be taken as zero when $L_{\mathrm{minD(j)}}$ is a negative value. Then, Eq. 3.4 will be calculated again by setting the value of $L_{\mathrm{minD(j)}}$ to zero.

It is important to note that, in this model, the focus is on an average (over the time period of the cycle) growth rate of all crystals of an enantiomer during the cooling part of the cycle.

The ratio of the growth rates of the *S*-crystals to the growth rate of the *R*-crystals decays over time and is dependent on the number of cycle *j* that the crystals have experienced. This is since both crystals are maturing due to the growth and dissolution cycles; however, the *R*-crystals are healing at a faster rate than the *S*-crystals. Initially, the ratio of the growth rates is unity; after the first cycle, the ratio decreases via an exponential decay function until it reaches some constant value, $\mathrm{G}_{\mathrm{j}\to\infty}^{\mathrm{S}-}/\mathrm{G}_{\mathrm{j}\to\infty}^{\mathrm{R}-}$, as shown by Eq. 3.9:

$$\frac{\bar{\mathrm{G}}_{(\mathrm{j})}^{S-}}{\bar{\mathrm{G}}_{(\mathrm{j}\to\infty)}^{R-}} = \frac{\bar{\mathrm{G}}_{(\mathrm{j}\to\infty)}^{S-}}{\bar{\mathrm{G}}_{(\mathrm{j}\to\infty)}^{R-}} + \left[1 - \frac{\bar{\mathrm{G}}_{(\mathrm{j}\to\infty)}^{S-}}{\bar{\mathrm{G}}_{(\mathrm{j}\to\infty)}^{R-}}\right] \cdot \exp\left(-\frac{\mathrm{j}}{\tau_{\mathrm{G}}^{S-}}\right) \tag{3.9}$$

where j = 1,2,3, ...

The variable τ_G^{S-} (which may also be considered as its inverse *b* in the exponential decay model) is a time constant that determines the rate at which the growth activity of the fast growing enantiomorph exceeds the value of the slow grower.

The average values of crystal growth activities for *R*- and *S*- enantiomorphs are different, so that the change in length of an *R*- and *S*-crystal during a cycle will be related to the ratio of the growth activities, or equivalently the ratio of the mean growth rates, of the enantiomorphs during the cycle. The relation of changing in size between *R*- and *S*- enantiomorphs is given by:

$$\Delta \mathrm{L}_{\mathrm{G(j)}}^{S-} = \Delta \mathrm{L}_{\mathrm{G(j)}}^{R-} \cdot \frac{\bar{\mathrm{G}}_{(\mathrm{j})}^{S-}}{\bar{\mathrm{G}}_{(j)}^{R-}} \tag{3.10}$$

The last term on the right is the ratio of the growth activities of the two enantiomorphs during cycle *j*. Equation 3.10 allows the change in size for the *S*-crystals to be known in terms of the change in size of the *R*-crystals, and means that there is only one variable to be solved for in the equation for the known third moment. The value of the change in size of *S*-crystals is then found from the change in size of *R*-crystals. The equations for solving the minimum size of the *R*- and *S*- populations (L^{R-}_{minG}, L^{S-}_{minG}) after a growth period for any cycle *j* are the following expressions:

$$\mu^{R-}_{3,G(j)} + \mu^{S-}_{3,G(j)} = \mu^{T}_{3} \tag{3.11}$$

The equation for the third moment of the *R*- and *S*- populations are expressed below:

$$\mu^{R-}_{3,G(j)} = \int_{L^{R-}_{minG(j)}}^{\infty} \left\{ L^3 \cdot \frac{1}{(\sigma^{R-})\sqrt{2\pi}} \exp\left(-\frac{\left(L-\bar{L}^{R-}_{G(j)}\right)^2}{2(\sigma^{R-})^2} \right) \right\} dL \tag{3.12}$$

$$\mu^{S-}_{3,G(j)} = \int_{L^{S-}_{minG(j)}}^{\infty} \left\{ L^3 \cdot \frac{1}{(\sigma^{S-})\sqrt{2\pi}} \exp\left(-\frac{\left(L-\bar{L}^{S-}_{G(j)}\right)^2}{2(\sigma^{S-})^2} \right) \right\} dL \tag{3.13}$$

$$L^{i}_{minG(j)} = L^{i}_{minD(j)} + \Delta L^{i}_{G(j)} \tag{3.14}$$

where $\Delta L^{i}_{G(j)}$ is the change in the size of *i* crystals due to growth during the cooling period. The crystals at the mode of the Gaussian distribution ($\bar{L}^{i}_{G(j)}$) will also grow by the same amount, and therefore

$$\bar{L}^{i}_{G(j)} = \bar{L}^{i}_{D(j)} + \Delta L^{i}_{G(j)} \tag{3.15}$$

The *e.e.* in the crystalline phase is then calculated for each cycle after cooling period (based on the known population density of both enantiomorphs present) by the third moments.

$$e.e._{(j)} = \left| \frac{\mu_{3,G(j)}^{R-} - \mu_{3,G(j)}^{S-}}{\mu_{3,G(j)}^{R-} + \mu_{3,G(j)}^{S-}} \right| \text{ x } 100\% \qquad (3.16)$$

The simple mathematical model presented above has several parameters that can be varied; initial CSD, growth rate functions, the final ratio of the growth rates of the two enantiomers, the time constant of the growth rate divergence, the percentage of the crystal mass dissolving in the heating part of the cycle, and so on. Some of these parameters were chosen to be keep constant, based on likely conditions in the deracemization experiments. Some parameters of interest, such as the time constant for the growth rate divergence, the final ratio of growth rates between the two enantiomers, and the percentage of the crystal mass dissolved during a deracemization, were varied. The initial CSD of the two enantiomorphs were equal for all simulations using this model.

In this section, the effect of three key parameters on the crystals growth are investigated, considering time-varying changes in the relative growth rates of the two populations but no GRD. The enantiomorphs have the same initial CSD and mass at the beginning of the simulation. By solving this model, the parameters as in Table 3.2 are considered.

Table 3.2 Parameters for the simulations using Model 1.

Exp. no.	τ_D^{R-}	τ_D^{S-}	D^{R-}	D^{S-}	τ_G^{S-}	$\overline{G}_{(j\to\infty)}^{S-}/\overline{G}_{(j\to\infty)}^{R-}$	%Dissolved
1	0	0	0.1	0.1	2.5, 5, 10	0.50	20
2	0	0	0.1	0.1	2.5, 5, 10	0.667	20
3	0	0	0.1	0.1	5	0.5, 0.667	20,25,30

To have a quantitative understanding of the kinetics, a computer code was developed in Maple 9.5 to simulate the system described by Eqs. 3.1 - 3.16. The thermal cycle consists of heating steps during which the suspension is dissolved to a saturation point at the high temperature, and then a cooling step where the crystals in the suspension are grown until the solution reaches the saturation point at the low temperature. The temperature cycles are arbitrarily set at 1 h, to agree with the cycles in the earlier experimental work. These temperature cycles were continued over a large number of cycles until deracemization was substantial. The main structure of the code is as follows:

(a) Crystals of the two enantiomorphs in the suspension are partially dissolved during the heating period with an equal dissolution rate, *D*. The dissolution of all crystals is equal and size independent. The change in the size of crystals due to dissolution (ΔL_D) is calculated to reduce the third moment to the value required based on the fraction of crystals that is dissolved between the two temperatures in the cycle.

(b) When step (a) is completed, the minimum crystal sizes of both enantiomorphs are calculated. These two sizes will be used in next crystal regrowth step.

(c) The remaining crystals then regrow during the cooling period by consumption of the supersaturation in the solution phase, with different mean growth rates for *R*- and *S*-crystals. This step is based on the mass regrown being the same as the mass lost during the dissolution step. The total third moment of crystals, based on regrowth of crystals to the same crystal mass as initially given in the suspension, is used to calculate the increase in size of the crystals, ΔL_G^{R-}, and ΔL_G^{S-}, the ratio of which is the same as the ratio of the growth rates of *R*- and *S*- crystals.

(d) The minimum crystal sizes of the two enantiomorphs are calculated again. These two new sizes will be used for calculating the third moments of both populations, and for use in the next dissolution cycle.

(e) The two new third moments of the populations, after the cooling step, will be used to calculate the *e.e.* in the solid phase.

(f) The simulation will be run using the same steps, (a) - (e), until complete deracemization (> 99% *e.e.*) is achieved. For each new cycle, the relative growth rate of the *S*-enantiomorph to the *R*-enantiomorph must be recalculated according to the change in growth activity, via Eq. 3.9.

3.4.1 Simulations and Parameter Analysis of Model 1

The results are presented in three parts. The model could describe the complete chiral resolution by temperature fluctuations induced by dissolution and regrowth of crystals combined with fast racemization in the solution phase and the entrainment effect. Simulations are presented by varying four sets of parameters in order to validate the simple mathematical model. Initial experiments where the ratio of the growth rate ratio was maintained at a constant value (but not unity) produced an

e.e. that evolved to reach 100%, but the evolution was not sigmoidal. Since the simulation did not agree with the experimental results, this type of simulation was not continued.

However, when considering a condition in which the ratio of the growth rates of the enantiomorphs is initially unity but then decays due to the *R*-enantiomorph maturing more quickly than the *S*-enantiomorph (based on Eq. 3.9) down to a constant value, the sigmoidal function of the *e.e.* is found, as shown in the results of the next simulations which fit the form of the experimental data well.

3.4.1.1 Simulation 1A: effect of the time constant in the growth rate model

In this simulation, the deracemization with time-dependent difference in the growth rate activities of the *R*- and *S*- crystals, as described above, is investigated. The ratio of the growth activities is described by Eq. 3.9. The decay in the growth activity ratio has a time constant τ cycles, or b^{-1}.

The simulations were carried out with same initial conditions (initial crystal mass and initial CSD) and the same dissolution rates for both enantiomorphs. In the first simulations using this model, the total percentage of crystal mass dissolved during the heating period was set at 20%. The final growth rate ratio of *S*- and *R*- crystals $\left(\overline{G}^{S}_{(j\to\infty)}/\overline{G}^{R}_{(j\to\infty)}\right)$ was set at 0.5. This difference in the growth rates is a relatively large one, but not outside the expected values when experimental variations in growth rates are considered. A large value was initially used in the simulation to test the if the evolution of *e.e.* was consistent with experiments, without making the simulation too lengthy or continuing for too many

cycles. The effect of the exponential decay constant, *b*, on the evolution of *e.e.* of the solid was investigated by setting the value of *b* at 0.1, 0.2, or 0.4 h^{-1}.

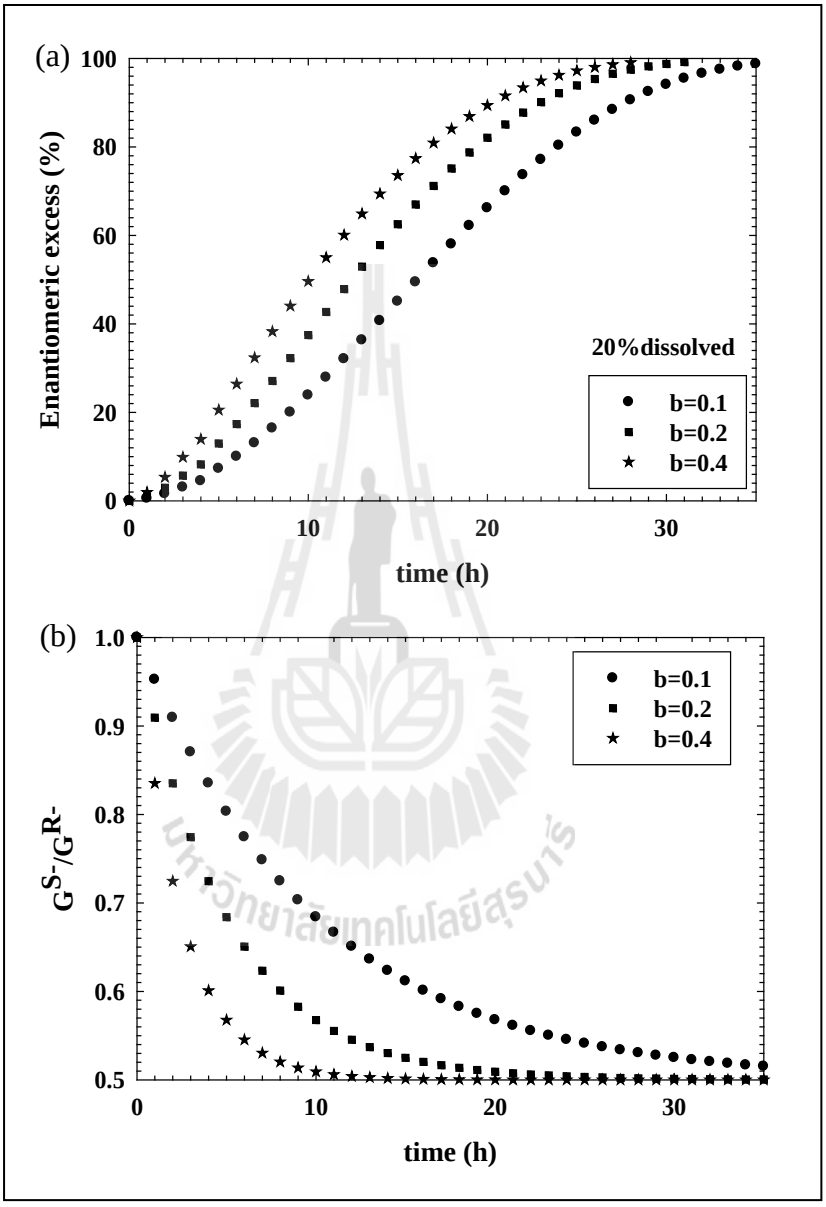

Figure 3.3 (a) Evolution of the solid phase *e.e.* when 20% of the crystal mass is dissolved in the heating step, based on growth rate ratios in (b). (b) Ratio of the growth rate of *S*- and *R*- enantiomorphs for a final value of 0.5 and various time constants, *b*.

The results for these simulations are illustrated in Figure 3.3, showing the effect of the exponential decay constant, b (the inverse of the decay time constant). This is a critical parameter since it will determine the effect of the mean crystal growth rate of the counter-enantiomer. Poor crystal perfection or poor maturation of the counter-enantiomer (arbitrarily assumed to be the *S*-enantiomorph here) will lead to a quicker decay in the growth rate (Figure 3.3b) and result in a smaller time required to achieve complete chiral purity (Figure 3.3a). The number of cycles needed in this simulation was smaller than seen in experimental results, presumably because of the large ratio of the growth rates of the two enantiomorphs.

It is also important to note that the same effect (a time-dependent ratio of the growth kinetics of the two enantiomorphs) may also be apparent if there is a chiral impurity in the system which, by transient adsorption onto the surface of one enantiomer, causes a time-dependent reduction in the growth rate of this enantiomer. The explanation of the maturation effect is preferred by the authors, since such chiral impurities were not evident in any of our experiments concerning the temperature cycle-induced deracemization.

3.4.1.2 Simulation 1B: effect of the steady state ratio of the growth rates of the two enantiomorphs

In this simulation, the same set of conditions was investigated as in Simulation 1A; however, the ratio of the growth rates of the two enantiomorphs at steady state is 0.667, rather than 0.5 as in Simulation 1A.

The evolution of the solid phase *e.e.* is shown in Figure 3.4a. In Simulations 1A and 1B, which differ only in the steady state growth rate ratio, the results show a similar tendency in the evolution of *e.e.*

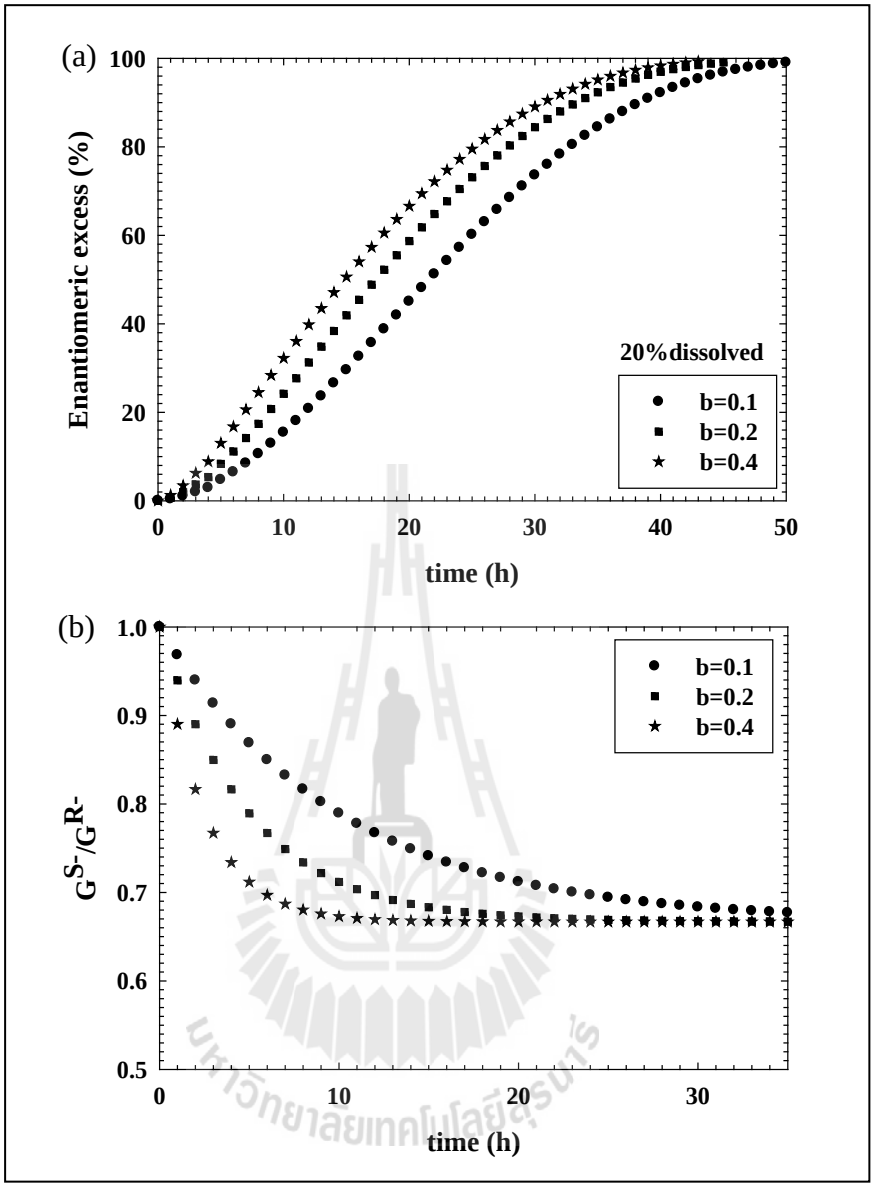

Figure 3.4 (a) Evolution of the solid phase *e.e.* when 20% of the crystal mass is dissolved in the heating step, based on the growth rate ratios in (b). (b) Ratio of the growth rate of the *S*- and *R*- enantiomorphs for a final value of 0.667 and various time constants, *b*.

The time required to achieve complete chiral purity is shorter when the counter-enantiomer (*S*-) has poorer crystal quality (higher values of *b* or

smaller value of τ), as illustrated in Figure 3.4a. Moreover, the evolution of *e.e.* when using different ratios of the final growth rates is different even when the same value of *b* is used. A smaller ratio results in a slower evolution of the *e.e.*

3.4.1.3 Simulation 1C: effect of the percentage of the crystal mass dissolved during a heating part of a cycle

The effect of the percentage of the crystal mass dissolved during a heating cycle on the evolution of *e.e.* was studied in this simulation. The simulations were carried out with the same conditions as in the first and the second simulations; however, here the percentage of crystal mass dissolved was set at 20%, 25%, or 30%. The simulation results are similar to the experimental results in a previously published article (Suwannasang et al., 2013); the time required to achieve complete resolution is shorter when the mass of crystals dissolved in the heating cycle increases, as shown in Figure 3.5. However, this result is only valid when the same temperature program is maintained for all cycles and only the total number of cycles required for deracemization is considered. Optimization of the process would likely involve larger temperature cycles (greater differences between the higher and the lower temperature in the cycle) at the beginning of the deracemization, followed by smaller, quicker cycles near the end of the deracemization; experimental optimization using damping in the series of temperature cycles is demonstrated in the Chapter IV.

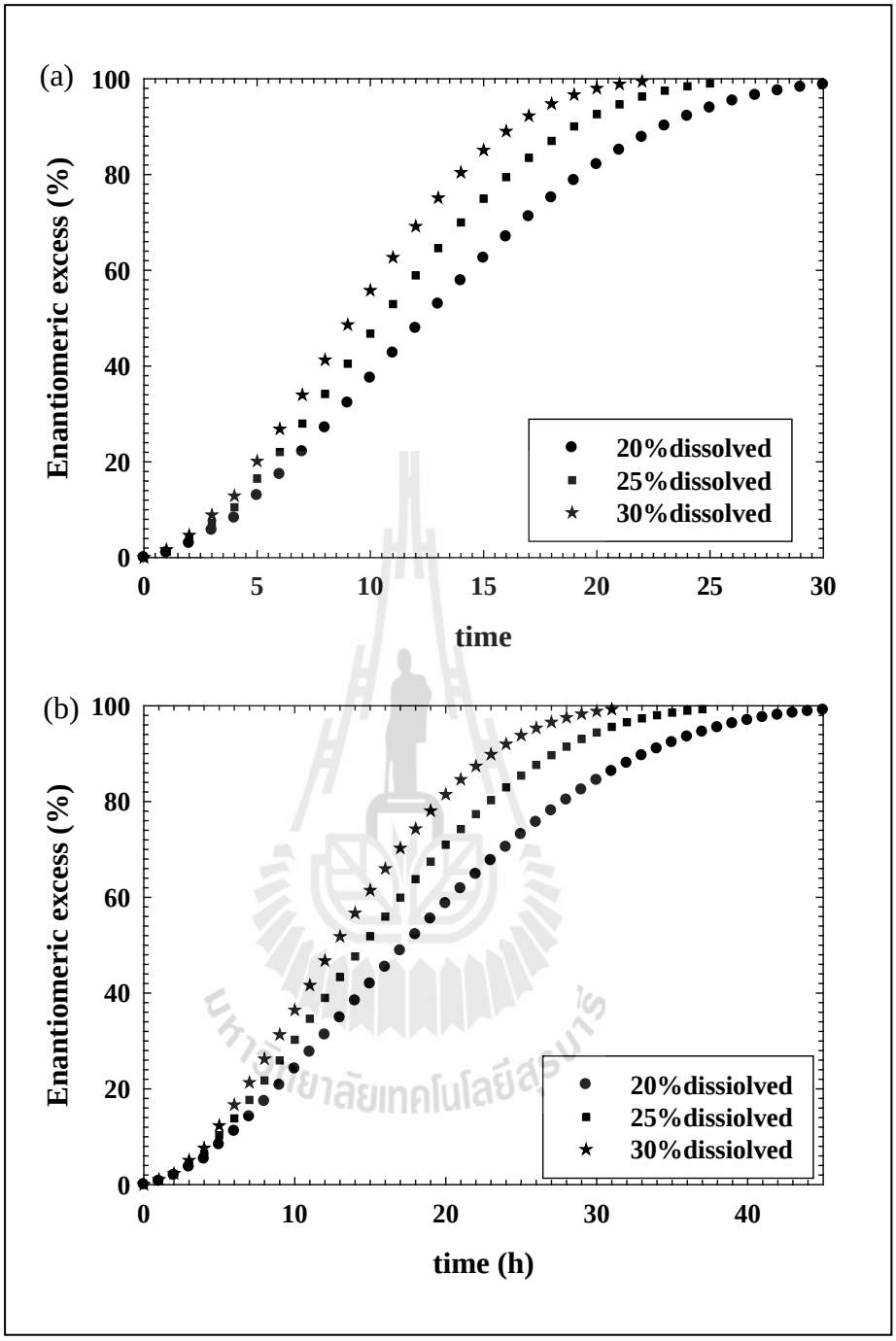

Figure 3.5 Evolution of the solid phase *e.e.* by setting the time constant at $b = 0.2$ and (a) $G^{S-}/G^{R-}_{(j\to\infty)} = 0.5$, (b) $G^{S-}/G^{R-}_{(j\to\infty)} = 0.667$, and by varying the percentage of the crystal mass dissolved in heating period.

3.5 Model 2: Simulation with Growth Rate Dispersion

A further set of simulations was performed with the assumption that the initial mass, the initial CSD (monosized crystals at 50 μm), and the mean of the crystal growth rate distributions of the two enantiomorphs were equal. However, the two enantiomorphs were assumed to have different levels of crystal growth dispersion. This is a difficult case to simulate since a two-dimensional (crystal size and crystal growth rate activity) population balance is required. Because it was uncertain whether this phenomenon could result in deracemization, it was decided to study a simple case that could be conveniently modeled. In this case, the population of growth activities is modeled with a small series of impulses rather than a continuous distribution of growth rate activities. These simulations can demonstrate whether this is a potential mechanism for the deracemization. The simulation of the system can then be performed in a similar way as for Model 1.

A simple case to simulate, for example, is when the mean crystal growth rates of the two enantiomorphs are equal but all *R*-crystals have a growth activity of 1 while half of the *S*-crystals have a growth activity of 1.1 (and are therefore fast growers) and the other half of the S-crystals have a growth activity of 0.9 (slow growers). This case is non-physical (the growth rate distributions are continuous functions in real systems), but it is a simple model that allows us to check whether GRD alone may be responsible for the deracemization of the suspension.

In solving this GRD model, the parameters in Table 3.3 were consider, where

- G_R is the growth rate of the *R*-crystals, G_S is the growth rate of the *S*-crystals
- $\overline{G}_R$ is the mean of the growth rate distribution of the *R*-crystals
- $\overline{G}_S$ is the mean of the growth rate distribution of the *S*-crystals

- FD is the fraction of mass dissolved, $L_{initial}$ is the initial size of crystals

Table 3.3 Initial parameters for the simulations of Model 2.

Exp. no.	G_R				$\overline{G}_R$	G_S				$\overline{G}_S$	FD	$L_{initial}$ (μm)
	1		2			1		2				
1	1.00		1.00		1.00	0.90		1.10		1.00	0.5	50
2	1.00		1.00		1.00	0.95		1.05		1.00	0.5	50
3	1.00		1.00		1.00	0.85		1.15		1.00	0.5	50
4	1.00		1.00		1.00	0.90		1.10		1.00	0.5	25
5	1.00		1.00		1.00	0.90		1.10		1.00	0.25	50
6	1.00	1.00	1.00	1.00	1.00	0.90	0.95	1.05	1.10	1.00	0.5	50
7	0.95		1.05		1.00	0.90		1.10		1.00	0.5	50

3.5.1 Simulations and Parameter Analysis of Model 2

The results of the simulations concerning GRD are shown in the Figures. 3.6 - 3.8. Simulations are presented by varying the GRD profile and the fraction of the suspension mass dissolved during the heating cycle, in order to determine whether GRD is a potential mechanism for the deracemization.

3.5.1.1 Simulation 2A: effect of the dispersion of the growth activity

The effect of dispersion of the growth activity of the two enantiomorphs is investigated during the recrystallization period. There are four crystals (or to extend the concept, four populations of crystals with the same number

of crystals in each population) considered in this simple simulation to model deracemization via GRD.

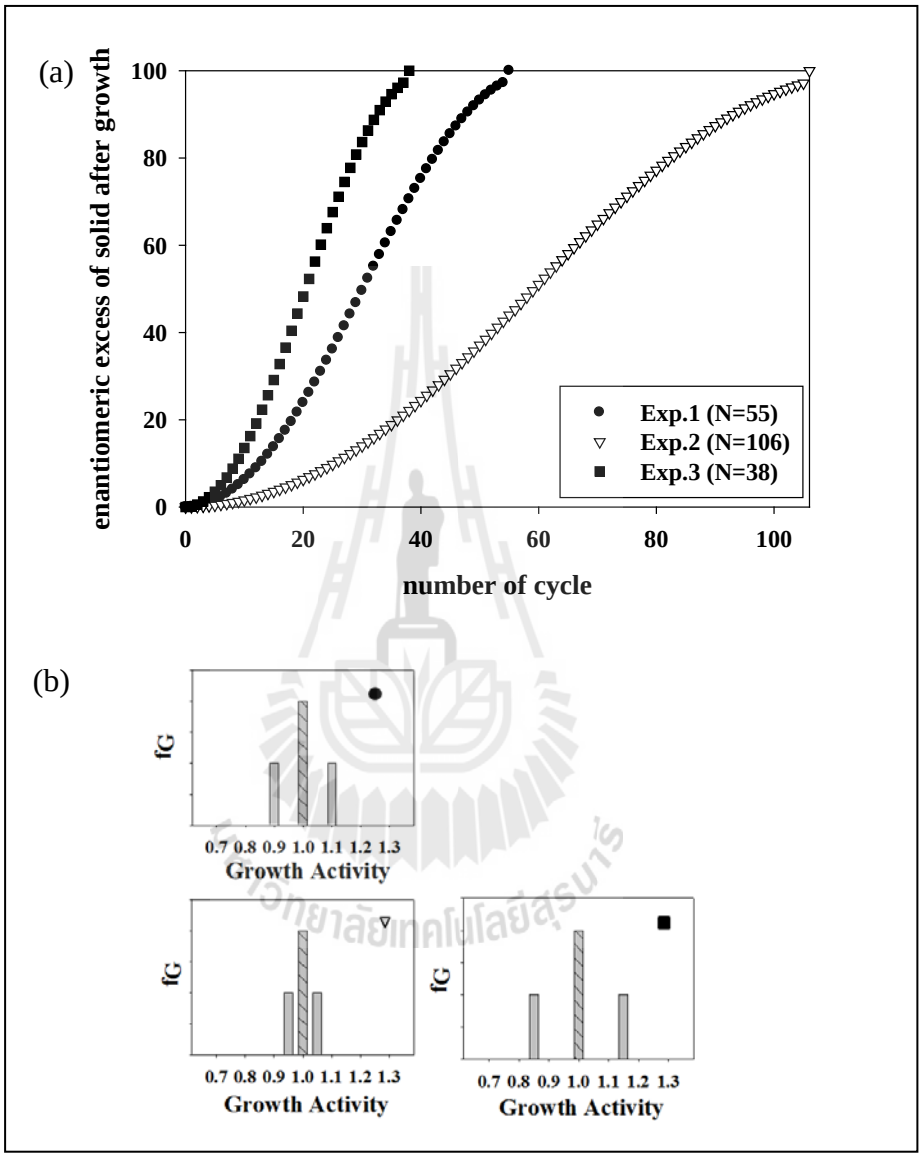

Figure 3.6 (a) Evolution of the solid phase *e.e* by dispersion of the growth activity when the two enantiomorphs have the same mean crystal growth rate activity. (b) The distribution of growth rate activity. The growth activity of *R*- is shown as the hatched bars.

The growth activity distributions for the *R*-enantiomorph and the *S*-enantiomorph are set based on the two enantiomorphs having the same mean growth rate activity but different levels of GRD. For example, the growth rate activity of two *R*-crystals can be set equal to unity, of the first *S*-crystal to less than unity, and of the other *S*-crystal to an equal amount greater than unity. The means of the growth rate distributions of both enantiomorphs are equal. The initial particle sizes of the four crystals are the same. The dissolution kinetics of the four crystals during the heating period are equal. The results of simulation 2A (Figure 3.6) show the progression of the deracemization as the GRD is varied, indicating that increasing the dispersion of rates in the more disperse crystal growth rate distribution hastens the deracemization.

3.5.1.2 Simulation 2B: effect of the initial size of the crystals

This simulation investigated the effect of the initial size of particles on the evolution of *e.e.* at a constant mass fraction of suspension dissolved. The distributions of the growth activities of both enantiomorphs are set by giving the two *R*-crystals a growth rate activity of 1 while one of the *S*-crystal populations has a growth activity of 0.9 and the other in the *S*-crystal population has a growth activity of 1.1. The experimental results are shown in Figure 3.7, which shows that the evolution of *e.e.* is not affected by the initial size of the crystals when the fraction dissolved is kept constant. Initially this result was surprising, but can be explained by the fact that a constant mass is dissolved; so, in each case, the fraction of the crystals dissolved in one cycle is the same, leading to a cycle displaying the same increase in *e.e*.

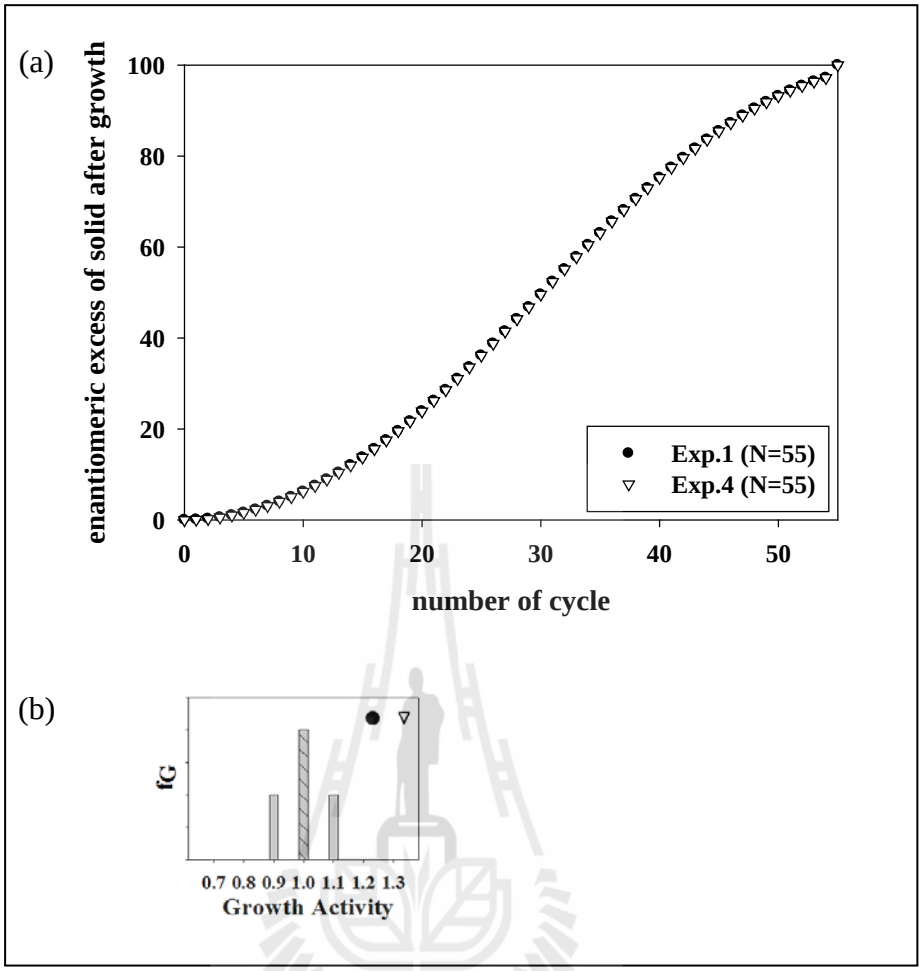

Figure 3.7 (a) Effect of the initial size of the two enantiomorphs on the evolution of the solid phase *e.e.* (●) Initial size = 50 μm; (▽) Initial size = 25 μm. (b) The distribution of growth rate activity. The growth activity of *R*- is shown as the hatched bars.

3.5.1.3 Simulation 2C: effect of the percentage of the crystal mass dissolved during a heating part of a cycle

The effect of the percentage of the suspension mass dissolved on the evolution of *e.e.* was investigated in simulation 2C. Simulations were performed with 25% and 50% of the crystal dissolving during the heating period of a

cycle. The percentage of the crystal mass dissolved can be experimentally varied either by varying the high and low temperatures in the cycle or by varying the suspension density in the vessel. The two populations have the same initial crystal size and have the growth rate distributions described in simulation 2A. The results of Simulation 2C are shown in Figure 3.8.

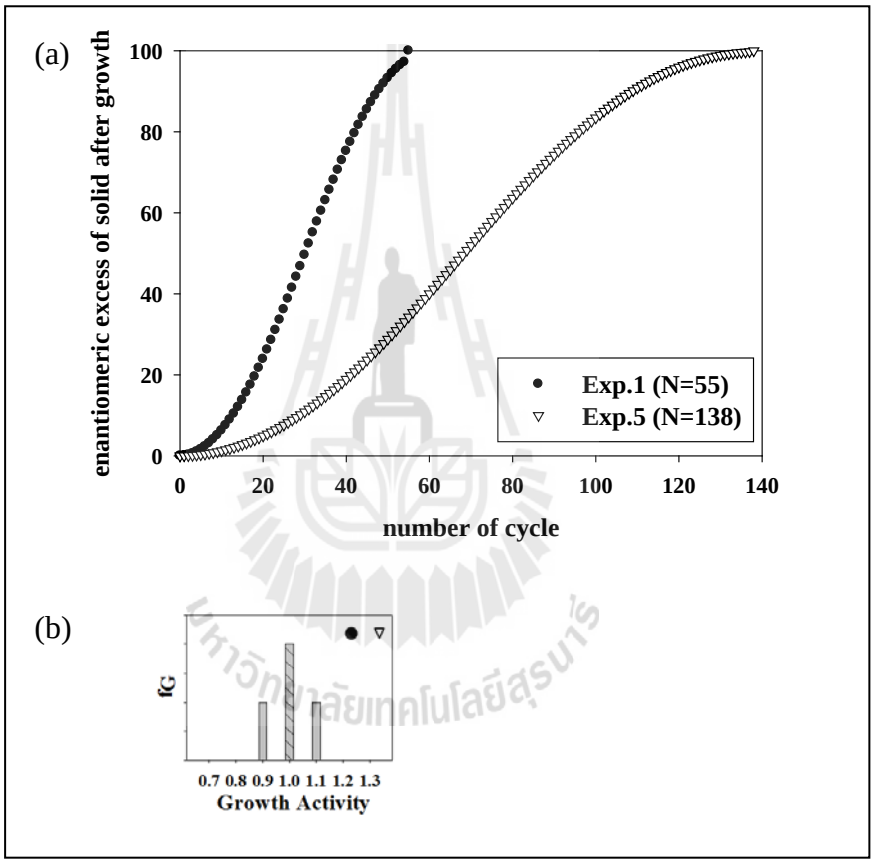

Figure 3.8 (a) Evolution of the solid phase *e.e.* when the percentage of the suspension mass dissolved is varied. (●) 50% dissolved, (▽) 25% dissolved. (b) The distribution of growth rate activity. The growth activity of *R*- is shown as the hatched bars.

Increasing the amount dissolved increases the rate of the deracemization, a result similar to the experimental results, where the number of cycles required is less when the amount of crystal dissolved is made larger (Suwannasang et al., 2013). However, there will be a limit to the improvement possible with higher amounts dissolved, because the higher amount dissolving will increase the driving force during the crystallization step, thus increasing the likelihood of nucleation of the two enantiomers occurs.

Further simulations were performed with different discretizations of the crystal growth rate distributions, e.g., smoothing the growth rate distribution of *S*- by using more discrete intervals, and also giving both *R*- and *S*- (different levels of) GRD. These results show similar trends to those already shown, and are not discussed here. Details and results of these simulations can be seen in Appendix C.2.

The models of the mechanism of deracemization due to crystal growth rate kinetics show the evolution of *e.e.* as a sigmoidal curve that matches the common experimental results of deracemization (Suwannasang et al., 2013). The two growth rate kinetic models are based on the population balance. The evolution in the *e.e.* could be explained by the fundamentals of crystal growth. In the growth kinetics model without GRD, the *e.e.* is increased due to the difference of the growth rate between the two enantiomorphs, which may be caused by the history of nucleation of the primary nuclei of the two enantiomorphs.

The other explanation for the mechanism of deracemization is crystal GRD. It can be seen that the slow grower of the disperse grower (the *S*-crystals) reduces to zero size relatively quickly; however, the *e.e.* of *S*-enantiomorph

still increases because the amount of mass gained by the fast grower of the *S*-crystals more than compensates for the loss in mass of the slow grower of the *S*-crystals. The *R*-crystals are eventually out-competed by the fast growing *S*-crystals, leading to complete deracemization. This last model (the GRD model) appears to be the most satisfactory explanation produced. The difference in the GRD may have resulted from the conditions experienced in the initial nucleation event (before the advent of the temperature cycles) as demonstrated in other materials by Jones and Larson (Jones and Larson, 1999), with the enantiomorphs having the larger GRD having initially nucleated at a higher supersaturation than the more well-behaved enantiomer with a smaller amount of GRD Experimental work following the particle size distribution event in deracemization due to temperature cycling could potentially clarify whether this mechanism is correct. In several types of deracemization experiment (Viedma ripening, deracemization with temperature cycles, deracemization using ultrasound), the time required to begin the deracemization varies strongly; perhaps the results presented here concerning the GRD of the enantiomorphs may help to explain why some deracemizations start evolving soon after the process is initiated while in other cases the initiation is slow.

3.6 Conclusions

In this work, the mechanism of chiral symmetry breaking towards a complete deracemization was described and tested by two simple mathematical models based on the fundamentals of crystal growth. A phenomenon relating to crystal growth may be responsible for the enhancement of *e.e.* when temperature cycling is applied to a racemic suspension of a conglomerate forming system where there is a swift

racemization in the solution phase. The possible mechanism for deracemization may come from the history of the nucleation, which is a stochastic process: The primary nuclei of the two enantiomorphs occur at slightly different times, and thus under the different levels of supersaturation and/or temperature, leading to different internal crystalline perfection and therefore slightly different thermodynamic stability. The results from the simulations are promising in that a very simple model can reproduce the sigmoidal form of the evolution in the enantiomeric excess. However, further experimental and modeling work is necessary to verify whether any of these hypotheses is correct. A study on the parameters associated with the crystal growth rate models could be a route to fill the gap in understanding of the deracemization process mechanism.

3.7 References

Cartwright, J. H. E., Piro, O., and Tuval, I. (2007). Ostwald Ripening, Chiral Crystallization, and the Common-Ancestor Effect. **Physical Review Letters.** 98: 165501.

G. Coquerel, P. (2007). **Springer GmbH**, pp. 1-50, ISSN: 0340-1022.

Gherase, D., Conroy, D., Matar, O. K., and Blackmond, D. G. (2014). Experimental and Theoretical Study of the Emergence of Single Chirality in Attrition-Enhanced Deracemization. **Crystal Growth & Design.** 14: 928-937.

Iggland, M., and Mazzotti, M. (2013). Solid state deracemisation through growth, dissolution and solution-phase racemisation. **CrystEngComm.** 15: 2319-2328.

John Garside, A. M., Jaroslav Nývlt, (2002). Measurement of Crystal Growth and Nucleation Rates. Second edition, **Institution of Chemical Engineers (IChemE)**. Rugby UK.

Jones, C. M., and Larson, M. A. (1999). Characterizing growth-rate dispersion of NaNO3 secondary nuclei. **AIChE Journal.** 45: 2128-2135.

Jones, C. M., and Larson, M. A. (2000). Using dislocations and integral strain to model the growth rates of secondary nuclei. **Chemical Engineering Science.** 55: 2563-2570.

Levilain, G., and Coquerel, G. (2010). Pitfalls and rewards of preferential crystallization. **CrystEngComm.** 12: 1983-1992.

McBride, J. M. (2008). Origins of Homochirality. A mechanism for deracemization by crystal grinding. **Lecture at NORDITA Workshop.** http://agenda.albanova.se/conferenceDisplay.py?confId=322.

Noorduin, W. L., van Enckevort, W. J. P., Meekes, H., Kaptein, B., Kellogg, R. M., Tully, J. C., McBride, J. M., and Vlieg, E. (2010). The Driving Mechanism Behind Attrition-Enhanced Deracemization. **Angewandte Chemie International Edition.** 49: 8435-8438.

Ricci, F., Stillinger, F. H., and Debenedetti, P. G. (2013). A computational investigation of attrition-enhanced chiral symmetry breaking in conglomerate crystals. **The Journal of Chemical Physics.** 139.

Steendam, R. R. E., Harmsen, B., Meekes, H., Enckevort, W. J. P. v., Kaptein, B., Kellogg, R. M., Raap, J., Rutjes, F. P. J. T., and Vlieg, E. (2013). Controlling the Effect of Chiral Impurities on Viedma Ripening. **Crystal Growth & Design.** 13: 4776-4780.

Suwannasang, K., Flood, A. E., Rougeot, C., and Coquerel, G. (2013). Using Programmed Heating–Cooling Cycles with Racemization in Solution for Complete Symmetry Breaking of a Conglomerate Forming System. **Crystal Growth & Design.** 13: 3498-3504.

Viedma, C. (2005). Chiral Symmetry Breaking During Crystallization: Complete Chiral Purity Induced by Nonlinear Autocatalysis and Recycling. **Physical Review Letters.** 94: 065504.

CHAPTER IV

BENEFIT OF TEMPERATURE FLUCTUATIONS IN A DAMPING PATTERN ON DERACEMIZATION OF A CONGLOMERATE SUSPENSION

4.1 Abstract

This current research has developed a new route for optimizing a process of deracemization via programmed heating-cooling cycles. Damped temperature cycles applied to a system in the presence of a swift racemization in solution phase has been investigated for deracemization of a racemic suspension of a conglomerate forming system. The difference of temperature between the high and the low parts of the cycles was reduced during the experimental period based on the response of the % *e.e.* in the solid phase, leading to an increase in the enantiomeric excess in the solid phase. Use of relatively large temperature swings initially helps to initiate the symmetry breaking of the racemic suspension faster, and once the response of the system accelerates the cycles can be made smaller and faster while still maintaining a good rate of evolution; therefore the system can be made more time and energy efficient. It was found that there was some grinding of crystals (due to the agitation) in an isothermal system however it was not sufficient to drive the *e.e* away from zero. Hence, the primary mechanisms resulting in deracemization in this system cannot be grinding nor Ostwald ripening. The SEM micrographs of the solid samples, which were taken during the experimental period, show that the amplification of the *e.e.* in

the solid phase is due to the dissolution and growth phenomenon induced by the damped temperature cycles. Racemization in solution, dissolution during the heating part of the cycles, crystal growth of the larger or faster growing crystals at the expense of the smaller or slower growing crystals during the cooling part of the cycles, and the entrainment effect where the mother liquor is maintained at 0% *e.e.* by the racemization reaction are responsible for this complete deracemization process.

4.2 Introduction

A pure enantiomer can be obtained from several methodologies such as chiral chromatography, biocatalytic processes, and resolution by crystallizations. Recently, a counterintuitive method, called Viedma ripening, has been used to obtain single handedness $NaClO_3$ crystals from a racemic suspension at a constant temperature by using a continuous abrasive grinding technique (Viedma, 2005). Three years later, inspired by Viedma, the group of Vlieg and Blackmond developed a new method for deracemization of an intrinsically chiral compound. This method combined the technique of Viedma ripening with a solution phase racemization (Noorduin et al., 2008a). The combined process has been rapidly extended to deracemize other organic chiral compounds (Levilain et al., 2009; Noorduin et al., 2009; Noorduin et al., 2008c; Tsogoeva et al., 2009; van der Meijden et al., 2009). Several scientists have attempted to explain the mechanism behind attrition-enhanced deracemization. (Cartwright et al., 2007; Iggland and Mazzotti, 2011; Katsuno and Uwaha, 2012; McBride, 2008; Noorduin et al., 2008b; Noorduin et al., 2010). However, their ideas on the mechanism of the attrition enhanced-deracemization have been in debate.

Recently, a new process of deracemization has been developed by our group, the use of programmed heating-cooling cycles combined with a swift racemization in solution for complete deracemization of a chiral organic compound (Suwannasang et al., 2013). The practical demonstration of this process was first shown for deracemization of 1-(4-chlorophenyl)-4,4-dimethyl-2-(1H-1,2,4-triazol-1-yl)pentan-3-one (Cl-Tak). This compound is a stable conglomerate and it is also easily racemized in the presence of a basic medium (Black et al., 1989). The novel deracemization process was also extended to deracemize another related organic compound as presented in this work. The model compound for this study is a 4,4-dimethyl-1-(p-toluyl)-2-(1H-1,2,4-triazol-1-yl)pentan-3-one (Me-Tak).

In the original experiments demonstrating the deracemization of Cl-Tak, a constant temperature difference between the high and low parts of the cycles was used throughout the entire period of the process. The experimental results showed a sigmoidal behavior in the evolution of *e.e.* in the solid phase (Suwannasang et al., 2013). This process appears to require a finite threshold in the *e.e.* to be achieved before the process becomes autocatalytic and the evolution in the *e.e.* becomes more rapid. This suggests that once the evolution in *e.e.* has been initiated then only smaller amounts of the minor enantiomer need to be dissolved. Hence, the use of constant amplitude temperature cycles seems to be suboptimal.

As a consequence, a new route for the optimization of the temperature cycle induced-deracemization process has been investigated. A pattern of temperature cycles was designed having large temperature swings in the cycles at the initial period of the process in order to initiate the symmetry breaking, and after that the amplitude of the later cycles is reduced based on the response of the *e.e.* in solid phase.

The chemical structures of the two compounds, Cl-Tak and Me-Tak investigated, are shown in Figure 4.

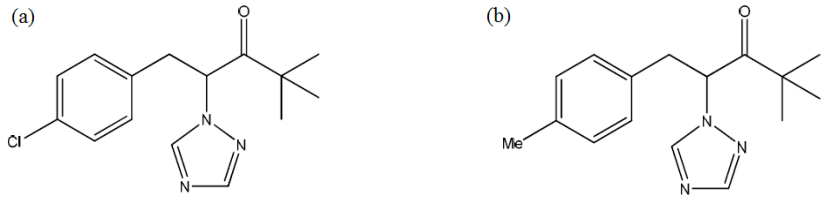

Figure 4.1 (a) Chemical Structure of Cl-Tak. (b) Chemical Structure of Me-Tak.

4.3 Experimental Section

4.3.1 Materials

Racemic 4,4-dimethyl-1-(p-toluyl)-2-(1H-1,2,4-triazol-1-yl)pentan-3-one (Me-Tak) was synthesized using the method of Rougeot (Rougeot, 2012).

Distilled water was used for deracemization experiments. HPLC-grade n-heptane and ethanol, and reagent-grade methanol were purchased from Fisher Scientific.

4.3.1.1 Starting Crystal Prepared by Solvent Evaporation (RM1)

Me-Tak was totally dissolved in a mixture of methanol/water (80/20 %wt) in the presence of NaOH (8 g per kg of solvent) as a racemizing agent. The solution was evaporated at 50°C under a vacuum of 270 mbar. Solids were washed with a sufficient amount of water to remove the rest of the sodium hydroxide. The solids were dried in an oven at 40°C. The preparation of this starting material is similar to the preparation of the starting material used in the Cl-Tak experiments.

4.3.1.2 Starting Crystals Prepared by Fast Cooling (RM2)

1.8 g of Me-Tak collected from RM1 was totally dissolved in 25 g of methanol/water mixture (65/35 %wt) in the presence of NaOH as a racemizing agent (0.2 g, i.e., 8 g per kg of solvent) at 35°C. The solvent mixture was chosen to ensure that an appropriate solubility of Me-Tak in the solvent mixture was achieved. The solutions were then filtrated using 0.2 micrometer pore size filters and dropped in a 50 mL round-bottomed thermostatted vessel at 35°C. The undersaturated solution was stirred by an oval magnetic bar operated at 500 rpm for 10 min in order to ensure that no nuclei remained in the system. Then the solution was cooled rapidly down to 20°C using cooling rate of 1 °C/min.

4.3.2 Deracemization Experiments

1.8 g of Me-Tak, 25 g of methanol/water mixture (65/35 %wt), and 0.2 g of NaOH were chosen as a standard solution for the Me-Tak experiments. One cycle in a loop of TPs consisted of four steps (Figure 4.2a); holding at 20°C for 5 min, heating up to the top temperature with a heating rate 2 °C/min, holding at the top temperature for 5 min, and then cooling down to 20°C with a cooling rate 10 °C/ 45 min. TP1 and TP2 were set with a constant amplitude of temperature fluctuations throughout the experiments (i.e. no damping pattern). The distinction between TP1 and TP2 is the maximum temperature in a cycle; TP1 has a maximum temperature of 25°C, while TP2 has a maximum temperature of 30°C (Figure 4.2a). TP3 is a set of damped temperature cycles consisting of large swings for the initial cycles and smaller temperature fluctuations in later cycles (in response to increases in the % *e.e.*) as depicted in Figure 4.2b.

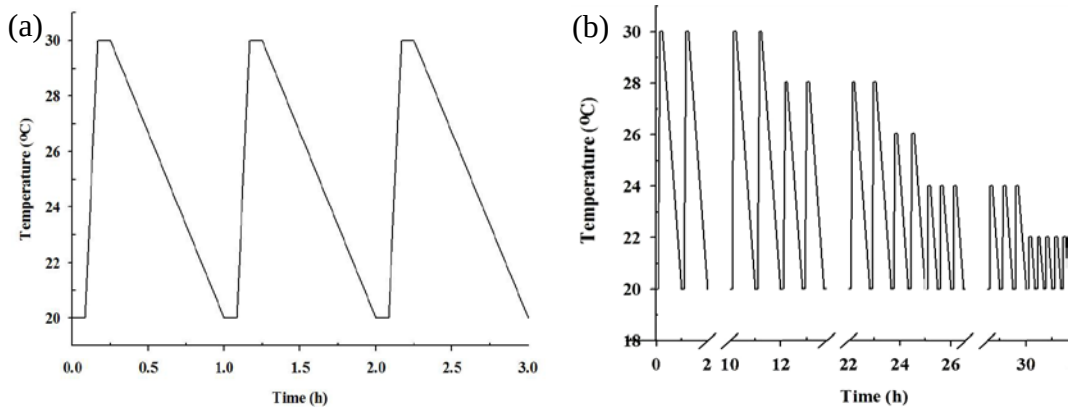

Figure 4.2 (a) Schematic representing constant amplitude of temperature cycles. (b) Temperature cycles with a damped pattern. TP1 and TP2 are the temperatures that fluctuate in a constant width between two saturated stages at 20°C and at a certain level of high temperature of cycles; at 25°C for TP1 and at 30°C for TP2. TP3 is a damped temperature variation, decreasing the upper temperature of cycles with time.

4.3.3 HPLC Analysis

The *e.e.* was monitored by chiral HPLC. Samples were taken at the end of cycles (at 20°C) using a plastic pipette. The solid was then filtered under vacuum and washed with a sufficient amount of water to remove the rest of the sodium hydroxide (the solubility of Me-Tak in water at 20°C is lower than 0.1%wt). A small amount of solid (*ca* 5 mg) was then dissolved into 1 mL of ethanol. A 20 µL sample of this solution was injected into a Chiracel OD column (250 × 4.6 mm) using a solution of 5 %vol ethanol in n-heptane as eluent at a flow rate of 1.5 $mL \cdot min^{-1}$. The two enantiomers were detected at retention times of *ca* 8 and *ca* 10 min using UV detection at a wavelength of 227 nm.

4.3.4 Solubility Measurement

Solubilities of the racemic mixture were determined at different temperatures using the gravimetric method as summarized in Table 4.1.

Table 4.1 Solubilities of Me-Tak in a 65/35 %wt methanol/water mixture containing 8 g of NaOH per kg of solvent. Solubilities are given in mass of Me-Tak per 100 g of the mixed solvent.

Temperature (°C)	Solubility of the racemic mixture Me-Tak (mass per 100g of mixed solvent)
20	3.8
25	4.7
30	6.1

4.3.5 Enantiomeric Excess in the Solid Phase

Enantiomeric excess (*e.e.*) in the crystal phase is defined in terms of the predominant enantiomer at complete deracemization (at the end of the experiment). The experimental results demonstrated that the direction of the deracemization was random; the final product of the deracemization could be either of the *R*-form or the *S*-form of the compound. The presentation here focuses on the absolute value of the *e.e.* in order to compare the results more conveniently. The enantiomer obtained as the final product from deracemization experiments is summarized in Table 4.2.

4.4 Experimental Results and Discussion

According to the previous studies of the deracemization process, the amplification of the evolution of *e.e.* in solid phase was expected to be strongly affected by the initial particle size distributions and/or a small imbalance of the initial mass of the two enantiomorphs in the suspension, chiral additives, impurities, etc. (Steendam et al., 2013; Viedma, 2005). Therefore, the starting crystals of Exp. I, Exp. II, Exp. III, and Exp. IV were collected from the racemic crystals of RM1 in order to eliminate bias due to differences in the properties of the initial crystals.

Exp. I was performed by stirring a suspension of Me-Tak in the presence of racemizing agent at a constant temperature throughout the experimental period in order to investigate the effect of the small amount of grinding produced by the agitation on the deracemization of the racemic suspension of a conglomerate forming system. 1.8 g of Me-Tak crystal was partially dissolved in 25 g of solution of 65 %wt methanol: 35 %wt distilled water with 0.2 g of NaOH as a racemizing agent. The suspension was gently agitated using an oval magnetic stirrer bar operated at 500 rpm in order to produce a uniform suspension. The experiment was carried out at 20°C without temperature cycles.

The result of experiment I was that there was no evolution in the *e.e.* over a period of 60 hours. Although the agitation caused a decrease in the crystal size it did not cause any symmetry breaking of the enantiomorphs in the suspension as shown in Figure 4.3a. This result was similar to what occurred in the deracemization of Cl-Tak (Suwannasang et al., 2013). Hence, it can be emphasized that the effect of grinding was not responsible for the deracemization occurring in the latter experiments.

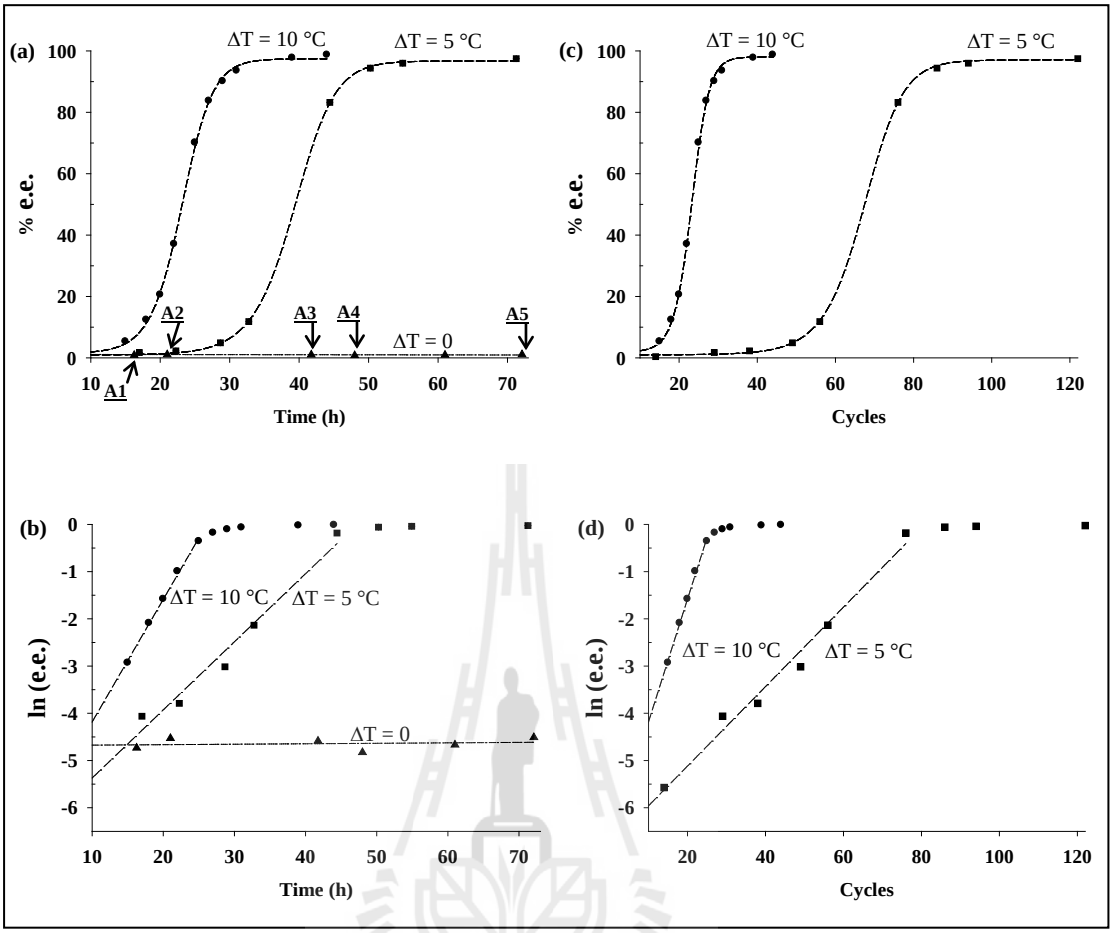

Figure 4.3 Effect of temperature difference (constant amplitude) on deracemization. (a) Evolution of *e.e.* versus time, (b) Evolution of ln *(e.e.)* versus time, (c) Evolution of *e.e.* versus the number of heating-cooling cycles, (d) Evolution of ln *(e.e.)* versus the number of heating-cooling cycles. ▲ Exp. I – constant temperature at 20°C (ΔT = 0), ■ Exp. II – TP1 (ΔT = 5°C), ● Exp. III – TP2 (ΔT = 10°C). Notes on Figure 4.3 (a) indicate that SEM micrographs were taken at that point in the experiment.

To prove that the amplification of the evolution of *e.e.* is due to the temperature cycles, Exp. II was then conducted under the same operating condition as

Exp. I – excepting that temperature cycles were used throughout the period of the experiment.

TP1 has a temperature gradient at 5°C, which was used to alter the symmetry breaking in Exp. II. It can be seen that the breaking of the symmetry of the racemic suspension was initiated after using *ca* 40 temperature cycles. Then, the autocatalytic process had begun so that an acceleration of the evolution of *e.e.* occurred. Finally, the complete deracemization was achieved at *ca* 90 temperature cycles as shown in Figure 4.3c.

The effect of the temperature differential on the evolution of *e.e.* was then investigated. Exp. III was carried out with the same conditions as in Exp. I and Exp. II, but with a different temperature program. TP2, which has a temperature difference of 10°C, was applied for Exp. III. The results show that the threshold of symmetry breaking in the system having a large temperature gradient ($\Delta T = 10°C$) was faster than the threshold of symmetry breaking in the system having a small temperature gradient ($\Delta T = 5°C$) as shown in Figure 4.3a. The rate of deracemization was also accelerated by the magnitude of the temperature gradient as shown in Figure 4.3b. This result was similar to the results in the experiments on the deracemization of Cl-Tak; that is an increase in the fraction of suspension mass dissolved in a cycle accelerated the evolution of the *e.e.* in solid phase (Suwannasang et al., 2013). It can be noticed that the temperature cycles can be used to initiate the symmetry breaking of a racemic suspension of a conglomerate forming system, independent of the effect of grinding. The ability and reproducibility of the use of temperature cycles for achieving a total deracemization have been proven by these three practical demonstrations.

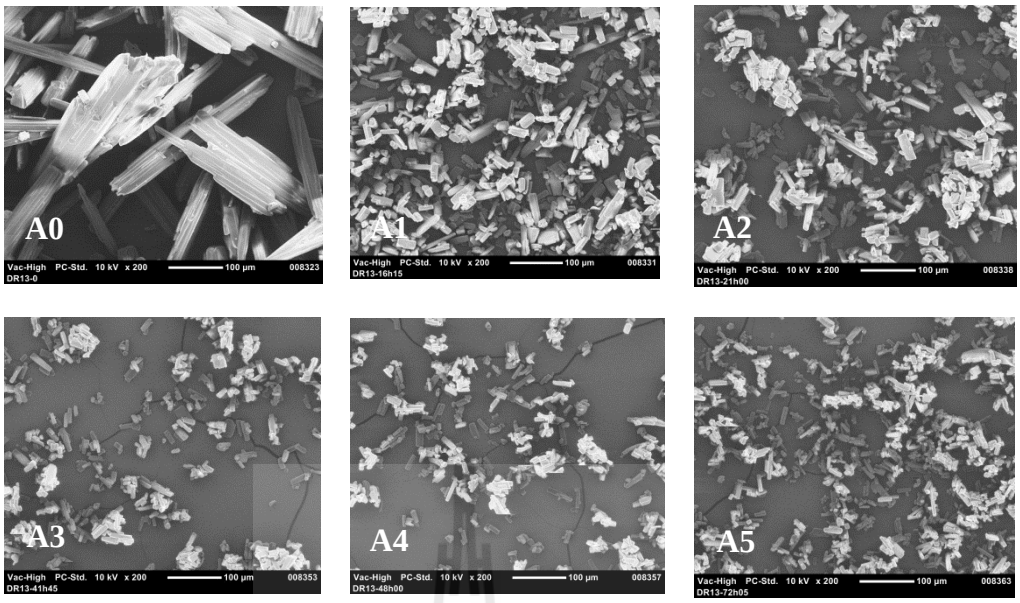

Figure 4.4 SEM micrographs of samples of Exp. I – deracemization without temperature cycles. Label A0 is a SEM micrograph of the initial crystals. Labels A1 - A5 correspond to the arrows indicated on Figure 4.3a (● Exp. I). The scale bar (0.7 cm) on the SEM micrographs is equivalent to 100 μm.

Crystalline samples were taken during the deracemization experiment and were analyzed by SEM. The SEM micrographs of the samples of Exp. I are shown in Figure 4.4. There were a lot of small crystals fragments occurring in the deracemization system due to the grinding. According to the labels on Figure 4.3a, indicating the point in the experiment the samples were taken, the effect of grinding was not significant on the symmetry breaking of the racemic suspension, since the *e.e.* of solid phase did not change away from 0%. This result clearly shows that the grinding is not responsible for the evolution of *e.e.* in this experiment.

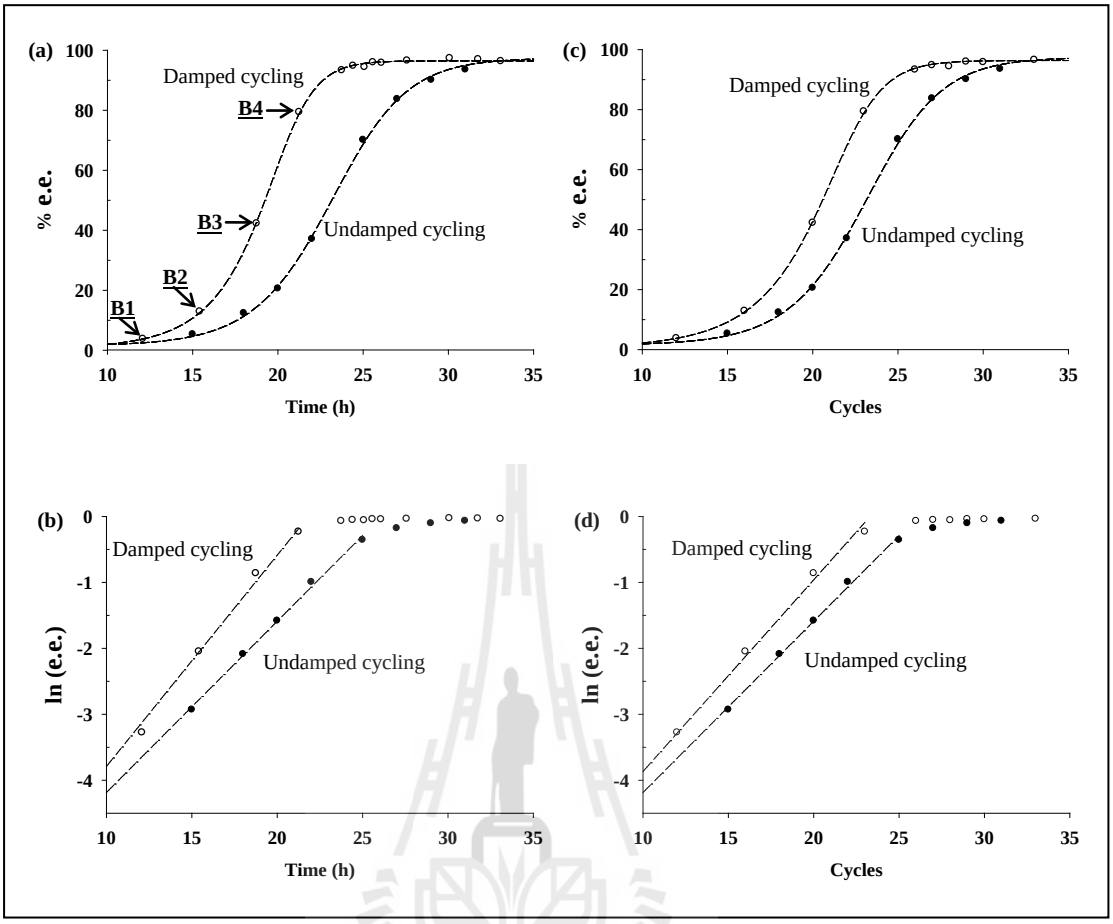

Figure 4.5 Effect of undamped cycles and damped cycles of temperatures on deracemization. (a) Evolution of *e.e.* versus time, (b) Evolution of ln*(e.e.)* versus time, (c) Evolution of *e.e.* versus the number of heating-cooling cycles, (d) Evolution of ln *(e.e.)* versus the number of heating-cooling cycles. ● Exp. III – TP2 (undamped cycles, ΔT = 10°C). ○ Exp. IV – TP3 (damped cycles, $\Delta T_{initial}$ = 10°C). Notes on Figure 4.5 (a) indicate the SEM micrographs that were taken at that point in the experiment.

The use of large temperature differences has been highlighted as a possible route for initiating the system to move away from the racemic state. However, after

breaking the symmetry the system appears autocatalytic and the amplitude of temperature cycles can be made smaller to reduce the dissolution of the major enantiomer and thus to enhance the deracemization rate. Indeed, the number of dominant enantiomer crystals being greater after the initiation of the evolution in *e.e.* will result in an enhancement in the effect of entrainment (Levilain and Coquerel, 2010; Levilain et al., 2009). As a consequence, TP3 was designed to be a damped system of temperature cycles.

Temperature program TP3 was used to deracemize Me-Tak in Exp. IV. TP3 has the same initial temperature difference ($\Delta T_{initial}$ = 10°C) as TP2 (used in Exp. III), however the top temperature of the cycles is deceased throughout the experiment based on the increase in the % *e.e.* (i.e. the cycle is damped based on the response of the *e.e.*).

Comparing the result of Exp. IV (damped cycling) and the result of Exp. III (undamped cycling), the symmetry breaking of both systems was initiated at about 10 h (i.e. 10 cycles) as shown in Figure 4.5a. However, it is important to note that the rate of deracemization of the damped cycling system was faster than the undamped cycling system as shown in Figure 4.5b. The later damped cycles are much faster cycles than the initial cycles, and therefore this experiment required *ca* 25% less time for complete deracemization than the experiment using the constant magnitude temperature fluctuations. The required number of cycles for the damped system is slightly smaller than the undamped system as depicted in Figure 4.5c.

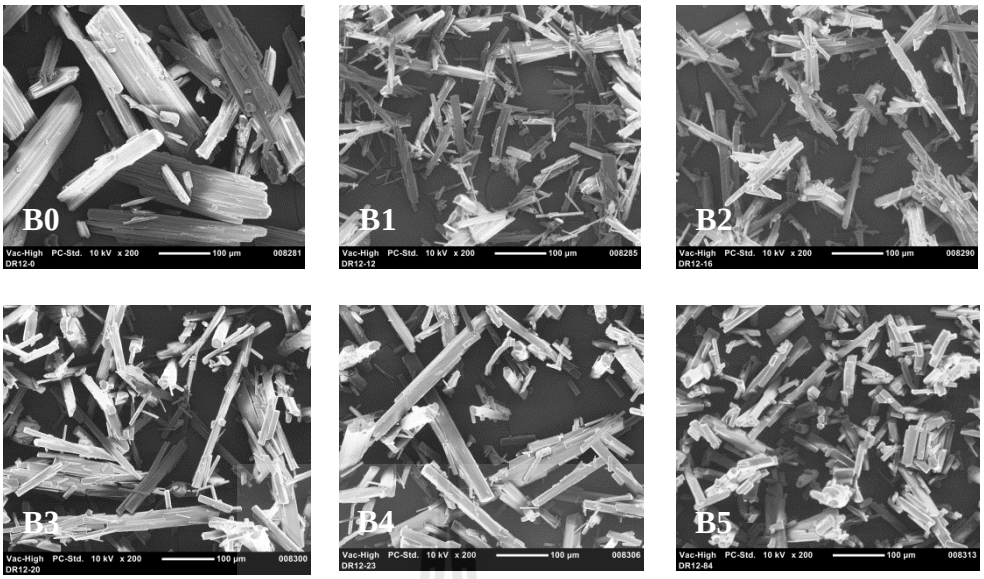

Figure 4.6 SEM micrographs of samples of Exp. IV – deracemization with damped temperature cycles. Label B0 and B5 are SEM micrographs of the initial crystals and the final crystals, respectively. Labels B1 – B4 correspond to the arrows indicated on Figure 4.5a (○ Exp. IV). The scale bar (0.7 cm) on the SEM micrographs is equivalent to 100 μm.

The SEM micrographs of the samples from Exp. IV are shown in Figure 4.6. It indicates that, after symmetry breaking at point B1 – as shown by the arrow on Figure 4.5a – the crystals were visibly bigger than the crystals obtained from the stirred isothermal system (Exp. I). The evolution of the *e.e.* in Figure 4.5a seems to be due to dissolution and recrystallization resulting in competition between the populations of the two crystals, with the stronger population out-competing the weaker one. There is no evidence of significant breakage, or of crystals small enough that Ostwald ripening would be significant.

Temperature cycles are responsible for enhancing the mass exchange between the solution phase and the crystal phase. The swift racemization in the solution phase

maintains an equal amount of the two enantiomers in the solution by conversion of the counter enantiomer to the preferred enantiomer, resulting in the two enantiomers having the same supersaturation even though one of the enantiomorphs is crystallizing at a faster rate than the other one. As a consequence, the entrainment effect of the preferred crystals during the cooling period of the cycles has not been limited. Although there was an eroding of crystals by the stirrer in the temperature cycling system, the rate of crystal growth seems to be faster than the rate of breakage as can be seen in the SEM micrographs. That shows the smooth surfaces and sharp edges of the crystals.

One of the hypotheses made in our modeling work (Suwannasang et al., 2014) concerns the effect of the initial nucleation event on the complete deracemization. In a fast solution phase racemization system, the nucleation of the two enantiomers could occur at different times and/or different conditions; hence, the later enantiomer therefore nucleates at lower supersaturation. This stochastic process of nucleation would result in a difference in the perfection of crystalline structure between the two enantiomorphs that leads to differences in the crystal growth rate activities, a small imbalance of mass and/or number, or crystal size distributions of the two enantiomorphs, or differences in the growth rate distributions of the two enantiomorphs. This memory effect indicates that the symmetry breaking of crystals may originate from the nucleation events.

Further experiments were conducted in order to investigate the effect of preparation of the crystals on the final outcome of deracemization. According to the procedure of RM1 and RM2, two different starting crystals were prepared independently. RM1 was prepared by the solvent evaporation technique under

vacuum in the presence of racemization in solution. RM2 was prepared by rapid nucleation in the vessel using a fast cooling technique. From a theoretical point of view, the creation of supersaturation by deep cooling causes the nucleation of the two enantiomers. Hence, the population of both enantiomorphs would be similar in both mass and crystal size. The outcome of the instantaneous nucleation systems is random. Once the systems starts with the same initial suspension, the outcome of these systems tends to be the same enantiomorphs as shown in Table 4.2. It can be noticed that the experimental result is consistent with the hypothesis of the nucleation event being significant on the outcome; even if the two populations nucleate essentially simultaneously there is no guarantee that their properties are exactly the same. This event would create differences in their crystal growth activities and that causes the symmetry breaking toward to a single chirality state as proposed in the previous article (Suwannasang et al., 2014).

Table 4.2 The number of times each enantiomer was obtained as the final product in the temperature induced-deracemization experiments.

Starting material	Final product analysis	
	Peak 1 of HPLC	Peak 2 of HPLC
Crystals produced via the RM1in Batch 1	0	5
Crystals produced via the RM1 in Batch 2	2	0
Crystals nucleated in vessel via the RM2	2	4

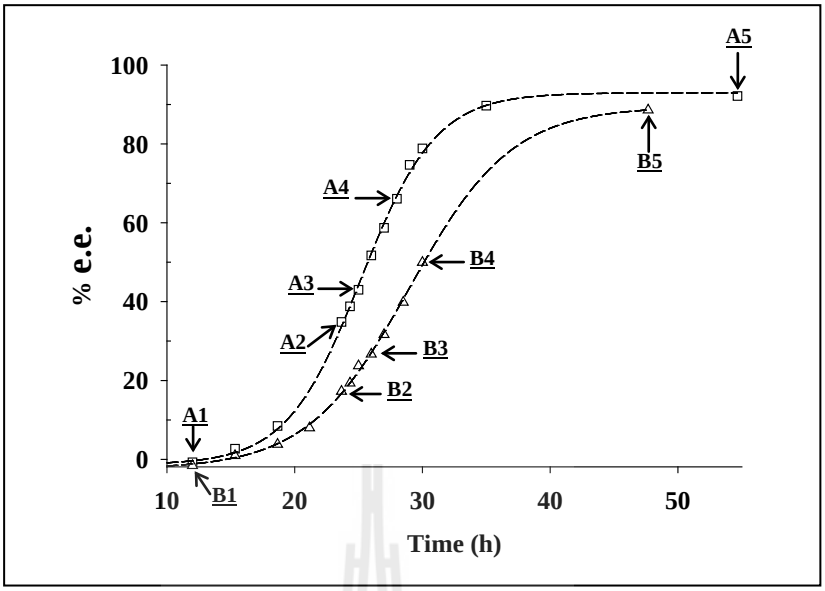

Figure 4.7 Effect of size of the initial crystals on the evolution of *e.e.*in deracemization via temperature cycles. □ Exp. V – small size of the initial population of crystals, Δ Exp. VI – large size of the initial population of crystals.

Two further experiments further conducted in order to investigate the effect of the initial crystals size on the amplification of the *e.e.* in the solid phase. The starting materials of these experiments were prepared in the same batch by anti-solvent addition – adding distilled water into the filtered saturated solution in the presence of a racemizing agent. Then the racemic conglomerate crystals in the suspension were separated from the mother liquor. The remaining sodium hydroxide on the surface of the crystals was washed by a sufficient amount of water. After that, the crystals were separated into two parts. The first part was used as the initial population of crystals of Exp. V. The second part was further dissolved in methanol without the racemization agent (NaOH) to prepare the initial population of crystals of Exp. VI. Then the solvent

was evaporated under vacuum at 30°C. A racemic mixture of crystals with large sizes was obtained. The starting population of crystals of Exp. V (A0) is thus smaller than the starting crystals of Exp. VI (B0) as shown in Figure 4.8. Deracemization experiment V and VI were carried out with the same condition as the Exp. IV. TP3 was used in the Exp. V and the Exp. VI.

As shown in Figure 4.7, the thresholds of symmetry breaking of the two systems were similar (*ca* 10 h, similar to the results obtained from the three initial experiments described above). Even though there are difference in crystal sizes at the beginning of the processes, the crystal size of the samples after the symmetry breaking of both systems are quite similar as shown Figure 4.8. Hence, the threshold of symmetry breaking is not related to the sizes of the initial population of crystals if there is the grinding effect. In contrast, the smaller sizes of the initial crystals (produced by nucleation before the experiment) were deracemized faster than the larger initial crystals (produced by redissolving the other haft of the nuclei in the absence of racemization in solution and producing larger crystals by slow evaporation at near ambient temperature under vacuum). It might be explained that the larger crystals of the two enantiomers (Exp. VI) were produced in a long period of time that might let them have more time to create their mature properties. Hence, they would take more time to finish the competition between them. In the maturing systems, the outcome seems to be determined at the initial state even though the initial *e.e.* in the solid phase is zero as shown in Table 4.2.

(a) Experiment V – Small crystals at the beginning.

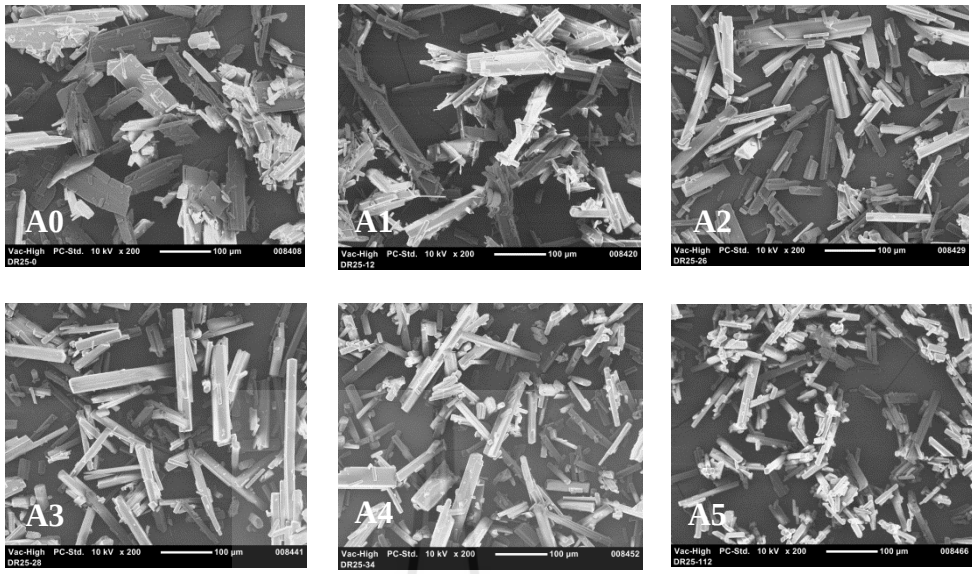

(b) Experiment VI – large crystals at the beginning.

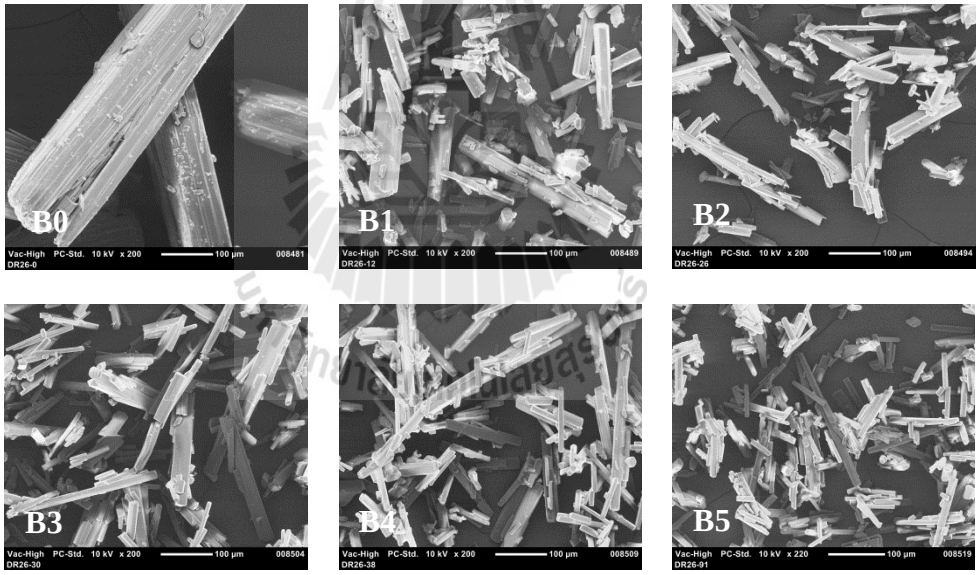

Figure 4.8 SEM micrographs of samples taken during the experimental period of Exp. V and Exp. VI. (a) Small size of the initial crystals. (b) Large size of the initial crystals. Label A0 and B0 are the SEM micrographs of the initial crystals of the smaller and larger populations, respectively. Labels A1 – A5 and labels B1 – B5 correspond to arrows indicated on

Figure 4.7a for Exp. V and Exp. VI, respectively. The scale bar (0.7 cm) on the SEM micrographs is equivalent to 100 μm.

The enantiomorphic outcome of the initial population of fine crystal systems is random as shown in Table 4.2. It might be due to the smaller crystals produced from the rapid nucleation event via an anti-solvent precipitation, so that there is not much time to differentiate the properties of the two enantiomorphs. The winning enantiomer probably depends on which enantiomorph has the higher growth rate activity as described in our modeling (Suwannasang et al., 2014). However, this point is still unclear. Therefore, further work is required for studying the effect of crystal growth rate on the deracemization process in order to have more understanding of the mechanism of this process.

The SEM micrographs of the initial population of crystals of Exp. VI as shown in Figure 4.8 (B0 - B1) show that the effect of grinding at the initial process on the crystal size is quite high. It was due to the fact that the breakage is dependent on the crystal size – large crystals tending to break at much larger rates than fine ones. However, there is no change of *e.e.* during this experimental period. The SEM micrographs also show that crystals remain at a certain size along a period of the increase of *e.e.*in the solid phase as can be seen in B1 - B5 of the SEM pictures in Figure 4.8. Therefore, the grinding may help the system to maintain the crystal size at a small value which creates a high surface area. That is an advantage for the mass exchange between the crystal phase and the solution phase during the cooling period of the temperature cycles.

4.5 Conclusions

Starting from a racemic suspension of Me-Tak in the presence of racemization in solution phase, the use of temperature cycles enables a breaking of the symmetry of the racemic mixture in the solid phase and drives the system to a single chiral solid state. The use of temperature cycles for deracemization of a conglomerate forming system have been proven by the results of this work. The temperature cycles have been modified by reducing the top temperature of the cycles. As a result, the time required to achieve a chiral pure crystalline state of the damped cycles is less than the undamped cycles by about 25%. During the experiment the only effect of breakage was to decrease the size of particles in the system. However, the crystals remained faceted so that there was no evidence of abrasive grinding. However, the *e.e.* in the solid phase did not evolve (there is no significant change away from 0%). The eroding of crystals by the stirrer may lead to the removal of some tiny crystals according to the Gibbs-Thomson effect but for this temperature cycling system that is not enough to break the symmetry of the enantiomorphs at least during this experimental period in which the complete deracemization can occur. Consequently, it can be emphasized that the amplification of the *e.e.* by temperature cycles is not induced by the grinding effect but rather by successive small entrainment effects at constant *e.e.* = 0 in the mother liquor.

4.6 References

Black, S. N., Williams, L. J., Davey, R. J., Moffatt, F., Jones, R. V. H., McEwan, D. M., and Sadler, D. E. (1989). The preparation of enantiomers of paclobutrazol: A crystal chemistry approach. **Tetrahedron**. 45: 2677-2682.

Cartwright, J. H. E., Piro, O., and Tuval, I. (2007). Ostwald Ripening, Chiral Crystallization, and the Common-Ancestor Effect. **Physical Review Letters.** 98: 165501.

Iggland, M., and Mazzotti, M. (2011). A Population Balance Model for Chiral Resolution via Viedma Ripening. **Crystal Growth & Design.** 11: 4611-4622.

Katsuno, H., and Uwaha, M. (2012). Appearance of a homochiral state of crystals induced by random fluctuation in grinding. **Physical Review E.** 86: 051608.

Levilain, G., and Coquerel, G. (2010). Pitfalls and rewards of preferential crystallization. **CrystEngComm.** 12: 1983-1992.

Levilain, G., Rougeot, C., Guillen, F., Plaquevent, J.-C., and Coquerel, G. (2009). Attrition-enhanced preferential crystallization combined with racemization leading to redissolution of the antipode nuclei. **Tetrahedron: Asymmetry.** 20: 2769-2771.

McBride, J. M. (2008). Origins of Homochirality: A mechanism for deracemization by crystal grinding. **Lecture at NORDITA Workshop.** http://agenda.albanova.se/conferenceDisplay.py?confId=322.

Noorduin, W. L., Izumi, T., Millemaggi, A., Leeman, M., Meekes, H., Van Enckevort, W. J. P., Kellogg, R. M., Kaptein, B., Vlieg, E., and Blackmond, D. G. (2008a). Emergence of a Single Solid Chiral State from a Nearly

Racemic Amino Acid Derivative. **Journal of the American Chemical Society.** 130: 1158-1159.

Noorduin, W. L., Kaptein, B., Meekes, H., van Enckevort, W. J. P., Kellogg, R. M., and Vlieg, E. (2009). Fast Attrition-Enhanced Deracemization of Naproxen by a Gradual In Situ Feed. **Angewandte Chemie International Edition.** 48: 4581-4583.

Noorduin, W. L., Meekes, H., Bode, A. A. C., van Enckevort, W. J. P., Kaptein, B., Kellogg, R. M., and Vlieg, E. (2008b). Explanation for the Emergence of a Single Chiral Solid State during Attrition-Enhanced Ostwald Ripening: Survival of the Fittest. **Crystal Growth & Design.** 8: 1675-1681.

Noorduin, W. L., Meekes, H., van Enckevort, W. J. P., Kaptein, B., Kellogg, R. M., and Vlieg, E. (2010). Enantioselective Symmetry Breaking Directed by the Order of Process Steps. **Angewandte Chemie International Edition.** 49: 2539-2541.

Noorduin, W. L., Meekes, H., van Enckevort, W. J. P., Millemaggi, A., Leeman, M., Kaptein, B., Kellogg, R. M., and Vlieg, E. (2008c). Complete Deracemization by Attrition-Enhanced Ostwald Ripening Elucidated. **Angewandte Chemie International Edition.** 47: 6445-6447.

Rougeot, C. (2012). Deracemisation of active compound precursors by physical treatments. Ph.D. Thesis. **University Paul Sabatier of Toulouse III.** Toulouse, France.

Steendam, R. R. E., Harmsen, B., Meekes, H., Enckevort, W. J. P. v., Kaptein, B., Kellogg, R. M., Raap, J., Rutjes, F. P. J. T., and Vlieg, E. (2013). Controlling

the Effect of Chiral Impurities on Viedma Ripening. **Crystal Growth & Design.** 13: 4776-4780.

Suwannasang, K., Coquerel, G., Rougeot, C., and Flood, A. E. (2014). Mathematical Modeling of Chiral Symmetry Breaking due to Differences in Crystal Growth Kinetics. **Chemical Engineering & Technology.** 37: 1329-1339.

Suwannasang, K., Flood, A. E., Rougeot, C., and Coquerel, G. (2013). Using Programmed Heating–Cooling Cycles with Racemization in Solution for Complete Symmetry Breaking of a Conglomerate Forming System. **Crystal Growth & Design.** 13: 3498-3504.

Tsogoeva, S. B., Wei, S., Freund, M., and Mauksch, M. (2009). Generation of Highly Enantioenriched Crystalline Products in Reversible Asymmetric Reactions with Racemic or Achiral Catalysts. **Angewandte Chemie International Edition.** 48: 590-594.

van der Meijden, M. W., Leeman, M., Gelens, E., Noorduin, W. L., Meekes, H., van Enckevort, W. J. P., Kaptein, B., Vlieg, E., and Kellogg, R. M. (2009). Attrition-Enhanced Deracemization in the Synthesis of Clopidogrel - A Practical Application of a New Discovery. **Organic Process Research & Development.** 13: 1195-1198.

Viedma, C. (2005). Chiral Symmetry Breaking During Crystallization: Complete Chiral Purity Induced by Nonlinear Autocatalysis and Recycling. **Physical Review Letters.** 94: 065504.

CHAPTER V

COMBINATION OF PREFERENTIAL CRYSTALLIZATION, SOLUTION PHASE RACEMIZATION AND TEMPERATURE CYCLES FOR RAPID SYMMETRY BREAKING OF A CONGLOMERATE FORMIMG SYSTEM

5.1 Abstract

An effective route to achieve a pure enantiomer from a racemic mixture has been developed. This current work shows that an ordinary deracemization process is able to be made more efficient by using a series of temperature cycles and a simultaneous in-situ racemization in solution combined with a preferential crystallization. The implementation of this process is very easy. Seeding of a small amount of the pure enantiomorph at the beginning of the process is able to initiate the symmetry breaking, where the system can move away from the racemic state, leading to a swift occurrence of an autocatalytic phenomenon. That makes the combined process require a short time for operation to achieve an enantiopure solid state. It also guarantees that the desired enantiomorph will be the product. The mechanisms involved in this novel process are dissolution/crystallization, a fast solution phase racemization and the entrainment effect. During the heating period of the temperature cycles, fine crystals/nuclei were partially and/or totally dissolved and the remaining

crystals were then regrown by consuming the supersaturation during the cooling part of the cycles. Thanks to the racemization in the solution phase, the counter enantiomer was simultaneously converted to the preferred one resulting in a decrease of the supersaturation and a suppression of the primary nucleation of the counter enantiomer. Those are advantages for the entrainment effect of the preferred enantiomorphs during the crystallization period. This combined process can also be made more efficient by monitoring the temperature profile during the operating period. As a result, the crystalline outcome of the combined process, which has a purity $>$ 99% *e.e.*, can be obtained within a few hours. Moreover, the novel process can achieve 100% yield of the desired enantiomer based on the total amount of the solute existing in the crystal phase of the suspension.

5.2 Introduction

The most direct route to synthesize material in the pharmaceutical and agrochemical industries produces a racemic mixture of the two enantiomeric forms (Jacques et al., 1981; Sheldon, 1993). Among the various methods of enantioseparation, perhaps the most significant one is preferential crystallization (PC) which is a direct crystallization for resolution of a racemic solution. The traditional PC is an effective and comparatively cheap process, which has been typically used for purification of a conglomerate forming chiral system. However, the overall yield of this process is limited at 50% since the undesired enantiomer is considered as an impurity. Several scientists have attempted to develop new routes of purification of chiral organic compounds. Recently, one of the most effective process was developed by the SMS laboratory (Coquerel et al., 1995), i.e., the auto-seeded polythermic

programmed preferential crystallization (AS3PC). Unfortunately, there is no a configuration change between the two enantiomers in the process. That limits AS3PC to 50% yield of the total solute in the suspension. In addition, even if there is a swift racemization in the solution phase of the PC process, the primary nucleation of the counter enantiomer eventually occurs resulting in a decrease in the product purity of the PC process (Levilain et al., 2009).

In 2005, a counterintuitive method of breaking the symmetry of racemic suspension of sodium chlorate (an achiral compound which forms an optically active crystal), named “Viedma ripening”, was first demonstrated by Cristobal Viedma (Viedma, 2005). This process was performed by using abrasive grinding to deracemize enantiomeric crystals in a suspension under near-equilibrium conditions by which the desired enantiomorph can be obtained from a racemic suspension. Several scientists have suggested that Ostwald ripening and the reincorporation of chiral clusters are responsible for the process of deracemization through grinding (Noorduin et al., 2010).

The application of the grinding technique has been extended for deracemization of an intrinsically chiral organic compound by the group of Blackmond in 2008 (Noorduin et al., 2008b). The new route of deracemization is the use of the grinding technique combined with a solution phase racemization for conversion of a racemic conglomerate crystals in a suspension to pure enantiomeric crystals. After this initial demonstration numerous organic conglomerate substances have been deracemized via this method (Levilain et al., 2009; Noorduin et al., 2008a; Noorduin et al., 2009; Tsogoeva et al., 2009; van der Meijden et al., 2009). However, the use of the grinding method for deracemization of organic substances has been

limited by the physical and chemical properties of the compounds. Those are the compounds must crystallize as a racemic conglomerate and must be easily racemizable in the solution phase at the same temperature where the compounds are relatively stable.

Recently, a practical demonstration of a new process of deracemization has been presented by our group (Suwannasang et al., 2013). A complete deracemization has been achieved via the use of programmed heating-cooling cycles combined with a simultaneous in-situ racemization in solution. The results of this novel process give a clearer picture of the mechanism involved in the deracemization process. It is likely to be due to energy input into the system; for instance boiling (Viedma and Cintas, 2011), ultrasound (Rougeot et al., 2015) and temperature variations (Suwannasang et al., 2013; Viedma et al., 2008).

According to the experimental results of the temperature cycles induced-deracemization process, it should be emphasized that the mechanism involved in the temperature cycling system is distinct from the grinding system (i.e. the Viedma ripening) as described previously (Suwannasang et al., 2014; Suwannasang et al., 2013). Temperature cycles can be used for complete deracemization of chiral organic compounds starting from a racemic suspension of a conglomerate forming system. Pure enantiomeric crystals can be obtained in a single step separation. The demonstration of the temperature cycles method clearly shows that a dissolution/recrystallization phenomenon, a swift solution phase racemization and the entrainment effect are responsible for conversion of a racemic suspension to a single chirality in crystalline phase. This process was also extended for deracemization of Me-Tak compound as experimentally demonstrated in Chapter V. However, it seems

to be suboptimal since the threshold of the symmetry breaking of the ordinary deracemization process is quite long (at *ca* 10 h).

As investigation of deracemization by a combination of heating-cooling cycles and an ordinary preferential crystallization, and with a swift racemization in solution was thus carried out. Seeding of pure enantiomeric crystals according to the ordinary PC process, aims to reduce the threshold of symmetry breaking which typically occurs in the ordinary deracemization process. The symmetry breaking will be initiated at the beginning of the process resulting in an acceleration of the system towards a pure chiral crystalline state. The use of temperature cycles and the solution phase racemization has focused on solving the problems of nucleation of the counter enantiomer and the limitation of the production yield of the traditional PC process. Furthermore, this enantiopurification was designed to be an easily implemented process. The scaling up for an industrial operation is therefore expected to be easily possible.

5.3 Experimental Section

5.3.1 Materials

Racemic 4,4-dimethyl-1-(p-toluyl)-2-(1H-1,2,4-triazol-1-yl)pentan-3-one (Me-Tak) was synthesized by Dr. Celine Rougeot (Rougeot, 2012). Distilled water was used for deracemization experiments. HPLC-grade n-heptane and ethanol, and reagent-grade methanol were purchased from Fisher Scientific.

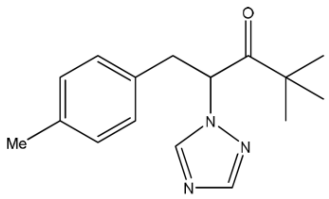

Figure 5.1 Chemical Structure of Me-Tak.

5.3.2 Experimental Procedure

1.8 g of Me-Tak (0.85 g of Me-Tak remains as solid at 20°C), 25 g of methanol/water mixture (65/35 %wt), and 0.2 g of NaOH were chosen as a standard solution. This mixture was totally dissolved at 40°C for 5 min (saturated at *ca* 33°C). The solution was filtrated by a warmed 0.2 micrometer pore size filter. The solution was then added to the crystallizer at 35 °C and held at constant temperature for 5 min. After that the solution was cooled down to 20°C with a cooling rate 10 °C/45 min. 10 mg of seed was introduced into the solution at 30°C. After the solution reached 20°C, the temperature program (TP) was started and applied throughout the experimental period until the *e.e.* reached the homochiral state in the crystal phase.

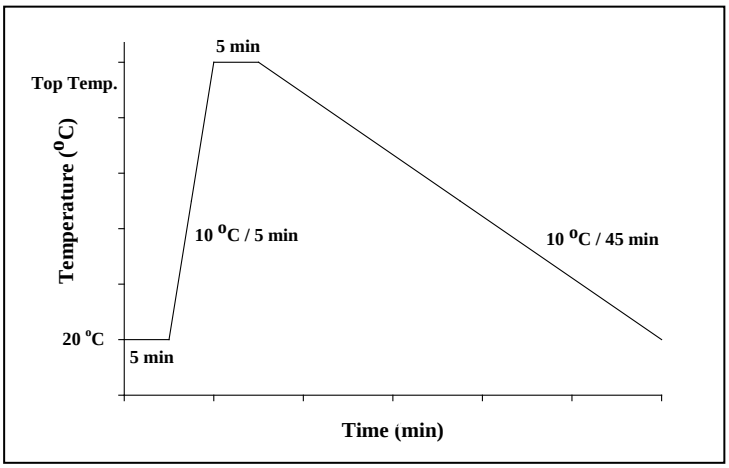

Figure 5.2 Schematic representing a cycle of temperature program versus time.

One cycle in a series of TPs consisted of four steps; holding at 20°C for 5 min, heating up to the top temperature with a heating rate 2 °C/min, holding at the top temperature for 5 min, and then cooling down to 20°C with cooling rate 10 °C/45 min as shown in Figure 5.2.

5.3.3 HPLC Analysis

The *e.e.* was monitored by chiral HPLC. Samples were taken at the end of the cycles (at 20°C) using a plastic pipette. The solid was then filtered under vacuum and washed with a sufficient amount of water to remove the rest of the sodium hydroxide (the solubility of Me-TAK in water at 20°C is lower than 0.1 %wt). A small amount of solid (*ca* 5 mg) was then dissolved into 1 mL of ethanol. A 20 μL sample of this solution was injected into a Chiracel OD column (250 × 4.6 mm) using a solution of 5 %vol ethanol in n-heptane as eluent at a flow rate of 1.5 mL min^{-1}. The two enantiomers were detected at retention times of *ca* 8 and *ca* 10 min using UV detection at a wavelength of 227 nm.

5.3.4 Solubility Measurement

Solubilities of the racemic mixture of Me-Tak under racemizing conditions were determined at different temperatures using the gravimetric method with the results shown previously in Table 4.1.

5.3.5 Enantiomeric Excess in the Solid Phase

Enantiomeric excess (*e.e.*) in the crystal phase is defined in terms of the predominant enantiomeric crystal, which is seeded into the solution at the beginning of the process. The final product of this combination process is either of the *R*-form or the *S*-form of the compound depending on the seeded crystals.

5.4 Experimental Results and Discussion

Preliminary experiments were conducted to investigate the feasibility of this process for enantiopurification by using an ordinary preferential crystallization (PC mode), PC in cooperation with a solution phase racemization (PCR mode), and a combination of temperature cycles and PC with in-situ solution phase racemization (PCRT mode).

The PC mode was carried out in Exp. I – without the use of racemizing agent and temperature cycles. The experimental result shows that after seeding with a pure enantiomorph the amplification of the *e.e.* in the solid phase did not occur since the solution was over the Ostwald limit where the primary nucleation occurs, resulting in a decrease of the *e.e.* in the solid phase. As a result, the *e.e.* did not obviously change away from 0% as shown in Figure 5.3. It can be explained that the entrainment effect had taken place for a very short time but it was stopped due to the Ostwald limit being exceeded. That leads to the system moving to the equilibrium quickly, where the mother liquor and the suspension both consist of an equal amount of the two enantiomers.

As a consequence, solution phase racemization was introduced into the system, namely the “PCR process”. Experiment II was performed with the same operating conditions as the PC process (in Exp. I) - excepting for the addition of the racemizing agent in solution. The mechanisms involved in the PRC process consist of PC and solution phase racemization. The result shows that the % *e.e.* in the solid phase can be obtained at *ca* 25%. It indicates that the PCR mode is not effective enough for access to chiral purity in the solid phase. However, the *e.e* of the crystal outcome of the PCR process is higher than the outcome of the PC process (0% *e.e.*). It

is important to note that the induction time of primary nucleation of the counter enantiomer can be extended by a solution phase racemization since the counter enantiomer is simultaneously converted to the desired enantiomer resulting in a decrease of the supersaturation of the counter enantiomer during the crystallization period. However, the primary nucleation of the counter enantiomer eventually occurs even if there is a fast racemization as can be seen in the PCR process. This may be caused by a competition between crystal growth and nucleation. The crystal growth rate of the preferred enantiomer is not fast enough to keep the supersaturation low. The solution eventually moves over the Ostwald limit resulting in the formation of primary nuclei of the counter enantiomer. The evolution of *e.e.* in the solid phase was therefore stopped as shown in Figure 5.3. It can be seen that the fast solution phase racemization is an advantage for the entrainment effect for a while that results in an increase of % *e.e.* in the solid phase from 0% (obtained from PC process) to *ca* 25% (obtained from PCR process). However, the entrainment effect is not limited by the thermodynamic limit if the PCR process is carried out with a fast racemization in solution and a very slow cooling rate.

In order to solve the problem of primary nucleation of the unwanted enantiomer occurring in the PCR process, a PCRT process was thus carried out in Exp. III. The PCRT process is composed of a swift solution phase racemization, PC and the use of temperature cycles – thus also incorporating temperature cycles into the PCR process. This process has been developed for improvement of the % *e.e.* in the solid product. The temperature profile used in the PCRT process is depicted in Figure 5.3. The experimental result of Exp. III shows that the temperature cycles can be used for acceleration of the evolution of *e.e* in the solid phase. It can be seen that after

seeding (before initiating the temperature cycles), the % *e.e.* in the solid phase was decreased due to the nucleation of the counter enantiomer. However, those small crystals/nuclei were dissolved during the heating part of the first cycles. Hence, the entrainment effect was not further limited because of the repetition of using of the temperature cycles. That is an advantage for enabling the access of 100% *e.e.* in the solid phase as shown in Figure 5.3.

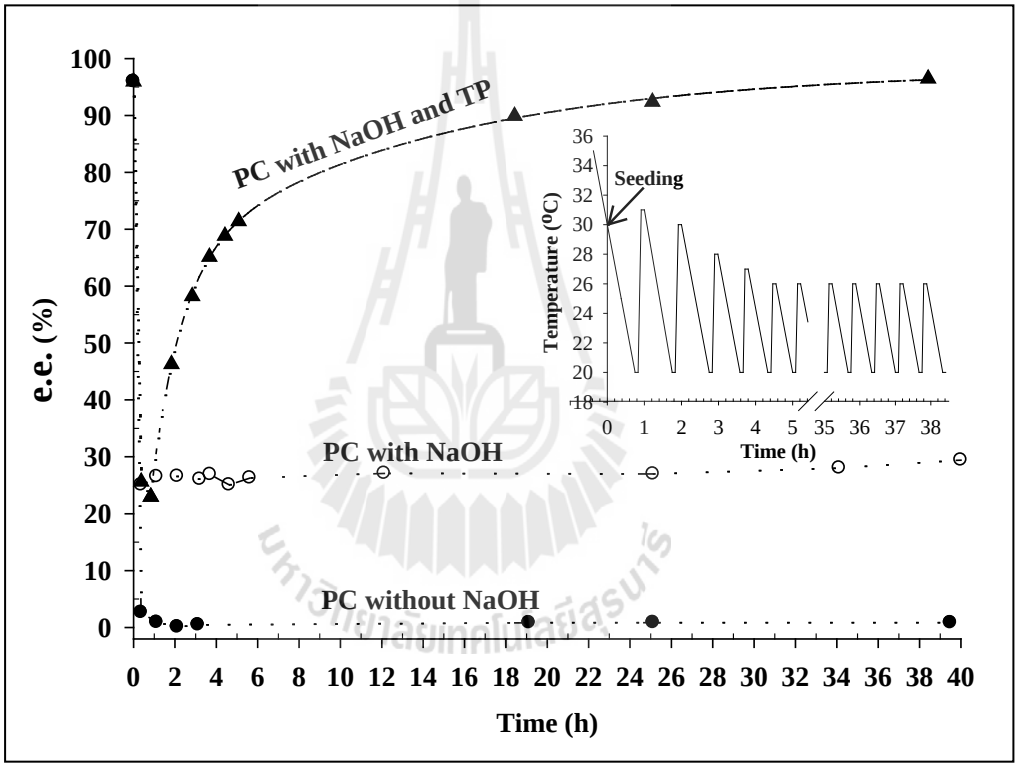

Figure 5.3 Evolution of *e.e.* versus time. ● Exp. I – use of an ordinary PC process without racemization and temperature cycles (a PC process), ○ Exp. II – use of a PC combined with a solution phase racemization without temperature cycles (a PCR process), ▲ Exp. III – use of a PC combined with a solution phase racemization and damped temperature cycles (a PCRT process).

The experimental result obtained from the PCRT process is quite similar to the result obtained from the deracemization process as previously shown in Chapter IV. The use of temperature cycles and solution phase racemization can drive the system towards a single enantiomorph solid state. The problem of nucleation has been removed by the temperature cycles and the racemization reaction. This is an advantage for the entrainment effect during the crystallization period of the cycle. Therefore, it can be concluded that the use of temperature cycles combined with a fast solution phase racemization in corporation with PC is able to obtain a pure crystalline product.

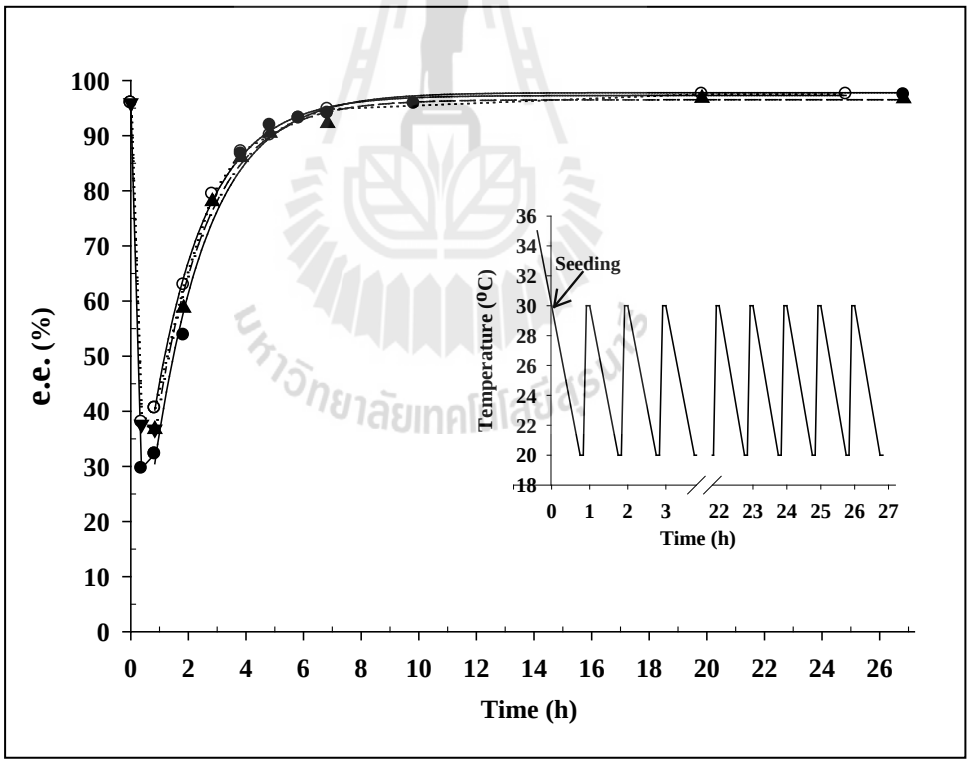

Figure 5.4 Evolution of *e.e.* versus time; ● Exp. IV, ○ Exp. V and ▲ Exp. VI (operated with the same operating condition as the Exp. III – excepting for the use of temperature profile).

Moreover, the PCRT process allows us to be able to modify a suitable temperature profile (based on the response of % *e.e.* in the solid phase) during the production period for a better effectiveness in producing pure enantiomorphs.

Further experiments (Exp. IV to Exp. VIII) were performed in order to investigate the reproducibility of the PCRT process. The experimental results of these five experiments are shown in Figure 5.4 (Exp. IV - VI) and Figure 5.5 (Exp. VII - VIII). The results indicate that the evolution of *e.e.* was due mainly to the temperature cycles. The time required to reach the pure crystalline state seems to be equal if the initial *e.e.* (before using the cycles) of the solid phase is equal, as shown in Figure 5.4. Otherwise, the time required to reach a pure enantiomorphic state seems to be different if there is a difference in the initial *e.e.* The difference of the initial *e.e.* may be due to the unpredictable process of nucleation, which can occur even if there is a swift racemization in the system as shown in Figure 5.5. The results show that the time needed for the system to reach the single enantiomorphic crystalline state was dependent on the initial *e.e.* of solid. It is important to note that even if, at the beginning of the process, there is an equal *e.e.* in the solid phase, there is no guarantee that the time required for the system to achieve an enantiopure crystals will be the same (Rougeot, 2012). The evolution of the *e.e.* in the solid phase in a temperature cycling system probably depends on the difference of the crystal growth rates of the two enantiomorphs as discussed in the previous publication (Suwannasang et al., 2014).

A symmetry breaking of the enantiomorphs in the suspension can be quantitatively performed by seeding pure desired enantiomorph-crystals at the beginning of the PCRT process. The seeding is an advantage for the PCRT process

that can break the threshold of the symmetry breaking which typically occurs in the deracemization process. As a result, the time required to achieve a complete single enantiomorphic solid state of the PCRT process (*ca* 8 h for Me-Tak if the initial *e.e.* is *ca* 35%) is less than the ordinary deracemization process (*ca* 40 h for Me-Tak if the initial *e.e* is *ca* 0%). It can be explained that in the PCRT process the symmetry of solid in the suspension was broken swiftly at the beginning of the process due to the seeding. The autocatalytic process was thus initiated earlier than what occurs in the ordinary deracemization process which requires *ca* 10 h for the threshold as shown in Chapter IV, resulting in a decrease of the operation time for complete deracemization.

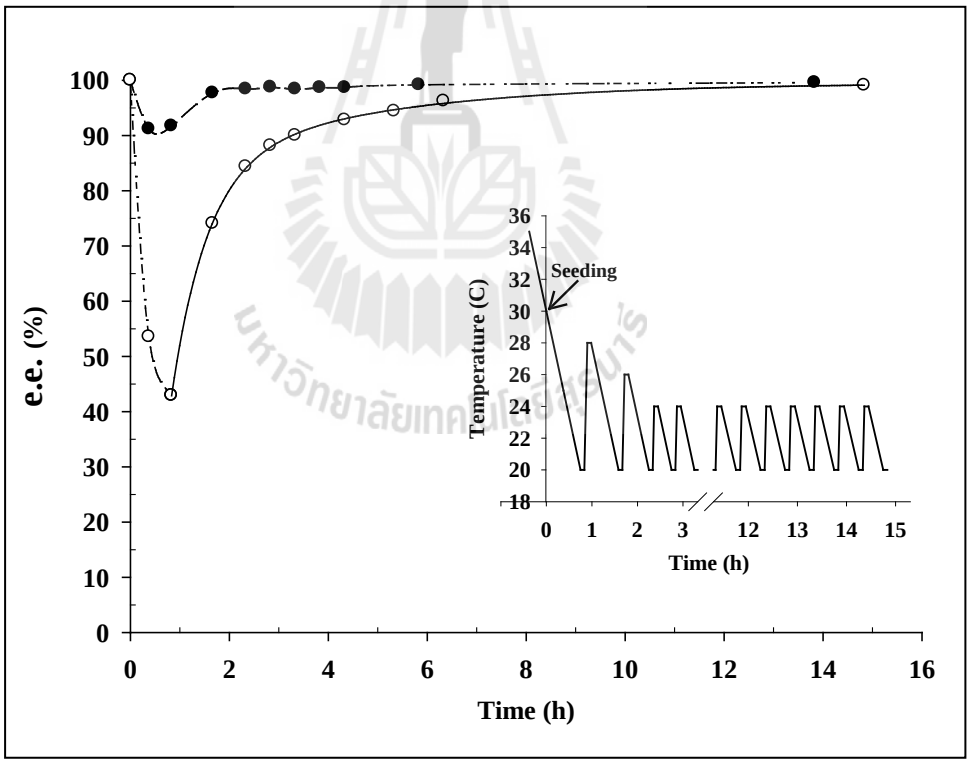

Figure 5.5 Evolution of *e.e.* versus time; ● Exp. VII and ○ Exp. VIII (operated with the same operating condition as the Exp. III – excepting for the use of temperature profile).

The last experiment (Exp. IX) was conducted to investigate the change in crystal size during the PCRT process. This experiment was performed by stirring an excess amount of Me-Tak under racemization conditions overnight at 35°C. The remaining crystals were quickly separated from a saturated solution using a warmed-glass filter under vacuum. The saturated solution was then preheated in a vessel at 40°C to avoid nucleation for 5 min. Then the solution was cooled down to 20°C for 90 min. 10 mg of a pure enantiomorph was injected into the solution after the solution had been maintained at the saturation temperature (35°C) for one minute. At the cooling period (before using temperature cycles), solid samples were taken at 30°C, 25°C, and 20°C, respectively. After applying the cycles, the samples were taken at the end of the cycle at 20°C. The solid sample was filtered under vacuum and then washed of the remaining NaOH on the crystal surface by a sufficient amount of water. The solid was dried in an oven and then analyzed by HPLC and SEM.

In the first cooling period, nucleation occurred after a few minutes after seeding resulting in a decrease of the *e.e.* in the solid phase. There are a lot of small crystals occurring in the system at point B, as seen in Figure 5.7. The HPLC result indicates that the decrease in the % *e.e.* of the solid phase was due to the primary nucleation of the counter enantiomer.

The results show that there is an increase of the *e.e.* in the solid phase after a few cycles, as shown in Figure 5.6 at point C to point E. It can be seen that fine crystals of the counter enantiomer were dissolved. That causes the acceleration of the evolution of *e.e.* in the solid phase. This result is not surprising since temperature cycles were shown to raise the *e.e.* in the previous article (Suwannasang et al., 2013). The SEM micrograph of the sample at point C evidently shows that there was crystal

growth during the use of the temperature cycles. Other SEM micrographs of the samples at point D and point E also show that the grinding did not have much effect on the crystal since the crystals still apparently have a good shape and also have clear edges.

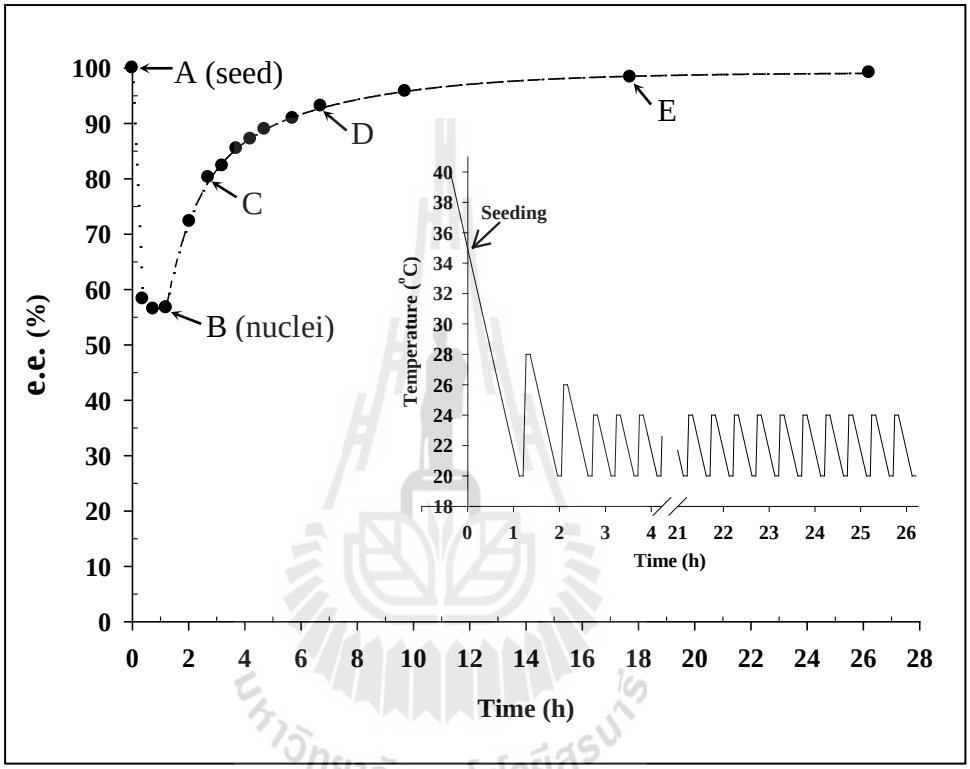

Figure 5.6 Evolution of *e.e.* versus time. Exp. IX – PCRT mode with damped temperature profile.

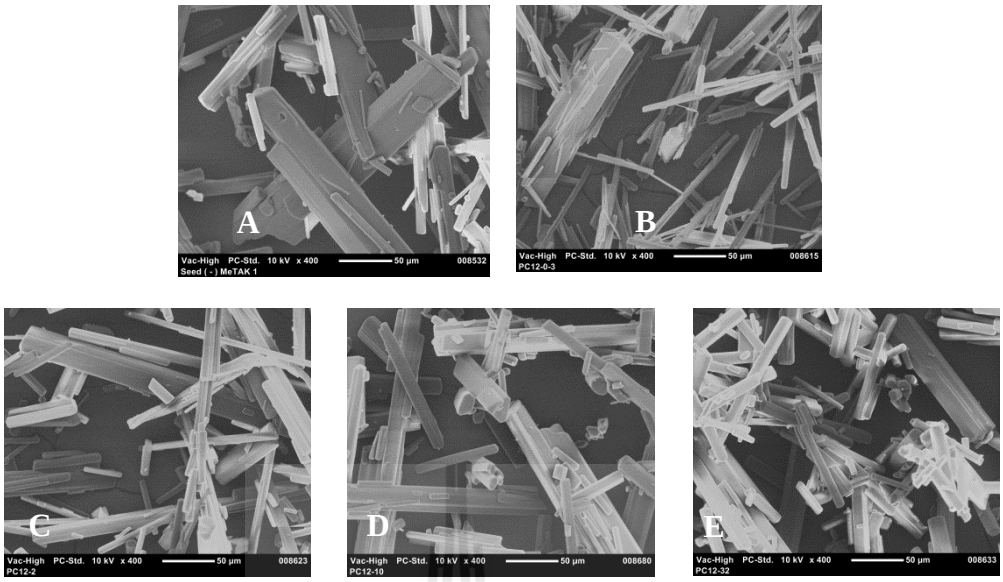

Figure 5.7 SEM micrographs of samples taken during the experimental period of Exp. IX. Deracemization by PCRT mode. Labels A - E corresponds to the arrows indicated on Figure 5.6. The scale bar (0.7 cm) on the SEM micrographs is equivalent to 100 μm.

5.5 Conclusions

The use of a series of temperature cycles combined with an ordinary preferential crystallization in the presence of a swift racemization in solution can be used for purification of enantiomers. The PCRT process has achieved 100% yield of the desired enantiomer based on the crystallized solute in the suspension. Seeding with a small amount of pure enantiomorph at the beginning of the PCRT process is an advantage for the symmetry breaking of the racemic suspension resulting in a decrease of time required for access a single enantiomorphic in solid phase. As a result, the crystalline product with an enantiomeric excess more than 99% can be obtained in a few hours. It could be emphasized that there are three main mechanisms

responsible for the PCRT process; these are dissolution/recrystallization, the fast solution phase racemization and the entrainment effect. The Ostwald ripening and Viedma ripening are not considered as the major mechanisms of this process. Since the implementation of the PCRT process is very simple, it should be able to be scaled up easily.

5.6 References

Coquerel, G., Petit, M.-N., and Bouaziz, R. (1995). Procédé de dédoublement (AS3PC) de deux antipodes optiques par entraînement polythermique programmé et auto-ensemencé. **Patent WO1995/008522.**

Jacques, J., Collet, A., and Wilen, S. H. (1981). **Enantiomers, Racemates, and Resolutions.** John Wiley & Sons, New York.

Levilain, G., Rougeot, C., Guillen, F., Plaquevent, J.-C., and Coquerel, G. (2009). Attrition-enhanced preferential crystallization combined with racemization leading to redissolution of the antipode nuclei. **Tetrahedron: Asymmetry.** 20: 2769-2771.

Noorduin, W. L., Izumi, T., Millemaggi, A., Leeman, M., Meekes, H., Van Enckevort, W. J. P., Kellogg, R. M., Kaptein, B., Vlieg, E., and Blackmond, D. G. (2008a). Emergence of a Single Solid Chiral State from a Nearly Racemic Amino Acid Derivative. **Journal of the American Chemical Society.** 130: 1158-1159.

Noorduin, W. L., Kaptein, B., Meekes, H., van Enckevort, W. J. P., Kellogg, R. M., and Vlieg, E. (2009). Fast Attrition-Enhanced Deracemization of Naproxen by

a Gradual In Situ Feed. **Angewandte Chemie International Edition.** 48: 4581-4583.

Noorduin, W. L., Meekes, H., van Enckevort, W. J. P., Millemaggi, A., Leeman, M., Kaptein, B., Kellogg, R. M., and Vlieg, E. (2008b). Complete Deracemization by Attrition-Enhanced Ostwald Ripening Elucidated. **Angewandte Chemie International Edition.** 47: 6445-6447.

Noorduin, W. L., van Enckevort, W. J. P., Meekes, H., Kaptein, B., Kellogg, R. M., Tully, J. C., McBride, J. M., and Vlieg, E. (2010). The Driving Mechanism Behind Attrition-Enhanced Deracemization. **Angewandte Chemie International Edition.** 49: 8435-8438.

Rougeot, C. (2012). Deracemisation of active compound precursors by physical treatments. Ph.D. Thesis, **University Paul Sabatier of Toulouse III.** Toulouse, France.

Rougeot, C., Guillen, F., Plaquevent, J.-C., and Coquerel, G. (2015). Ultrasound-Enhanced Deracemization: Toward the Existence of Agonist Effects in the Interpretation of Spontaneous Symmetry Breaking. **Crystal Growth & Design.**

Sheldon, R. A. (1993). Industrial Synthesis of Optically Active Compounds. **Chirotechnology.** Marcel Dekker: New York.

Suwannasang, K., Coquerel, G., Rougeot, C., and Flood, A. E. (2014). Mathematical Modeling of Chiral Symmetry Breaking due to Differences in Crystal Growth Kinetics. **Chemical Engineering & Technology.** 37: 1329-1339.

Suwannasang, K., Flood, A. E., Rougeot, C., and Coquerel, G. (2013). Using Programmed Heating–Cooling Cycles with Racemization in Solution for

Complete Symmetry Breaking of a Conglomerate Forming System. **Crystal Growth & Design.** 13: 3498-3504.

Tsogoeva, S. B., Wei, S., Freund, M., and Mauksch, M. (2009). Generation of Highly Enantioenriched Crystalline Products in Reversible Asymmetric Reactions with Racemic or Achiral Catalysts. **Angewandte Chemie International Edition.** 48: 590-594.

van der Meijden, M. W., Leeman, M., Gelens, E., Noorduin, W. L., Meekes, H., van Enckevort, W. J. P., Kaptein, B., Vlieg, E., and Kellogg, R. M. (2009). Attrition-Enhanced Deracemization in the Synthesis of Clopidogrel - A Practical Application of a New Discovery. **Organic Process Research & Development.** 13: 1195-1198.

Viedma, C. (2005). Chiral Symmetry Breaking During Crystallization: Complete Chiral Purity Induced by Nonlinear Autocatalysis and Recycling. **Physical Review Letters.** 94**:** 065504.

Viedma, C., and Cintas, P. (2011). Homochirality beyond grinding: deracemizing chiral crystals by temperature gradient under boiling. **Chemical Communications.** 47: 12786-12788.

Viedma, C., Ortiz, J. E., Torres, T. d., Izumi, T., and Blackmond, D. G. (2008). Evolution of Solid Phase Homochirality for a Proteinogenic Amino Acid. **Journal of the American Chemical Society.** 130: 15274-15275.

CHAPTER VI

GENERAL CONCLUSION AND RECOMMENDATIONS

6.1 General Conclusion

This research has developed novel routes of purification of chiral organic compounds. Enantiopurification has been achieved in two effective and uncomplicated processes. The new methods can be used for chiral discrimination and are expected to be used for purification of pharmaceutical ingredients. The new methods can achieve 100% chiral purification at a yield of 100% of the solute, i.e. all the solute material in the crystal phase of the suspension can be recovered as the desired enantiomer.

Two related organic compounds, Cl-Tak and Me-Tak, were chosen as model compounds since they can be racemized rapidly in a basic medium and they also crystallize as a conglomerate forming system, which are the basic criteria of chiral symmetry breaking of organic materials. Evidence of chiral discrimination of the two collected compounds via the effect of dissolution/crystallization phenomenon induced by programmed-temperature cycles are proposed, independent of the grinding effect.

Although the abrasive technique in the presence of racemization in solution conducted at a constant temperature can be used to achieve a pure enantiomer of several organic compounds, the mechanisms behind this process are still uncertain. Indeed, the mechanical effect from abrasion would produce a lot of localized volumes

of high energy in the system leading to creation of a lot of micro-temperature cycles even through the macroscopic measured temperature seems to be constant. The temperature gradients occurring in the system may drive the system to a single crystalline phase upon destruction of small crystals and growth of the larger ones by consuming supersaturation produced by the dissolution. This process, however, takes time to reach a complete deracemization. Furthermore, several separation units are required for this process, increasing the operating cost and the loss of product in the additional separation units.

The boiling technique is the one of the techniques which can be used for complete deracemization. This process was recently demonstrated by Viedma. Deracemization via boiling of a suspension is driven by temperature gradients between the hot and the cool zones of the flask. The boiling was carried out in the absence of agitation in which case agglomeration would occur. The control of this process would appear to be difficult.

The use of programmed heating-cooling cycles combined with a fast solution phase racemization has thus been designed as a new process of deracemization. The magnitude of the temperature difference between the hot and cold parts of the cycle, which is used to promote the dissolution and recrystallization phenomena occurring in the system, can be programmed during the deracemization process. The implementation of this process is quite easy. The temperature cycles are run continuously until the crystal phase of the suspension completely changes to a pure enantiomer. This process can be highlighted as a single unit separation. After proving the possibility of this new process for deracemizing the model compounds, we conclude that

- The effect of grinding is not a major mechanism driving deracemization of the temperature cycles process. It was found that in the isothermal system (i.e. without temperature cycles) even if the suspension was agitated by a magnetic stirrer bar in order to create a uniform suspension of the crystals (avoiding agglomeration at the bottom of the flask), the evolution of enantiomeric excess in the solid phase did not occur, at least during the experimental period in which systems with temperature cycles could completely deracemize.

- In the temperature cycles process, all crystals are either partially or totally dissolved at the heating period of the cycles and the remaining crystals (those that do not fully dissolve) are regrown during the cooling period of the cycles. This is distinct from the dissolution/crystallization phenomenon occurring in the grinding system that is related to the Gibbs-Thomson effect. The size-dependent solubility, thus, is not counted as a primary mechanism of the temperature cycling induced-deracemization.

- The mechanism driving the deracemization in the temperature cycling system (a kinetic phenomenon) is far from Ostwald ripening (a process relation to thermodynamic stability) since the evolution of the enantiomeric excess is too fast for this to be driven by the Gibbs-Thomson effect.

- When the programmed heating-cooling cycles were introduced to the suspension of a racemic mixture of the two enantiomorphs operated with a fast racemization in solution phase, the evolution of enantiomeric excess begins and subsequently accelerated due to an autocatalytic phenomenon. Our hypothesis for the major mechanisms involved in this deracemization is the interplay between (i) dissolution and regrowth with crystal growth and/or dissolution rate dispersion as

described in the chapter III, (ii) racemization in solution and (iii) the entrainment effect (a kinetic phenomenon).

Enantiopurification via deracemization, however, may need an initial finite threshold to be created in order to send the process in the right direction. The direction of the deracemization could not predicted (the final crystalline state may be the pure *R*- or the pure *S*- enantiomer) but use of the same initial suspension tended to produce products of the same enantiomorph. We also noticed that the starting point of symmetry breaking is an unpredictable even through there are similar conditions. Therefore, we designed the use of temperature cycles having large swings of temperature between the high and the low parts of the cycles, with the same heating and cooling rates at the initial period, in order to accelerate the symmetry breaking. The amplitude of temperature difference was then reduced based on the change in the enantiomeric excess in solid phase as demonstrated in chapter IV.

As an economic aspect, the modification of the preferential crystallization was considered. The traditional PC has been typically used for the enantioseparation process in industry due to its effectiveness and because it has also a low operating cost compared with other enantioseparation techniques such as a chiral HPLC. PC is such a cyclic operating process, separating the two enantiomorphs at different times and usually in different vessels. PC, however, has been limited at 50% of the overall yield due to the unwanted enantiomer is considered as an impurity. The combination of using programmed heating-cooling cycles technique and preferential crystallization with simultaneous in-situ racemization in solution was designed. The combined process can be very effective in producing pure enantiomorphs. It takes a short time compared with the deracemization process. The direction of the outcome can be

assigned by seeding the desired enantiomorph. The symmetry breaking appears at the beginning of the process. Thanks to racemization in solution, the unwanted enantiomer can be converted to the desired enantiomer. This allows the combined process to achieve 100% yield based on the combined amount of *R*- and *S*-, and the racemization also helps by suppressing the primary nucleation of the undesired enantiomer. However, without temperature cycles the primary nucleation of the unwanted enantiomer eventually occurs resulting in a decrease in the product purity during the preferential crystallization. To solve this problem, temperature cycles (with or without damping) can be used to dissolve the small crystals of the unwanted enantiomorphs until only the desired enantiomorphic crystals remain in suspension.

6.2 Recommendations

Although the new route of enantiopurification based upon the temperature cycles has been successful, the mechanisms involved in complete deracemization have to be further investigated. A practical demonstration to prove the hypothesis of crystal growth rate dispersion being responsible for the deracemization still needs to be performed.

The limitations of this enantiopurification process are that the compound must crystallize as a conglomerate forming system and it must be easily racemizable at a temperature where the compound is relatively stable. Unfortunately, there are only 5 – 10% of intrinsically chiral organic molecules crystallizing as a conglomerate. However, most of primary amines can be modified by reacting with aldehydes to form Schiff bases, which are derivatives of the compound. Some derivative molecules probably crystallize as a conglomerate. Furthermore, the Schiff base derivatives are

easily racemizable in basic mediums. These may be unstable in the presence of acid and water. This is an advantage for the hydrolysis of the derivative into the starting compound after the separation process. In addition, the screening of aldehyde agents to make the desired derivatives has been encouraging.

The investigation of the use of temperature cycles for deracemizing other chiral compounds is also interesting. The optimization of the use of temperature cycles in the enantiopurification process should be further investigated. In addition, a route of scaling up the new process to purify the intrinsically chiral organic pharmaceutical ingredients is of great interest for practical applications of this new process.

APPENDIX A

PROPERTIES OF THE TRIAZOLYL KETONES

A.1 Synthesis of the Triazolyl Ketones

Dr. Céline Rougeot synthesized the two studied triazolyl ketones (i.e. Cl-Tak and Me-Tak) in the SMS laboratory at the University of Rouen, France, according to the procedure of synthesis described in a patent (Balasubramanyan and Shephard, 1977). During the period of her Ph.D. study, Dr. Rougeot synthesized a range of triazolyl ketone derivatives (Rougeot, 2012).

The first compound studied is 1-(4-chlorophenyl)-4,4-dimethyl-2-(1H-1,2,4-triazol-1-yl)pentan-3-one (Cl-Tak). This compound is a precursor of Paclobutrazol, a plant growth regulator. Cl-Tak crystallizes as a stable conglomerate without detectable solid solution (Black et al., 1989) and can be easily racemized using an alkaline aqueous solution (Black et al., 1990). These two properties are the basis for choosing this as a model compound for this research.

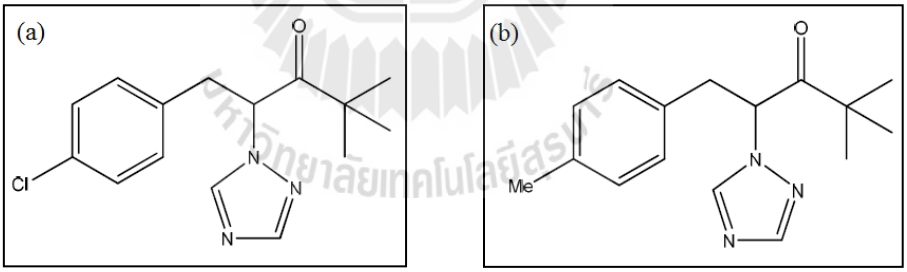

Figure A.1 Chemical structure of Tak derivatives; (a) Cl-Tak, (b) Me-Tak.

The second compound studied is 4,4-dimethyl-1-(p-toluyl)-2-(1H-1,2,4-triazol-1-yl)pentan-3-one (Me-Tak). Like Cl-Tak, this compound is rapidly racemizable in a basic medium and is a stable conglomerate compound so it also fits well with the criteria of this research (Rougeot, 2012).

A.2 Thermal Analysis of the Triazolyl Ketones

The physical properties of Cl-Tak and Me-Tak were reported as summarized in Table A.1;

Table A.1 Thermal analysis of Cl-Tak and Me-Tak.

	Cl-Tak	Me-Tak
Chemical Formula	$C_{15}H_{18}ClN_3O$	$C_{16}H_{21}N_3O$
Molecular weight (g/gmol)	291.77	271.36
Crystal System / Space group	Orthorhombic / $P2_12_12_1$ †, ‡	Orthorhombic / $P2_12_12_1$ †
Eutectic melting temperature (°C)	124.0	103.8
Melting temperature of pure compound (°C)	152.7	128.6 *

† SMS laboratory's data, ‡ (Black et al., 1989), * 97%e.e.

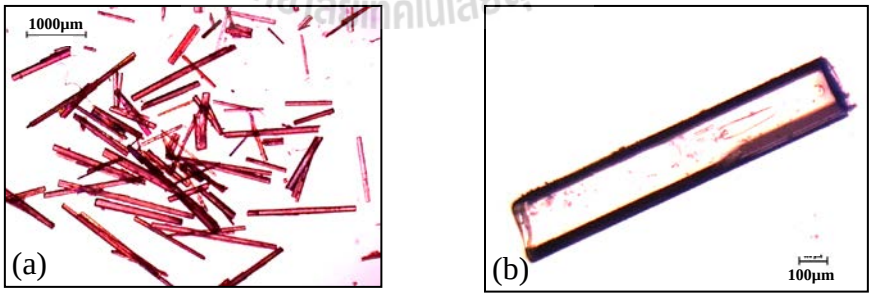

Figure A.2 Crystals of (a) Cl-Tak and (b) Me-Tak obtained from saturated solution (a) in methanol/water 80/20 from 30°C to room temperature, (b) in methanol from 35°C to room temperature.

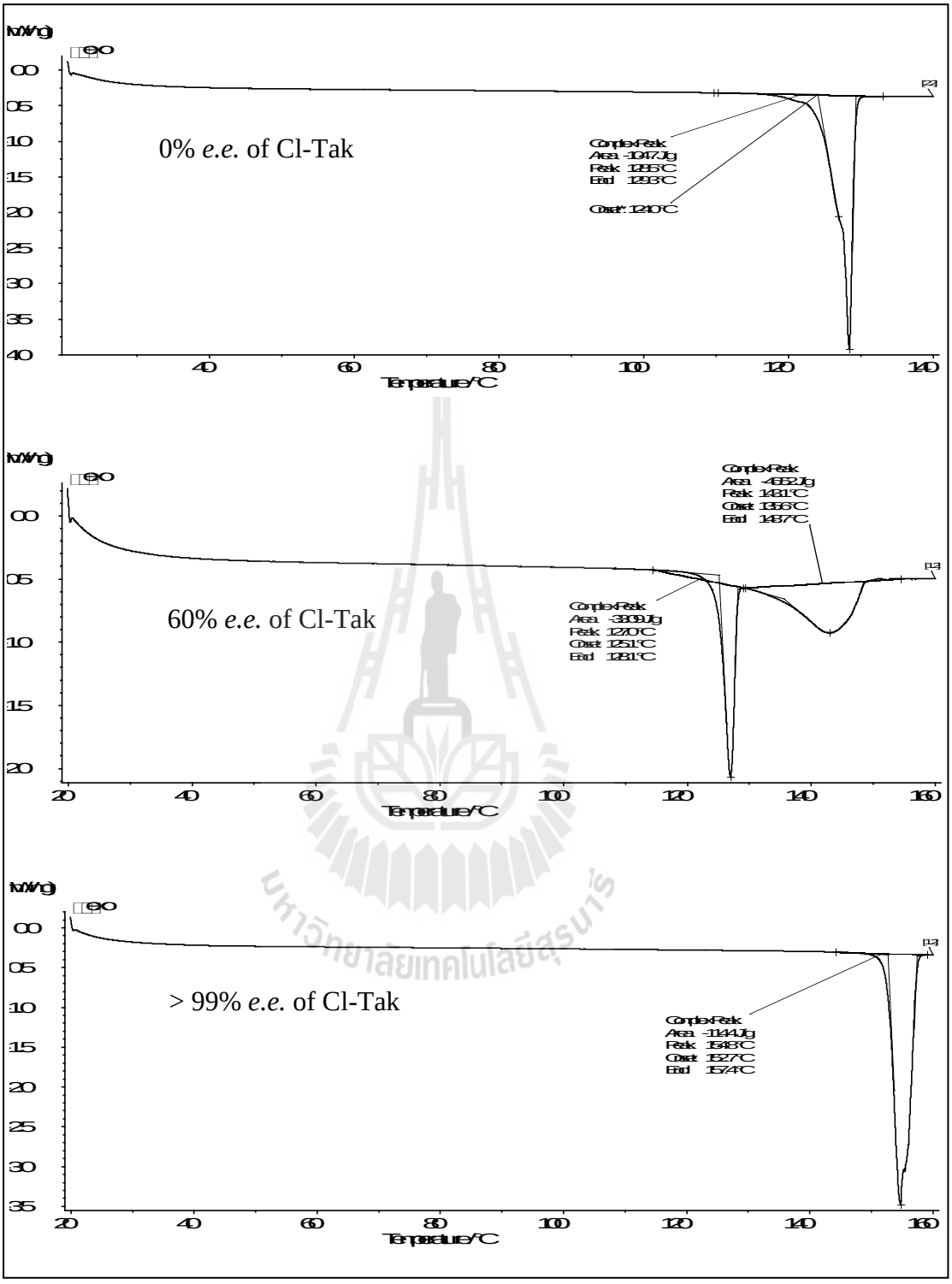

Figure A.3 DSC analysis of three different compositions of Cl-Tak.

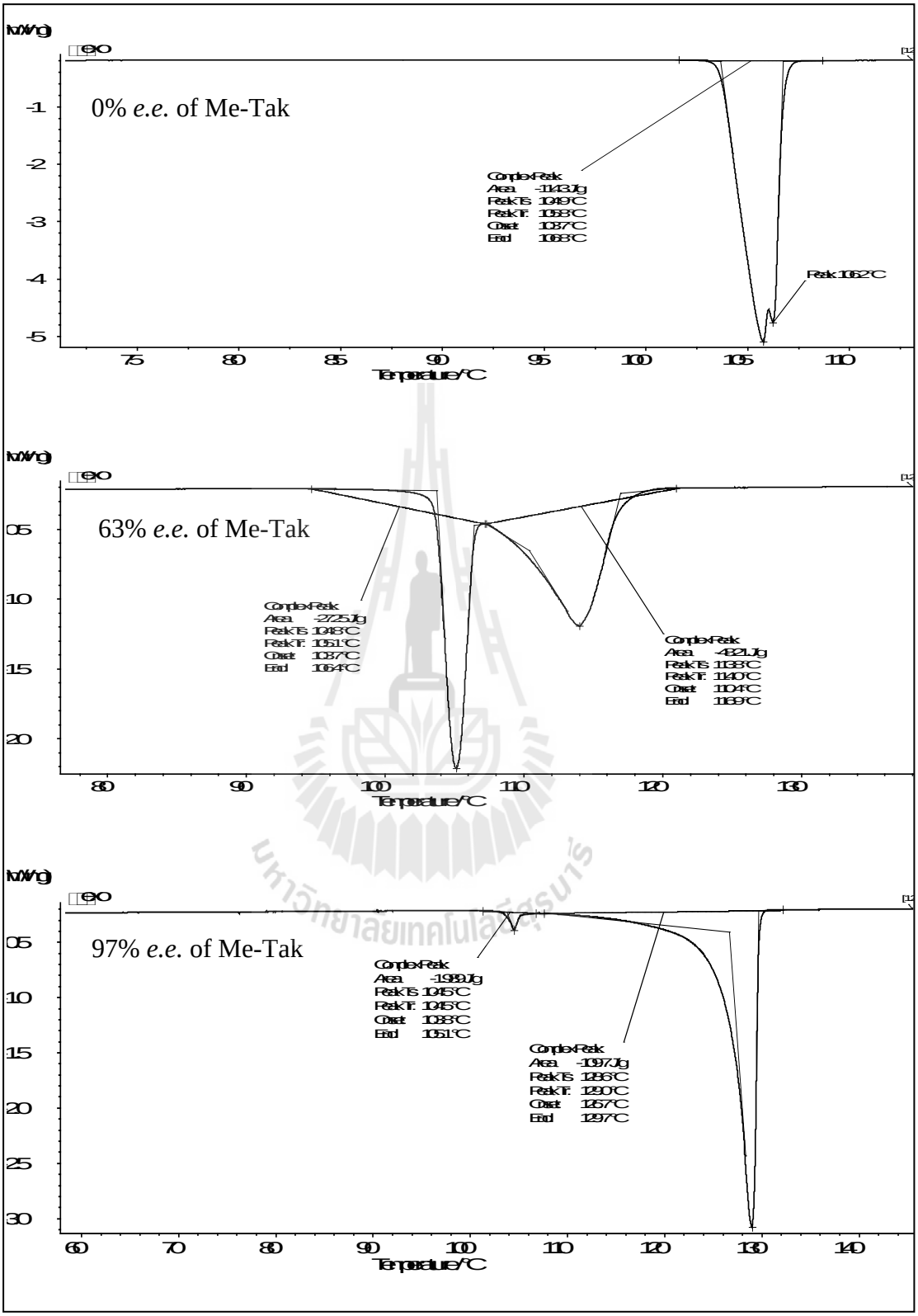

Figure A.4 DSC analysis of three different compositions of Me-Tak.

A.3 X ray Powder Diffraction (XRPD) of the Triazolyl Ketones

Racemic mixtures of Cl-Tak and Me-Tak were analyzed by powder X-ray diffraction. An analysis of their XRPD patterns shows that they are very similar as depicted in Figure A.5. These results preliminary indicated that the two Tak derivative compounds are isomorphous.

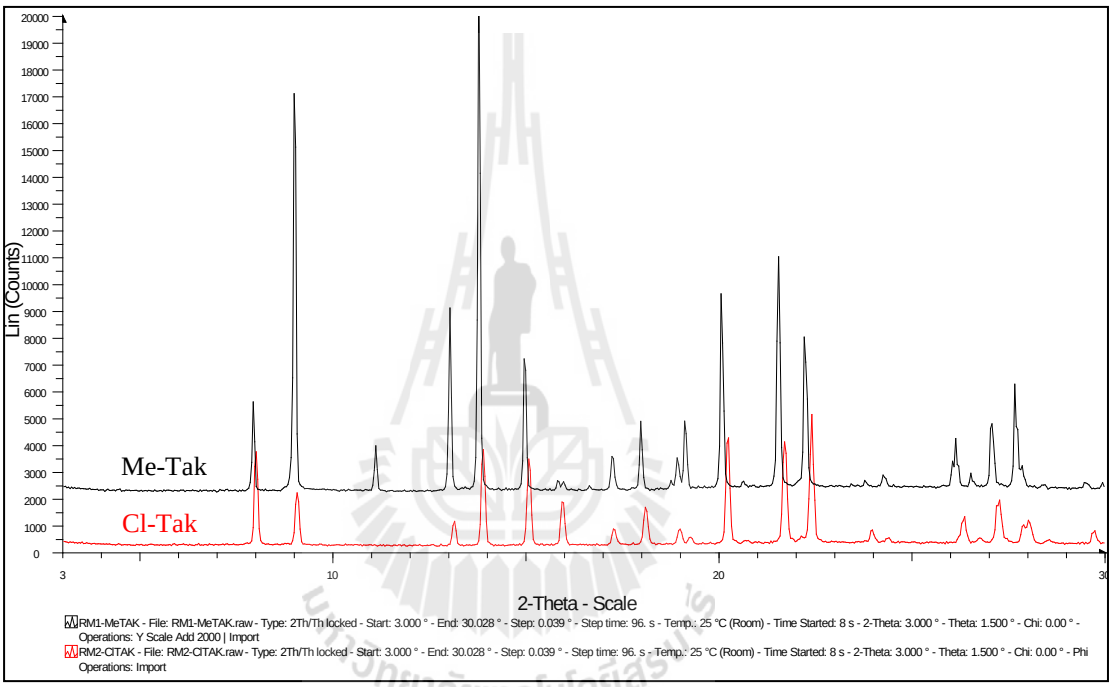

Figure A.5 XRPD analysis of the two Tak derivatives.

The crystals were also collected during the deracemization experiments and then the crystalline samples were analyzed using XRPD. The results show there is no change of XRPD pattern of the samples taken off during the deracemization experiments of Cl-Tak and Me-Tak as depicted in the Figure A6 and Figure A7, respectively. The DSC analysis and the perfect superimposition of the patterns pointed out that these Taks are a stable conglomerate in the experimental conditions.

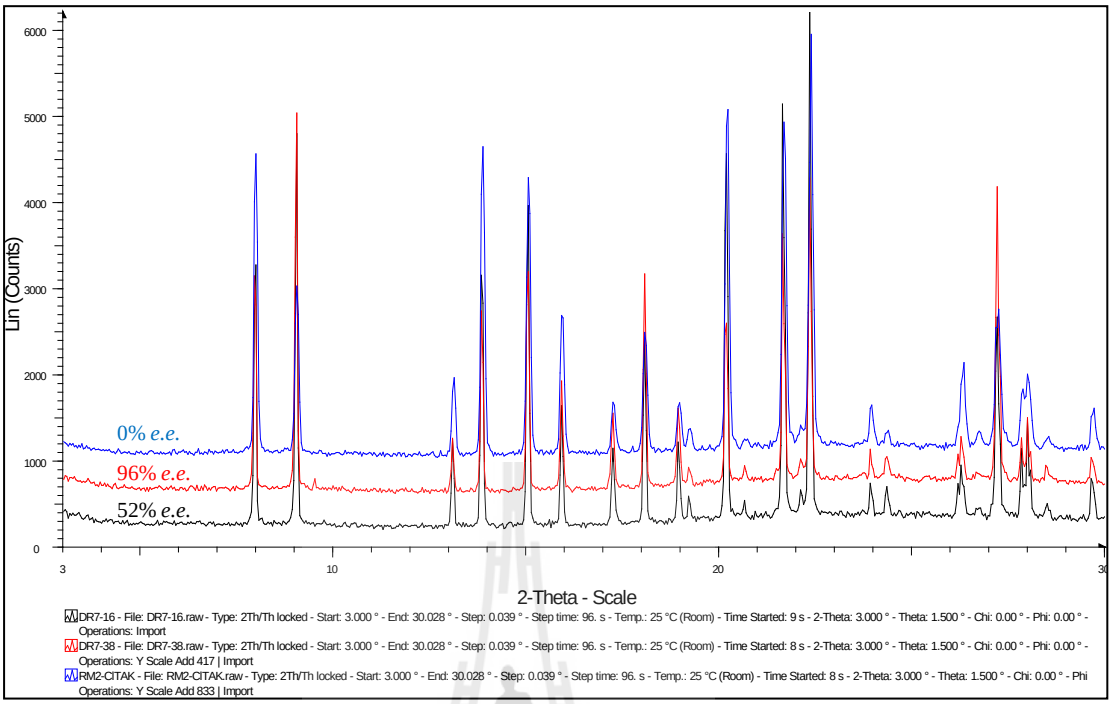

Figure A.6 XRPD analysis of the samples collected during deracemization of Cl-Tak.

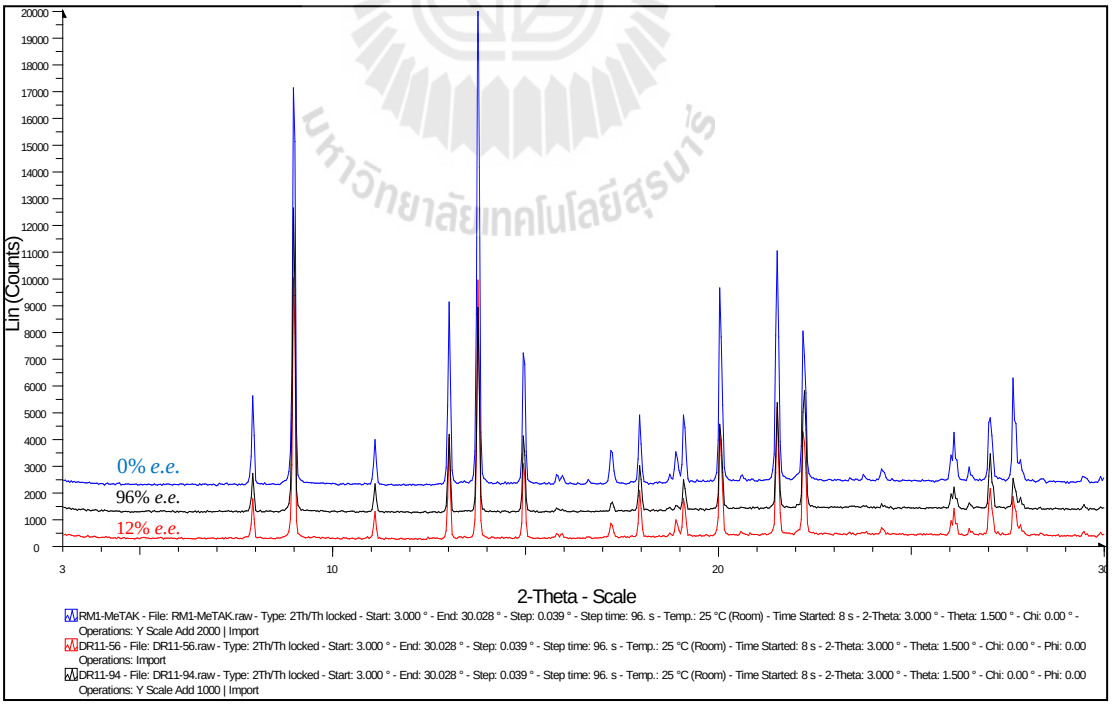

Figure A.7 XRPD analysis of the samples collected during deracemization of Me-Tak.

A.4 Solubility of the Triazolyl Ketones

As the solvent mixture used for preferential crystallization of Cl-Tak (Black et al., 1989), the mixture of methanol and distilled water as a solvent is suitable for the two model compounds. Solubilities of the racemic mixture and of the pure enantiomer of Cl-Tak were determined at different temperatures using the gravimetric method. The mixed solvents of 80 %wt methanol: 20 %wt water and of 65% methanol: 35% water were used for Cl-Tak and Me-Tak, respectively. The different composition of the solvent is due to the difference in solubilities of the two compounds in the mixed solvents.

According to Meyerhoffer's double solubility rule (Meyerhoffer, 1904), without the racemizing agent the two crystalline phase behave independently of another one. Hence, the solubility of the racemic composition should have exactly double the solubility of each of the pure enantiomers in g/g solution (not g/g solvent). Without racemization (i.e. in a 80/20 methanol/water mixture), the solubilites of the racemic mixture and of the pure enantiomer at 25°C are 5.0% and 2.4%, respectively (Suwannasang et al., 2013) which are in accordance with Meyerhoffer's rule within the accuracy of the technique.

Under racemizing conditions, the solubilities of the racemic mixture and of the pure enantiomer are very close (Table A.2), probably because both the solid phases are in equilibrium with a racemic liquid phase.

Table A.2 Solubilities of Cl-Tak in an 80/20 %wt methanol/water mixture containing 8 g of NaOH per kg of solvent. Solubilities are given in mass of Cl-Tak per 100 g of saturated solution.

Temperature (°C)	Solubility of the racemic mixture Cl-Tak (%)	Solubility of pure enantiomer of Cl-Tak (%)
20	3.9	3.6
25	4.6	4.4
30	5.8	5.5

Table A.3 Solubilities of Me-Tak in a 65/35 %wt methanol/water mixture containing 8 g of NaOH per kg of Solvent. Solubilities are given in mass of Me-Tak per 100 g of the mixed solvent.

Temperature (°C)	Solubility of the racemic mixture Me-Tak (%)
20	3.8
25	4.7
30	6.1

A.5 References

Balasubramanyan, S., and Shephard, M. C. (1977). Fungicidal compounds. **Patent US4243405 A.**

Black, S. N., Williams, L. J., Davey, R. J., Moffatt, F., Jones, R. V. H., McEwan, D. M., and Sadler, D. E. (1989). The preparation of enantiomers of paclobutrazol: A crystal chemistry approach. **Tetrahedron.** 45: 2677-2682.

Black, S. N., Williams, L. J., Davey, R. J., Moffatt, F., McEwan, D. M., Sadler, D. E., Docherty, R., and Williams, D. J. (1990). Crystal chemistry of 1-(4-chlorophenyl)-4,4-dimethyl-2-(1H-1,2,4-triazol-1-yl)pentan-3-one, a paclobutrazol intermediate. **The Journal of Physical Chemistry.** 94: 3223-3226.

Meyerhoffer, W. (1904). Stereochemische Notizen. **Berichte.** 37: 2604.

Rougeot, C. (2012). Deracemisation of active compound precursors by physical treatments. Ph.D. Thesis. **University Paul Sabatier of Toulouse III.** Toulouse, France.

Suwannasang, K., Flood, A. E., Rougeot, C., and Coquerel, G. (2013). Using Programmed Heating–Cooling Cycles with Racemization in Solution for Complete Symmetry Breaking of a Conglomerate Forming System. **Crystal Growth & Design.** 13: 3498-3504.

APPENDIX B

EXPERIMENTAL AND ANALYTICAL APPARATUS

B.1 Experimental Setup

The experimental setup used for the study of temperature cycles induced-deracemization is shown in Figure B.1. The experiments were carried out in a 50 mL double jacket round-bottom flask (Figure B.2). The temperature was controlled using a thermostat (Lauda RP 890;$\pm$0.02 ℃), Figure B.3. The suspension was stirred with an oval magnetic bar (length 2 cm) at 500 rpm.

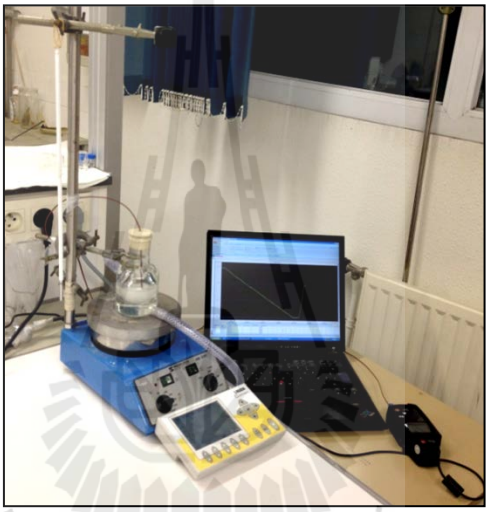

Figure B.1 Picture of the experimental setup used for study of the deracemization and preferential crystallization in the presence of racemization in solution.

Figure B.2 Picture of the reactor used for the study of deracemization and preferential crystallization in the presence of racemization in solution.

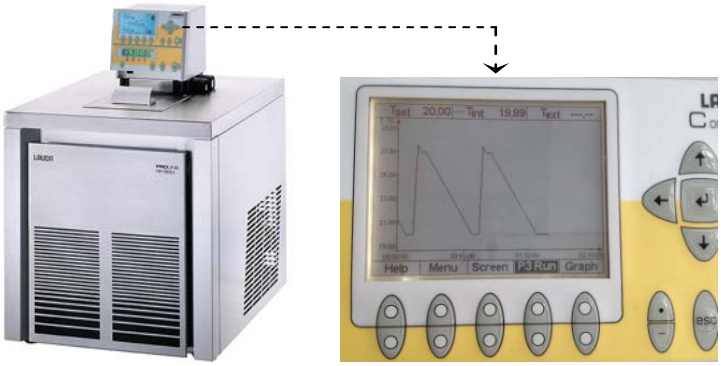

Figure B.3 Picture of LAUDA Proline RP 890 used as a cooling thermostat.

B.2 Temperature Monitoring

The temperature of suspension was monitored using a wire Teflon coated PT100 thermocouple connected to the Testo equipment for online temperature measuring.

Figure B.4 Picture of the Testo 177-T4 V01.10 Datalogger Unit with 0554 1765 USB interface and software used for measuring the temperature of the systems.

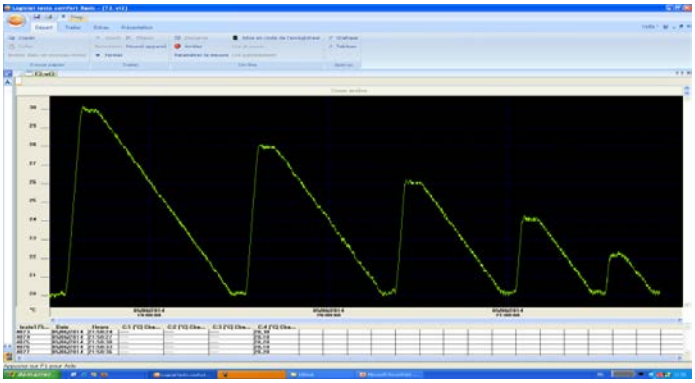

Figure B.5 Picture of a temperature profile in a damped pattern.

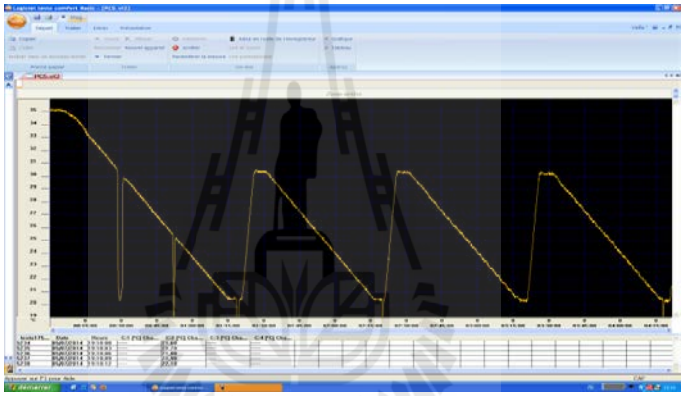

Figure B.6 Picture of a temperature profile measuring at the beginning of the experiment.

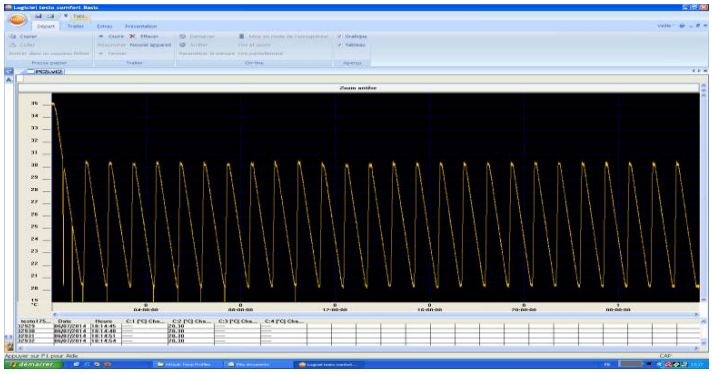

Figure B.7 Picture of temperature measuring throughout an experiment.

B.3 X ray Powder Diffraction (XRPD)

The XRPD apparatus located in the SMS laboratory at the University of Rouen was used for analysis of a powder sample of the crystal as shown in Figure B.8.

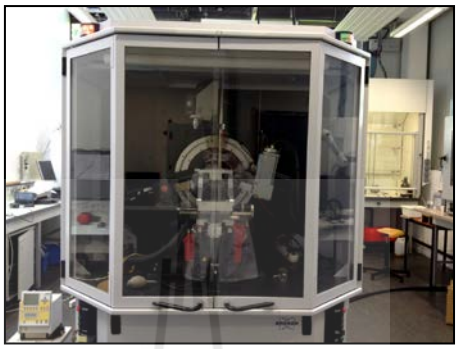

Figure B.8 Picture of XRPD equipment used for analyzing the crystalline samples.

B.4 High-Performance Liquid Chromatography (HPLC)

The enantiomeric excess of the solid samples was monitoring by chiral HPLC. A small amount of solid (*ca* 5 mg) was dissolved into 1 mL of ethanol. A 20 μL sample of this solution was injected into a Chiracel OD column (250 × 4.6 mm) using a solution of 5 % vol ethanol in *n*-heptane as eluent at a flow rate of 1.5 mL.min^{-1}.

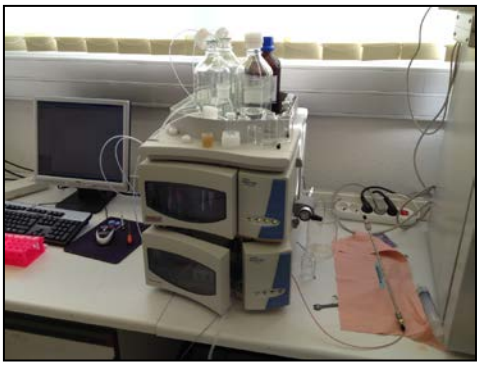

Figure B.9 Picture of HPLC equipment used for analyzing the samples.

Figure B.10 Picture of a ChiralCel OD column used for analyzing the *e.e.*

The two enantiomers of Cl-Tak were detected at retention times of *ca* 8.7 and *ca* 10.1 min using UV detection at a wavelength of 227 nm. For the Me-Tak, the retention times were at *ca* 7.6 and *ca* 9.1 minutes as shown in the Figures below.

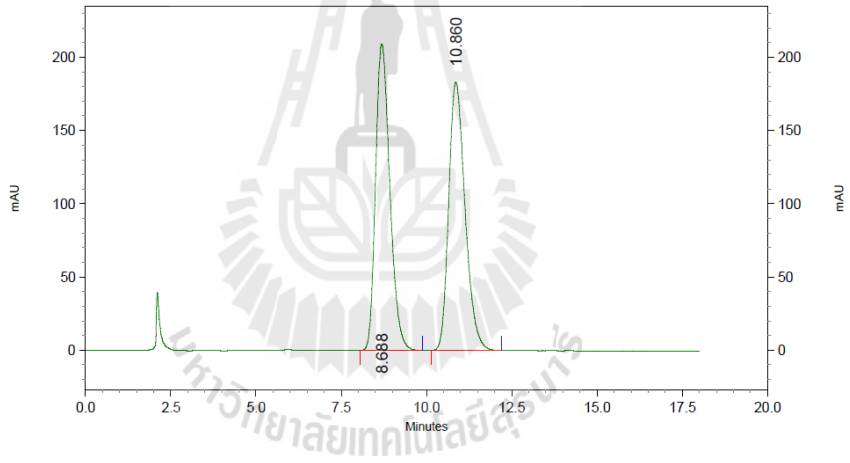

Figure B.11 Chromatogram of the sample of Cl-Tak.

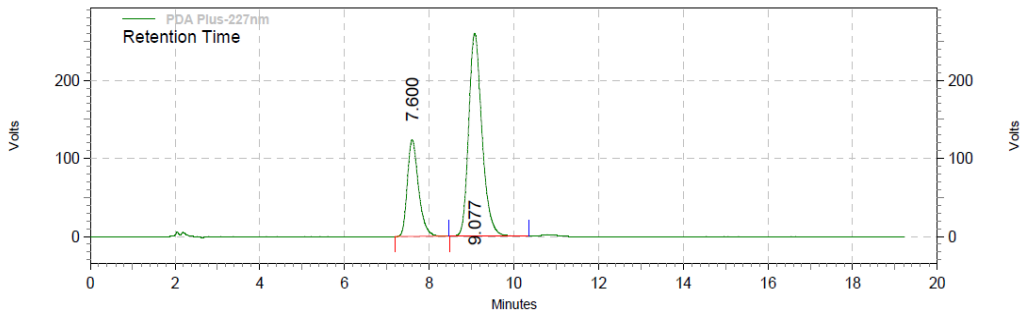

Figure B.12 Chromatogram of the sample of Me-Tak.

APPENDIX C

SUPPORTING INFORMATION AND EXAMPLE OF CALCULATION OF THE MATHEMATICAL MODELING

C.1 Schematic of Simulation for Dissolution and Growth Cycles based on McCabe's ΔL law

An initial concept for the mechanism of deracemization was that the two enantiomorphs have a difference in their mean size but the smaller size population (in this case *S*-) contains more crystals, such that the total initial mass in the smaller sized population is the same as in the larger sized population (in this case *R*-). A schematic of the simulation results for this model is shown in Figure C.1. This model assumes the system remains within the MSZW (i.e. there is no nucleation). During the first of these cycles the number of particles should decrease, causing the final size of the particles to be slightly larger than the initial size. After the first cycle, no more particles completely disappear, the smallest particles only approaching zero size by the end of the heating cycle. In a typical case this will not result in more than a fractional amount of change in the *e.e.*

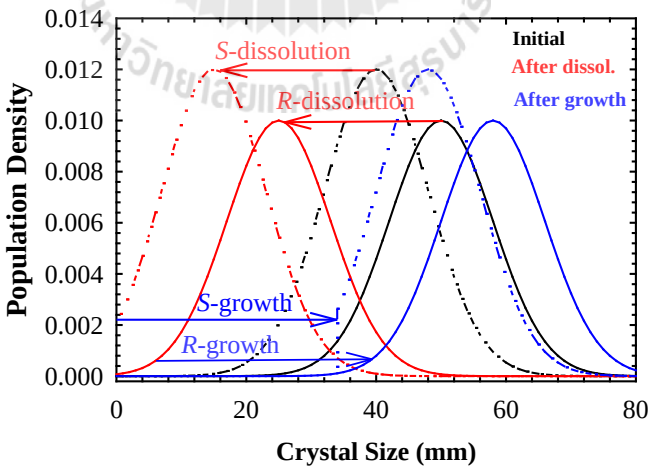

Figure C.1 Simulations for cycles based on dissolution and growth based on McCabe's ΔL law. By the second cycle the crystal size distributions begin to repeat and no further increase in *e.e.* was found.

The dissolution and regrowth phenomena based upon McCabe's ΔL law could be responsible for complete deracemization, but only under unusual conditions. The dissolution and growth might eventually destroy the smaller sized population of crystals (via Ostwald ripening for the crystals approaching zero size) leaving the other enantiomorph surviving, and thus eventually produce complete deracemization. The dominant enantiomorph, which has a bigger crystal mean size, could be the winner by consuming the solute produced during dissolution of the counter enantiomorph during the growth period.

C.2 Additional Simulations using the Growth Rate Dispersion Model

C.2.1 Simulation Model 2D

In order to get a better idea of the deracemization in systems with continuous growth rate activity distributions, the dispersion of growth rate activity is investigated by increasing the number of crystal of two populations from 2 crystals to 4 crystals of each enantiomorph; this helps bring the growth activity distributions slightly closer to continuous distributions. (Apart from the increasing number of discretizations of the growth rate distributions the model is the same as that presented in the paper under the section of the growth rate dispersion model). The distributions of growth activities of the two enantiomorphs are set by giving the four *R*-crystals a growth rate activity of 1 while *S*-crystals have the growth activities of 0.90, 0.95, 1.05 and 1.10, respectively. The mean growth rate distributions of both populations are still the same. The initial particle sizes of all crystals are 50 μm and the fraction of crystal dissolved in the suspension during the heating cycle is 50%. The results of this

experiment are shown in Figure A. The results indicate that the smoothing of the growth rate distribution of the disperse form slows the evolution of *e.e.* slightly.

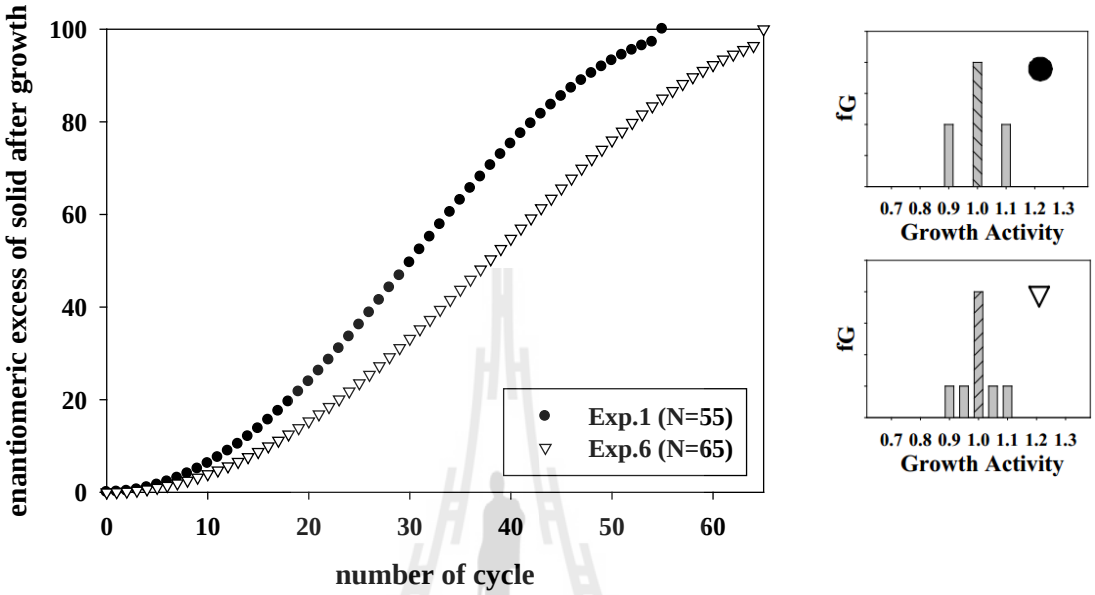

Figure C.2 Evolution of the solid phase enantiomeric excess when the functional form of the growth rate activity distribution is varied.

C.2.2 Simulation Model 2E

A simulation to model the case where both populations have GRD, but where the amount of dispersion is not the same for the two enantiomorphs, was performed in Simulation B. The growth rate activities of the two *R*-crystals are set at 0.95 and 1.05 (a narrow distribution of growth rate activity) and the growth rate activities of the two *S*-crystals are set at 0.90 and 1.10 (a wider distribution of growth rate activity). The results are shown in Figure B. The mean of the growth rate distributions of the two populations are equal at 1. The initial particle sizes of all crystals and the percentage of mass dissolved are given equal for the two

enantiomorphs. The result of this simulation is that the evolution of the *e.e.* is slowed when both enantiomorphs have dispersion in their growth rate distributions.

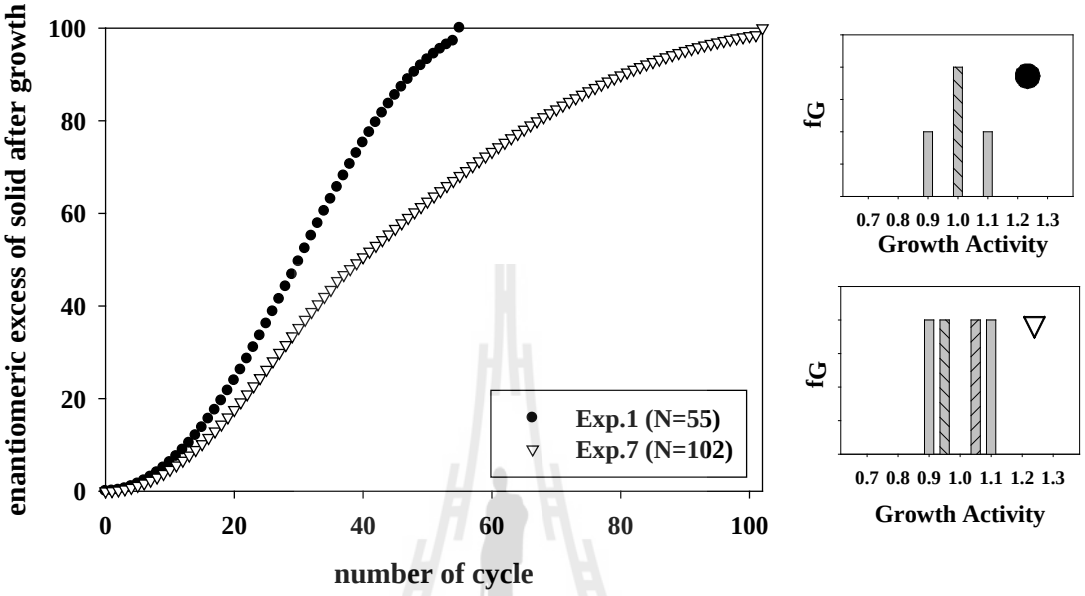

Figure C.3 Evolution of the solid phase enantiomeric excess when the functional form of the growth rate activity distribution is varied.

C.3 Flowchart of Calculation Procedure of Mathematical Modeling

As described in Chapter III, the main structure of the code of calculation of mathematical modelling is as follows:

a) Using equation 3.4 (of chapter III) to calculate the change in the size of crystals due to dissolution ($\Delta L^{i}_{D(j)}$). The third moment is reduced to the value required based on the fraction of crystals dissolved (FD) by an increase in the temperature from the low temperature in the cycle to the high temperature of the cycle.

b) When step (a) is completed the minimum crystal size ($L^{i}_{minD(j)}$) of both enantiomorphs are calculated, via equation 3.7. After that the rechecking of the value of $L^{i}_{minD(j)}$ is required; if it is negative value then sets it as zero and calculate step (a) again.

c) After cooling period of the cycle, the increase in size ($\Delta L^{i}_{G(j)}$) of remaining crystals is calculated by equation 3.11. The minimum crystal sizes of the two enantiomorphs ($L^{i}_{minG(j)}$) are calculated again using equation 3.14. The two new third moments of the populations ($\mu^{i}_{3,G(j)}$), after the cooling step, will be used to calculate the enantiomeric excess in the solid phase ($e.e._{(j)}$) by equation 3.16.

d) The simulation will be run using the same steps as described above, until complete deracemization (*e.e.* > 99%) is achieved.

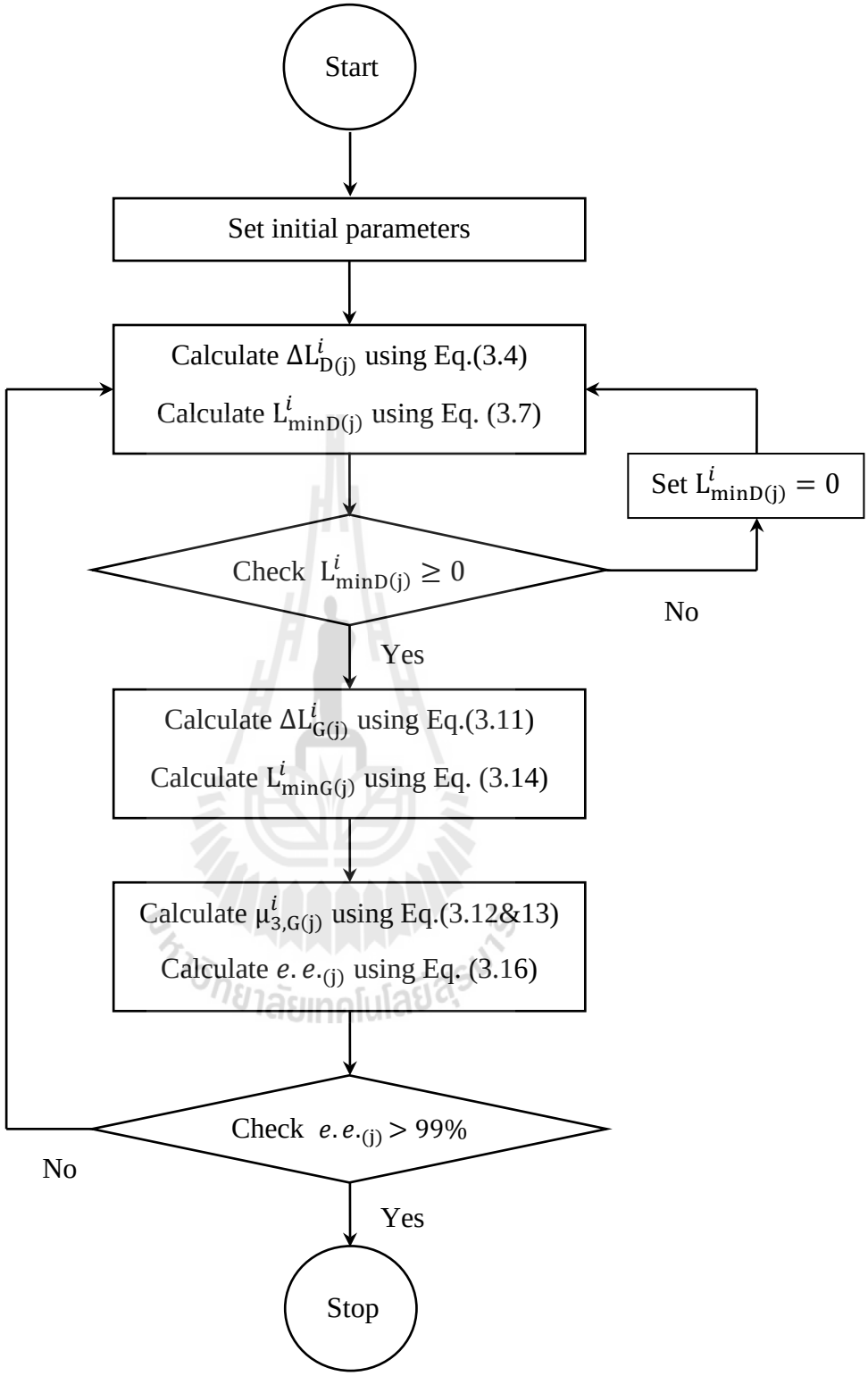

Figure C.4 Flowchart of the calculation procedure of the simulation.

C.4 Example of Calculation of Simulations Based on McCabe's ΔL law using Maple 9.5

C.4.1 Initial populations

```
> restart; DR := 0.5; DS := 0.5; GR := 0.5; GS := 0.5;

> LminGofR0 := 0;

> LminGofS0 := 0;

> LaveGofR0 := 5;

> LaveGofS0 := 4;

> nR := (1)*exp(-(l - LaveGofR0)^2/(2*1^2))/sqrt(2.*π);

> nS := (1.842105217)*exp(-(l - LaveGofS0)^2/(2*1^2))/sqrt(2.
      *π);

> mu3ofR := int(nR*l^3, l = 0 .. ∞);

                              140.000000

> mu3ofS := int(nS*l^3, l = 0 .. ∞);

                              140.000000

> ThirdMoment := mu3ofR + mu3ofS;

                              280.000000

> ee0 = 100*(mu3ofR - mu3ofS)/(mu3ofR + mu3ofS);

                              ee0 = 0.

> plot([nR, nS], l = -3 .. 10, title = "population density", linestyle
      = [SOLID, DASH], color = [blue, blue], legend = ["nR", "nS"]);
```

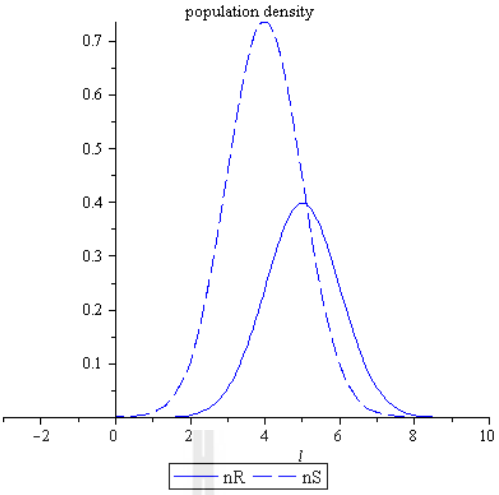

C.4.2 Length of R- and S- crystals after dissolution

```
> LminDofR1 := LminGofR0 - DR·t1;

> LminDofS1 := LminGofS0 - DS·t1;;

> LaveDofR1 := LaveGofR0 - DR·t1;

> LaveDofS1 := LaveGofS0 - DS·t1;

> DissOfnR1 := 1.*exp(-(l - LaveDofR1)^2/(2*1^2))/sqrt(2.
      *π);

> DissOfnS1 := (1.842105217)*exp(-(l - LaveDofS1)^2/(2*1^2))
      /sqrt(2.*π);

> Dissolve1 := int(DissOfnR1*l^3, l = LminDofR1 .. ∞)
      + int(DissOfnS1*l^3, l = LminDofS1 .. ∞);

> t1 := fsolve(Dissolve1 = ThirdMoment*(50/100), t1);
```

C.4.2.1 Checking the minimum size of *i* crystal after dissolution

```
> LminDofR1 := LminGofR0 - DR·t1;
```

-1.02192310

```
> LminDofS1 := LminGofS0 - DS·t1;
```

$$-1.02192310^{8}$$

C.4.2.1.2 If $L_{min} < 0$ then set $L_{min} = 0$

```
> LminDofR1new := 0;
```

$$0$$

```
> LminDofS1new := 0;;
```

$$0$$

C.4.2.1.3 Recalculation of the crystal length

```
> LaveDofR1new := LaveGofR0 - DR·t1new;

> LaveDofS1new := LaveGofS0 - DS·t1new;

> DissOfnR1new := 1.*exp(-(l - LaveDofR1new)^2/(2*1^2))
    /sqrt(2.*π);

> DissOfnS1new := (1.842105217)*exp(-(l - LaveDofS1new)^2/(2
    *1^2))/sqrt(2.*π);

> Dissolve1new := int(DissOfnR1new *l^3, l = LminDofR1new .. ∞)
    + int(DissOfnS1new *l^3, l = LminDofS1new .. ∞);

> t1new := fsolve(Dissolve1new = ThirdMoment*(50/100), t1new);

> plot([DissOfnR1new, DissOfnS1new], l = -1 .. 10, linestyle
    = [SOLID, DASH], color = [blue, blue]);
```

C.4.3 Length of R- and S- crystals after growth

```
> LminGofR1 := LminDofR1new + GR·t2;

> LminGofS1 := LminDofS1new + GS·t2;;
```

```
> LaveGofR1 := LaveDofR1new + GR·t2;

> LaveGofS1 := LaveDofS1new + GS·t2;

> GrowthOfnR1 := 1.*exp(-(l - LaveGofR1)^2/(2*1^2))/sqrt(2.
      *π);

> GrowthOfnS1 := (1.842105217)*exp(-(l - LaveGofS1)^2/(2*1
      ^2))/sqrt(2.*π);

> Growth1 := int(GrowthOfnR1*l^3, l = LminGofR1 .. ∞)
      + int(GrowthOfnS1*l^3, l = LminGofS1 .. ∞);

> t2 := fsolve(Growth1 = ThirdMoment*(100/100), t2);
```

C.4.4 Calculation of enantiomeric excess in solid phase

```
> ee1 := 100*(int(GrowthOfnR1*l^3, l = LminGofR1 .. ∞)
      -int(GrowthOfnS1*l^3, l = LminGofS1 .. ∞))
      /(int(GrowthOfnR1*l^3, l = LminGofR1 .. ∞)
      + int(GrowthOfnS1*l^3, l = LminGofS1 .. ∞));
```

0.000448785714

```
> plot([GrowthOfnR1, GrowthOfnS1], l = -1 .. 10, linestyle
      = [SOLID, DASH], color = [blue, blue]);
```

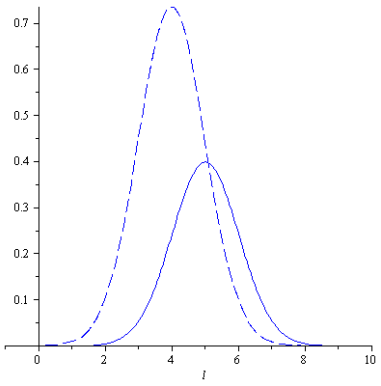

C.4.5 Similar steps of calculation for next cycles

```
> LminDofR2 := LminGofR1 - DR·t3;

> LminDofS2 := LminGofS1 - DS·t3;

> LaveDofR2 := LaveGofR1 - DR·t3;

> LaveDofS2 := LaveGofS1 - DS·t3;

> DissOfnR2 := 1.*exp(-(l - LaveDofR2)^2/(2*1^2))/sqrt(2.
      *π);

> DissOfnS2 := (1.842105217)*exp(-(l - LaveDofS2)^2/(2*1^2))
      /sqrt(2.*π);

> Dissolve2 := int(DissOfnR2*l^3, l = LminDofR2 .. ∞)
      + int(DissOfnS2*l^3, l = LminDofS2 .. ∞);

> t3 := fsolve(Dissolve2 = ThirdMoment*(50/100), t3);

> LminDofR2 := LminGofR1 - DR·t3;

                              0.

> LminDofS2 := LminGofS1 - DS·t3;

                              0.

> plot([DissOfnR2, DissOfnS2], l = -1 .. 10, linestyle = [SOLID,
      DASH], color = [blue, blue]);

> LminGofR2 := LminDofR2 + GR·t4;

> LminGofS2 := LminDofS2 + GS·t4;

> LaveGofR2 := LaveDofR2 + GR·t4;

> LaveGofS2 := LaveDofS2 + GS·t4;

> GrowthOfnR2 := 1.*exp(-(l - LaveGofR2)^2/(2*1^2))/sqrt(2.
      *π);
```

```
> GrowthOfnS2 := (1.842105217)*exp(-(l - LaveGofS2)^2/(2*1
      ^2))/sqrt(2.*π);

> Growth2 := int(GrowthOfnR2 *l^3, l = LminGofR2 .. ∞)
        + int(GrowthOfnS2 *l^3, l = LminGofS2 .. ∞);

> t4 := fsolve(Growth2 = ThirdMoment*(100/100), t4);

> ee2 := 100*(int(GrowthOfnR2 *l^3, l = LminGofR2 .. ∞)
      -int(GrowthOfnS2 *l^3, l = LminGofS2 .. ∞))
      /(int(GrowthOfnR2 *l^3, l = LminGofR2 .. ∞)
       + int(GrowthOfnS2 *l^3, l = LminGofS2 .. ∞));

                          0.000448785714

> plot([GrowthOfnR2, GrowthOfnS2], l = -1 .. 10, linestyle
      = [SOLID, DASH], color = [blue, blue]);

> ee3 := 100*(int(GrowthOfnR3 *l^3, l = LminGofR3 .. ∞)
      -int(GrowthOfnS3 *l^3, l = LminGofS3 .. ∞))
      /(int(GrowthOfnR3 *l^3, l = LminGofR3 .. ∞)
       + int(GrowthOfnS3 *l^3, l = LminGofS3 .. ∞));

                          0.000448785714

> plot([GrowthOfnR3, GrowthOfnS3], l = -1 .. 10, linestyle
      = [SOLID, DASH], color = [blue, blue]);
```

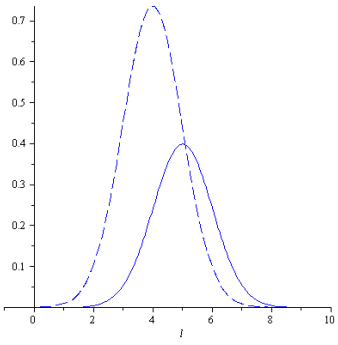

C.5 Example of Calculation of Simulations with Difference in Growth Rate Kinetics using Maple 9.5

C.5.1 Initial populations

```
> restart; DR := 0.1; DS := 0.1; GRinf := 0.1; GSinf := 0.05; T := 1/0.2; GR := GRinf;

> LminGofR0 := 0; LminGofS0 := 0; LaveGofR0 := 5; LaveGofS0 := 5;

> nR := (1)*exp(-(l-LaveGofR0)^2/(2*1^2))/sqrt(2.*π);

> nS := (1)*exp(-(l-LaveGofS0)^2/(2*1^2))/sqrt(2.*π);

> mu3ofR := int(nR*l^3, l = 0 .. ∞);

                              140.000000

> mu3ofS := int(nS*l^3, l = 0 .. ∞);

                              140.000000

> ThirdMoment := mu3ofR + mu3ofS;

                              280.000000

> ee0 = 100*(mu3ofR-mu3ofS)/(mu3ofR + mu3ofS);

                              ee0 = 0.

> plot([nR, nS], l = -3 .. 10, title = "population density", linestyle = [SOLID, DASH], color = [blue, blue], legend = ["nR", "nS"]);
```

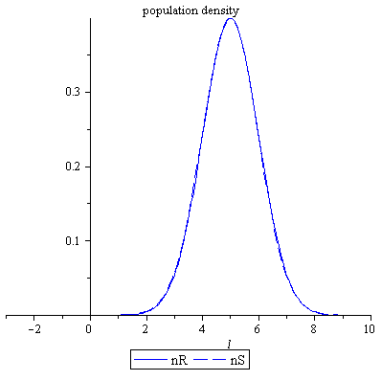

C.5.2 Length of R- and S- crystals after dissolution

```
> LminDofR1 := LminGofR0 - DR·t1;
> LminDofS1 := LminGofS0 - DS·t1;;
> LaveDofR1 := LaveGofR0 - DR·t1;
> LaveDofS1 := LaveGofS0 - DS·t1;
> DissOfnR1 := (1)*exp(-(l - LaveDofR1)^2/(2*1^2))/sqrt(2.
      *π);
> DissOfnS1 := (1)*exp(-(l - LaveDofS1)^2/(2*1^2))/sqrt(2.
      *π);
> Dissolve1 := int(DissOfnR1*l^3, l = LminDofR1 .. ∞)
      + int(DissOfnS1*l^3, l = LminDofS1 .. ∞);
> t1 := fsolve(Dissolve1 = ThirdMoment*(70/100), t1);
```

C.5.2.1 Checking the minimum size of *i* crystal after dissolution

```
> LminDofR1 := LminGofR0 - DR·t1;
```

$$-0.606295401$$

```
> LminDofS1 := LminGofS0 - DS·t1;
```

$$-0.606295401$$

C.5.2.1.2 If $L_{min} < 0$ then set $L_{min} = 0$

```
> LminDofR1new := 0;
```

$$0$$

```
> LminDofS1new := 0;
```

$$0$$

C.5.2.1.3 Recalculation of the crystal length

```
> LaveDofR1new := LaveGofR0 - DR·t1new;

> LaveDofS1new := LaveGofS0 - DS·t1new;

> DissOfnR1new := (1)*exp(-(l - LaveDofR1new)^2/(2*1^2))
      /sqrt(2.*π);

> DissOfnS1new := (1)*exp(-(l - LaveDofS1new)^2/(2*1^2))
      /sqrt(2.*π);

> Dissolve1new := int(DissOfnR1new*l^3, l = LminDofR1new .. ∞)
      + int(DissOfnS1new*l^3, l = LminDofS1new .. ∞);

> t1new := fsolve(Dissolve1new = ThirdMoment*(70/100), t1new);

> plot([DissOfnR1new, DissOfnS1new], l = -1 .. 10, linestyle
      = [SOLID, DASH], color = [red, red]);
```

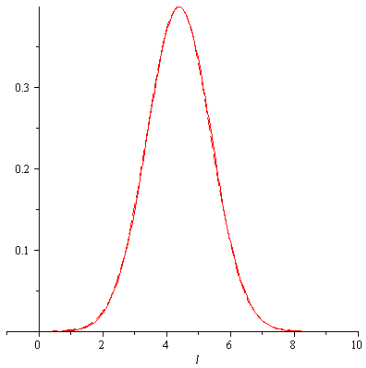

C.5.3 Length of R- and S- crystals after growth

> $GS1 := GSinf + (GRinf - GSinf) \cdot \exp\left(-\frac{1}{T}\right);$

> $LminGofR1 := LminDofR1new + GR \cdot t2;$

> $LminGofS1 := LminDofS1new + GS1 \cdot t2;;$

> $LaveGofR1 := LaveDofR1new + GR \cdot t2;$

> $LaveGofS1 := LaveDofS1new + GS1 \cdot t2;$

> $GrowthOfnR1 := 1.*\exp(-(l - LaveGofR1)\text{^}2/(2*1\text{^}2))/\mathrm{sqrt}(2.*\pi);$

> $GrowthOfnS1 := 1.*\exp(-(l - LaveGofS1)\text{^}2/(2*1\text{^}2))/\mathrm{sqrt}(2.*\pi);$

> $Growth1 := int(GrowthOfnR1*l\text{^}3,\ l = LminGofR1 .. \infty) + int(GrowthOfnS1*l\text{^}3,\ l = LminGofS1 .. \infty);$

> $t2 := fsolve(Growth1 = ThirdMoment*(100/100), t2);$

C.5.4 Calculation of enantiomeric excess of cycle1

> $ee1 := 100*(int(GrowthOfnR1*l\text{^}3,\ l = LminGofR1 .. \infty) - int(GrowthOfnS1*l\text{^}3,\ l = LminGofS1 .. \infty)) / (int(GrowthOfnR1*l\text{^}3,\ l = LminGofR1 .. \infty) + int(GrowthOfnS1*l\text{^}3,\ l = LminGofS1 .. \infty));$

1.60294964

> $plot([GrowthOfnR1, GrowthOfnS1], l = -1 .. 10, linestyle = [SOLID, DASH], color = [blue, blue]);$

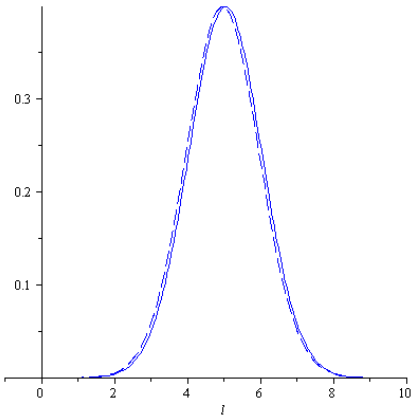

C.5.5 Similar steps of calculation for next cycles

```
> LminDofR2 := LminGofR1 - DR·t3;

> LminDofS2 := LminGofS1 - DS·t3;

> LaveDofR2 := LaveGofR1 - DR·t3;

> LaveDofS2 := LaveGofS1 - DS·t3;

> DissOfnR2 := 1.*exp(-(l - LaveDofR2)^2/(2*1^2))/sqrt(2.
      *π);

> DissOfnS2 := 1.*exp(-(l - LaveDofS2)^2/(2*1^2))/sqrt(2.*π);

> Dissolve2 := int(DissOfnR2*l^3, l = LminDofR2 .. ∞)
      + int(DissOfnS2*l^3, l = LminDofS2 .. ∞);

> t3 := fsolve(Dissolve2 = ThirdMoment*(70/100), t3);

> LminDofR2 := LminGofR1 - DR·t3;

                          0.028593211

> LminDofS2 := LminGofS1 - DS·t3;

                          -0.028951486

> LminDofR2new := LminGofR1 - DR·t3new;

                  0.6349085564 - 0.1 t3new
```

```
> LminDofS2new := 0;

> LaveDofR2new := LaveGofR1 - DR·t3new;

> LaveDofS2new := LaveGofS1 - DS·t3new;

> DissOfnR2new := (1)*exp(-(l - LaveDofR2new)^2/(2*1^2))
      /sqrt(2.*π);

> DissOfnS2new := (1)*exp(-(l - LaveDofS2new)^2/(2*1^2))
      /sqrt(2.*π);

> Dissolve2new := int(DissOfnR2new *l^3, l = LminDofR2new .. ∞)
      + int(DissOfnS2new *l^3, l = LminDofS2new .. ∞);

> t3new := fsolve(Dissolve2new = ThirdMoment*(70/100), t3new);

> plot([DissOfnR2new, DissOfnS2new], l = -1 .. 10, linestyle
      = [SOLID, DASH], color = [red, red]);
```

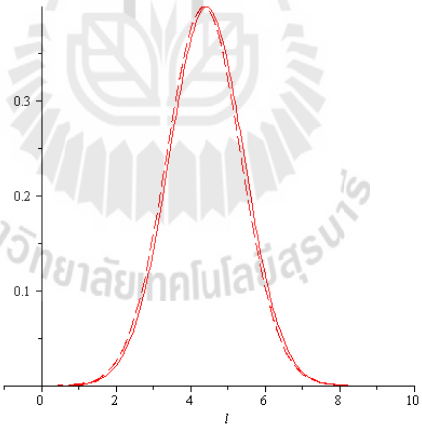


```
> GS2 := GSinf + (GRinf - GSinf)·exp(-2/T);

> LminGofR2 := LminDofR2new + GR·t4;

> LminGofS2 := LminDofS2new + GS2·t4;

> LaveGofR2 := LaveDofR2new + GR·t4;

> LaveGofS2 := LaveDofS2new + GS2·t4;
```

```
> GrowthOfnR2 := 1.*exp(-(l - LaveGofR2)^2/(2*1^2))/sqrt(2.
    *π);

> GrowthOfnS2 := 1.*exp(-(l - LaveGofS2)^2/(2*1^2))/sqrt(2.
    *π);

> Growth2 := int(GrowthOfnR2 *l^3, l = LminGofR2 .. ∞)
    + int(GrowthOfnS2 *l^3, l = LminGofS2 .. ∞);

> t4 := fsolve(Growth2 = ThirdMoment*(100/100), t4);

> ee2 := 100*(int(GrowthOfnR2 *l^3, l = LminGofR2 .. ∞)
    -int(GrowthOfnS2 *l^3, l = LminGofS2 .. ∞))
    /(int(GrowthOfnR2 *l^3, l = LminGofR2 .. ∞)
    + int(GrowthOfnS2 *l^3, l = LminGofS2 .. ∞));
```

4.62948703

```
> plot([GrowthOfnR2, GrowthOfnS2], l = -1 .. 10, linestyle
    = [SOLID, DASH], color = [blue, blue]);

> ee3 := 100*(int(GrowthOfnR3 *l^3, l = LminGofR3 .. ∞)
    -int(GrowthOfnS3 *l^3, l = LminGofS3 .. ∞))
    /(int(GrowthOfnR3 *l^3, l = LminGofR3 .. ∞)
    + int(GrowthOfnS3 *l^3, l = LminGofS3 .. ∞));
```

8.88800542

```
> plot([GrowthOfnR3, GrowthOfnS3], l = -1 .. 10, linestyle
    = [SOLID, DASH], color = [blue, blue]);
```

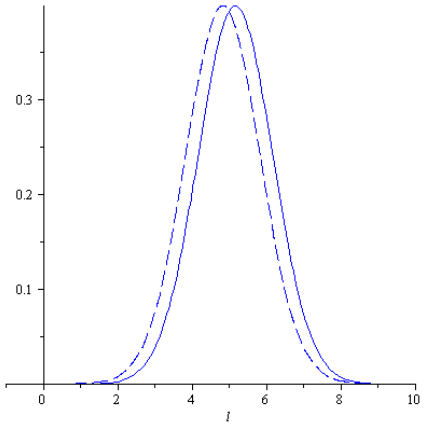

C.6 Example of Calculation of Simulations with Growth Rate Dispersion using Maple 9.5

C.6.1 Main code of calculation

for i **from** 2 **by** 1 **to** n **do**

$lrd(i,1) := lrg(i-1,1) - d(1,1)\cdot x$:
$lrd(i,2) := lrg(i-1,2) - d(2,1)\cdot x$:
$lsd(i,1) := lsg(i-1,1) - d(1,2)\cdot x$:
$lsd(i,2) := lsg(i-1,2) - d(2,2)\cdot x$:

$t(i,1) := fsolve\left(\left((\mathrm{lrd(i,1)})^3 + (\mathrm{lrd(i,2)})^3 + (\mathrm{lsd(i,1)})^3 + (\mathrm{lsd(i,2)})^3\right) = (1 - \mathrm{Fd})\cdot \mathrm{V}, \mathrm{x}\right)$:

$lrd(i,1) := lrg(i-1,1) - d(1,1)\cdot t(i,1)$:
$lrd(i,2) := lrg(i-1,2) - d(2,1)\cdot t(i,1)$:

$lsd(i,1) := lsg(i-1,1) - d(1,2)\cdot t(i,1)$:
$lsd(i,2) := lsg(i-1,2) - d(2,2)\cdot t(i,1)$:

$CEE(\mathrm{i},2) := 100 \cdot \left(\left(\left((lsd(i,1))^3 + (lsd(i,2))^3\right) - \left((lrd(i,1))^3 + (lrd(i,2))^3\right)\right)\right)$:

$lrg(i,1) := lrd(i,1) + g(1,1)\cdot y$:
$lrg(i,2) := lrd(i,2) + g(2,1)\cdot y$:
$lsg(i,1) := lsd(i,1) + g(1,2)\cdot y$:
$lsg(i,2) := lsd(i,2) + g(2,2)\cdot y$:

$t(i,2) := fsolve\left(\left((\mathrm{lrg(i,1)})^3 + (\mathrm{lrg(i,2)})^3 + (\mathrm{lsg(i,1)})^3 + (\mathrm{lsg(i,2)})^3\right) = \mathrm{V}, \mathrm{y}\right)$:

$lrg(i,1) := lrd(i,1) + g(1,1)\cdot t(i,2)$:
$lrg(i,2) := lrd(i,2) + g(2,1)\cdot t(i,2)$:

$lsg(i,1) := lsd(i,1) + g(1,2)\cdot t(i,2)$:
$lsg(i,2) := lsd(i,2) + g(2,2)\cdot t(i,2)$:

$CEE(i,1) := i - 1$:
$CEE(\mathrm{i},3) := 100 \cdot \left(\left(\left((lsg(i,1))^3 + (lsg(i,2))^3\right) - \left((lrg(i,1))^3 + (lrg(i,2))^3\right)\right)\right)$:

od:

C.6.2 Calculation of the cycle 1-9

C.6.2.1 Initial condition

> restart; n := 10; Fd := 1/2; Linitial := 50;

>

$LRd := Matrix(1..n, 1..2, lrd)$:
$lrd(1,1) := Linitial$:
$lrd(1,2) := lrd(1,1)$:

$LSd := Matrix(1..n, 1..2, lsd)$:
$lsd(1,1) := lrd(1,1)$:
$lsd(1,2) := lrd(1,1)$:

$V := 4 \cdot (lrd(1,1))^3$;

Time := $Matrix(1..n, 1..2, t)$:
$t(1,1) := 0$:
$t(1,2) := 0$:

$dissolutionrate := Matrix(1..2, 1..2, d)$:
$d(1,1) := 1$:
$d(2,1) := 1$:
$d(1,2) := 1$:
$d(2,2) := 1$:

$growthrate := Matrix(1..2, 1..2, g)$:
$g(1,1) := 1$:
$g(2,1) := 1$:
$g(1,2) := 0.9$:
$g(2,2) := 1.1$:

$LRg := Matrix(1..n, 1..2, lrg)$:
$lrg(1,1) := Linitial$:
$lrg(1,2) := lrd(1,1)$:

$LSg := Matrix(1..n, 1..2, lsg)$:
$lsg(1,1) := lrd(1,1)$:
$lsg(1,2) := lrd(1,1)$:

$crytalenanex := Matrix(1..n, 1..3, CEE)$:
$CEE(1,1) := 0$:
$CEE(1,2) := 0$:
$CEE(1,3) := 0$:

$V := 500000$

C.6.2.2 Enantiomeric excess in solid phase

> *crytalenanex* ;

0	0	0
1	0.	0.06369432000
2	0.1010958240	0.2541608600
3	0.4032541038	0.5704425401
4	0.9045058327	1.011536320
5	1.602512016	1.576388180
6	2.494554695	2.263885879
7	3.577521631	3.072849501
8	4.847884750	4.002019962
9	6.301672496	5.050045021

C.6.2.3 Length of R- and S- crystals after dissolution

> *LRd*;

50	50
39.68502630	39.68502630
39.67164849	39.67164849
39.63161061	39.63161061
39.56501259	39.56501259
39.47189797	39.47189797
39.35225549	39.35225549
39.20602109	39.20602109
39.03307999	39.03307999
38.83326908	38.83326908

> *LSd*;

50	50
39.68502630	39.68502630
38.64121292	40.70208406
37.57257950	41.69064172
36.47866805	42.65135713
35.35897079	43.58482515
34.21293052	44.49158046
33.03994147	45.37210071
31.83935036	46.22680962
30.61045790	47.05608026

C.6.2.4 Length of R- and S- crystals after growth

> *LRg*;

50	50
49.98938203	49.98938203
49.95760392	49.95760392
49.90474489	49.90474489
49.83083895	49.83083895
49.73587586	49.73587586
49.61980201	49.61980201
49.48252121	49.48252121
49.32389553	49.32389553
49.14374612	49.14374612

> *LSg*;

50	50
48.95894646	51.01981760
47.89857281	52.01663503
46.81840035	52.99108943
45.71791177	53.94376613
44.59655089	54.87520083
43.45372239	55.78588163
42.28879158	56.67625084
41.10108435	57.54670671
39.88988724	58.39760500

C.6.3 Calculation of the cycle 27-36

C.6.3.1 Initial condition

>

$LRd := Matrix(1..n, 1..2, lrd)$:
$lrd(1,1) := 41.83061894$:
$lrd(1,2) := lrd(1,1)$:

$LSd := Matrix(1..n, 1..2, lsd)$:
$lsd(1,1) := 13.09688705$:
$lsd(1,2) := 70.56435082$:

$Vcal := 2(lrd(1,1))^3 + (lsd(1,1))^3 + (lsd(1,2))^3$;
$V := 4 \cdot (Linitial^3)$;

Time $:= Matrix(1..n, 1..2, t)$:
$t(1,1) := 12.13283989$:
$t(1,2) := 11.50449944$:

$dissolutionrate := Matrix(1..2, 1..2, d)$:
$d(1,1) := 1$:
$d(2,1) := 1$:
$d(1,2) := 1$:
$d(2,2) := 1$:

$growthrate := Matrix(1..2, 1..2, g)$:
$g(1,1) := 1$:
$g(2,1) := 1$:
$g(1,2) := 0.9$:
$g(2,2) := 1.1$:

$LRg := Matrix(1..n, 1..2, lrg)$:
$lrg(1,1) := lrd(1,1)$:
$lrg(1,2) := lrd(1,2)$:

$LSg := Matrix(1..n, 1..2, lsg)$:
$lsg(1,1) := lsd(1,1)$:
$lsg(1,2) := lsd(1,2)$:

$crytalenanex := Matrix(1..n, 1..3, CEE)$:
$CEE(1,1) := 27$:
$CEE(1,2) := 55.37579328$:
$CEE(1,3) := 41.44380358$:

$Vcal := 4.99999999810^5$ $V := 500000$

C.6.3.2 Length of R- and S- crystals after dissolution

> *LRd*;

$$\begin{bmatrix} 41.83061894 & 41.83061894 \\ 29.57614621 & 29.57614621 \\ 28.80192845 & 28.80192845 \\ 28.00595004 & 28.00595004 \\ 27.19120946 & 27.19120946 \\ 26.36122268 & 26.36122268 \\ 25.51999690 & 25.51999690 \\ 24.67196998 & 24.67196998 \\ 23.82191336 & 23.82191336 \\ 22.97480079 & 22.97480079 \end{bmatrix}$$

> *LSd*;

$$\begin{bmatrix} 13.09688705 & 70.56435082 \\ 0.84241432 & 58.30987809 \\ -1.09168855 & 58.69554544 \\ -3.05673269 & 59.06863276 \\ -5.04929396 & 59.43171287 \\ -7.06524049 & 59.78768584 \\ -9.09974331 & 60.13973710 \\ -11.14732686 & 60.49126681 \\ -13.20196369 & 60.84579040 \\ -15.25721305 & 61.20681462 \end{bmatrix}$$

C.6.3.3 Recalculation due to the negative value of length

>

$lrd1 := 41.17499730 - 11.28138030 - d(1,1)\cdot x:$
$lrd2 := 41.17499730 - 11.28138030 - d(2,1)\cdot x:$
$lsd1 := 11.28138030 - 11.28138030:$
$lsd2 := 71.06861429 - 11.28138030 - d(2,2)\cdot x:$

$t1 := fsolve\left(\left((lrd1)^3 + (lrd2)^3 + (lsd1)^3 + (lsd2)^3\right) = ((1 - Fd)\cdot V), x\right);$

$$t1 := 1.09177352$$

> $lrd1 := 41.17499730 - 11.28138030 - d(1,1)\cdot t1;$
> $lrd2 := 41.17499730 - 11.28138030 - d(2,1)\cdot t1;$
> $lsd1 := 11.28138030 - 11.28138030;$
> $lsd2 := 71.06861429 - 11.28138030 - d(2,2)\cdot t1;$
> $crystalVol = (\mathrm{lrd1})^3 + (\mathrm{lrd2})^3 + (\mathrm{lsd1})^3 + (\mathrm{lsd2})^3;$

$lrd1 := 28.8018434$ $lrd2 := 28.8018434$

$lsd1 := 0.$ $lsd2 := 58.6954604$

$crystalVol = 2.50000000110^5$

> $CEE := 100\cdot \frac{\left(\left((lsd1)^3 + (lsd2)^3\right) - \left((lrd1)^3 + (lrd2)^3\right)\right)}{\left(\left((lsd1)^3 + (lsd2)^3\right) + \left((lrd1)^3 + (lrd2)^3\right)\right)};$

$CEE := 61.7720648$

>
> $lrg1 := lrd1 + g(1,1)\cdot y :$
> $lrg2 := lrd2 + g(2,1)\cdot y :$
> $lsg1 := 0 :$
> $lsg2 := lsd2 + g(2,2)\cdot y :$
>
> $t2 := fsolve\left(\left((\mathrm{lrg1})^3 + (\mathrm{lrg2})^3 + (\mathrm{lsg1})^3 + (\mathrm{lsg2})^3\right) = \mathrm{V}, y\right);$

$t2 := 11.7220842$

>
> $lrg1 := lrd1 + g(1,1)\cdot t2;$
> $lrg2 := lrd2 + g(2,1)\cdot t2;$
> $lsg1 := 0;$
> $lsg2 := lsd2 + g(2,2)\cdot t2;$
> $crystalVol = (\mathrm{lrg1})^3 + (\mathrm{lrg2})^3 + (\mathrm{lsg1})^3 + (\mathrm{lsg2})^3;$

$lrg1 := 40.5239277$

$lrg2 := 40.5239277$

$lsg1 := 0$

$lsg2 := 71.5897531$

$crystalVol = 4.99999999910^5$

> $CEE := 100\cdot \frac{\left(\left((lsg1)^3 + (lsg2)^3\right) - \left((lrg1)^3 + (lrg2)^3\right)\right)}{\left(\left((lsg1)^3 + (lsg2)^3\right) + \left((lrg1)^3 + (lrg2)^3\right)\right)};$

$CEE := 46.7616503$

C.6.4 Calculation of the cycle 29-38

C.6.4.1 Initial condition

>

$LRd := Matrix(1..n, 1..2, lrd)$:
$lrd(1,1) := 40.52392776$:
$lrd(1,2) := lrd(1,1)$:

$LSd := Matrix(1..n, 1..2, lsd)$:
$lsd(1,1) := 0$:
$lsd(1,2) := 71.58975318$:

$Vcal := 2(lrd(1,1))^3 + (lsd(1,1))^3 + (lsd(1,2))^3$;
$V := 4 \cdot (Linitial^3)$;

Time $:= Matrix(1..n, 1..2, t)$:
$t(1,1) := T$:
$t(1,2) := 11.72208428$:

$dissolutionrate := Matrix(1..2, 1..2, d)$:
$d(1,1) := 1$:
$d(2,1) := 1$:
$d(1,2) := 1$:
$d(2,2) := 1$:

$growthrate := Matrix(1..2, 1..2, g)$:
$g(1,1) := 1$:
$g(2,1) := 1$:
$g(1,2) := 0.9$:
$g(2,2) := 1.1$:

$LRg := Matrix(1..n, 1..2, lrg)$:
$lrg(1,1) := lrd(1,1)$:
$lrg(1,2) := lrd(1,2)$:

$LSg := Matrix(1..n, 1..2, lsg)$:
$lsg(1,1) := lsd(1,1)$:
$lsg(1,2) := lsd(1,2)$:

$crytalenanex := Matrix(1..n, 1..3, CEE)$:
$CEE(1,1) := 29$:
$CEE(1,2) := 61.77206486$:
$CEE(1,3) := 46.76165031$:

$V := 500000$ $Vcal := 4.99999999910^5$

C.6.4.2 Enantiomeric excess in solid phase

> *crytalenanex* ;

$$\begin{bmatrix} 29 & 61.77206486 & 46.76165031 \\ 30 & 64.86965117 & 49.57098327 \\ 31 & 67.87614093 & 52.34791979 \\ 32 & 70.78440418 & 55.08882131 \\ 33 & 73.58724948 & 57.78988888 \\ 34 & 76.27746577 & 60.44715703 \\ 35 & 78.84787633 & 63.05648911 \\ 36 & 81.29140621 & 65.61357401 \\ 37 & 83.60116603 & 68.11392550 \\ 38 & 85.77055453 & 70.55288431 \end{bmatrix}$$

C.6.4.3 Length of R- and S- crystals after dissolution

> *LRd*;

$$\begin{bmatrix} 40.52392776 & 40.52392776 \\ 28.00189955 & 28.00189955 \\ 27.17915246 & 27.17915246 \\ 26.33287362 & 26.33287362 \\ 25.46231474 & 25.46231474 \\ 24.56671191 & 24.56671191 \\ 23.64529109 & 23.64529109 \\ 22.69727508 & 22.69727508 \\ 21.72189260 & 21.72189260 \\ 20.71838971 & 20.71838971 \end{bmatrix}$$

> *LSd*;

$$\begin{bmatrix} 0 & 71.58975318 \\ 0 & 59.06772497 \\ 0 & 59.42460861 \\ 0 & 59.76580047 \\ 0 & 60.09097882 \\ 0 & 60.39981436 \\ 0 & 60.69197454 \\ 0 & 60.96712892 \\ 0 & 61.22495613 \\ 0 & 61.46515251 \end{bmatrix}$$

C.6.4.4 Length of R- and S- crystals after growth

> *LRg*;

$$\begin{bmatrix} 40.52392776 & 40.52392776 \\ 39.79820681 & 39.79820681 \\ 39.05385946 & 39.05385946 \\ 38.29024590 & 38.29024590 \\ 37.50669840 & 37.50669840 \\ 36.70252187 & 36.70252187 \\ 35.87699497 & 35.87699497 \\ 35.02937194 & 35.02937194 \\ 34.15888529 & 34.15888529 \\ 33.26474960 & 33.26474960 \end{bmatrix}$$

> *LSg*;

$$\begin{bmatrix} 0 & 71.58975318 \\ 0 & 72.04366296 \\ 0 & 72.48678631 \\ 0 & 72.91890998 \\ 0 & 73.33980085 \\ 0 & 73.74920532 \\ 0 & 74.14684881 \\ 0 & 74.53243547 \\ 0 & 74.90564809 \\ 0 & 75.26614839 \end{bmatrix}$$

APPENDIX D

LIST OF PUBLICATIONS

LIST OF PUBLICATIONS

D.1 Selected International Publications

Suwannasang, K., Flood, A. E., Rougeot, C., and Coquerel G. (2013). Using Programmed Heating–Cooling Cycles with Racemization in Solution for Complete Symmetry Breaking of a Conglomerate Forming System. **Crystal Growth & Design** 13 (8): 3498-3504. (2014 Impact factor = 4.558)

Suwannasang, K., Coquerel G., Rougeot, C., and Flood, A. E. (2014). Mathematical Modeling of Chiral Symmetry Breaking due to Differences in Crystal Growth Kinetics. **Chemical Engineering & Technology** 37(8): 1329-1339. (2014 Impact factor = 2.175)

D.2 Selected Conference Proceeding

Suwannasang, K., Flood, A. E., Rougeot, C., and Coquerel G. (2012). Using a Programmed Heating-Cooling Cycle with Racemization for Symmetry Breaking of a Chiral Organic Compound. **Conference Proceedings of the 10th International Workshop on Crystal Growth of Organic Materials (CGOM10)**, June 11-14. Limerick, Ireland.

Suwannasang, K., Flood, A. E., and Coquerel G. (2013). Potential Mechanisms for the Symmetry Breaking of a Racemic Suspension due to Temperature Cycles. **Conference Proceedings of the 20th International Workshop on Industrial Crystallization (BIWIC)**, September 18 – 20. University of Southern Denmark.

Flood, A. E., Suwannasang, K., Rougeot, C., and Coquerel G. (2014). Use of Temperature Cycles and Solution Phase Racemization Agent for Complete Deracemization of a Suspension of a Conglomerate. **The 4th TIChE International Conference**, December 18 – 19. Chiang Mai, Thailand.

CRYSTAL GROWTH & DESIGN

Article

pubs.acs.org/crystal

Using Programmed Heating–Cooling Cycles with Racemization in Solution for Complete Symmetry Breaking of a Conglomerate Forming System

Published as part of a Crystal Growth and Design virtual special issue of selected papers presented at the 10th International Workshop on the Crystal Growth of Organic Materials (CGOM10)

K. Suwannasang,[†] A. E. Flood,*[,†] C. Rougeot,[‡] and G. Coquerel[‡]

[†]School of Chemical Engineering, Suranaree University of Technology, Nakhon Ratchasima 30000, Thailand

[‡]Normandie Univ, France, SMS Unité de Crystallogénèse EA3233, Université de Rouen, 76821, Mont-Saint-Aignan Cedex, France

ABSTRACT: A deracemization technique using periodic temperature fluctuations on a conglomerate forming system undergoing a swift racemization in solution is demonstrated. The method uses heating and cooling periods of the suspension in order to create cycles of partial dissolution of the crystal phase followed by crystal regrowth: this enables symmetry breaking in the solid phase. The technique is an effective, simple, and cheap operation, and can promote understanding of the effects of dissolution and recrystallization on chiral symmetry breaking in the solid phase. The heating period leads to the decrease of the size of crystals and the destruction of small crystals; the surviving crystals can then grow during the cooling period. A succession of such cycles allows the autocatalytic transformation from a racemic suspension into pure enantiomer, with an enantiomeric excess (*ee*) > 99% within a few days. The results demonstrate a possible mechanism for the emergence of homochirality of molecules of biological significance on Earth.

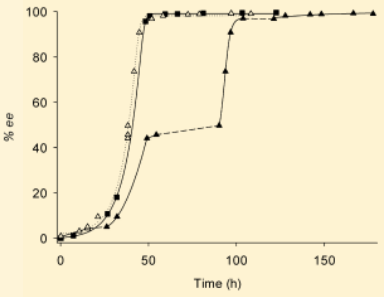

INTRODUCTION

Access to pure enantiomers remains an important scientific and industrial issue. Recently, a new crystallization process called Viedma ripening was designed.[1] Viedma showed that it was possible to completely break the symmetry of a racemic mixture of D- and L-crystals of $NaClO_3$ by using a continuous grinding technique in suspension. Though achiral in solution, $NaClO_3$ has the special feature to crystallize in the chiral space group $P2_13$,[2] giving two kinds of enantiomorphous crystals. An older technique named total symmetry breaking, which was described by Kipping and Pope in 1898, was used to obtain an enantiomeric excess over 90% by seeding a saturated solution of $NaClO_3$ with solid composed of pure enantiomorphous crystals.[3] In 2008, the first example of the total symmetry breaking of an intrinsically chiral component, an amino acid derivative, was jointly given by a Dutch consortium and the group of Blackmond by combining Viedma ripening and *in situ* racemization in solution.[4] After this initial research, further chiral organic compounds have been deracemized.[5−10] Unfortunately, the number of candidates is limited by the important restrictions of this process: compounds must crystallize as a conglomerate (i.e., a physical mixture of the two enantiomers) and must undergo a fast racemization in solution under the same operating conditions. The number of publications on the topic has also significantly increased as researchers attempt to explain how racemic suspensions in contact with a saturated solution and a racemizing agent are able to evolve toward an enantiopure final state. Additionally, the full resolution of the mechanism of the deracemization could give the keys to understand why only one enantiomer of many natural chiral compounds is prevalent in nature. The understanding of how biological systems may have naturally become homochiral is one of the most important questions for scientists.[11−14]

Numerous studies have been carried out to explain the mechanism of chiral symmetry breaking of the crystal phase. After vigorous debates, the current standard model involves the combination of Ostwald ripening and the reincorporation of chiral clusters by crystals of the same chirality.[5,10,15−17] Indeed, attrition produced by grinding enables the production of a high number of chiral clusters that increase the exchange of matter between particles and thus the rate of the evolution of the *ee* of the solid phase. Moreover, due to the minimization of the energy surfaces, the smaller particles produced by grinding are quickly dissolved to the benefit of the growth of the larger ones (Ostwald ripening) which also speeds up the evolution of the *ee*. Numerous computer models have been produced to simulate the evolution of such a process by taking in account the reincorporation of clusters, the effect of Ostwald ripening, the size dependent solubility, the agglomeration of particles,

Received: March 24, 2013
Revised: June 22, 2013
Published: June 25, 2013

dx.doi.org/10.1021/cg400436r | *Cryst. Growth Des.* 2013, 13, 3498−3504

and of course, the crystallization as a conglomerate together with fast racemization in solution.[18−23] These studies also demonstrated that the grinding and the resulting processes were not necessary to complete deracemization, but they serve to significantly accelerate the evolution of the *ee*.[5] Ripening occurs somewhere between the solubility of an infinite size crystal and the solubility of a nucleus, which will result in slow kinetics since these two limits are very close and both dissolution and growth processes will occur at very low levels of supersaturation.

In 2011, Viedma and Cintas showed that boiling suspensions of sodium chlorate can also lead to chiral symmetry breaking of the crystals.[24] They suggested that dissolution/crystallization cycles due to the temperature gradient existing between the bottom of the flask (in contact with a hot plate) and the top of the flask (in contact with atmosphere at ambient temperature) are responsible for the process of deracemization. Recent modeling performed by Iggland and Mazzotti[25] has shown that simultaneous growth of crystals larger than the critical size and dissolution of crystals smaller than the critical size may be able to produce relatively fast chiral symmetry breaking. It should be emphasized that this process (a form of ripening) is very distinct from growth and dissolution cycles due to temperature gradient where essentially all the crystals in the suspension grow in the lower temperature part of the gradient and dissolve (either partially or totally) in the upper temperature part. It is possible that similar effects occur in suspensions undergoing grinding. Indeed, attrition induces localized volumes of high energy/temperature in the system, which leads to the dissolution/recrystallization phenomenon.

This paper aims at contributing to a better understanding of deracemization in heterogeneous systems. This study is focused on the effect of temperature fluctuations at near ambient conditions in a gently stirred system on the deracemization of a model compound, 1-(4-chlorophenyl)-4,4-dimethyl-2-(1*H*-1,2,4-triazol-1-yl)pentan-3-one **1** (Figure 1). This compound,

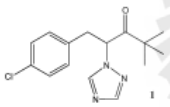

Figure 1. Chemical structure of **1**.

a precursor of Paclobutrazol, a plant growth inhibitor,[26] is known to crystallize as a stable conglomerate without detectable solid solution and can be easily racemized using an alkaline aqueous solution.[27] The deracemization of this compound was previously described in the literature at 25 °C.[6] This compound was thus an appropriate candidate to study the possibility to perform deracemization by means of temperature cycles at near ambient conditions to simulate the natural temperature cycling and in order to address the question of how chiral symmetry breaking occurs

■ EXPERIMENTAL SECTION

Materials. Racemic 1-(4-chlorophenyl)-4,4-dimethyl-2-(1*H*-1,2,4-triazol-1-yl)pentan-3-one (**1**) was synthesized according to the literature.[28]

Distilled water was used for deracemization experiments. HPLC-grade *n*-heptane and ethanol, and reagent-grade methanol were purchased from Fisher Scientific.

Deracemization Experiments. The deracemizations were carried out as follows: in a 50 mL round-bottom thermostatted flask, **1** was suspended in a methanol/water mixture (80/20 wt %, 25 g) and then the racemising agent, sodium hydroxide (0.2 g, i.e., 8 g per kg of solvent), was added. An oval magnetic stirrer operated at 500 rpm was used to ensure a uniform distribution of particles and temperature in the heterogeneous system, and then a temperature program (TP) was applied. Different masses of **1** and different TPs (Figure 2) were used to achieve the symmetry breaking in the study, as summarized in Table 1. The first temperature program TP1 consisted of four steps: holding

Table 1. Required Number of Cycles and Required Time to Achieve Complete Symmetry Breaking (Defined As Reaching an *ee* > 98%) for the Experiments Described

	TP	total mass of **1** (g)	required time to complete deracemization (h)	number of cycles required to complete deracemization
experiment I	1	3.3	91	91
experiment II	2	2.5	51	86
experiment III	3	2.5	51	121
experiment IV	4	2.5	51	67
experiment V	2	1.8	32	55

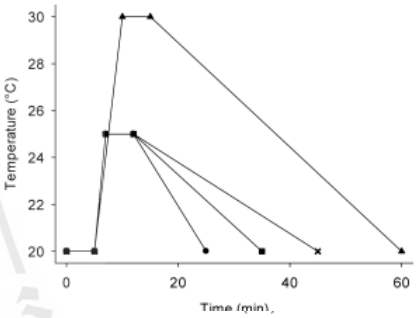

Figure 2. The different temperature programs. ▲ TP1, ■ TP2, ● TP3, and × TP4.

at 20 °C for 5 min, ramping up to 30 °C over a period of 5 min, holding at 30 °C for 5 min, and then ramping down to 20 °C over a period of 45 min. The second temperature program TP2 starting by holding the temperature of the suspension at 20 °C for 5 min, then ramping it up to 25 °C over a period of 2 min, then holding it at 25 °C for 5 min, and finally ramping it down to 20 °C over 23 min. The third temperature program TP3 and fourth temperature program TP4 were identical to TP2 with the exception that the final ramp from 25 to 20 °C occurred over periods of 13 min (TP3) and 33 min (TP4). These temperature cycles were continued over a large number of cycles until deracemization was substantial. The suspension was partially dissolved during the heating period. The remaining crystals then recrystallize and grow during the cooling period by consumption of the supersaturation in the solution phase. The recrystallized amount is the same as the mass lost during the heating step.

HPLC. The *ee* was monitored by chiral HPLC.[6] Samples were taken off at the end of cycles (at 20 °C) using a plastic pipet. The solid was then filtered under a vacuum and washed with a sufficient amount of water to remove the rest of the sodium hydroxide (the solubility of **1** in water at 20 °C is lower than 0.1%[6]). A small amount of solid (ca. 5 mg) was then dissolved into 1 mL of ethanol. A 20 μL sample of this solution was injected into a Chiracel OC column (250 × 4.6 mm) using a solution of 5 vol% ethanol in *n*-heptane as eluent at a flow rate of 1.5 mL·min^{-1}. The two enantiomers were detected at retention

times of ca. 8 and ca. 10 min using UV detection at a wavelength of 227 nm.

Solubility. Solubilities of the racemic mixture and of the pure enantiomer of **1** were determined at different temperatures using the gravimetric method. Without racemization (i.e., in a 80/20 methanol/water mixture), the solubilites of the racemic mixture and of the pure enantiomer are 5.0% and 2.4%, respectively at 25 °C and are in accordance with Meyerhoffer's rule. Under racemizing conditions, the solubilities of the racemic mixture and of the pure enantiomer are very close (Table 2), probably because both the solid phases are in equilibrium with a racemic liquid phase. The presence of sodium hydroxide seems to decrease the solubility of **1**. It should be noted that HPLC analyses confirmed that the chirality of the solid phases was the expected chirality (racemic for determination of the solubility of racemic **1**, enantiomerically pure for determination of the solubility of pure enantiomer of **1**) and that the liquid phases (that is to say, the dry extracts) were racemic.

Table 2. Solubilities of 1 in an 80/20 wt % Methanol/Water Mixture Containing 8 g of NaOH per kg of Solvent[a]

temperature (°C)	solubility of the racemic mixture **1** (%)	solubility of pure enantiomer of **1** (%)
20	3.9	3.6
25	4.6	4.4
30	5.8	5.5

[a]Solubilities are given in mass of **1** per 100 g of saturated solution.

Enantiomeric Excess (*ee*) in the Solid Phase. Enantiomeric excess in the solid phase is defined in terms of the predominant enantiomer at complete deracemization (at the end of the experiment). The experimental results demonstrated that the deracemization was random; the final product of the deracemization could be either of the R-form or the S-form of the compound. The presentation here is focused on the absolute value of the *ee* in order to compare the results more conveniently.

RESULTS

First, experiments were carried out to give the proof that temperature cycles at near ambient conditions were able to totally break the symmetry of the solid phase. TP1 and TP2, respectively experiment I (Figure 3a) and experiment II (Figure 4a), were applied to a suspension of **1**. After a few dozens of hours (ca. 90 h and ca. 50 h, respectively) and cycles (ca. 90 cycles and ca. 85 cycles, respectively), the solid phase became enantiomerically pure. The time required to achieve complete deracemization in the solid phase using the temperature cycling technique is shorter than when using grinding by small glass beads at constant temperature, which requires around a week for complete deracemization. These results indicate that it is possible to achieve total symmetry breaking of the solid phase by using cyclic temperature fluctuations in the system. The behavior of the conversion is a sigmoidal curve with an exponential part as illustrated by the curve $\ln(ee) = f(t)$ (see Figure 3b).

TP2 is shorter than TP1 and with smaller temperature fluctuations (between 20 and 25 °C instead of 20 and 30 °C for TP1). Therefore, for a usual ds/dT — variation of solubility versus temperature — there is no need for a high temperature gradient to break the symmetry.

It is known that grinding due to a magnetic stirrer is also able to perform deracemization.[29] Similar experiments were thus conducted in the same operating conditions than experiments I and II but with some periods of constant temperature to demonstrate that the symmetry breaking found in this study was due to temperature cycling rather than grinding. Experiment I′ was carried out at constant temperature (20 °C) for the first 142 h, and then TP1 cycles were applied (Figure 3a). No evolution of the *ee* is visible in the absence of temperature cycles during the observation period. But, once TP1 is applied, symmetry breaking of the solid phase significantly increases, leading to complete deracemization at ca. 90 temperature cycles (90 h) after the initiation of the temperature program. Figure 3b shows that the linear part of the curve $\ln(ee) = f(t)$ of experiment I and I′ is parallel, meaning that the evolution of the *ee* is not disturbed by the initial constant temperature period.

In the case of experiment II′, three periods of constant temperature were applied between periods of temperature cycles (Figure 4a). The evolution of the *ee* of the solid phase when the temperature is constant is much slower (almost without evolution) than during the TP2 periods even at high values of *ee* (≈45%). When merging the TP2 periods together (removing data at constant temperature), the evolution of *ee* in the solid phase (dotted line) is similar to the continuous use of TP2 throughout the experiment. The curves $\ln(ee) = f(t)$ are also superimposable (Figure 4b).

The fast evolution of the *ee* observed in this study is therefore due to the temperature fluctuations applied to the suspension and not due to the grinding ensured by the magnetic stirrer.

The effect of the cooling rate on the evolution of *ee* of the solid was investigated; the temperature programs TP2, TP3,

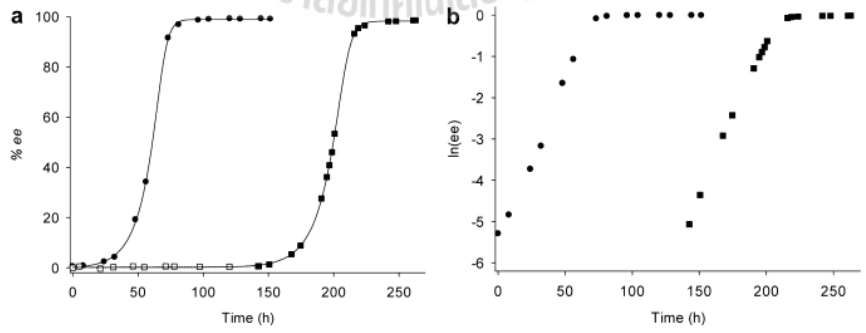

Figure 3. Deracemization by using TP1. (a) Evolution of *ee* versus time. (b) Evolution of ln(*ee*) versus time. ● Experiment I, □ Experiment I′ - constant temperature period (20 °C), ■ Experiment I′ - TP1 period.

dx.doi.org/10.1021/cg400436r | *Cryst. Growth Des.* 2013, 13, 3498−3504

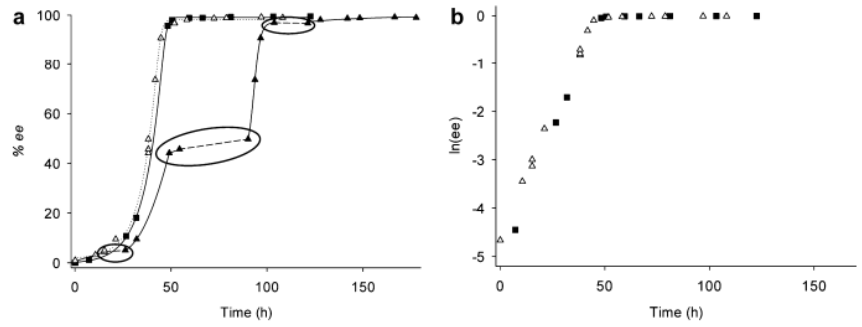

Figure 4. Deracemization by using TP2. (a) Evolution of *ee* versus time. (b) Evolution of ln(*ee*) versus time. ■ Experiment II, ▲ Experiment II′, full line: TP2 periods, dashed line: constant temperature periods (20 °C). (The constant temperature periods are encircled.) △ Experiment II′ ignoring the constant temperature periods.

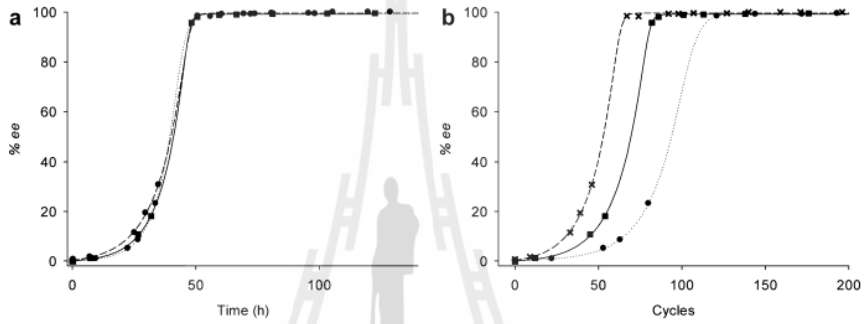

Figure 5. Effect of the cooling rate on deracemizations. (a) Evolution of the *ee* versus time, (b) evolution of *ee* versus the number of heating−cooling cycles. ■ Experiment II (TP2), ● experiment III (TP3), × experiment IV (TP4).

and TP4 were compared. They differ only by the duration of the ramp to return to 20 °C (Figure 5). This is a critical parameter since it will determine the evolution of the supersaturation during the crystal growth period; faster cooling rates will lead to larger supersaturation values during the crystallization and therefore a greater likelihood of nucleation during the crystallization period rather than simply growth of existing crystals. The cooling rates of TP2, TP3, and TP4 are 13 °C h^{-1}, 23 °C h^{-1}, and 9 °C h^{-1}, respectively. The results show that the evolution of *ee* over time is unchanged for the three temperature programs used (Figure 5a). The programs have no significant effect on the time required to achieve complete chiral purity. However, when the evolution of *ee* in the solid phase is plotted against the number of heating−cooling cycles (Figure 5b), the evolution of the *ee* is different. The faster cooling rate system requires more cycles than the lower cooling rate system. In the case of a rapid cooling, the creation of a high supersaturation puts the solution point beyond the Ostwald limit,[30] and the enantiomer in minor amount can produce small crystals by secondary nucleation, resulting in a time delay for complete conversion. However, in the case of a slow cooling, the crystallization of the major enantiomer is favored and not limited by the decrease of its concentration due to racemization in the liquid phase.

The effect of the amount of solid to deracemize on the duration of the experiment was studied. Two experiments were carried out in the same operating conditions, except for the initial mass of **1**: 2.5 g (experiment II) and 1.8 g (experiment V) were used. In the two cases, the same mass of solid is dissolved during the heating period. The resulting masses and the resulting supersaturations are therefore the same, as illustrated in Figure 7. It is not surprising that the time required to achieve complete chiral purity is shorter when the mass of solid is smaller (Figure 6), the amount of **1** to deracemize being smaller. However, the relative percentage of

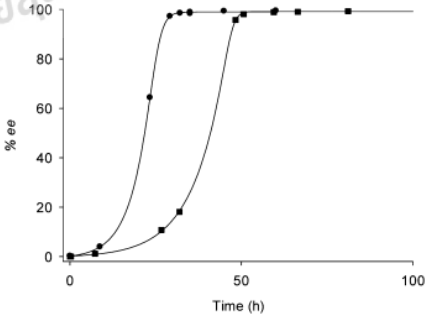

Figure 6. Comparison between two deracemizations carried out in the same experimental conditions, using TP2, except for the total mass of **1**: ■ experiment II: 2.5 g of **1** and ● experiment V: 1.8 g of **1**.

dx.doi.org/10.1021/cg400436r | *Cryst. Growth Des.* 2013, 13, 3498−3504

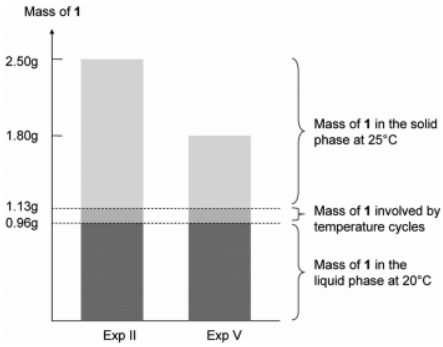

Figure 7. Schematic representation of the distribution of **1** in the different phases of the suspension for the experiments II and V.

solid involved in each cycle is different: ca. 10% of the solid phase is dissolved in the experiment II instead of ca. 20% in the experiment V. It is therefore possible that all the processes that occur due to dissolution/recrystallization are magnified when a higher percentage of solid is involved by the temperature fluctuations, accelerating the evolution of the *ee*.

DISCUSSION

The results presented in this study demonstrate conclusively that deracemization can also occur in the absence of abrasive grinding. The evolution of a racemic mixture of a chiral compound to single handedness is possible due to the combination of racemization in solution and dissolution/recrystallization cycles in the system. These temperature fluctuations are responsible for two phenomena that result in an increase of the *ee* of the solid phase: (i) dissolution of the racemic mixture during heating periods, (ii) growth of crystals and entrainment effect during cooling periods.

During the heating periods, according to thermodynamic principles and for low and medium *ee* in the solid phase, only the racemic mixture is dissolved (obviously, if the ee of the solid phase is too high, the enantiomer in excess will be also dissolved). Proportionally, crystals of the less abundant enantiomer are more dissolved than crystals of the enantiomer in excess; the *ee* of the solid phase is therefore magnified. Then, during the cooling periods, a supersaturation is created and the remaining crystals can grow.[31]

For a system in equilibrium without racemization, the initial and the final compositions of a heating/cooling event must be the same: a racemic liquid phase in equilibrium with two mirror related solid phases. The entrainment effect is therefore limited to a short period of time, when the system is out of equilibrium. In the most favorable case, the enantiomer in default is completely dissolved at the highest temperature. The system is autoseeded by the crystals of the single enantiomer remaining in the solid phase.[31−33] The entrainment effect takes place as soon as the system is cooled, and it is exhausted when the mother liquor reaches the metastable solubility of the crystallizing enantiomer. The return to equilibrium corresponds to the crystallization of the second enantiomer, and then the *ee* of the mother liquor decreases down to zero.

With racemization in solution, the composition of the liquid phase is always racemic. Therefore, the entrainment effect has no thermodynamic limit.

A preferential crystallization method called second order asymmetric transition (SOAT)[34] is based on this concept. The combination of a controlled cooling with racemization in solution prevents, up to a certain point, the crystallization of the counter enantiomer and improves the efficiency of the preferential crystallization. If the enantiomeric excess in the solid is not high enough, they are actually two simultaneous SOATs, but the larger the imbalance in the two solid phases the higher the imbalance in the crystal growth so the faster the evolution of toward high *ee*. The net result is therefore an autocatalytic effect.

Viedma previously described a similar model, the "*thermodynamic-kinetic feedback near equilibrium*", to explain the spontaneous chiral symmetry breaking observed for $NaBrO_3$.[33] The appearance of a single handedness was due to a "*feedback between the thermodynamic control of dissolution and the kinetics of the growth process near equilibrium*". This model was described for the slight growth−dissolution cycles that occur at constant temperature (Ostwald ripening), but he suggested that this model could be applied to intrinsically chiral molecules.

Recently, Viedma's research group in collaboration with Blackmond's group gave the proof that deracemization can be achieved only through the use of a temperature gradient, at high temperatures (ca.105 °C), due to the type of heating used, but without grinding.[35] This is likely to be due to a similar mechanism as in the current work, since crystals may cycle through regions of different temperatures; however, the use of deliberate temperature cycling may result in a clearer picture of the mechanism of the deracemization which is still matter of debate.

The general consensus is that Viedma ripening occurs due to Ostwald ripening and the reincorporation of chiral clusters. At the initial stage of the deracemization, a difference between the two enantiomers can be created by any departure from a perfectly symmetric situation: stochastic slight variation of *ee* or of the crystal size distribution due to continuous exchanges of matter between the solid and the liquid phase, presence of an impurity[4] which promotes or disrupts the crystallization of one of the two enantiomers, etc. This imbalance is then progressively increased due to Ostwald ripening and reincorporation of chiral clusters. It is evident however that grinding also introduces fluctuations in energy and therefore fluctuations in temperature in a suspension. Friction induced by glass beads may cause high numbers of small localized cycles of heating/cooling in the system. These fluctuations (with respect to time and space) in temperature will lead to the creation of local dissolution and thus supersaturation after cooling and then entrainment.

In this report, we demonstrate deracemization using a technique that is not dependent on grinding. The phenomenon of dissolution/growth in our system has been induced by controlled temperature cycles similar to those occurring in nature. All crystals are simultaneously dissolved during the heating period; the same mass of the two enantiomers is affected. The crystals remaining after the heating cycle are then grown during the cooling period by consuming the excess of the solute molecules in the supersaturated solution. Since the solution has rapid racemization, the supersaturation of the *R*- and *S*-components are equal throughout the crystallization period and the entrainment effect can efficiently occur. Possible mechanisms for the phenomena do not necessarily require an initial asymmetry in either the solution or the crystalline phase;

dx.doi.org/10.1021/cg400436r | *Cryst. Growth Des.* 2013, 13, 3498−3504

a very slight imbalance stochastically created by statistical fluctuations is sufficient to trigger the evolution of the whole system. It is possible that there are different histories involved in the nucleation and growth of the two populations (due to the stochastic nature of some of the phenomena) which may have been carried over from events occurring before the temperature cycles where initiated that may result in an imbalance in the kinetics of the two enantiomorphs.

The results may also have implications for the origin of the homochirality of biologically significant molecules on Earth.

Natural temperature cycles occur over short time intervals due to natural convection and buoyancy induced flow, and over longer time intervals due to diurnal and annual temperature cycles. Thus, if deracemization can occur due only to repeated temperature cycles at near ambient conditions, it seems a highly likely cause for homochirality in nature. There is no need for a racemization agent in the liquid phase for the deracemization in a crystalline phase to occur, since amino acids will naturally racemize in solution over very long periods of time, which is plausible since geological time frames were available for the event.

Another well-known theory is that undersea volcanic vents (hydrothermal vents) might have been the original source of life on earth, and this has been reviewed recently by Holm.[36] These vents will result in strong temperature gradients due to the temperature difference between the vent and the surrounding deep water, creating buoyancy flow. This creates a natural temperature cycle for pockets of fluid around the vent and potentially has led to a deracemization event due to these temperature cycles. It can be noted that such systems have the necessary precursor compounds required to form amino acids and also suitable reaction conditions.

CONCLUSIONS

This work presents a possible mechanism of complete chiral symmetry breaking occurring in the system via temperature fluctuations, and this is independent from grinding. The dissolution and recrystallization phenomena induced by temperature fluctuations in the system are enough to break the symmetry and finally to achieve complete deracemization. The interplay between (i) dissolution and regrowth with dispersion of rates,[37] (ii) racemization in solution, and (iii) the entrainment effect seems to be responsible for this process.

The heating/cooling cycle can be produced by several procedures, such as friction caused by glass beads in agitated systems or sonication, causing localized energy inputs into the system, temperature programming via the use of a thermostat, or temperature fluctuations in nature. Their effects are therefore to be added to the effect of the other phenomena, such as Ostwald ripening or reincorporation of clusters.

Our results help to fill crucial gaps in the understanding of the mechanism of the deracemization process.

To optimize this novel procedure, the temperature programming has to be adjusted. Optimal programming may use large temperature swings for the initial cycles in order to initiate the breaking of symmetry, followed by smaller temperature variations in later cycles where the preferred enantiomer has a significant excess. In the latter situation, only a small amount of crystal needs to be dissolved to remain in the biphasic domain at high temperature: crystals of a single enantiomer in equilibrium with a racemic saturated solution. This procedure should produce an optimum set of conditions, and the evolution of enantiomeric excess may tend toward an exponential increase to 100%, for conglomerates without partial solid solution,[38] rather than the sigmoidal shape as found in this work.

A combination of techniques using preferential crystallization in addition to periodic temperature fluctuations in order to completely deracemize conglomerate systems may accelerate the complete deracemization and yield high product purity and yield for industrial applications.

This method could also lead to a variety of industrial applications for deracemization; the process involving cycles of growth and dissolution due to temperature fluctuations is easier to implement at a large scale than a continuous grinding.

AUTHOR INFORMATION

Corresponding Author

*Phone: +66 44 224497. Fax+66 44 224609. E-mail: adrianfl@sut.ac.th.

Notes

The authors declare no competing financial interest.

ACKNOWLEDGMENTS

This work was supported by the Thailand Research Fund (TRF) in collaboration with Suranaree University of Technology (SUT) through the Royal Golden Jubilee Ph.D. Program (1.C.TS/51/B.1) and was partially funded by the French embassy in Thailand. A.F. also thanks the University of Rouen for funding for a study leave in 2011.

REFERENCES

(1) Viedma, C. *Phys. Rev. Lett.* **2005**, *94*, 065504.
(2) Abrahams, S. C.; Bernstein, J. L. *Acta Crystallogr.* **1977**, *B33*, 3601−3604.
(3) Kipping, F. S.; Pope, W, J. *J. Chem. Soc. Trans.* **1898**, *73*, 606−617.
(4) Noorduin, W. L.; Izumi, T.; Millemaggi, A.; Leeman, M.; Meekes, H.; Van Enckevort, W. J. P.; Kellogg, R. M.; Kaptein, B.; Vlieg, E.; Blackmond, D. G. *J. Am. Chem. Soc.* **2008**, *130*, 1158−1159.
(5) Noorduin, W. L.; Vlieg, E.; Kellogg, R. M.; Kaptein, B. *Angew. Chem., Int. Ed.* **2009**, *48*, 9600−9606.
(6) Levilain, G.; Rougeot, C.; Guillen, F.; Plaquevent, J. C.; Coquerel, G. *Tetrahedron Asymmetry* **2009**, *20*, 2769−2771.
(7) Van der Meijden, M. W.; Leeman, M.; Gelens, E.; Noorduin, W. L.; Meekes, H.; van Enckevort, W. J. P.; Kaptein, B.; Vlieg, E.; Kellogg, R. M. *Org. Process. Res. Dev.* **2009**, *13*, 1195−119.
(8) Noorduin, W. L.; Kaptein, B.; Meekes, H.; Van Enckevort, W. J. P.; Kellogg, R. M.; Vlieg, E. *Angew. Chem. Int. Ed* **2009**, *48*, 4581−4583.
(9) Noorduin, W. L.; Meekes, H.; Van Enckevort, W. J. P.; Kaptein, B.; Kellogg, R. M.; Vlieg, E. *Angew. Chem., Int. Ed.* **2010**, *49*, 2539−2541.
(10) Noorduin, W. L.; van Enckevort, W. J. P.; Meekes, H.; Kaptein, B.; Kellogg, R. M.; Tully, J. C.; McBride, J. M.; Vlieg, E. *Angew. Chem., Int. Ed.* **2010**, *49*, 8435−8438.
(11) Frank, F. C. *Biochim. Biophys. Acta* **1953**, *11*, 459−463.
(12) Soai, K.; Shibata, T.; Morioka, H.; Choji, K. *Nature (London)* **1995**, *378*, 767−776.
(13) Sato, I.; Omiya, D.; Igarashi, H.; Kato, K.; Ogi, Y.; Tsukiyama, K.; Soai, K. *Tetrahedron Asymmetry* **2003**, *14*, 975.
(14) Saito, Y.; Hyuga, H. *J. Cryst. Growth* **2011**, *318*, 93−98.
(15) Cartwright, J. H. E.; Piro, O.; Tuval, I. *Phys. Rev. Lett.* **2007**, *98*, 165501.
(16) Crusats, J.; Vientemillas-Verdaguer, S.; Ribó, J. M. *Chem.—Eur. J.* **2006**, *12*, 7776−7781.
(17) Hein, J. E.; Cao, B. H.; Viedma, C.; Kellogg, R. M.; Blackmond, D. G. *J. Am. Chem. Soc.* **2012**, *134*, 12629−12639.
(18) Uwaha, M. *J. Phys. Soc. Jpn.* **2004**, *73* (10), 2601−2603.

(19) Noorduin, W. L.; Meekes, H.; Bode, A. A. C.; Van Enckevort, W. J. P.; Kaptein, B.; Kellogg, R. M.; Vlieg, E. *Cryst. Growth Des.* **2008**, *8* (5), 1675−1681.
(20) McBride, J. M.; Tully, J. C. *Nature* **2008**, *452*, 161−162.
(21) Saito, Y.; Huyga, H. *J. Phys. Soc. Jpn.* **2004**, *73*, 33−35.
(22) Skrdla, P. J. *Cryst. Growth Des.* **2011**, *11*, 1957−1965.
(23) Iggland, M.; Mazzotti, M. *Cryst. Growth Des.* **2011**, *11*, 4611−4622.
(24) Viedma, C.; Cintas, P. *Chem. Commun.* **2011**, *47*, 12786−12788.
(25) Iggland, M.; Mazzotti, M. *CrystEngComm* **2013**, *15*, 2319−2328.
(26) Black, S. N.; Williams, L. J.; Davey, R. J.; Moffatt, F.; Jones, R. V. H.; McEwan, D. M.; Sadler, D. E. *Tetrahedron* **1989**, *45*, 2677−2682.
(27) Black, S. N.; Williams, L. J.; Davey, R. J.; Moffatt, F.; McEwan, D. M.; Sadler, D. E; Docherty, R.; Williams, D. J. *J. Phys. Chem.* **1990**, *94*, 3223−3226.
(28) Balasubramanyan, S.; Shephard, M. C. Fungicidal Compounds. U.S. 4243405, August 19, 1977.
(29) Viedma, C. *J. Cryst. Growth* **2004**, *262*, 118−121.
(30) Ostwald, F. W. *Z. Phys. Chem.* **1900**, *34*, 495−503.
(31) Levilain, G.; Coquerel, G. *CrystEngComm* **2010**, *12* (7), 1983−1992.
(32) Coquerel, G. *Preferential crystallization*; Springer-Verlag: Berlin Heildelberg; *Topics in Current Chemistry*, 2007; Vol *269*, pp 1−51.
(33) Viedma, C. *Astrobiology* **2007**, *7* (2), 312−319.
(34) Sheldon, R. A. *Chirotechnology: Industrial Synthesis of Optically Active Compounds*; Marcel Dekker, New York, 1993, and Collins, A. N.; Sheldrake, G. N.; Crosby, J. *Chirality in Industry: The Commercial Manufacture and Applications of Optically Active Compounds*; Wiley, Chichester, 1992.
(35) Viedma, C.; Ortiz, J. E.; de Torres, T.; Izumi, T.; Blackmond, D. G. *J. Am. Chem. Soc.* **2008**, *130*, 15274−15275.
(36) Holm, N. G. *Origins Life Evol. Biosphere* **1992**, *22* (1−4), 5−14.
(37) Flood, A. E. *CrystEngComm* **2010**, *12* (2), 313−323.
(38) Gonella, S.; Levilain, G.; Coquerel, G. *J. Therm. Anal. Calorim.* **2011**, *103*, 125−129.

Chemical Engineering & Technology Research Article 1329

Kittisak Suwannasang[1]
Gerard Coquerel[2]
Celine Rougeot[2]
Adrian E. Flood[1]

[1]School of Chemical Engineering, Suranaree University of Technology, Nakhon Ratchasima, Thailand.

[2]Crystal Genesis Unit SMS EA3233, Université de Rouen, Mont Saint Aignan, France.

Supporting Information available online

Mathematical Modeling of Chiral Symmetry Breaking due to Differences in Crystal Growth Kinetics

Two simple models are proposed and tested for the mechanism of ripening of a conglomerate suspension to a single enantiomorph by temperature cycles. In both models, the initial crystal size distributions and masses of the two enantiomorphs are equal, but either the crystal growth rate or the growth rate distribution is varied. The difference in the crystal growth kinetics of the two enantiomorphs may be caused by the intrinsic thermodynamic stability of the crystals occurring in the initial suspension. The initial nucleation of one of the two enantiomers will occur earlier than that of the counter-enantiomer. This results in the formation of two populations occurring under different conditions, leading to different internal crystalline perfection and therefore different thermodynamic stability.

Keywords: Chiral symmetry breaking, Crystal growth, Crystal dissolution, Population balance modeling

Received: January 22, 2014; *revised:* April 03, 2014; *accepted:* April 04, 2014

DOI: 10.1002/ceat.201400056

1 Introduction

Recently, a new process was experimentally demonstrated to obtain an enantiopure suspension from a racemic suspension of a conglomerate-forming system, using a series of temperature cycles combined with swift racemization in the solution phase [1]. The material chosen as a model compound was 1-(4-chlorophenyl)-4,4-dimethyl-2-(1*H*-1,2,4-triazol-1-yl)pentan-3-one (Cl-Tak), because it is a conglomerate-forming system and because it is rapidly racemized in the presence of sodium hydroxide. The previous study [1] showed that ripening by temperature cycles can achieve complete deracemization from an initially racemic suspension within 2–4 d (see Fig. 1 for an example of experimental results). During the periods when temperature cycling is stopped there was negligible change in enantiomeric excess (ee) in the crystalline phase. This demonstrated clearly that deracemization is caused by temperature cycling, not by grinding. This new ripening process appears distinct from Viedma ripening, and Ostwald ripening could not be the primary mechanism involved since the deracemization is too fast [2–5].

Deracemization by temperature cycling occurs due to repeated cycles of partially dissolving the suspension during the heating period and then regrowth of the remaining crystals during the cooling period, which consumes the supersaturation in the solution phase. The mass of crystalline material regrown is the same as the mass lost during the heating step since the system fluctuates between saturated states at high and low temperature. However, this new phenomenon of ripening is not well understood.

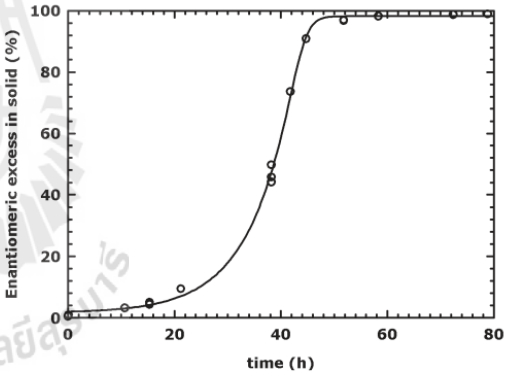

Figure 1. Deracemization of Cl-Tak using temperature cycling. Evolution of ee versus time during periods of temperature cycling; temperature cycles each with 1 h of duration.

Although the original racemic solution may be perfectly symmetric, this does not guarantee that the two enantiomorphs will nucleate or crystallize simultaneously. Garside et al. [6] have noted that "as an example, the induction periods for aqueous solution of KCl show that the scatter of experimental data is rather large. This is often found and arises from the stochastic character of nucleation". This suggests that the two enantio-

Correspondence: Prof. Adrian Flood (adrianfl@sut.ac.th), School of Chemical Engineering, Suranaree University of Technology, Nakhon Ratchasima 30000, Thailand.

morphs can nucleate at different times even though their properties are identical. Jones and Larson [7] have shown that crystals nucleating under different supersaturation levels have different levels of growth rate activity and different levels of crystal growth rate dispersion (GRD). If the two enantiomorphs nucleate under different supersaturations or different temperatures, then the crystal growth rate kinetics of the two populations will be different, i.e., there is a memory effect.

One of the hypotheses is that deracemization may originate from the original nucleation events for the two enantiomorphs. Although the original racemic solution may be perfectly symmetric, this does not guarantee that the two enantiomorphs will nucleate or crystallize simultaneously since nucleation is known as a stochastic phenomenon that does not occur at predictable times. Thus, deracemization might be caused – at least partially – by differences in crystal growth kinetics between the two enantiomorphs, which are caused by the initial formation of nuclei of the two enantiomers occurring at slightly different times, and therefore under different levels of supersaturation. Under rapid racemization in the solution phase, the enantiomorph nucleating first will nucleate at high supersaturation and will consume the solute of both enantiomers in the solution phase before the formation of the other enantiomer begins; the solution temperature may also change between the two nucleation events. This creates two populations of crystals that commenced nucleation at (slightly) different times and therefore under different conditions, leading to different internal crystalline perfection and thus slightly different thermodynamic stability. The current study aims to use models of growth and dissolution kinetics under various assumptions for crystal growth and to determine whether such models are able to fit the functional forms of the experimental data in the deracemizations. It is important to note that the aim of this study is not to try and achieve predictive models of the deracemization; the simple models are used to determine (i) whether the mechanism produces a time evolution of the ee and (ii) whether the functional form of the evolution in ee is similar to that seen in the experimental results in Fig. 1. Experimental studies of deracemization of chiral compounds tend to be very expensive, time consuming, and necessarily use small amounts of material. This is because the species involved must be conglomerate-forming compounds and easily and quickly racemize in solution; this combination is very rare, and hence the compounds used are often not available commercially but need to be prepared and purified within the laboratory. This makes it beneficial to highlight some potential mechanisms and exclude other mechanisms based on the results of fundamental models using the mechanisms being investigated. In this way experimental studies can be optimized in order to search mainly the most probable mechanisms for the process.

Other studies have applied different mathematical modeling techniques to model Viedma ripening (deracemization in systems using grinding) and Oswald ripening based on considerations including growth and dissolution. Iggland and Mazzotti [8] solved the full population balance including the use of size-dependent solubility to model Ostwald ripening and concluded that the size-dependent solubility could induce deracemization. Ricci et al. [9] investigated Viedma ripening using Monte-Carlo simulations. They conclude that "size-dependent crystal solubility alone is insufficient to reproduce most of the experimental signatures of Viedma ripening, and that some form of a solid-phase chiral feedback mechanism must be invoked in order to reproduce experimentally observed behavior". The apparent contradiction between these two results indicates that further work modeling such systems using a range of methods is warranted. Further work modeling Viedma ripening was made by Gherase et al. [10], who modified the population balance formulation of Iggland and Mazzotti to include a surface area dependence for the mass transfer coefficient as well as the size-dependent solubility model. This model suggests that the main factors driving deracemization may be the differences in the sizes and surface areas of the crystals of the two enantiomorphs, which is related to differences in sizes and numbers of crystals. In this model, agglomeration of "like-handed" particles is not needed to achieve amplification of the ee.

Steendam et al. [11] have recently experimentally investigated the effect of chiral impurities on Viedma ripening. It is known that even very small levels of impurities can have significant effects on crystal growth (and potentially dissolution) kinetics. Chiral impurities will have different effects for the two enantiomorphs and thus may influence the deracemization; in fact, it is shown that the deracemization does not progress to either one of the two enantiomorphs with equal probability, thus clearly illustrating the effect of the chiral impurity. However, this effect can be removed by enhancing the grinding, thus increasing the ratio of surface area to impurity concentration. The effect could also be removed with small amounts of chiral additive. This has a bearing on the present study since it shows that, under certain circumstances, the crystal growth kinetics of the two enantiomorphs may differ.

2 Conceptual Model Development

An initial thought was that deracemization could occur in systems where there is no difference between the crystal growth rate kinetics of the two enantiomorphs, and where there is no crystal GRD (growth rate occurs according to McCabe's ΔL[1)] law) if there is an initial asymmetry in the crystal size distributions (CSD) of the two enantiomorphs. It could be imagined that dissolution cycles destroy more of the population of the enantiomorph having a smaller mean crystal size, thus altering the ee. Initial simulations modeling this effect show that this phenomenon does change the ee in the first dissolution-recrystallization cycle, but after this first cycle the two crystal populations oscillate between two fixed particle size distributions, and subsequent cycles make no change in the ee. This mechanism is not a potential cause of the deracemization and will not be discussed further. It should be noted that, if the initial mean particle sizes of the two enantiomorphs are very large and a very large fraction of the suspension is dissolved, then a small population of the crystals of the larger enantiomorph survive to grow (in an autoseeded preferential crystallization [12, 13]) during the cooling part of the cycle, potentially leading to 100 % ee in a single cycle. This has clearly not occurred in the

1) List of symbols at the end of the paper.

experiments described in the prior experimental work [1]. An illustration of a simulation of this model is shown in the Supporting Information.

Based on the inability of McCabe's ΔL law with equal growth kinetics for the two enantiomorphs to explain the deracemization, two potential mechanisms are proposed that might explain the temperature-induced deracemization, and simple mathematical models, based on fundamental laws of crystal growth and dissolution kinetics, were made in order to check whether the proposed mechanisms are possible causes of the deracemization. The models should be able to reproduce the sigmoidal evolution of ee in the solid phase that is typically found in the deracemization experiments. The physical system to be modeled is illustrated in Fig. 2. If simulation of a particular mechanism produces changes in ee that closely match the experimental trends, it provides a starting point for experimental validation of the mechanism for the process of deracemization.

In a typical deracemization experiment, a cycle in a temperature program consists of four steps: holding at 20 °C for 5 min, ramping to 30 °C over a period of 5 min, holding at 30 °C for 5 min, then ramping down to 20 °C over a period of 45 min. In this program, the time required for a cycle is 1 h. The cooling part of the cycle is deliberately performed slowly in order to promote crystal growth by maintaining a small supersaturation level and thus to inhibit crystal nucleation. The crystals in suspension were partially dissolved during the heating period. The remaining seeds then recrystallize and grow during the cooling period by consumption of the supersaturation in the solution phase. The amount recrystallized is the same amount as the mass lost during the heating step.

It is assumed in the simulations that the cycles are short enough and that the supersaturation during growth is low enough so that nucleation does not occur for either enantiomorph. Crystal breakage and agglomeration are unlikely for the gentle agitation used in the experiments and are not considered in the models.

Two models are proposed to provide possible explanations of the experimental results. In the first model (Model 1), the two enantiomorphs have slightly different mean crystal growth rates, but the initial CSD and mass of the two populations are the same. In this model there is no crystal GRD for either enantiomorph. In the second model (Model 2), the two populations have the same initial CSD and mass: The two enantiomorphs have slightly different amounts of GRD but their mean crystal growth rate is equal.

3 Model 1: Simulation with Difference in Growth Rate Kinetics

The first model considers what can occur if there is a difference in the crystal growth rate kinetics of the two enantiomorphs related to the history of the crystals in the suspension. The two enantiomorphs possibly nucleate at different times where the primary nuclei of the two enantiomorphs occur at different levels of supersaturation and/or temperature. This causes the populations of the two enantiomorphs to have different crystal growth kinetics due to differences in internal crystal perfection or thermodynamic stability.

The assumptions in this model are: (i) there is no crystal GRD for either enantiomorph, (ii) size-independent crystal growth, (iii) no nucleation, breakage nor agglomeration occur during the crystallization. The model uses only the average growth rate (or dissolution rate) during a cooling (or heating) part of a cycle. This is sufficient to find the CSD at the beginning and end of a cycle since each crystal in a particular population will grow or dissolve by the same ΔL, and therefore the CSD can be found by knowing the mass of crystal that is present at saturation. This is known since the solution of the population balance for a system in which there is no nucleation, agglomeration nor breakage is a traveling wave, and hence the CSD at the end of a cycle will be the same function as at the beginning of the cycle, but shifted along the length axis. The ratio of the average growth rates of the two forms will be in the same range as the ratio of the crystal growth activities (and therefore the ratio of the two growth rates at any point in time during a cooling cycle). The model uses the same dissolution rate kinetics for the two forms (since dissolution is often assumed to be mass transfer controlled).

Initial simulations were performed with the growth rates of the *R*- and *S*- forms being a constant ratio, for instance $G_{S-} = 0.8\ G_{R-}$. The ee evolved over time up to 100 %; however, the evolution did not show the sigmoidal curve characteristic of the experimental results. Since the simulation results did not show the same functional form as the experimental results, the simulations were modified such that the two populations start with the same reduced growth rates (due to poor quality in the nuclei initially formed), but the crystals of both enantiomorphs undergo maturation due to the heating and cooling cycles such that their growth rates change. The model assumes that this maturation or healing process occurs at different rates for the two enantiomorphs, with the maturation of the *R*- crystals being

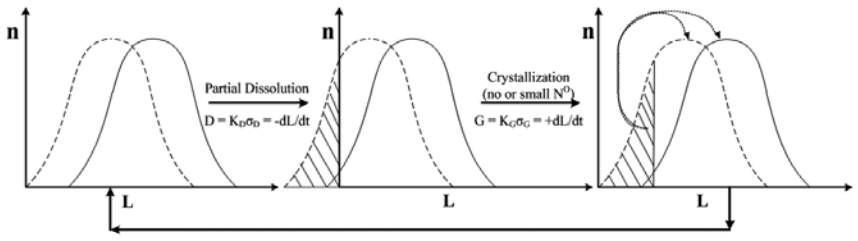

Figure 2. Schematic representation of the CSD during a partial dissolution/recrystallization cycle. In the solution phase, fast racemization occurs to maintain equal amounts of the two enantiomers in solution.

significantly faster than that for the *S*- crystals, perhaps due to the poorer internal perfection of the *S*-crystals. The ratio of the growth rates (rate of slow maturing crystal/rate of fast maturing crystal) followed an exponential decay down to a constant value. This is due to the assumption that the slow maturing *S*- crystals nucleated under harsher conditions than the *R*- crystals [7, 14].

The first model is initiated with two equal population densities of *R*- and *S*-enantiomorphs. The CSD are assumed to be normal (Gaussian) distributions for the modeling here, with the exception that, due to the dissolution process, some of the smallest crystals completely disappear and are not replaced by nucleation (therefore, the number of particles decreases during the process), leaving the CSD without a lower tail; the distribution is cut at a size L_{min}. The CSD for the *S*-crystals after growth (Fig. 2) illustrates this phenomenon. Tab. 1 summarizes the conditions used in this model (and the second model used).

The key to the present models is that, under the conditions assumed (no nucleation, agglomeration nor breakage in a batch system), solving the full population balance over time is not necessary, since the solution is known to be a traveling wave. The shape of the CSD at the end of a heating or cooling cycle (assuming that equilibrium has been reached at that time) can be related to the initial CSD and a shift in size. The total masses of crystals at the beginning and end of the cycle are known (based on a mass balance for the solution and the saturation concentration at the high and low temperatures in the cycle). Thus, the correct solution can be found exactly via solving the third moment for the unknown parameter in the solution for the CSD, which is the amount by which the mode of the distribution has been shifted. The third moment and the number density distribution are defined by the equations:

$$\mu_3^{(i)} = \int_{L_{min}^{(i)}}^{\infty} \left\{ \left(L^{(i)}\right)^3 n_t^{(i)} \right\} dL^{(i)} \quad \text{where } i = R\text{-}, S\text{-} \tag{1}$$

$$n^{(i)} = \begin{cases} 0 & \text{for } L < L_{min} \\ \frac{1}{(\sigma^{(i)})\sqrt{2\pi}} \exp\left(-\frac{\left(L^{(i)} - \bar{L}^{(i)}\right)^2}{2(\sigma^{(i)})^2} \right) & \text{for } L_{min} \le L < L_{\infty} \end{cases} \tag{2}$$

The third moment of the enantiomorph is proportional to the mass of this enantiomorph in the crystal phase. The initial total third moment is defined as:

$$\mu_{3,(j=0)}^{T} = \mu_{3,(j=0)}^{R\text{-}} + \mu_{3,(j=0)}^{S\text{-}} \tag{3}$$

Table 1. Key features of the two models.

	Model 1	Model 2
Initial CSD of *R*- and *S*-	equal; normal distributions	equal; monosize
Initial masses of *R*- and *S*-	equal	equal
Mean crystal growth rate	different, with the ratio $\bar{G}_S/\bar{G}_R$ being time dependent	equal (until slow growers in the distribution are fully dissolved)
Crystal GRD	none	modeled using discrete GRD

This is also the total third moment for the suspension after the saturation point has been reached at the lower temperature for any cycle *j* because the same amount of crystal must occur whenever the system reaches saturation at this temperature.

The linear measure of particle size, rather than the volume of the particle, is chosen as the independent variable because the crystal growth rate is usually found to be approximately size independent if formulated in the term of an increase in a linear dimension. The growth rate is a strong function of size if described in term of a volumetric increase, and so this form is unsuited to this modeling.

The average dissolution rates of all crystals of both enantiomorphs are the same during every heating cycle. At the end of the dissolution period, the minimum sizes ($L_{minD}^{R\text{-}}$, $L_{minD}^{S\text{-}}$) of both populations are calculated using Maple 9.5. The equations to solve at the dissolution part at any cycle *j* are the following expressions:

$$\mu_{3,D(j)}^{R\text{-}} + \mu_{3,D(j)}^{S\text{-}} = (1 - \mathrm{FD})\mu_{3,G(j-1)}^{T} \tag{4}$$

where FD is the fraction of the suspension mass dissolved due to the change in the saturation temperature. The third moments of the *R*- and *S*- populations are

$$\mu_{3,D(j)}^{R\text{-}} = \int_{L_{minD(j)}^{R\text{-}}}^{\infty} \left\{ L^3 \frac{1}{(\sigma^{R\text{-}})\sqrt{2\pi}} \exp\left(-\frac{\left(L - \bar{L}_{D(j)}^{R\text{-}}\right)^2}{2(\sigma^{R\text{-}})^2} \right) \right\} dL \tag{5}$$

$$\mu_{3,D(j)}^{S\text{-}} = \int_{L_{minD(j)}^{S\text{-}}}^{\infty} \left\{ L^3 \frac{1}{(\sigma^{S\text{-}})\sqrt{2\pi}} \exp\left(-\frac{\left(L - \bar{L}_{D(j)}^{S\text{-}}\right)^2}{2(\sigma^{S\text{-}})^2} \right) \right\} dL \tag{6}$$

The lower limits of the populations ($L_{minD(j)}^{S\text{-}}$ and $L_{minD(j)}^{R\text{-}}$) may be zero if the smallest crystals in the population are entirely destroyed in the dissolution step or may be greater than zero if the amount of mass dissolved is not sufficient to destroy the smallest crystals.

The means of both populations will also change during a cycle (*j*) by the decrease in size due to dissolution ($\Delta L_{D(j)}^{(i)}$) during the heating period, and the increase in size of the crystals due to crystal growth ($\Delta L_{G(j)}^{(i)}$) during the cooling period. However, the shapes of the populations at the beginning and the end of the cycle are the same (since all crystals in the population may be assumed to be growing or dissolving with the same rate at any particular time), with the possible exception of the amount of the lower tail which no longer exists. Therefore

$$L_{minD(j)}^{i} = L_{minG(j-1)}^{i} - \Delta L_{D(j)}^{i}$$
$$L_{minG(j=0)}^{i} = 0 \quad i = R\text{-}, S\text{-} \tag{7}$$

where $L^{i}_{\mathrm{minD}(j)}$ is the minimum size of i crystals after the heating period of cycle j, $L^{i}_{\mathrm{minG}(j)}$ is the minimum size of i crystals after the cooling period of cycle j, and $\Delta L^{i}_{D(j)}$ is the change in the size of any i crystals due to dissolution during the heating period j.

$$\bar{L}^{i}_{D(j)} = \bar{L}^{i}_{G(j-1)} - \Delta L^{i}_{D(j)} \qquad \bar{L}^{i}_{G(j=0)} = \bar{L}^{i}_{\mathrm{initial}} \tag{8}$$

where $\bar{L}^{i}_{D(j)}$ is the mean of the population density of the i enantiomorph after the heating period of cycle j, and $\bar{L}^{i}_{G(j-1)}$ is the mean of the population density of the i enantiomorph after the previous cooling period.

The crystal size (L) cannot take on negative values; thus, the lower integration limit will be taken as zero when $L_{\mathrm{minD}(j)}$ is a negative value. Then, Eq. (4) will be calculated again by setting the value of $L_{\mathrm{minD}(j)}$ to zero.

It is important to note that, in this model, the focus is on an average (over the time period of the cycle) growth rate of all crystals of an enantiomer during the cooling part of the cycle.

The ratio of the growth rates of the *S*- crystals to the growth rate of the *R*- crystals decays over time and is dependent on the number of cycles j that the crystals have experienced. This is since both crystals are maturing due to the growth and dissolution cycles; however, the *R*- crystals are healing at a faster rate than the *S*- crystals. Initially, the ratio of the growth rates is unity; after the first cycle, the ratio decreases via an exponential decay function until it reaches some constant value, $\bar{G}^{S\text{-}}_{j\to\infty}/\bar{G}^{R\text{-}}_{j\to\infty}$, as shown by Eq. (9):

$$\frac{\bar{G}^{S\text{-}}_{(j)}}{\bar{G}^{R\text{-}}_{(j\to\infty)}} = \frac{\bar{G}^{S\text{-}}_{(j\to\infty)}}{\bar{G}^{R\text{-}}_{(j\to\infty)}} + \left[1 - \frac{\bar{G}^{S\text{-}}_{(j\to\infty)}}{\bar{G}^{R\text{-}}_{(j\to\infty)}}\right] \exp\left(-\frac{j}{\tau^{S\text{-}}_{G}}\right) \tag{9}$$

$j = 1, 2, 3, \ldots$

The variable $\tau^{S\text{-}}_{G}$ (which may also be considered as its inverse b in the exponential decay model) is a time constant that determines the rate at which the growth activity of the fast growing enantiomorph exceeds the value of the slow grower.

The average values of crystal growth activities for the *R*- and *S*- enantiomorphs are different, so that the change in length of an *R*- and *S*- crystal during a cycle will be related to the ratio of the growth activities, or equivalently the ratio of the mean growth rates, of the enantiomorphs during the cycle. The relation of changing in size between the *R*- and *S*- enantiomorphs is given by:

$$\Delta L^{S\text{-}}_{G(j)} = \Delta L^{R\text{-}}_{G(j)} \frac{\bar{G}^{S\text{-}}_{(j)}}{\bar{G}^{R\text{-}}_{(j)}} \tag{10}$$

The last term on the right is the ratio of the growth activities of the two enantiomorphs during cycle j. Eq. (10) allows the change in size for the *S*- crystals to be known in terms of the change in size of the *R*- crystals, and means that there is only one variable to be solved for in the equation for the known third moment. The value of the change in size of the *S*- crystals is then found from the change in size of the *R*- crystals. The equations for solving the minimum size of the *R*- and *S*- populations ($L^{R\text{-}}_{\mathrm{minG}}$, $L^{S\text{-}}_{\mathrm{minG}}$) after a growth period for any cycle j are the following expressions:

$$\mu^{R\text{-}}_{3,G(j)} + \mu^{S\text{-}}_{3,G(j)} = \mu^{\mathrm{T}}_{3} \tag{11}$$

The equation for the third moment of the *R*- and *S*- populations are expressed below:

$$\mu^{R\text{-}}_{3,G(j)} = \int_{L^{R\text{-}}_{\mathrm{minG}(j)}}^{\infty} \left\{ L^3 \frac{1}{(\sigma^{R\text{-}})\sqrt{2\pi}} \exp\left(-\frac{\left(L - \bar{L}^{R\text{-}}_{G(j)}\right)^2}{2(\sigma^{R\text{-}})^2} \right) \right\} \mathrm{d}L \tag{12}$$

$$\mu^{S\text{-}}_{3,G(j)} = \int_{L^{S\text{-}}_{\mathrm{minG}(j)}}^{\infty} \left\{ L^3 \frac{1}{(\sigma^{S\text{-}})\sqrt{2\pi}} \exp\left(-\frac{\left(L - \bar{L}^{S\text{-}}_{G(j)}\right)^2}{2(\sigma^{S\text{-}})^2} \right) \right\} \mathrm{d}L \tag{13}$$

$$L^{i}_{\mathrm{minG}(j)} = L^{i}_{\mathrm{minD}(j)} + \Delta L^{i}_{G(j)} \tag{14}$$

where $\Delta L^{i}_{G(j)}$ is the change in the size of i crystals due to growth during the cooling period. The crystals at the mode of the Gaussian distribution ($\bar{L}^{i}_{G(j)}$) will also grow by the same amount, and therefore

$$\bar{L}^{i}_{G(j)} = \bar{L}^{i}_{D(j)} + \Delta L^{i}_{G(j)} \tag{15}$$

The ee in the crystalline phase is then calculated for each cycle after the cooling period (based on the known population density of both enantiomorphs present) by the third moments.

$$\mathrm{ee}_{(j)} = \left| \frac{\mu^{R\text{-}}_{3,G(j)} - \mu^{S\text{-}}_{3,G(j)}}{\mu^{R\text{-}}_{3,G(j)} + \mu^{S\text{-}}_{3,G(j)}} \right| 100\,\% \tag{16}$$

The simple mathematical model presented above has several parameters that can be varied: initial CSD, growth rate functions, the final ratio of the growth rates of the two enantiomers, the time constant of the growth rate divergence, the percentage of the crystal mass dissolving in the heating part of the cycle, and so on. Some of these parameters were chosen to be kept constant, based on likely conditions in the deracemization experiments. Some parameters of interest, such as the time constant for the growth rate divergence, the final ratio of growth rates between the two enantiomers, and the percentage of the crystal mass dissolved during a deracemization, were varied. The initial CSD of the two enantiomorphs were equal for all simulations using this model.

In this section, the effects of three key parameters on the crystal growth are investigated, considering time-varying changes in the relative growth rates of the two populations but no GRD. The enantiomorphs have the same initial CSD and mass at the beginning of the simulation. By solving this model, the parameters as given in Tab. 2 are considered.

Table 2. Parameters for the simulations using Model 1.

Exp. no.	τ_D^R	τ_D^S	D^R	D^S	τ_G^S	$\bar{G}^S_{(j\to\infty)}/\bar{G}^R_{(j\to\infty)}$	% Dissolved
1	0	0	0.1	0.1	2.5, 5, 10	0.50	20
2	0	0	0.1	0.1	2.5, 5, 10	0.667	20
3	0	0	0.1	0.1	5	0.5, 0.667	20, 25, 30

To have a quantitative understanding of the kinetics, a computer code was developed in Maple 9.5 to simulate the system described by Eqs. (1)–(16). The thermal cycle consists of heating steps during which the suspension is dissolved to a saturation point at the high temperature, and then a cooling step where the crystals in the suspension are grown until the solution reaches the saturation point at the low temperature. The temperature cycles are arbitrarily set at 1 h, to agree with the cycles in the earlier experimental work. These temperature cycles were continued over a large number of cycles until deracemization was substantial. The main structure of the code is as follows:

(a) Crystals of the two enantiomorphs in the suspension are partially dissolved during the heating period with an equal dissolution rate, D. The dissolution of all crystals is equal and size independent. The change in the size of the crystals due to dissolution (ΔL_D) is calculated to reduce the third moment to the value required based on the fraction of crystals that is dissolved between the two temperatures in the cycle.

(b) When step (a) is completed, the minimum crystal sizes of both enantiomorphs are calculated. These two sizes will be used in the next crystal regrowth step.

(c) The remaining crystals then regrow during the cooling period by consumption of the supersaturation in the solution phase, with different mean growth rates for the *R*- and *S*- crystals. This step is based on the mass regrown being the same as the mass lost during the dissolution step. The total third moment of crystals, based on regrowth of crystals to the same crystal mass as initially given in the suspension, is used to calculate the increase in size of the crystals, $\Delta L_G{}^{R-}$ and $\Delta L_G{}^{S-}$, the ratio of which is the same as the ratio of the growth rates of the *R*- and *S*- crystals.

(d) The minimum crystal sizes of the two enantiomorphs are calculated again. These two new sizes will be used for calculating the third moments of both populations, and for use in the next dissolution cycle.

(e) The two new third moments of the populations, after the cooling step, will be used to calculate the ee in the solid phase.

(f) The simulation will be run using the same steps, (a)–(e), until complete deracemization (> 99 % ee) is achieved. For each new cycle, the relative growth rate of the *S*- enantiomorph to the *R*- enantiomorph must be recalculated according to the change in growth activity, via Eq. (9).

3.1 Simulations and Parameter Analysis of Model 1

The results are presented in three parts. The model could describe the complete chiral resolution by temperature fluctuations induced by dissolution and regrowth of crystals combined with fast racemization in the solution phase and the entrainment effect. Simulations are presented by varying four sets of parameters in order to validate the simple mathematical model. Initial experiments where the ratio of the growth rate ratio was maintained at a constant value (but not unity) produced an ee that evolved to reach 100 %, but the evolution was not sigmoidal. Since the simulation did not agree with the experimental results, this type of simulation was not continued.

However, when considering a condition in which the ratio of the growth rates of the enantiomorphs is initially unity but then decays due to the *R*- enantiomorph maturing more quickly than the *S*- enantiomorph (based on Eq. 9) down to a constant value, the sigmoidal function of the ee is found, as shown in the results of the next simulations which fit the form of the experimental data well.

Simulation 1.1

In this simulation, the deracemization with a time-dependent difference in the growth rate activities of the *R*- and *S*- crystals, as described above, is invetigated. The ratio of the growth activities is described by Eq. (9). The decay in the growth activity ratio has a time constant τ, or b^{-1}.

The simulations were carried out with the same initial conditions (initial crystal mass and initial CSD) and the same dissolution rates for both enantiomorphs. In the first simulations using this model, the total percentage of crystal mass dissolved during the heating period was set at 20 %. The final growth rate ratio of the *S*- and *R*- crystals $\left(\bar{G}^S_{(j\to\infty)}/\bar{G}^R_{(j\to\infty)}\right)$ was set at 0.5. This difference in the growth rates is a relatively large one, but not outside the expected values when experimental variations in growth rates are considered. A large value was initially used in the simulation to test if the evolution of ee was consistent with experiments, without making the simulation too lengthy or continuing for too many cycles. The effect of the exponential decay constant, b, on the evolution of ee of the solid was investigated by setting the value of b at 0.1, 0.2, or 0.4 h^{-1}.

The results of these simulations are illustrated in Fig. 3, showing the effect of the exponential decay constant, b (the inverse of the decay time constant). This is a critical parameter since it will determine the effect of the mean crystal growth rate of the counter-enantiomer. Poor crystal perfection or poor maturation of the counter-enantiomer (arbitrarily assumed to be the *S*- enantiomorph here) will lead to a quicker decay in the growth rate (Fig. 3 b) and result in a smaller time required to achieve complete chiral purity (Fig. 3 a). The number of cycles needed in this simulation was smaller than seen in experimental results, presumably because of the large ratio of the growth rates of the two enantiomorphs.

It is also important to note that the same effect (a time-dependent ratio of the growth kinetics of the two enantiomorphs) may also be apparent if there is a chiral impurity in the system

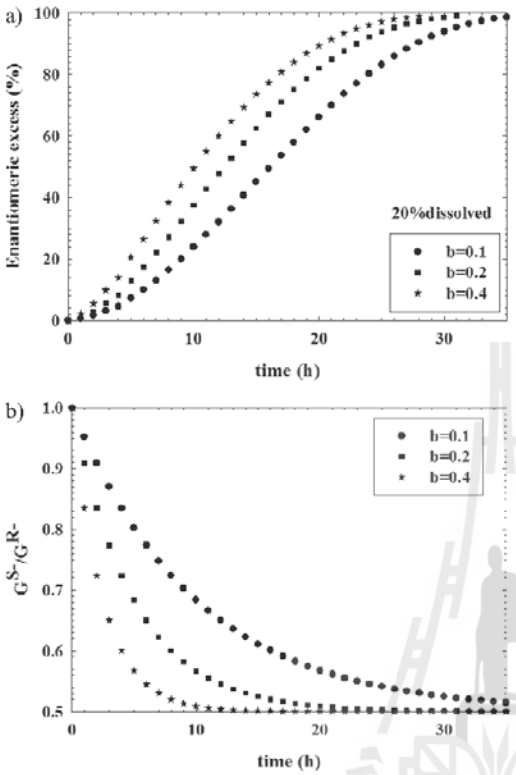

Figure 3. (a) Evolution of the solid phase ee when 20% of the crystal mass is dissolved in the heating step, based on the growth rate ratios in (b). (b) Ratio of the growth rates of the *S*- and *R*- enantiomorphs for a final value of 0.5 and various time constants, *b*.

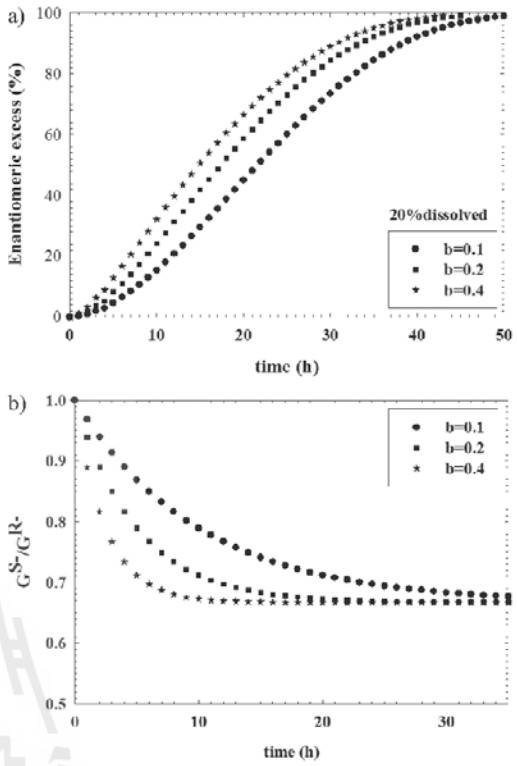

Figure 4. (a) Evolution of the solid phase ee when 20% of the crystal mass is dissolved in the heating step, based on the growth rate ratios in (b). (b) Ratio of the growth rates of the *S*- and *R*- enantiomorphs for a final value of 0.667 and various time constants, *b*.

which, by transient adsorption onto the surface of one enantiomer, causes a time-dependent reduction in the growth rate of this enantiomer. The explanation of the maturation effect is preferred by the authors, since such chiral impurities were not evident in any of the experiments concerning the temperature cycle-induced deracemization.

Simulation 1.2

In this simulation, the same set of conditions was investigated as in Simulation 1.1; however, the ratio of the growth rates of the two enantiomorphs at steady state is 0.667, rather than 0.5 as in Simulation 1.1.

The evolution of the solid phase ee is shown in Fig. 4 a. In Simulations 1.1 and 1.2, which differ only in the steady-state growth rate ratio, the results show a similar tendency in the evolution of ee The time required to achieve complete chiral purity is shorter when the counter-enantiomer (*S*-) has a poorer crystal quality (higher values of b or smaller value of τ), as illustrated in Fig. 4 a. Moreover, the evolution of ee when using different ratios of the final growth rates is different even when the same value of b is used. A smaller ratio results in a slower evolution of the ee.

Simulation 1.3

The effect of the percentage of the crystal mass dissolved during a heating cycle on the evolution of ee was studied in this simulation. The simulations were carried out with the same conditions as in the first and the second simulations; however, here the percentage of crystal mass dissolved was set at 20%, 25%, or 30%. The simulation results are similar to the experimental results in a previously published article [1]; the time required to achieve complete resolution is shorter when the mass of crystals dissolved in the heating cycle increases, as shown in Fig. 5. However, this result is only valid when the same temperature program is maintained for all cycles and only the total number of cycles required for deracemization is considered. Optimization of the process would likely involve larger temperature cycles (greater differences between the higher and the lower temperature in the cycle) at the beginning of deracemization, followed by smaller, quicker cycles near the end of the de-

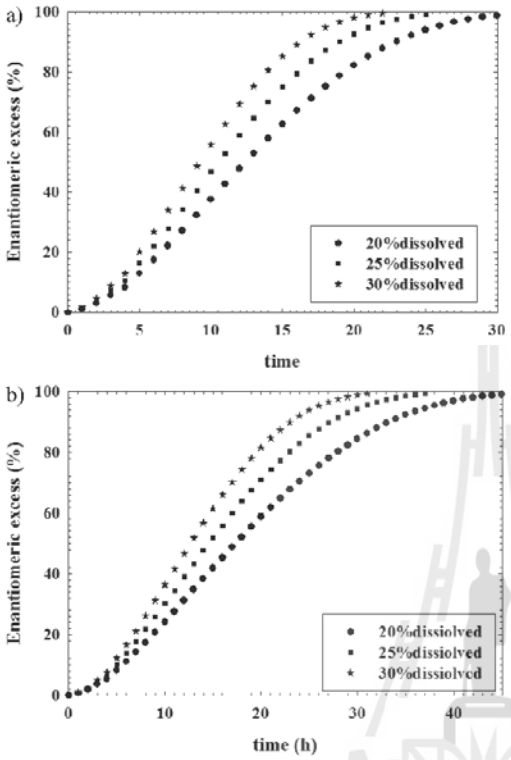

Figure 5. Evolution of the solid phase ee by setting the time constant at $b = 0.2$ and (a) $(G_S/G_R)(j\to\infty) = 0.5$, (b) $(G_S/G_R)(j\to\infty) = 0.667$, and by varying the percentage of the crystal mass dissolved in the heating period.

racemization; experimental optimization using damping in the series of temperature cycles is currently in progress.

4 Model 2: Simulation with Growth Rate Dispersion

A further set of simulations was performed with the assumption that the initial mass, the initial CSD (monosized crystals at 50 µm), and the mean of the crystal growth rate distributions of the two enantiomorphs were equal. However, the two enantiomorphs were assumed to have different levels of crystal growth dispersion. This is a difficult case to simulate since a two-dimensional (crystal size and crystal growth rate activity) population balance is required. Because it was uncertain whether this phenomenon could result in deracemization, it was decided to study a simple case that could be conveniently modeled. In this case, the population of growth activities is modeled with a small series of impulses rather than a continuous distribution of growth rate activities. These simulations can demonstrate whether this is a potential mechanism for the deracemization. The simulation of the system can then be performed in a similar way as for Model 1.

A simple case to simulate, for example, is when the mean crystal growth rates of the two enantiomorphs are equal but all *R*- crystals have a growth activity of 1 while half of the *S*- crystals have a growth activity of 1.1 (and are therefore fast growers) and the other half of the *S*- crystals have a growth activity of 0.9 (slow growers). This case is non-physical (the growth rate distributions are continuous functions in real systems), but it is a simple model that allows us to check whether GRD alone may be responsible for the deracemization of the suspension.

In solving this GRD model, the parameters in Tab. 3 were considered, where

- G_R is the growth rate of the *R*- crystals
- G_S is the growth rate of the *S*- crystals
- $\bar{G}_R$ is the mean of the growth rate distribution of the *R*- crystals
- $\bar{G}_S$ is the mean of the growth rate distribution of the *S*- crystals
- FD is the fraction of mass dissolved
- $L_{initial}$ is the initial size of the crystals

4.1 Simulations and Parameter Analysis of Model 2

The results of the simulations concerning the GRD are shown in Figs. 6–8. Simulations are presented by varying the GRD profile and the fraction of the suspension mass dissolved during the heating cycle, in order to determine whether GRD is a potential mechanism for the deracemization.

Simulation 2.1

The effect of dispersion of the growth activity of the two enantiomorphs is investigated during the recrystallization period. There are four crystals (or to extend the concept, four populations of crystals with the same number of crystals in each population) considered in this simple simulation to model deracemization via GRD. The growth activity distributions for the *R*- enantiomorph and the *S*- enantiomorph are set based on

Table 3. Initial parameters for the simulations of Model 2.

Exp. no.	G_R		$\bar{G}_R$	G_S		$\bar{G}_S$	FD	$L_{initial}$ [µm]
	1	2		1	2			
1	1.00	1.00	1.00	0.90	1.10	1.00	0.5	50
2	1.00	1.00	1.00	0.95	1.05	1.00	0.5	50
3	1.00	1.00	1.00	0.85	1.15	1.00	0.5	50
4	1.00	1.00	1.00	0.90	1.10	1.00	0.5	25
5	1.00	1.00	1.00	0.90	1.10	1.00	0.25	50
6	1.00, 1.00	1.00, 1.00	1.00	0.90, 0.95	1.05, 1.10	1.00	0.5	50
7	0.95	1.05	1.00	0.90	1.10	1.00	0.5	50

the two enantiomorphs having the same mean growth rate activity but different levels of GRD. For example, the growth rate activity of two *R*- crystals can be set equal to unity, of the first *S*- crystal to less than unity, and of the other *S*- crystal to an equal amount greater than unity. The means of the growth rate distributions of both enantiomorphs are equal. The initial particle sizes of the four crystals are the same. The dissolution kinetics of the four crystals during the heating period are equal. The results of Simulation 2.1 (Fig. 6) show the progression of the deracemization as the GRD is varied, indicating that increasing the dispersion of rates in the more disperse crystal growth rate distribution hastens the deracemization.

Simulation 2.2

This simulation investigated the effect of the initial size of the particles on the evolution of ee at a constant mass fraction of suspension dissolved. The distributions of the growth activities of both enantiomorphs are set by giving the two *R*- crystals a growth rate activity of 1 while one of the *S*- crystal populations has a growth activity of 0.9 and the other *S*- crystal population has a growth activity of 1.1. The experimental results are shown in Fig. 7, which shows that the evolution of ee is not affected by the initial size of the crystals when the fraction dissolved is kept

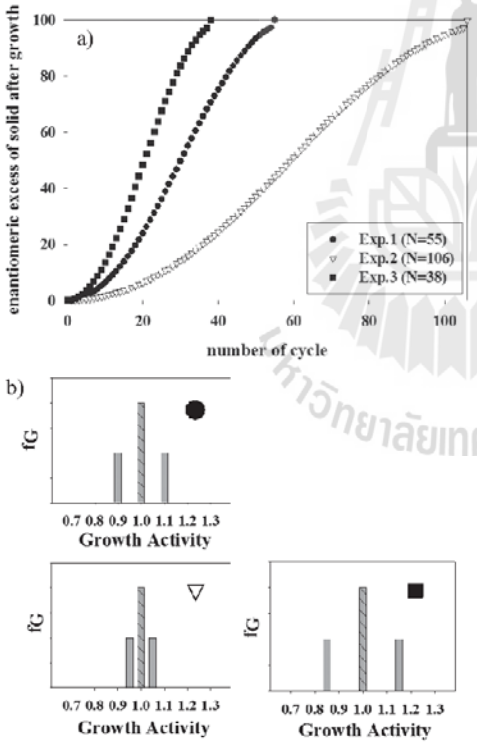

Figure 6. Evolution of the solid phase ee by dispersion of the growth activity when the two enantiomorphs have the same mean crystal growth rate activity (the growth activity of *R*- is shown as the hatched bars).

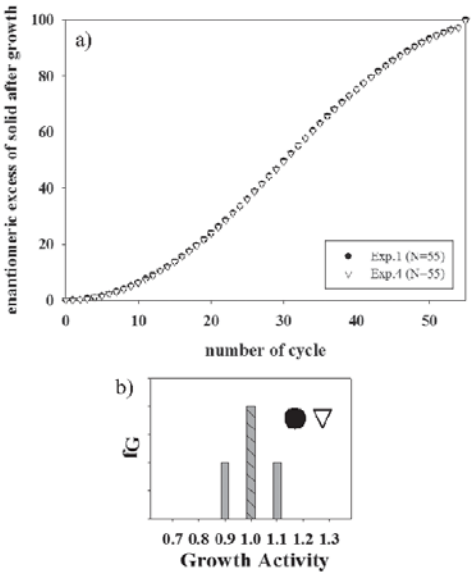

Figure 7. Effect of the initial size of the two enantiomorphs on the evolution of the solid phase ee (●) Initial size = 50 µm, (▽) initial size = 25 µm.

constant. Initially, this result was surprising, but can be explained by the fact that a constant mass is dissolved; so, in each case, the fraction of the crystals dissolved in one cycle is the same, leading to a cycle displaying the same increase in ee.

Simulation 2.3

The effect of the percentage of the suspension mass dissolved on the evolution of ee was investigated in Simulation 2.3. Simulations were performed with 25 % and 50 % of the crystal dissolving during the heating period of a cycle. The percentage of the crystal mass dissolved can be experimentally varied either by varying the high and low temperatures in the cycle or by varying the suspension density in the vessel. The two populations have the same initial crystal size and have the growth rate distributions described in Simulation 3.1. The results of Simulation 2.3 are shown in Fig. 8.

Increasing the amount dissolved increases the rate of the deracemization, a result similar to the experimental results, where the number of cycles required is less when the amount of crystal dissolved is made larger [1]. However, there will be a limit to the improvement possible with higher amounts dissolved, because the higher amount dissolving will increase the driving force during the crystallization step, thus increasing the likelihood that nucleation of the two enantiomers occurs.

Further simulations were performed with different discretizations of the crystal growth rate distributions, e.g., smoothing the growth rate distribution of *S*- by using more discrete intervals, and also giving both *R*- and *S*- (different levels of) GRD. These results show similar trends to those already shown, and are not discussed here. Details and results of these simulations can be seen in the Supporting Information.

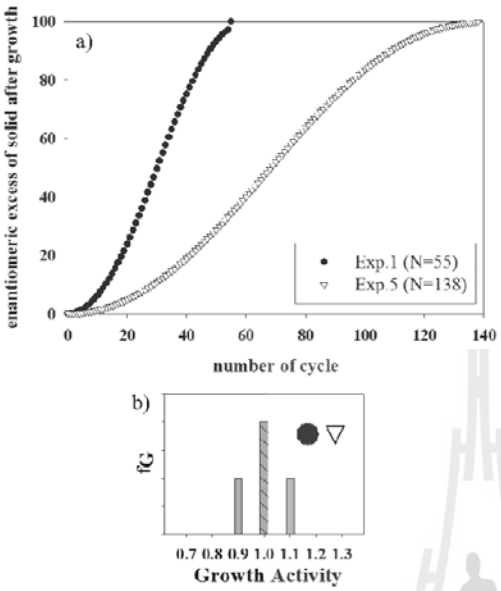

Figure 8. Evolution of the solid phase ee when the percentage of the suspension mass dissolved is varied. (●) 50 % dissolved, (▽) 25 % dissolved.

The models of the mechanism of deracemization due to the crystal growth rate kinetics show the evolution of ee as a sigmoidal curve that matches the common experimental results of deracemization [1]. The two growth rate kinetic models are based on the population balance. The evolution in the ee could be explained by the fundamentals of crystal growth. In the growth kinetics model without GRD, the ee is increased due to the difference in the growth rate between the two enantiomorphs, which may be caused by the history of nucleation of the primary nuclei of the two enantiomorphs.

The other explanation for the mechanism of deracemization is crystal GRD. It can be seen that the slow grower of the disperse grower (the *S*- crystals) reduces to zero size relatively quickly; however, the ee of the *S*- enantiomorph still increases because the amount of mass gained by the fast grower of the *S*- crystals more than compensates for the loss in mass of the slow grower of the *S*- crystals. The *R*- crystals are eventually out-competed by the fast growing *S*- crystals, leading to complete deracemization. This last model (the GRD model) appears to be the most satisfactory explanation produced. The difference in the GRD may have resulted from the conditions experienced in the initial nucleation event (before the advent of the temperature cycles), as demonstrated in other materials by Jones and Larson [7], with the enantiomorphs having the larger GRD having initially nucleated at a higher supersaturation than the more well-behaved enantiomer with a smaller amount of GRD. Experimental work following the particle size distribution event in deracemization due to temperature cycling could potentially clarify whether this mechanism is correct. In several types of deracemization experiments (Viedma ripening, deracemization with temperature cycles, deracemization using ultrasound), the time required to begin the deracemization varies strongly; perhaps the results presented here concerning the GRD of the enantiomorphs may help to explain why some deracemizations start evolving soon after the process is initiated while in other cases the initiation is slow.

5 Conclusions

In this work, the mechanism of chiral symmetry breaking towards complete deracemization was described and tested by two simple mathematical models based on the fundamentals of crystal growth. A phenomenon relating to crystal growth may be responsible for the enhancement of ee when temperature cycling is applied to a racemic suspension of a conglomerate-forming system where there is a swift racemization in the solution phase. The possible mechanism for deracemization may come from the history of the nucleation, which is a stochastic process: The primary nuclei of the two enantiomorphs occur at slightly different times, and thus under different levels of supersaturation and/or temperature, leading to different internal crystalline perfection and therefore slightly different thermodynamic stability. The results from the simulations are promising in that a very simple model can reproduce the sigmoidal form of the evolution of the ee However, further experimental and modeling work is necessary to verify whether any of these hypotheses is correct. A study on the parameters associated with the crystal growth rate models could be a route to fill the gap in understanding of the deracemization process mechanism.

Acknowledgment

This work was supported by the Thailand Research Fund (TRF), in collaboration with Suranaree University of Technology (SUT) through the Royal Golden Jubilee Ph.D. Program (1.C.TS/51/B.1).

The authors have declared no conflict of interest.

Symbols used

b	[h^{-1}]	inverse of the time constant τ_G
ee	[%]	enantiomeric excess in the solid phase
FD	[–]	fraction of the crystal dissolved during the heating part of the cycle
G	[$m\,s^{-1}$]	crystal growth rate
$\bar{G}$	[$m\,s^{-1}$]	mean crystal growth rate of a population
L	[m]	specific length of a crystal
$\bar{L}$	[m]	parameter in the distribution describing the population density
n	[$\#\,m^{-4}$]	population density of the crystals

Greek symbols

Δ	[–]	change in a property over a specific part of the temperature cycle
μ_3	[m^3]	third moment about the origin for the crystal size distribution
σ	[m]	parameter in the distribution describing the population density
τ_G	[h]	time constant relating to the change in the growth rate ratio $\bar{G}^{S-}/\bar{G}^{R-}$

Subscripts/superscripts

D	property at the end of the dissolution part of the temperature cycle
G	property at the end of the growth part of the temperature cycle
i	pertaining to species *i* (*R*- or *S*-)
initial	property at the initiation of the temperature cycling
j	property of the *j*th temperature cycle
min	minimum
R-	property of the *R*- population
S-	property of the *S*- population
T	total (property of the combined *R*- and *S*- populations)

References

[1] K. Suwannasang, A. E. Flood, C. Rougeot, G. Coquerel, *Cryst. Growth Des.* **2013**, *13 (8)*, 3498.

[2] C. Viedma, *Phys. Rev. Lett.* **2005**, *94 (6)*, 065504.

[3] J. H. E. Cartwright, O. Piro, I. Tuval, *Phys. Rev. Lett.* **2007**, *98 (16)*, 165501.

[4] J. M. McBride, *Lecture at NORDITA Workshop "Origins of Homochirality"*, Stockholm **2008**, http://agenda.albanova.se/conferenceDisplay.py?confId=322.

[5] W. L. Noorduin, W. J. P. van Enckevort, H. Meekes, B. Kaptein, R. M. Kellogg, J. C. Tully, J. M. McBride, E. Vlieg, *Angew. Chem.* **2010**, *49 (45)*, 8435.

[6] J. Garside, A. Mersmann, J. Nývlt, *Measurement of Crystal Growth and Nucleation Rates*, 2nd ed., Institution of Chemical Engineers (IChemE), Rugby **2002**.

[7] C. M. Jones, M. A. Larson, *AIChE J.* **1999**, *45 (10)*, 2128.

[8] M. Iggland, M. Mazzotti, *CrystEngComm* **2013**, *15 (12)*, 2319.

[9] F. Ricci, F. H. Stillinger, P. G. Debenedetti, J. Chem. Phys. 2013, 139, 174503.

[10] D. Gherase, D. Conroy, O. K. Matar, D. G. Blackmond, *Cryst. Growth Des.* **2014**, *14 (3)*, 928.

[11] R. R. E. Steendam, B. Harmsen, H. Meekes, W. J. P. van Enckevort, B. Kaptein, R. M. Kellogg, J. Raap, F. P. J. T. Rutjes, E. Vlieg, *Cryst. Growth Des.* **2013**, *13 (11)*, 4776.

[12] G. Levilain, G. Coquerel, *CrystEngComm* **2010**, *12 (7)*, 1983.

[13] G. Coquerel, in *Topics in Current Chemistry (Novel Optical Resolution Technologies)* (Eds: K. Sakai, N. Hirayama, R. Tamura), Springer, New York **2007**.

[14] C. M. Jones, M. A. Larson, *Chem. Eng. Sci.* **2000**, *55 (14)*, 2563.

Supporting information

Part 1.

The McCabe ΔL Model.

An initial concept for the mechanism of deracemization was that the two enantiomorphs have a difference in their mean size but the smaller size population (in this case *S*-) contains more crystals, such that the total initial mass in the smaller sized population is the same as in the larger sized population (in this case *R*-). A schematic of the simulation results for this model is shown in Figure 3. This model assumes the system remains within the MSZW (i.e. there is no nucleation). During the first of these cycles the number of particles should decrease, causing the final size of the particles to be slightly larger than the initial size. After the first cycle, no more particles completely disappear, the smallest particles only approaching zero size by the end of the heating cycle. In a typical case this will not result in more than a fractional amount of change in the *ee*.

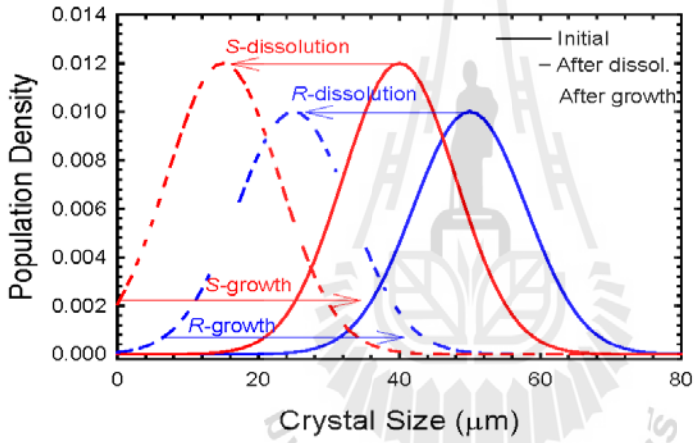

Figure 1. Simulations for cycles based on dissolution and growth based on McCabe's ΔL law. By the second cycle the crystal size distributions begin to repeat and no further increase in *ee* in found.

The dissolution and regrowth phenomena based upon McCabe's ΔL law could be responsible for complete deracemization, but only under unusual conditions. The dissolution and growth might eventually destroy the smaller sized population of crystals leaving the other enantiomorph surviving, and thus eventually produce complete deracemization. The dominant enantiomorph, which has a bigger crystal mean size, could be the winner by consuming the solute produced during dissolution of the counter enantiomorph during the growth period.

Simulations Analysis of Model 1

The results of the simulation show that dissolution and growth by McCabe's ΔL law cannot achieve complete deracemization except where there is an exceptionally large difference in the sizes of the two enantiomorphs at the initial condition. For most simulations there was no increase of the *ee* after the first cycle. However in extreme cases, where there is a substantial difference in the initial crystal size of the two enantiomorphs and the amount dissolved is very large, it is possible to reach 100% *ee* in one dissolution and growth cycle. Under these conditions the smaller enantiomorph completely dissolves during the dissolution part of the cycle leaving only a small population of the other enantiomorph to grow (in an Auto seeded preferential crystallization) during the cooling part

of the cycle. The fast racemization reaction maintains an equal supersaturation for the two enantiomorphs, and reduces the chance that the counter enantiomorph primary nucleates. In cases where the differences between the initial sizes of the two enantiomorphs is small there is some change in *ee* in the first cycle as more crystals of the smaller sized enantiomorph dissolve when compared to the larger sized enantiomorph (see Figure 1). During the cooling period of the cycle the two populations are regrown, but the smaller population has lost more of its tail, and hence its mass, causing an increase in the *ee* during this cycle. However, after the first cycle the two distributions simply cycle between two fixed points at the end of the dissolution and growth periods without any further improvement in the *ee*. It is clear a different model for growth or dissolution part of the cycle is required to predict the continuous evolution of the *ee* over a large number of cycles.

Part 2.

Additional Simulations using the Growth Rate Dispersion Model.

Simulation A. In order to get a better idea of the deracemization in systems with continuous growth rate activity distributions, the dispersion of growth rate activity is investigated by increasing the number of crystal of two populations from 2 crystals to 4 crystals of each enantiomorph; this helps bring the growth activity distributions slightly closer to continuous distributions. (Apart from the increasing number of discretizations of the growth rate distributions the model is the same as that presented in the paper under the section of the growth rate dispersion model). The distributions of growth activities of the two enantiomorphs are set by giving the four *R*-crystals a growth rate activity of 1 while *S*-crystals have the growth activities of 0.90, 0.95, 1.05 and 1.10, respectively. The mean growth rate distributions of both populations are still same. The initial particle sizes of all crystals are 50 μm and the fraction of crystal dissolved in the suspension during the heating cycle is 50%. The results of this experiment are shown in Figure A. The results indicate that the smoothing of the growth rate distribution of the disperse form slows the evolution of *ee* slightly.

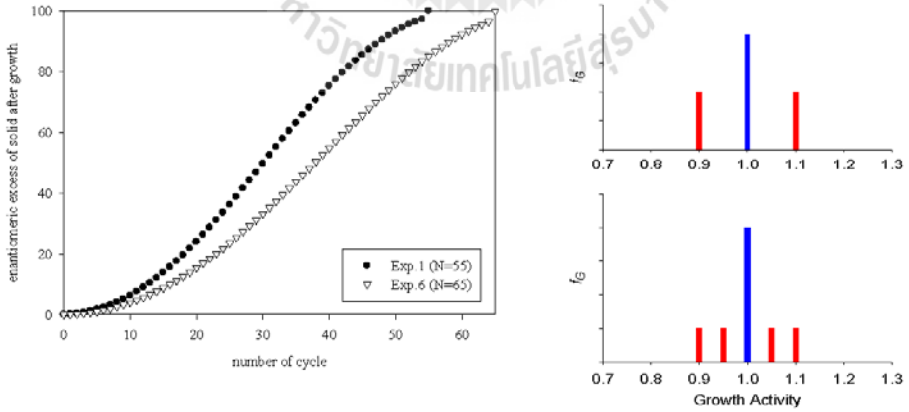

Figure A Evolution of the solid phase enantiomeric excess when the functional form of the growth rate activity distribution is varied.

Simulation B. A simulation to model the case where both populations have GRD, but where the amount of dispersion is not the same for the two enantiomorphs, was performed in Simulation B.

The growth rate activities of the two *R*-crystals are set at 0.95 and 1.05 (a narrow distribution of growth rate activity) and the growth rate activities of the two *S*-crystals are set at 0.90 and 1.10 (a wider distribution of growth rate activity). The results are shown in Figure B.

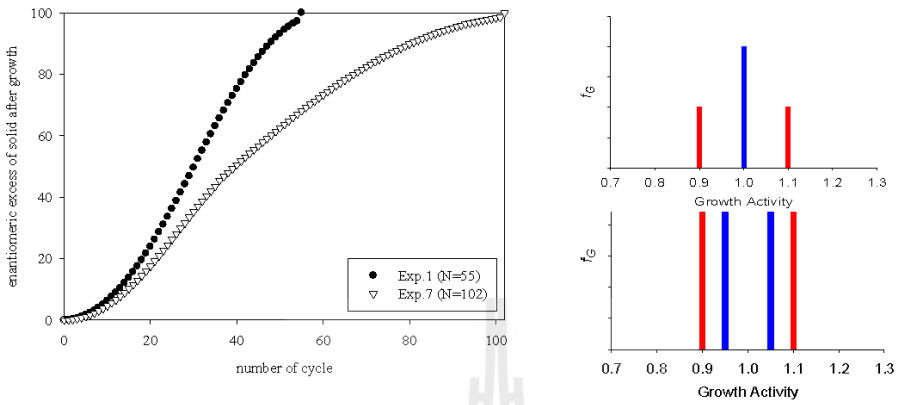

Figure B Evolution of the solid phase enantiomeric excess when both enantiomorphs have dispersion of growth rate activity compared to the evolution when only one enantiomorph has dispersion of growth activity.

The mean of the growth rate distributions of the two populations are equal at 1. The initial particle sizes of all crystals and the percentage of mass dissolved are given equal for the two enantiomorphs. The result of this simulation is that the evolution of the *ee* is slowed when both enantiomorphs have dispersion in their growth rate distributions.

BIOGRAPHY

Mr. Kittisak Suwannasang was born on December 27, 1986 in Chiang Rai, the northernmost province of Thailand. He continued his study towards a Ph.D. after he earned his bachelor's degree (first class honors) in Chemical Engineering at Suranaree University of Technology in 2009. He was awarded the honorable distinguished golden brooch for obtaining the highest GPAX of the graduating students from HRH Princess Maha Chakri Sirindhorn. Since the year 2009, Mr. Suwannasang has received the prestigious Royal Golden Jubilee Ph.D. Scholarship funded by the Thailand Research Fund (TRF) in collaboration with Suranaree University of Technology (SUT) for the study of the Doctor of Philosophy (Ph.D.) Program in Chemical Engineering at SUT. His research was under the supervision of Professor Dr. Adrian Evan Flood at SUT and Professor Dr. Gérard Coquerel at University of Rouen in France. He has spent seventeen months in France for studying his Ph.D. at the SMS laboratory in University of Rouen. His research articles have been published in the Crystal Growth & Design Journal and in the Chemical Engineering & Technology Journal as shown in Appendix D.